ROLE OF SILICA-BASED CO-ADDITIVES FOR EFFECTIVE TREATMENT OF EXPANSIVE SOILS

A Dissertation

by

NRIPOJYOTI BISWAS

Submitted to the Graduate and Professional School of
Texas A&M University
in partial fulfillment of the requirements for the degree of

DOCTOR OF PHILOSOPHY

Chair of Committee,	Anand J. Puppala
Committee Members,	Marcelo Sanchez
	Dallas N. Little
	Miladin Radovic
Head of Department,	Zachary Grasley

May 2022

Major Subject: Civil Engineering

ABSTRACT

Construction of pavements and other lightweight structures on expansive soils is a considerable cause of concern for transportation infrastructure practitioners around the globe, including in the state of Texas. Pavement undergoes rutting, cracking, shoulder dropping, and differential heaving during its service life due to non-uniform moisture cycles, and consequently, the long-term durability of the structures is severely impacted. Among the available methods, chemical stabilization using calcium-based stabilizers such as lime is one of the most commonly used techniques, considering the ease of construction and low cost of virgin materials for building the transportation infrastructures. The stabilization of high-plasticity soils with lime results in the formation of pozzolanic reactions products, which binds the soil matrix and imparts the desired engineering properties to the soil subgrade.

However, the pozzolanic reactions being a slow process, need considerable time before the final strength or stiffness is achieved. As a result, it results in significant traffic delays during the construction phase and increases the overall life-cycle cost of the project. Additionally, several expansive soil zones also have a considerable concentration of soluble sulfate minerals. Treatment of such sulfate-rich soils using calcium-based stabilizers could be counterproductive, resulting in the formation of a highly deleterious and expansive mineral, ettringite. Researchers have been extensively working on developing novel treatment techniques to mitigate such problems associated with traditional ground treatment techniques.

To overcome the problems associated with slow pozzolanic reactions, sulfate-related heave distresses and long-term durability of transportation infrastructures, a research study was designed to use novel silica-based co-additives, such as quarry-dust and laboratory-grade nano-silica compounds with lime stabilizer to treat high plasticity soils with different levels of sulfate concentration. The present studies showed that the application of these novel-co-additives with traditional dolomitic-hydrated lime significantly modified the reaction kinetics. Additionally, when used with lime to treat sulfate-rich soils, the presence of the additional silica phases suppressed the precipitation and subsequently swelling from ettringite crystals. The presence of the silica phases also improved the durability and permanency of the chemical stabilizer compared to traditional treatment alone. Overall the application of these new treatment techniques will be of immense help for transportation agencies and would help them to use new and more sustainable soil treatment techniques for improving the long-term performance of the transportation infrastructures.

DEDICATION

To all inquisitive minds

'Cerca Trova'

ACKNOWLEDGEMENTS

I would like to extend my sincere gratitude to Dr. Anand J. Puppala, my committee chair, for providing me with the opportunity and invaluable support to conduct this research. What I have learned working with him far exceeds the research that is documented in this dissertation.

I also wish to thank my graduate committee members, Dr. Dallas Little, Dr. Marcelo Sanchez, and Dr. Miladin Radovic, for their support and encouragement in pursuing this research. I also acknowledge the technical staff at the Center for Infrastructure Renewal (CIR) for their help in executing this research.

I appreciate the support of my colleague Dr. Sayantan Chakraborty who was directly involved in various stages of my research. I am also grateful to Dr. Surya Congress and Dr. Ashrafuzzaman Khan, who motivated me during this research. I also wish to thank Krishneswar Ramineni and Jungyeon Jang for providing valuable support in performing the microstructural studies at CIR. Special thanks to my other team members in the research group- Aritra, Jass, Danny, Rinu, Leila, Puneet, Burak, Prince, Amit, Hiramani and Kamron

I acknowledge the support and encouragement of my parents, Mr. Subhas Chandra Biswas and Mrs. Sahana Biswas, for always believing in me.

Finally, I thank friends who made my stay in Texas memorable- Sayantan, Aritra, Jass, Ajay, Ashraf, Atreye, Debranjan, Prince, and Akshay.

CONTRIBUTORS AND FUNDING SOURCES

Contributors

This work was supervised by a dissertation committee consisting of Dr. Anand J. Puppala [advisor and P.I.], Dr. Dallas Little, and Dr. Marcelo Sanchez of the Zachry Department of Civil and Environmental Engineering, and Dr. Miladin Radovic of the Department of Material Science and Engineering.

All other work conducted for the dissertation was completed by the student independently.

Funding Sources

This work was also made possible in part by NSF Industry-University Cooperative Research Center (I/UCRC) program funded ‘‘Center for Integration of Composites into Infrastructure (CICI)’’ site at Texas A&M University, NSF PD: Dr. Prakash Balan; Award #2017796 and #1954073 (Completed Aug 2021).

Its contents are solely the responsibility of the authors and do not necessarily represent the official views of the NSF-I/UCRC.

TABLE OF CONTENTS

Page

LIST OF FIGURES

Page

LIST OF TABLES

Page

1. INTRODUCTION

"*The most fruitful research grows out of practical problems*"

– Ralph. B. Peck (1912-2008)

1.1 Background

Pavements and lightweight structures constructed on problematic soils often suffer from distress induced by both traffic and environmental loads. The moisture migration within the pavement layers due to seasonal wet-dry cycles induces significant damage to the expansive soil subgrades. The expansive soils undergo volumetric expansion due to moisture intrusion, resulting in the reduction of strength and stiffness. Similarly, during dry seasons, the soils undergo major shrinkage strains causing the development of cracks near the top of the subgrade that gradually propagates to the surficial layers in the pavement. The cyclic wetting and drying coupled with repeated traffic loading induce detrimental impacts on the long-term performance of the transportation infrastructures.

Chemical treatment of expansive soils with traditional calcium-based stabilizers such as lime has been practiced extensively over several decades all over the world and in the state of Texas. These treatments help to improve the properties of expansive clays immediately during the construction stage and during their long-term serviceability. However, based on the previous experimental studies, some major short-comings for the calcium-based lime treatments were identified and are listed in the following:

- Stabilization of expansive soils using lime is a time-dependent phenomenon. This is primarily attributed to the slow pozzolanic reactions. Rehabilitation of transportation infrastructure using lime-stabilized layers could significantly

increase the traffic delays and hence an overall impact in the socio-economic aspects of the project.

- Lime treatments in sulfate-rich expansive soils are often counterproductive due to the formation of highly deleterious mineral ettringite.
- Although, several studies have been performed on co-additives that are rich in alumino-silicate sources, no major research has been focused on the utilization of novel silica-based co-additives such as crystalline silica and nano-silica to mitigate the problems with lime treatment in expansive soils with different levels of sulfate concentrations.
- Limited studies have been performed on the resilient modulus properties of treated expansive soils with both lime and silica-based co-additives.
- Durability and long-term performance of novel co-additive treatments with Ca-based stabilizers are necessary for improving infrastructure serviceability.

Considering the above research gaps, a study was designed to treat problematic soils with a commercially available traditional calcium (Ca)-based stabilizer (dolomitic-hydrated lime) and different silica-based novel materials as co-additives. This study explored engineering properties as well as microscale studies along with comprehensive durability studies. These results are used to address silica additives and their impacts on the effective treatment of plastic soils.

1.2 Research Problem Descriptions

1.2.1 Utilization of Silica-based Co-additives to Modify the Reaction Kinetics

The utilization of commercially available lime for treating expansive soils has been practiced by TxDOT for several decades. Lime treatments are generally recommended for treating plastic clays (Plasticity Index (PI)>20). However, the chemical reactions involved in improving the performance of the problematic soils are often time-consuming. The application of industrial lime improves the treated soil performance over a long time through pozzolanic reactions. These reactions help in the formation of cementitious compounds that help in binding the soil matrix and subsequently enhance the performance of the stabilized soils. The pozzolanic reactions often take several months to complete, and during this time, the construction or rehabilitation activities for the pavements are significantly delayed. This also impacts traffic flow on the roads and increases congestions and time delays during that period. Overall, it culminates into significant socio-economic problems and losses for the transportation agencies during the construction and maintenance phases. As a result, research studies are necessary to address these problems and accelerate the reactions rates for the formation of cementitious binding gels. Rapid formation and hardening of the binding gels using silica-based co-additives would help to reduce the construction time for such pavements and subsequently improve the socio-economic benefits of the treatment process.

1.2.2 Application of Silica-based Co-additives to Reduce Ettringite in Sulfate-rich Soils

Application of Ca-based stabilizers to treat high-plastic problematic soils having significant concentration of soluble sulfates (>3000 ppm) is often counterproductive, and sometimes leads to major detrimental impacts on the rehabilitated structures. This primarily occurs due to the formation of a deleterious calcium alumino-sulfate hydrate mineral 'ettringite.' The precipitated ettringite crystals are hydrophilic in nature and undergo significant volumetric expansion causing severe damages to pavement and light-weight structure. Ettringite induced heaving are often termed as man-made heaving problem, and the state transportation agencies (DOTs) are persistently looking towards sustainable alternatives to address the problems associated with it. In this present research, the application of silica-based co-additives with lime is expected to mitigate the problems associate with ettringite-induced heave in high-sulfate soils.

1.2.3 Durability and Permanency of Stabilizer with Silica-based Co-additive Treatments

Another major concern associated with the treatment of high plasticity soils is the durability or permanency of the Ca-based treatments. The durability issues of low and high sulfate soils not having an appreciable amount of organic matter have been primarily attributed to moisture intrusion, leaching, carbonation, and exposure to extreme environmental conditions. Leaching, carbonation of stabilizers, and exposure to extreme environmental conditions are time-dependent phenomena, and their deleterious impact is observed over a longer period after treatment. In contrast, moisture exposure during the

early curing periods has been reported to cause immediate degradation in engineering properties of lime-treated soils. The application of silica-based co-additives is expected to improve the permanency of the soil treatment through the possible formation of additional cementitious phases. These cementitious phases are expected to improve the bonding of the soil matrix and subsequently counteract the repulsive forces from water molecules.

1.3 Dissertation Research Objectives

In the light of these problems associated with the application of traditional lime treatments, a research study was planned and designed to address the main research objective of developing a comprehensive guideline regarding the utilization of novel silica-based co-additives with traditional dolomitic-hydrated lime to improve both short-term as well as the long-term performance of problematic high-plastic clays. As a part of the evaluation of the research objective, several specific research goals are developed and presented in the following:

- Experimentally study and then develop a treatment methodology to modify the reaction kinetics of cementitious compounds and consequently rapidly improve the soil properties using silica-based co-additives.
- Investigate utilization of silica-based co-additive with traditional Ca-based stabilizer for treating high-sulfate soils.
- Study the effects of these novel treatment techniques on the durability and permanency for both short-term and long-term curing periods.

1.4 Dissertation Outline

The dissertation is organized as follows:

Chapter 1 is an introduction to the overall topic, which includes the background for this research, problem statements, dissertation research objectives, and dissertation outline.

Chapter 2 includes the literature review for chemical treatments in expansive soils, existing studies on mineralogy of expansive soil, traditional treatment techniques, use of different co-additives, past studies on stabilizing sulfate-rich soils, and literature on the durability and permanency of the chemical treatments.

Chapter 3 provides a comprehensive overview of all the raw materials used for the research study. Furthermore, this section also discusses an array of engineering and chemical tests, and subsequently followed by micro-structural studies that were performed during the course of this research.

Chapter 4 presents the studies where the effects of silica-based co-additives were studied in accelerating the development of engineering properties after treatment through the formation of additional cementitious phases in high-plastic soils.

Chapter 5 presents a study on the utilization of the silica-based co-additives to treat high-sulfate plastic soils when used with a traditional Ca-based stabilizer.

Chapter 6 discusses the efficacy of the novel treatment technique with the silica-based co-additives to improve both immediate and long-term durability and permanency of the treatments.

Chapter 7 provides an overall summary and conclusion for the dissertation and some recommendations for the scope of future studies.

2. LITERATURE REVIEW

2.1 Introduction

This chapter provides an overview of the existing literature related to the field of chemical stabilization of expansive soils. The literature reviews are classified into four major sections. The first section focuses on expansive soils and chemical stabilization using traditional techniques. The next section focuses on sulfate-rich soils and the problems associated with traditional stabilization techniques. The third section provides an overview of non-traditional approaches using the addition of several co-additives to modify the chemical reactions, such that problems associated with the traditional techniques could be mitigated. In the last section, previous studies related to the long-term durability and performance of the chemical stabilizers are presented. This chapter aims to introduce the readers to some existing studies on the chemical stabilizers and expansive soils with or without soluble sulfates and discuss some literature gaps that could possibly be addressed using this present research program.

2.2 Literature Review

2.2.1 Chemical Treatment of Expansive Soils

Construction of pavements and other lightweight transportation infrastructures on problematic soils is a considerable cause of concern for engineering practitioners (Estabragh et al. 2013, Saride and Dutta 2016). The use of the expansive soils for constructing pavement subgrades are motivated by some major factors, including local availability of geomaterials, low cost of hauling and transportation and traditional

knowledge of construction methodologies (Puppala et al. 2017b, Khan et al. 2020, Biswas et al. 2021c). However, the use of such soils as a supporting layer often leads to several distresses in the long-term serviceability of the pavements (Puppala 2016, Jafari et al. 2019). The majority of the problems arise due to a seasonal influx of moisture within the soil layers. The moisture ingress and egress due to rainfall events result in distress, including rutting, cracking, and differential heaving of such soils (Puppala et al. 1996, Petry and Little 2002, Chakraborty and Nair 2020, Puppala 2021). The behavior of such soils could be primarily attributed to its clay mineralogy and different concentrations of secondary minerals present in the soil layers (Pedarla et al. 2011, Puppala and Pedarla 2017, Chittoori et al. 2018).

2.2.1.1 Mineralogy of Expansive Soils

Expansive soils are primarily classified as high-plastic clays and, due to its genesis, could be composed of one or more of the three major clay minerals- Illite, Kaolinite and Montmorillonite (Little 1995, Mitchell et al. 2005, Chittoori et al. 2018). The major concentration of one or the other basic clay minerals dictates the macrostructural behavior of the soil layers. The common building block of soil is shown in Figure 2.1. These are silica tetrahedron and alumina octahedron blocks formed when oxygen is in coordination with other multivalent cations.

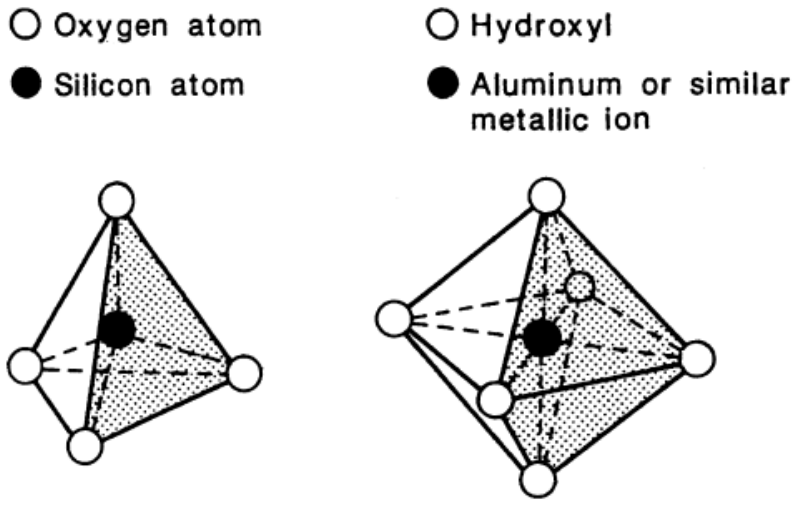

Figure 2.1 Basic building blocks of soil a) Silica-tetrahedron and b) Alumina octahedron (Little 1995)

The clay minerals are layered structures also known as phyllosilicates (Mitchell 1981, Petry and Little 2002). The layers consist of sheets of tetrahedral silica and octahedral alumina bonded with each other in either 1:1 arrangement or 2:1 arrangement to form layers of basic clay minerals (Bell 1996, Little and Nair 2009a, Puppala et al. 2017a). Kaolinites are 1:1 layered structures with silica and alumina sheets bonded by sharing the basal oxygen atoms and hydroxyl atoms. The Kaolinite clay minerals are generally classified as non-plastic. Illites and Montmorillonites are 2:1 layered structures where an octahedral alumina sheet is sandwiched between two tetrahedral silica sheets on either side.

During the formation of some clay minerals or 'genesis,' due to isomorphous substitution, one or more Si^{+4} ions in the tetrahedral sheet or Al^{+3} in the octahedral sheet are replaced by other positive cations having lower valency. This phenomenon of

isomorphous substitution induces a charge imbalance in the minerals, due to which the surfaces of these layered clay minerals develop a net negative charge. As a result, the clay surfaces become reactive to several positive cations or water molecules. The reactivity of a clay mineral is directly proportional to the amount of isomorphous substitutions. Montmorillonite minerals undergo the highest isomorphous substitution because approximately one in every six trivalent aluminum atoms are replaced by divalent magnesium atoms. As an outcome, the smectites develop abundant reactive surfaces, which are more likely to absorb positively charged hydroxyl ions and other positive cations to impart distinct properties to the soil. In Kaolinites, the isomorphous substitution is less prevalent as compared to smectites, as only one in about every 400 tetravalent silica atoms are replaced by trivalent aluminum atoms. This makes the Kaolinites less reactive and subsequently has limited availability of negatively charged surface ions for chemical reactions.

The negatively charged clay surfaces and the mineral structures strongly influence the mechanism through which the basic building blocks of minerals are linked together to form different clay minerals. The three primary clay minerals are shown in Figure 2.2. The 2:1 Illite sheets are bonded by intermittent K^+ ions, making the surface charge neutral and forming strongly bonded sheets or layers (Gaudette et al. 1964, Deng et al. 2006, Konan et al. 2007, Safehian et al. 2018). This neutralization of surface charges makes Illites less prone to absorb water or hydroxyl molecules. Similarly, the 1:1 sheets of Kaolinite are linked by secondary hydrogen bonds in between the OH^- ions at the surface of the octahedral sheet and the oxygen atoms at the base of the tetrahedral sheet (Schroth

and Sposito 1997, Wang and Siu 2006). Unlike the primary valence bonds, these secondary valence bonds (hydrogen bonds) are relatively weak. However, they are strong enough to prevent the ingress of water molecules or positively charge cations in-between the clay layers. This impediment to the cations from external sources to migrate in between the clay layers makes Kaolinites a significant stable mineral and consequently less plastic in nature.

Smectites or Montmorillonites have 2:1 layered structure and a significant concentration of surface negative charges due to large isomorphous substitutions (Odom 1984, Kloprogge et al. 1999, Janek and Lagaly 2001). The negative surface charges are satisfied by the absorption of loosely bonded exchangeable cations. The weak linkage of cations to the clay surfaces induces a major potential for the development of weak cleavage planes. Consequently, there is a breakage of clay particles to smaller fragments and a generation of large specific surface area (~800 m^2/gm), and making it more prone to absorb positive cations or bi-polar hydroxyl ions. The swelling of smectite clays is extensively dependent on the presence of a cation concentration in the interacting fluid.

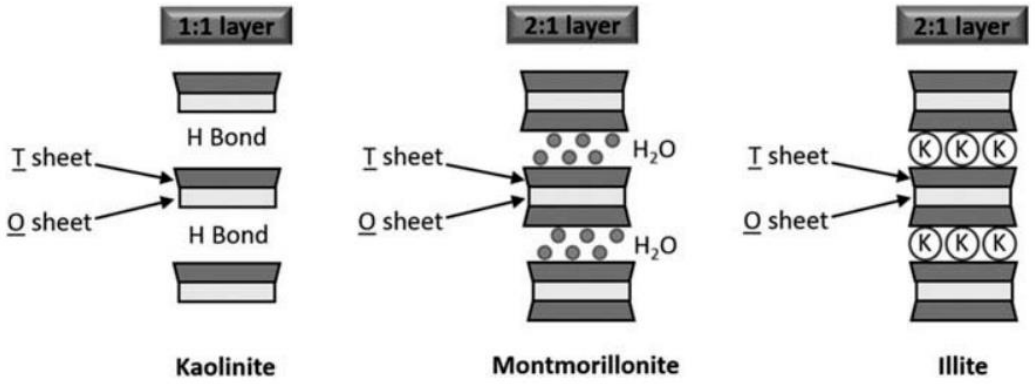

Figure 2.2 Primary clay mineral a) Kaolinite and b) Montmorillonite, and c) Illite (Chen and Peng 2018)

Figure 2.3 shows the mechanism of clay and water interaction using the double diffused layer (DDL) (Mitchell et al. 2005). The negative surface charge of the clay particles tends to be surrounded by positive disorderly arranged cations to equilibrate the surface charges. A second layer of water molecules diffuse towards the positive cations and are held in position by weak hydrogen bonding or diffusion gradient. The negatively charged surfaces of the clay minerals absorb hydroxyl ions when exposed to moisture conditioning and form dispersed structures. This occurs due to the loss of particle to particle contact due to the formation of a thin layer of water molecules and positive cations around clay particles known as DDL theory.

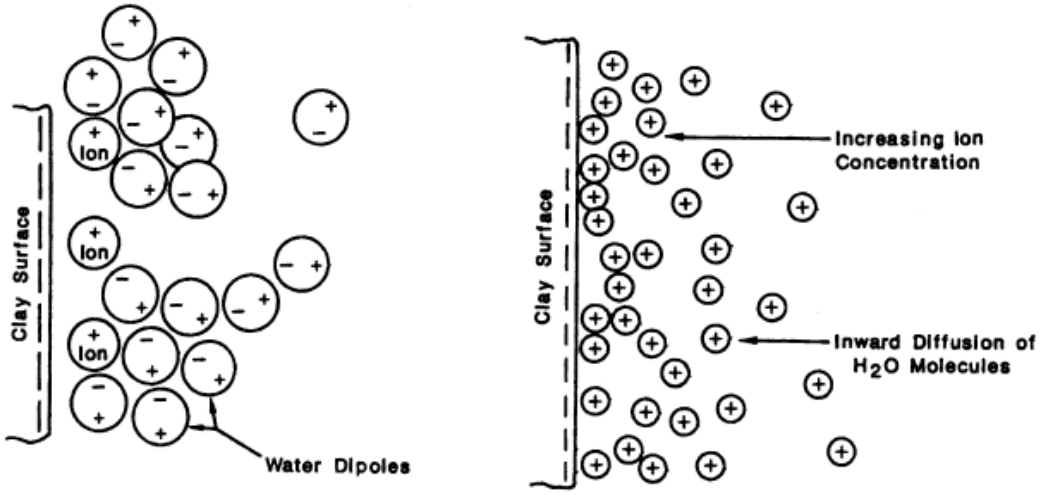

Figure 2.3 Interaction between clay and water molecules in clay minerals (Mitchell and Soga 2005)

The thickness of the DDL is dependent on the amount of negative surface charges and the size and valency of the cations present in the clay minerals. Due to the formation of DDL and dispersed structures, the clay particles undergo loss in strength and develop internal pressure that results in the swelling of the clay matrix. The swelling of clay minerals due to moisture intrusion can cause significant damage to the overlying structures. Alternatively, in the dry seasons, the removal of moisture results in the development of cracks and fissures near the surface layers and reduces the serviceability of the layers (Nahlawi and Kodikara 2006, Morris et al. 2011).

As a result, several research studies in the past have focused on using chemical stabilizers such as lime and cement additives to improve the performance of such soils when exposed to moisture conditioning.

2.2.1.2 Traditional Treatment Techniques

Traditional Ca-based stabilizers such as lime and cement have been used for several decades to treat expansive soils (Nelson and Miller 1992, Consoli et al. 2002, 2009, 2011, Puppala et al. 2006a, 2009, Si and Herrera 2007, Pedarla et al. 2011, Saldanha and Consoli 2016). The use of these stabilizers has been motivated by their low economic costs, ease of construction techniques, and reliability of performance during the design life of the infrastructures (Dempsey and Thompson 1968, Little 1995). The selection of an appropriate stabilizer is based on several criteria including, the objective of treatment, the target engineering or material property, the environmental and economic impacts of treatment, and the soil mineralogy and classification. Texas Department of Transportation (TxDOT) provides a flow-chart to select the type of stabilizer based on the soil classification information as shown in Figure 2.4.

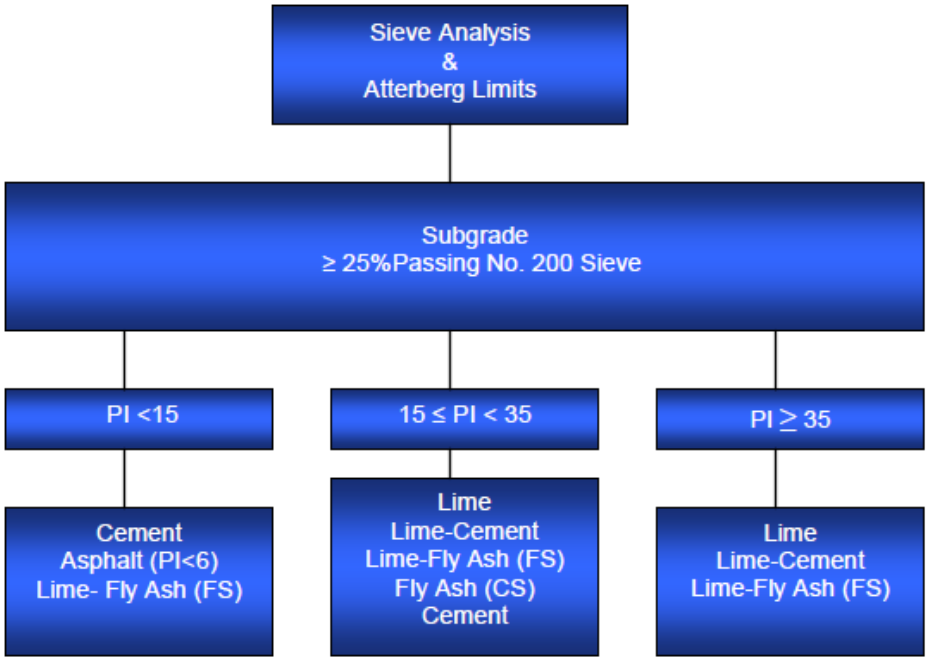

Figure 2.4 Additive selection criterial based on % passing #200 sieve and PI (Texas Department of Transportation 2005)

Among the Ca-based stabilizers, cement is mostly used for soils that are granular in nature or have low plasticity index (PI) values (PI<15). Due to a quick reactivity of the cement to form final cementitious products, it is generally not recommended to be used with high plastic clays, since it requires longer mixing time before final layer compaction (Texas Department of Transportation 2005, Hoyos et al. 2006). TxDOT recommends the use of lime either independently or mixed with cement or other stabilizers for stabilizing soils with PI>15. For soils with PI>35, it is strongly recommended to be treated with lime alone or with lime and cement or fly ash.

Treatment of expansive soils with lime helps to improve the performance through two basic reaction mechanisms: immediate 'modification' reactions and long-term pozzolanic reactions (Arabi and Wild 1986, Little 1995, Bell 1996, Little et al. 2000, Rao and Shivananda 2005, Puppala et al. 2006b, Al-Mukhtar et al. 2010, Dash and Hussain 2012, Talluri et al. 2013b, 2013a, Chakraborty and Nair 2020). Ca-based stabilizers such as lime are mixed with soil either in dry powder form (CaO) or in a hydrated form ($Ca(OH)_2$) to the target soil. Both the calcium oxides or hydroxides when mixed with water, dissolves to release free Ca^{+2} ions and OH^- ions in the system. The increase in Ca^{+2} concentrations in the soil matrix facilitates the mechanism of cation exchange (Figure 2.5). This cation exchange results in the replacement of monovalent cations from the clay layer interfaces by divalent calcium ions. The cation exchange capacity depends on the valency (Lyotropic series- larger cations replace smaller cations) and the concentrations of the ions involved in the process.

As a result of cation exchange, the clay layers undergo a reduction in the thickness of the DDL. Consequently, due to the reduction in the thickness of the DDL, the clay particles can form either edge to face bonds and result in flocculation of clay particles. The flocculation is often enhanced in the presence of high pH from the OH^- ions as well as a high electrolytic concentration in the pore fluid. A group of flocculated clay particles often bond through edges and agglomerate to form bigger sized particles. The flocculation-agglomeration reactions help to improve the soil behavior by forming granular aggregates and subsequently changing the gradation of the treated soil. The entire process of cation exchange, flocculation and agglomeration is collectively termed as

'modification' reactions. The immediate modification reaction helps to reduce the moisture affinity, reduces the soil plasticity, improves the workability and friability due to textural changes, helps to improve the internal friction and also helps to develop an immediate strength in the treated soil layers.

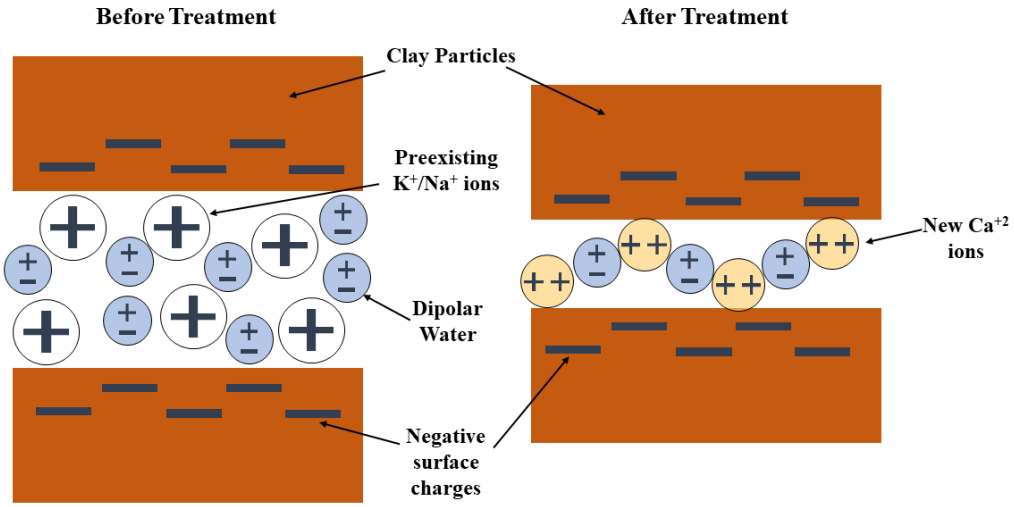

Figure 2.5 Cation exchange of monovalent cations (+1 valency) in between the clay layers by divalent calcium ions (+2 valency).

During long-term pozzolanic reactions, the OH^- ions from the dissolution of calcium oxides or hydroxides help to increase the soil pH. The increase in the pH of the soil results in the enhancement of the soil alkalinity that facilitates the dissolution of soil silicates and aluminates. A pH >10.5, helps in the dissolution of soil minerals to form Aluminum hydroxides and Silicic acid (H_4SiO_4) (Figure 2.6). Subsequently, the Silicic acids dissolve and reacts with the available Ca^{+2} from the Ca-based stabilizers to form Calcium-Silicate-Hydrates (C-S-H) compounds. Similarly, the Aluminum hydroxides

($Al(OH)_4^-$) from the dissolution of clay minerals reacts with the available Ca^{+2} ions to form Calcium-Aluminate-Hydrates (C-A-H) compounds.

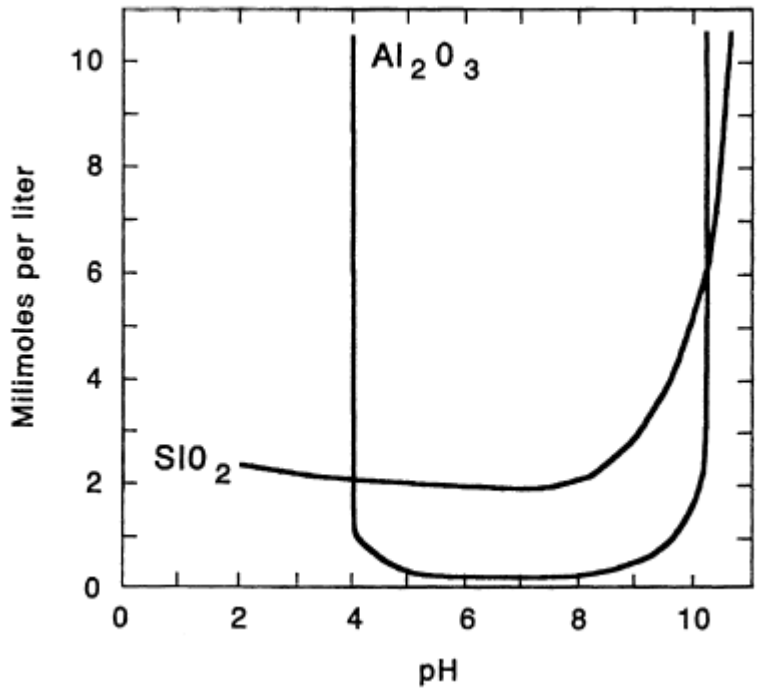

Figure 2.6 Effect of high pH on the dissolution of soil silicates and aluminates (Keller 1964)

The C-S-H and C-A-H are the major cementitious compounds that help to bind the soil matrix during the longer curing periods (Ho and Handy 1963, Diamond and Kinter 1966, Ormsby and Kinter 1973, Cabrera and Nwakanma 1979, Arabi and Wild 1986, Rajasekaran and Narasimha Rao 1997, Khattab et al. 2007). This helps to enhance the long-term strength, durability, and overall performance of the treated soil layers (Al-Rawas and Goosen 2006, Puppala 2016). However, the pozzolanic reactions are a generally slow process and require a considerable time before the target performance is

achieved. This results in a longer duration of traffic closure and consequently affects the project costs and sustainability goals (Das 2018, Das et al. 2019). The chemically treated soils retain a significant strength and undergo minimal strength loss after a prolonged curing period (Thompson 1970). Although lime-treated soils continue to gain strengths even after several years of treatment, substantial strength gain is generally observed during the first few months (Townsend and Donaghe 1976). However, considering the growing needs of pavements and transportation infrastructures to support the growing traffic, maintenance and rehabilitation of pavements using traditional stabilization techniques could often lead to longer delay periods due to slow chemical reactions.

Several research studies in the past have indicated that accelerated strength gain could often be obtained through changing the curing conditions (Rao and Shivananda 2005, Mooney and Toohey 2010, Al-Mukhtar et al. 2010, De Windt et al. 2014, Ali and Mohamed 2019). Research study by Little et al. (2010) have shown that 7 day curing at 40ºC is equivalent to 28 days of curing at standard room temperature of 23±2ºC. However, increasing the chemical reactions by increasing the temperature is generally not a feasible option for construction practice. Furthermore, several researchers have also reported that curing at higher temperature conditions is not conservative and can yield a considerable error in the predicted engineering properties (Mooney and Toohey 2010, Toohey et al. 2013). High-temperature curing affects the nature of the microstructures of the cementitious compounds formed and might not be the best representation of the actual field conditions (Townsend and Donaghe 1976). In a given problematic soil, the kinetics of the pozzolanic reaction between clay minerals and the stabilizer and formation of

cementitious compounds cannot be altered at room temperature conditions without increasing the stabilizer dosage or introducing an additive that can accelerate the pozzolanic reaction. Selecting a very high stabilizer dosage may be uneconomical and even counterproductive, as reported by previous research studies (Thompson 1970, Bell 1996, Kumar et al. 2007, Dash and Hussain 2012).

Additionally, the application of Ca-based stabilizers is a considerable cause of concern in the areas plagued with high-sulfate concentration. The presence of soluble sulfates results in the formation of a highly deleterious mineral- Ettringite, which causes major distress to the transportation infrastructures. The next section discusses the detrimental effects of the traditional treatment techniques in high-sulfate soils.

2.2.2 Sulfate-rich Soils

The application of Ca-based stabilizers such as lime or cement has been a cause of concern for soils with a major concentration of soluble sulfates in the form of anhydrite or gypsum (Figure 2.7). The sulfates ions from anhydrites or gypsum, reacts with the calcium ions to precipitate a deleterious reaction product known as Ettringite (Figure 2.8). The precipitation and stability of an ettringite crystal is dependent on several geochemical, environmental and engineering factors such as soil composition, pH, ion activity and ion migration, availability of moisture, and the construction methods to control the soil void structures (Petry and Little 1992, Little et al. 2005, Puppala et al. 2005, Nair and Little 2009, Chakraborty et al. 2020).

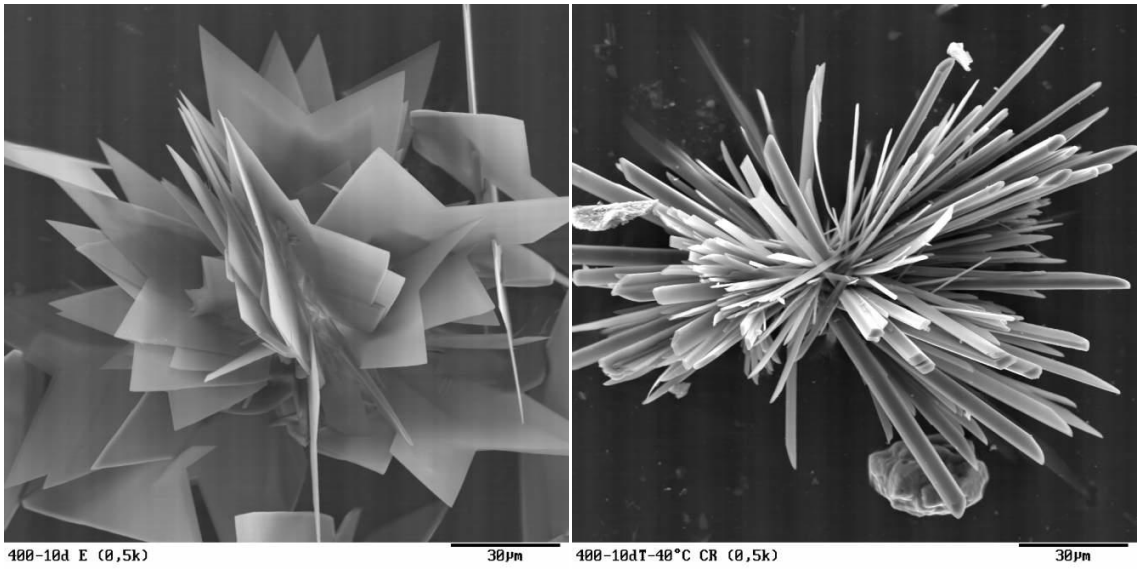

(a) (b)

Figure 2.7 SEM images of fully grown gypsum crystals (Kutschera et al. 2011)

Sulfate ions form a major constituent in the precipitation of ettringite and thaumasite mineral. The sulfate concentration in a given soil component is expressed as parts per million (ppm) or mg/kg (where 1 ppm ~ 1 mg/kg), or as a percentage of dry unit weight of the soil (where 10,000 ppm ~ 1 percent by mass). In this research study, the concentration of the soluble sulfates in different soils was measured using the colorimetric technique as outlined in Tex-145-E. Several research studies in the past have outlined the level of risk associated with different concentrations of sulfate levels in the soil. The studies have documented that sulfate concentration ranging from 1,000 ppm to 10,000 ppm have the potential to precipitate ettringite in the presence of Ca-based stabilizer treatments (Hunter 1988, Mitchell and Dermatas 1992, Puppala et al. 2002, Little et al. 2005).

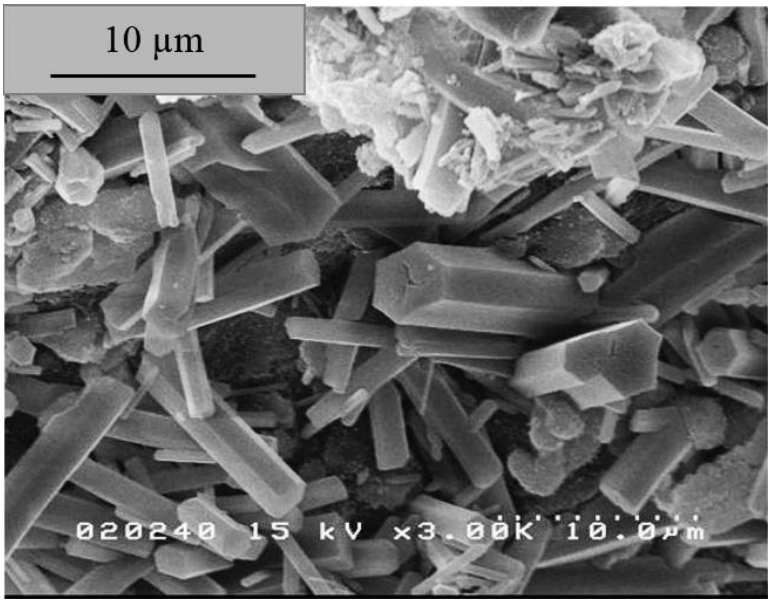

Figure 2.8 SEM images of precipitated ettringite (Jewell et al. 2015).

Table 2.1 from the NCHRP-145 synthesis manual on high-sulfate soils indicates the different levels of risk associated with sulfate concentrations. The TxDOT sulfate guidelines indicate a safe sulfate concentration of 3,000 ppm, beyond which there is moderate to high risk associated with Ca-based treatment. Research studies by Puppala et al. (2002) also indicated that sulfate concentrations as low as 0.1-0.2% have a significant effect on sulfate-related distress. The differences in the observed results could be partially attributed to the soil chemistry and the ease of the release of soil alumina, which is a key ingredient for ettringite formation (Petry and Little 1992). Therefore, identification of sulfate concentration in addition to standard test methods to determine the volumetric expansion of expansive soils is necessary to determine the long-term durability and permanency of chemical treatments.

Table 2.1 Risk associated with different levels of sulfate concentrations (Little and Nair 2009c)

Risk Involved	**Soluble Sulfate Concentrations**	
	Parts per million	**Percent dry weight**
Low Risk	Below 3,000 ppm.	Below 0.3%
Moderate Risk	Between 3,000 and 5,000 ppm	Between 0.3% and 0.5%
Moderate to High Risk	Between 5,000 and 8,000 ppm	Between 0.5% and 0.8%
High to Unacceptable Risk	Greater than 8,000 ppm	Greater than 0.8%
Unacceptable Risk	Greater than 10,000 ppm	Greater than 1.0%

The geochemical processes involved in the precipitation of ettringite was first explained by Hunter (1988) in the Las Vegas Stewart Avenue case study (Figure 2.9) and subsequently being studied and explained by several other researchers and is represented as follows:

$$6Ca^{2+} + 2Al(OH)_4^- + 4OH^- + 3(SO_4)^{2-} + 26H_2O \rightarrow Ca_6[Al(OH)_6]_2.(SO_4)_3.26H_2O$$

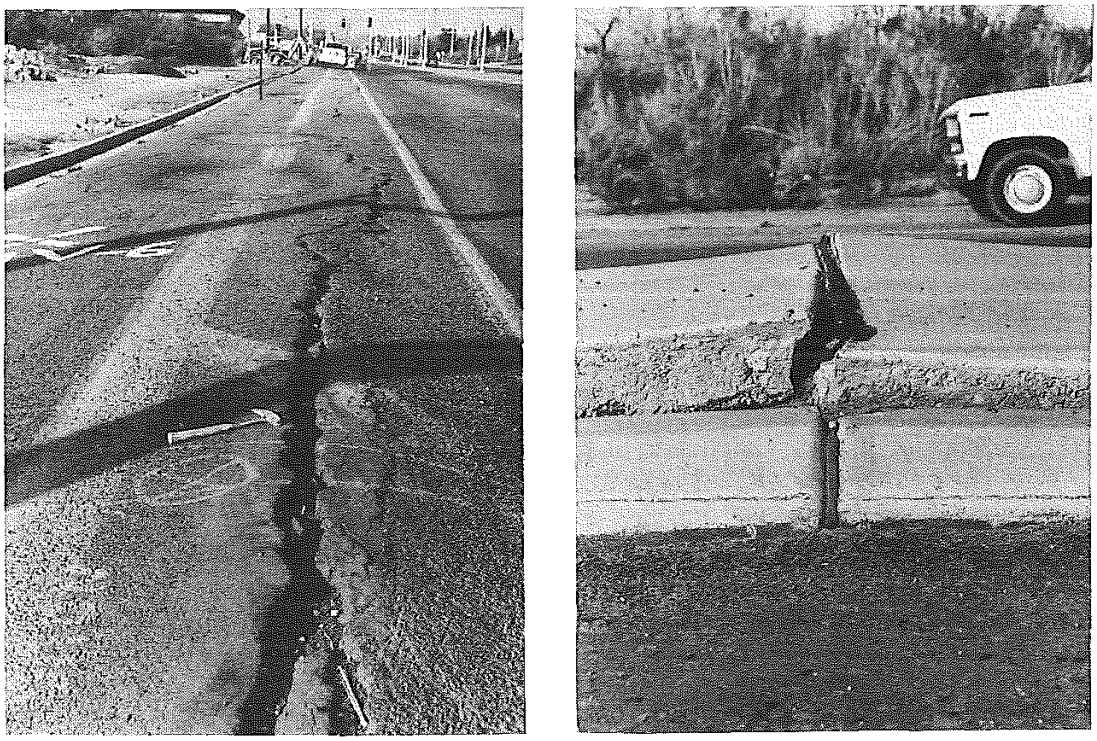

Figure 2.9 Stewart Avenue Failure, Los Angeles, California (Hunter 1988).

The ettringite is a calcium-alumino-sulfate hydrate mineral that precipitates under pH>10.5 in soils with significant sulfate concentrations (Petry and Little 1992, Kota et al. 1996). The application of a Ca-based stabilizer increases the soil alkalinity through dissociation of $Ca(OH)_2$ to release free OH^- ions. An increase in soil pH (>10.5) imparts dissolution of soil aluminates from oxyhydroxides and phyllosilicates (Myneni et al. 1998). Although multiple sulfate-bearing phases are formed during the geochemical process, the mono- and tri-sulfate phases are the most stable and significantly detrimental to the infrastructures (Lerch et al. 1925, Dermatas 1995).

The chemical process outlined by Hunter (1988) indicates that for the formation of 1 mole of ettringite, the necessary ingredients include 6 moles of Ca^{+2}, 3 moles of SO_4^{-2},

2 moles of Al^{+3}, and 32 moles of water. The Ca^{+2} is provided by the lime or cement additives, and the sulfates are provided by the dissolution of sulfate bearing soil or by migration of sulfate ions dissolved with water which diffuses into the soil matrix (Mitchell and Dermatas 1992, Dermatas 1995, Puppala et al. 2005, Ouhadi and Yong 2008, Nair and Little 2009, Little and Nair 2009c, Talluri et al. 2020, Chakraborty et al. 2020). Among different sulfate sources available for ettringite formation, gypsum is one of the primary sources commonly observed in the natural soil (Czerewko et al. 2003, Little and Nair 2009a). The solubility of the gypsum is about 2.58 g/L, and it can approximately provide around 1,400 ppm of sulfate ions per liter of water through dissolution (Burkart et al. 1999).

At low temperatures (<15° C) and due to intensive carbonation, ettringite crystals often undergo isostructural substitution to form different phases of alumino-sulfate compound known as thaumasite ($Ca_6[Si(OH)_6]_2. (CO_3)_2 .(SO_4)_2. 24H_2O$) (Hunter 1988, Bensted 2000). The thaumasite minerals derive the silicon from the decomposition of the C-S-H phases formed during the pozzolanic reactions (Crammond 2003, Köhler et al. 2006). Although both ettringite and thaumasite have detrimental effects on soil stabilization. Thaumasite is known to have a lesser expansive nature as compared to tri-sulfate phase ettringite (Little and Nair 2009a).

The ettringite crystal is a needle-shaped tubular structure with approximate lengths up to 200 μm, where the aluminum octahedrons and the calcium polyhedrons form the part of the columns running parallel to the *c*-axis in the tube (Moore and Taylor 1970; Dermatas 1995; Moon et al 2007). The trigonal prisms of calcium polyhedrons consist of

water and hydroxyl ions at four apices. The tubular structure is formed by combining three alumina octahedrons to a single calcium polyhedron which repeats to form the $\{Ca_6[Al(OH)_6]_2.\ 24H_2O\}^{+6}$ structure (Figure 2.10). The calcium and aluminum polyhedrons are bounded by shared hydroxy ions and form a continuous chain along the c-axis. The water molecules complete the co-ordination polyhedron.

The SO_4^{-3} ions occupy the intermediate channels and bind the columns through H-bond with calcium-coordinated water molecules (Puppala et al. 2005, Little and Nair 2009b). Water molecules form a significant part of the structure of the ettringite crystal and contribute to the stability of the crystal. Exchangeable water molecules could be accommodated in the crystal structure by calcium and sulfate ions which contributes to the stability of the crystals. Furthermore, the channel structures along the c-axis have the capability to hold additional water molecules when sufficient water is available from an external source (Mehta 1973). This is one of the primary reasons for the anisotropic swelling behavior of the ettringite mineral and the subsequent development of the swelling pressure on the soil and other lightweight structures.

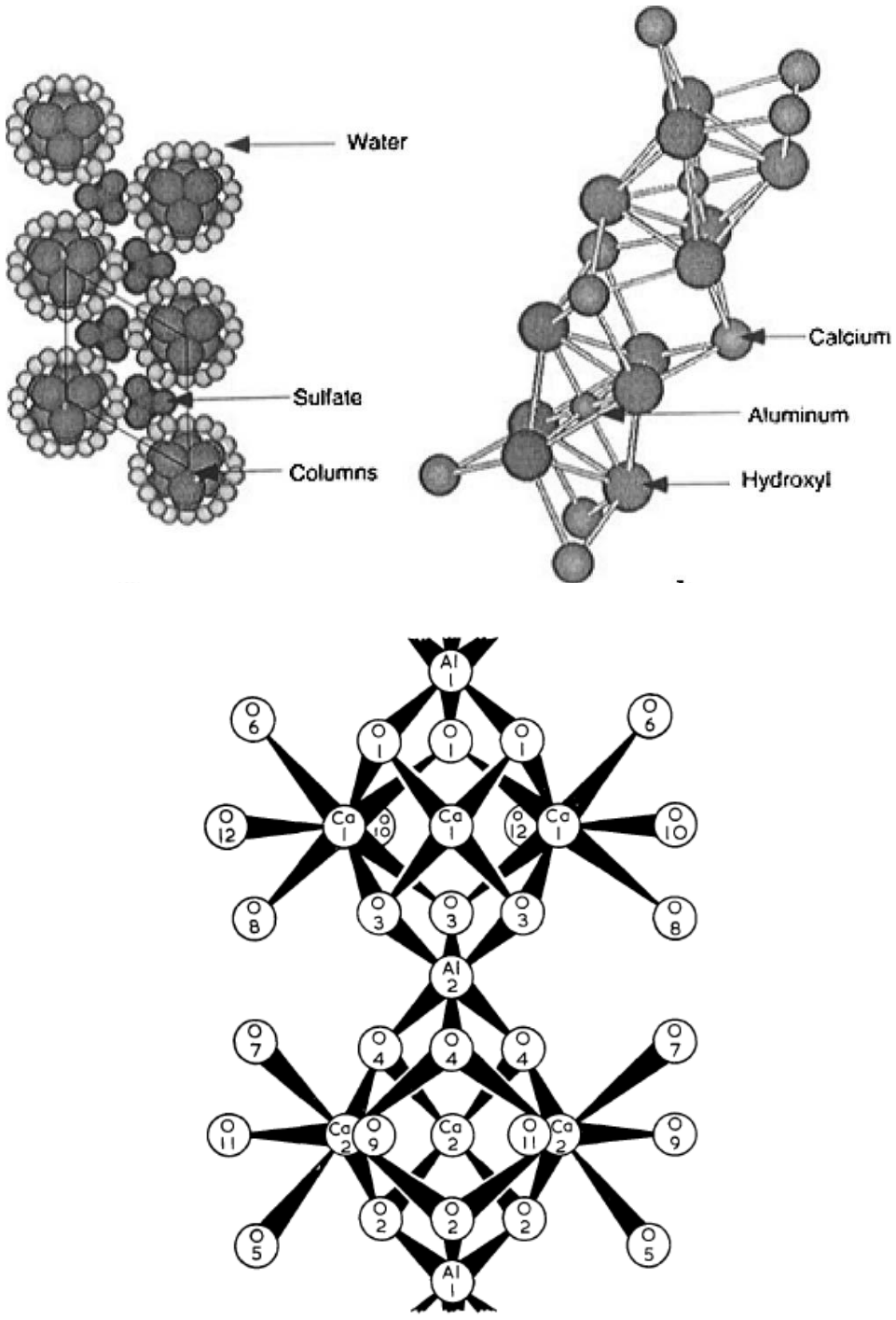

Figure 2.10 Structure of an ettringite crystal (Moore and Taylor 1968, Little and Nair 2009a).

Research studies in the past have indicated two possible mechanisms for the formation and precipitation of the ettringite crystals (Skalny et al. 2001). The first theory is based on topochemical reactions, where the growth of ettringite occurs at the interface of soil solids and solution (Odler and Gasser 1988, Nair and Little 2009). Topochemical reactions are favored when the rate of dissolution of the reactants is slower than the rate of formation of the crystals. This occurs when a significant contribution of calcium and sulfate ions are present in the soil matrix; however, the aluminum ions fail to dissolve sufficiently and migrate far away from the source. As a result, the ettringite crystals precipitate near the source of the aluminum bearing phases in this precipitation mechanism (Min and Mingshu 1994). The second mechanism involves random precipitation of the ettringite crystals in a liquid state when the solution attains a supersaturation phase. This occurs when the concentration of lime in any particular location in the soil matrix is low, and subsequently, the aluminum ions have a favorable condition to dissolve and migrate in the solution and form supersaturated solutions (Min and Mingshu 1994).

The expansion due to ettringite crystal could be attributed to either topochemical formation and anisotropic crystal growth or through absorption of water molecules and subsequent expansion of the crystal (Mehta 1973, Ogawa and Roy 1982, Puppala et al. 2005, Chakraborty et al. 2020, Biswas et al. 2021b, Jang et al. 2022). Due to the presence of negative surface charges, high surface area, and loosely bonded crystal structure of the ettringite, the crystal undergoes expansion due to inter-particular repulsion from the absorption of water molecules (Mehta 1973, Little et al. 2010). The mechanism of expansion through water absorption is similar to the electrostatic attraction of polar water

molecules. Consequently, water plays a significant role that determining the intensity of the expansion of the ettringite crystals, and both the mechanism partially attribute to the expansion and growth of the crystals (Mehta 1973, Ogawa and Roy 1982, Min and Mingshu 1994). Overall, the external source of water plays a significant role in causing a deleterious expansion of the stabilized soils.

The stoichiometric calculations to determine the changes in the molar volume of the ettringite crystal due to water absorption indicates that a fully hydrated ettringite crystal has a molar volume of 1.37 times higher than a non-hydrated reactant forming the crystals (Nair and Little 2009, Chakraborty et al. 2020). Furthermore, some studies have also estimated the volumetric expansion due to ettringite could reach up to 250% in treated soil layers due to their hydration and growth when exposed to external water sources (Puppala and Cerato 2009, Zhang et al. 2015).

Overall, the presence of soluble sulfates and the source of moisture affect the longevity of the lime-stabilized matrix. Therefore, research studies are extensively focused on using several alternatives, including the application of co-additives to mitigate the problems associated with ettringite-induced failures. The next sections discuss the use of different co-additives to improve the traditional stabilization techniques.

2.2.3 Application of Co-additives to Modify Reaction Kinetics

Several co-additives such as Ground Granulated Blast Furnace Slag (GGBFS), Class-C or Class-F Fly Ash (FA), Cement Kiln Dusts (CKD), Lime Kiln Dusts (LKD), Rice Husk Dusts (RHA), bagasse fibers, Silica Fumes (SF), and Nano-materials has been blended with lime to enhance the performance of the treated soil matrix (Misra 1998, Wild et al.

1999, Çokça 2001, Hilbig and Buchwald 2006, Si and Herrera 2007, Peethamparan et al. 2008a, Chen et al. 2009, Kalkan 2011, Kumar and Gupta 2016, Behnood 2018). These co-additives are the source of additional pozzolanic phases of silicates and aluminates, which react in the presence of Ca-based stabilizers to form additional cementitious compounds (Çokça 2001, Puppala et al. 2003, Behnood 2018). Discussions of some traditional alumina and silica-based pozzolanic compounds are presented below:

2.2.3.1 Ground Granulated Blast Furnace Slags

Ground Granulated Blast Furnace Slag is a commonly used alumino-silicate material having both amorphous and crystalline phases of silica compounds (Ozyildirim 1990, Tasong et al. 1999, Puppala et al. 2003, Puppala 2016). The GGBFS is a byproduct of an iron blast furnace formed from the siliceous components of iron ore and the limestone flux used in the process of smelting the iron (Sherwood 1993). Past studies have shown that the application of GGBFS as a co-additive with traditional stabilizer resulted in the improvement of several engineering properties including, increase in the unconfined strength and shear strength properties, reduction in soil plasticity, and swell-shrink potentials in a treated soil (Nidzam and Kinuthia 2010, Yi et al. 2014, Vakili et al. 2016, Keramatikerman et al. 2016).

Furthermore, the application of GGBFS has the potential to improve the hydraulic properties of the treated soil by reducing soil permeability (Ozyildirim 1990). The presence of silica and alumina phases in the GGBFS affects the reaction kinetics through accelerating to precipitation of C-S-H and C-A-H phases in the treated soil (James et al. 2008, Keramatikerman et al. 2016). In the case of problematic soils having a major

concentration of sulfates, the application of GGBFS with lime has the potential to reduce the precipitation of ettringite and subsequent problems associated with sulfate-induced heaving (Wild et al. 1999, Puppala et al. 2003, Puppala 2021).

2.2.3.2 Fly Ash

Fly Ash (FA) materials are the byproducts of coal combustion in power generation plants (Hoyos et al. 2004, Puppala et al. 2008a, Phetchuay et al. 2016). The principle components include the amorphous and crystalline phases of silica oxides, aluminum oxides, and calcium oxide. The two common classes of FA are Class-C and Class-F fly ash (McCarthy et al. 1984, Kolias et al. 2005, Horpibulsuk et al. 2009, 2011). The Class-C FA is traditionally produced from the combustion of sub-bituminous coals and is rich in both pozzolanic phases as well oxides of Calcium (CaO). As a result, it has both pozzolanic as well as self-cementing characteristics. The Class-F FA has a significantly low percentage of calcium oxides due to its production from anthracite or bituminous coal. Consequently. Class-F FA is used in combination with certain cementitious compounds, such as lime or cement, to enhance the pozzolanic reactions in the treated soils.

Majority of the FA related studies have observed that the application of FA with lime or cement treatment has significantly improved the strength, stiffness, and hydraulic properties of the treated soils (McCarthy et al. 1984, Puppala et al. 2003, Horpibulsuk et al. 2012, Saride et al. 2013, Saride and Dutta 2016). However, some past researchers have documented that even though FA enhance long-term engineering properties, due to slow reaction rates, additional sources of alkali activators are needed to accelerate the hydration

reactions (Wild et al. 1999, Bakharev et al. 1999, Kukko 2000, Brough and Atkinson 2002).

2.2.3.3 Cement Kiln Dust (CKD)

Cement Kiln Dusts are rich in oxides of calcium (CaO) and certain alkali-bearing byproducts generated in the cement industry (Baghdadi and Rahman 1990, Baghdadi et al. 1995, Miller and Azad 2000, Peethamparan et al. 2008a). The fineness of the materials, high alkali concentration, and significant amount of free lime content make the CKDs an effective stabilizing agent. The application of CKDs as co-additives has resulted in significant improvement in the engineering properties for both immediate (7 days) and longer curing periods (Sreekrishnavilasam et al. 2007, Peethamparan and Olek 2008, Peethamparan et al. 2008b). However, the CKDs have been found to be effective in stabilizing low-PI soils as compared to the high-PI clays (Miller and Azad 2000). Furthermore, the durability of CKD-treated soil has also been a cause of concern, as reported in previous study by USACE (Kampala et al. 2014).

2.2.3.4 Lime Kiln Dust (LKD)

Lime Kiln Dusts are the byproducts of the quick lime manufacturing process and have a significant concentration of reactive calcium (Kakrasul et al. 2017, Behnood 2018). The availability of free lime in the LKDs helps to increase its reactivity and makes it suitable for stabilizing high plastic clays (Chesner et al. 2002). The application of LKDs have improved several engineering properties such as soil plasticity, swell potential, strength and durability properties in treated soil matrix (Chen et al. 2009, Jung et al. 2011, Kakrasul et al. 2017). The application of LKDs has been associated with dusting and handling

problems because of its fine powdery nature and reduced cementitious potential due to premature hydration of the available free lime (Behnood 2018).

Although some of the studies indicate potential benefits of adding these co-additives for modifying the kinetics in lime-treated soil, researchers are continuously striving to identify novel co-additives that could be used with lime for enhancing the reaction rate for chemically treated soils. In the following paragraphs, research studies related to two new novel silica-based co-additives are provided, which have the potential to be used as an additional silicate source with traditional treatment techniques in high-plastic clays.

2.2.3.5 Quarry Dust

The quarry dusts are primarily produced from the crushing of the boulders and rocks in a rubble crusher unit (Figure 2.11) (McKennon et al. 1994, Chesner et al. 2002, Soosan et al. 2005, Sridharan et al. 2006, Puppala et al. 2008b, Kufre Etim et al. 2021, Amulya et al. 2021). Several million tons of these quarry byproducts are generated in the United States, which has an excellent potential to be used for different engineering purposes (Chesner et al. 2002, Lamb 2005, Ingalkar and Harle 2017, Biswas et al. 2021b). The physical and chemical composition of these quarry dust is significantly dependent on the source of production or parent rock. Although the mineralogical composition of the quarry fines is relatively uniform at any particular quarry location, some studies suggest that the quarry fines from different sources have a marginal difference in compaction and gradation characteristics (Wood and Marek 1993, Soosan et al. 2005).

Figure 2.11 Quarry dust generation from rock crushing (https://www.generatorsource.com/ n.d.).

The quarry dust is composed of crystalline silica phases and has a relatively large specific surface area owing to its fine powdery nature (Soosan et al. 2005, Chakraborty et al. 2020). This enhances the cementitious reactions when used with calcium-based cementing compounds. The presence of crystalline phases in the quarry fines also increases the shear strength properties when used to stabilize the geomaterials (Okamura and Ouchi 1998). The angular grains of the crushed fines help to develop a strong soil matrix which improves the strength and also reduces the plasticity and swell characteristics in the treated soil (Ingles and Metcalf 1972, Chakraborty et al. 2020, Biswas et al. 2021a, Jang et al. 2021). Figure 2.12 shows a Scanning Electron Microscope

image of quarry fines showing predominant crystalline components (framework SiO_2). However, the crystalline silica fines are often considered a health hazard and cause significant geoenvironmental problems when disposed of in landfills (Bahoria et al. 2018).

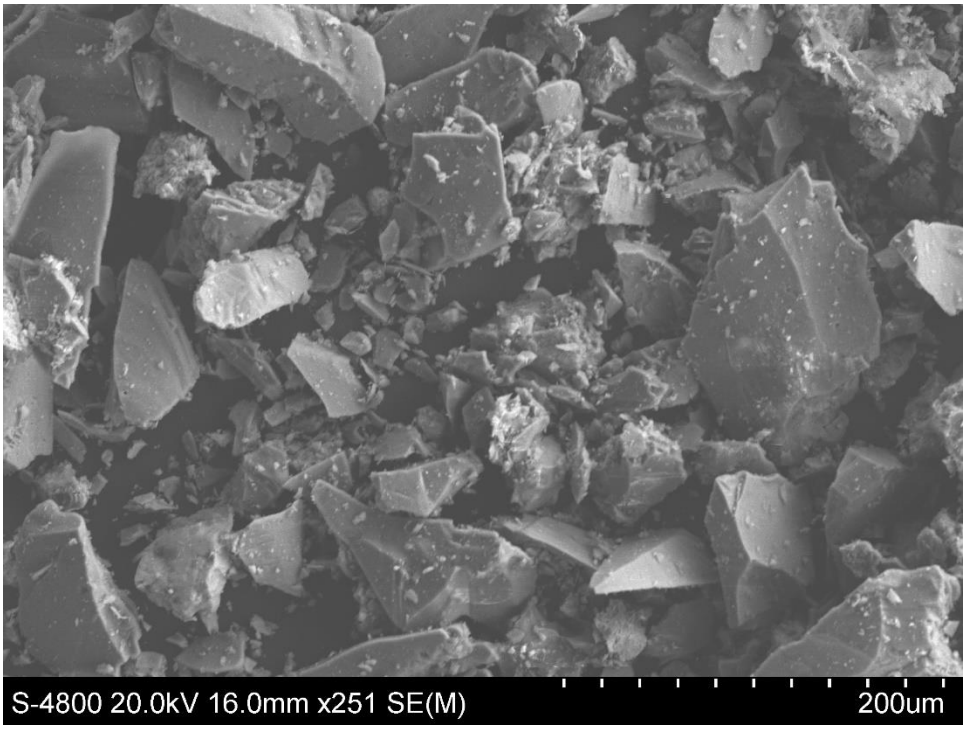

Figure 2.12 SEM image of quarry fines (crystalline silica) (Chakraborty et al. 2020).

It is generally assumed, based on some studies, that the amorphous phases of silica co-additives are more reactive than the crystalline phases (Sivapullaiah and Moghal 2011, Bahmani et al. 2014, Consoli et al. 2019). However, the crystalline co-additives at an elevated temperature and longer curing periods, with high lime dosages, have the potential to develop significant cementitious binding phases (C-S-H) (Dash and Hussain 2012, Dhar and Hussain 2019).

2.2.3.6 Nano-materials

In the past decade, there has been a major focus on the use of nanomaterials to nanotechnologies for the enhancement of the properties of cementitious reaction products (Niroumand et al. 2013, Pham and Nguyen 2014, Correia et al. 2015, Correia and Rasteiro 2016, Changizi and Haddad 2017, Abbasi et al. 2018, Kehew 2021, Ciardi et al. 2021). The application of nano-materials as a co-additive with traditional treatment techniques has primarily been motivated by their novel material properties such as high specific surface area, high surface energy, and significant cation exchange capacity. Different types of nano-materials have been investigated in the past to identify their efficacy in improving cementitious reactions. Certain major nano-materials include, nano-TiO_2, nano-Al_2O_3, nano-carbon tubes, and nano-SiO_2 (Figure 2.13). The application of amorphous nano-silica to cement composites improves the microstructure by developing a denser matrix by filling pores and enhancing the rate of the pozzolanic reactions (Sobolev et al. 2009, Stefanidou and Papayianni 2012, Givi et al. 2013).

The application of nano-silica has also resulted in significant improvements of several engineering properties, such as reducing volumetric strains and improving the compaction characteristics and compressive strength of the treated soils (Taha and Taha 2012, Niroumand et al. 2013, Bahmani et al. 2014, 2016, Kalhor et al. 2019). The application of nano-particles also impacts the hydraulic properties of the treated soils by substantially reducing the permeability in high-plastic clays (Changizi and Haddad 2017). Therefore, most of the studies concluded that the nano-particles when added as a co-admixture with cement or lime has improved the engineering properties. However, the

majority of the studies are focused on the application of nano-silica on coarse-grained particles. Additionally, limited literatures have indicated the effects of moisture intrusion and durability of the treated soils.

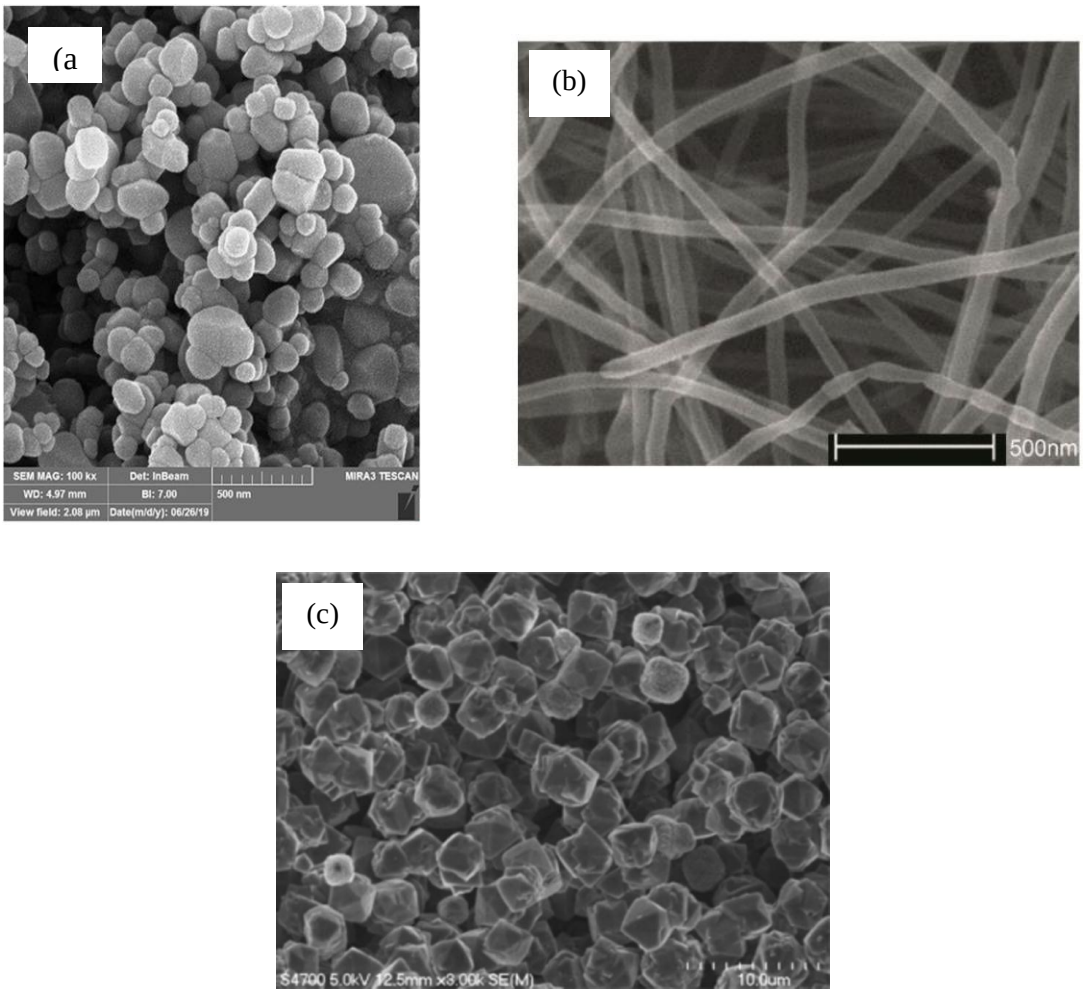

Figure 2.13 SEM images of a) Nano- TiO_2 (Gohari et al. 2020) b) Nano-carbon tubes (Yuan and Chen 2016) c) Nano-silica (Shafabakhsh and Ani 2015).

The application of one or more of the aluminate or silicate phases has the potential to improve the engineering properties of chemically treated soils. However, the long-term serviceability and durability performance of these pozzolanic compounds should be

properly established before recommending the treatment techniques for transportation practitioners. The next section discusses the effects of long-term durability problems associated with traditional chemical treatment techniques.

2.2.4 Durability of Chemically Treated Soils

Extensive studies have been undertaken in the past to better understand the behavior of lime stabilized or lime-fly ash stabilized expansive soils (Sherwood 1993, Little 1995, Bell 1996, Khattab et al. 2007, Sivapullaiah and Moghal 2011, Puppala et al. 2013, Puppala and Pedarla 2017, Chakraborty and Nair 2018). Similarly, several research studies have been performed on different cement-treated soils, including granular materials, silts, and clays (Mitchell 1981, Tatsuoka et al. 1997, O'Rourke et al. 1998, Hoyos et al. 2004, Saride et al. 2013, Puppala and Pedarla 2017). Strength and durability are considered as the two key parameters to assess the efficacy of a stabilizer mix design. Although stabilization improves engineering properties of soils under normal conditions, water intrusion, leaching, and other environmental conditions like freeze-thaw and wet-dry cycles can influence the long-term performance and durability of stabilized layers (Little and Nair 2009a, Puppala 2016, Puppala et al. 2017a). Dempsey and Thompson (1968) defined durability as "the ability of materials to retain their stability, integrity and maintain an adequate amount of long-term residual strength so as to provide sufficient resistance to climatic conditions."

Recent researches have also indicated that the durability issues are often a concern due to degradation and reversal of cementitious compounds due to carbonation and removal of stabilizers by moisture intrusion and leaching (McCallister and Petry 1992,

Little and Yusuf 2001, Christopher et al. 2006, Nakarai and Yoshida 2015, Puppala 2016, Puppala and Pedarla 2017). Some studies indicated preferential dissolution of ingredient components (Ca or Si) from the cementitious C-S-H phases, in the presence of water (Harris et al. 2002, Baston et al. 2012). After a few years of the chemical treatment, some field studies have also reported: "problems with disappearing stabilizers" (Syed and Scullion 1998, Little and Yusuf 2001, Harris et al. 2009).

The durability of lime-treated soil is affected by different factors such as ingress of moisture, exposure to freeze-thaw and wet-dry cycles, carbonation and leaching of lime, and presence of organic compounds and soluble sulfates (Syed and Scullion 1998, Christopher et al. 2006, Aldaood et al. 2015). Majority of the durability-related issues in chemically treated layers are attributed to moisture intrusion. Water can infiltrate into the stabilized layers by different mechanisms, such as percolation of water through cracks on the road surface, moisture ingress through construction joints, rainwater infiltration through the shoulder edges, and upward movement of water by capillary action (Reid et al. 2006). These phenomena increase the degree of saturation and water content of the stabilized soil layer.

Soaking increases the degree of saturation up to 90 percent in stabilized soil layers (Dumbleton 1962, Thompson 1970). Although optimum moisture conditions are required to support the pozzolanic reactions, the intrusion of water from external sources can weaken the stabilized layers (Little and Yusuf 2001, Little and Nair 2009a, Khoury et al. 2013). The extent of strength loss depends on the time of water intrusion and the extent of the pozzolanic reaction. Strength loss of up to 40% has been observed when moisture

intrusion occurred in the early stages of curing (Dempsey and Thompson 1968, Thompson 1968, Little 1996, Little and Nair 2009a). However, the extent of strength reduction is significantly lower after prolonged curing (Thompson 1970, Little and Nair 2009a). The degree of strength loss in a stabilized layer is dependent on the nature of the soil, the type of clay minerals present, and the stabilizer type and dosage used for treatment (Kennedy et al. 1987, McCallister and Petry 1992, Chittoori et al. 2013a).

The durability of the stabilized layers against harsh environmental conditions primarily depends on the lime treatment dosage (McCallister 1990, McCallister and Petry 1992, Chakraborty and Nair 2020). Optimum lime content (or more) is required to satisfy the initial soil-lime reaction and have excess available lime to sustain time-dependent strength gain by pozzolanic reaction (Little 1995, Little and Nair 2009a). Insufficient lime dosages have resulted in significant deterioration of stabilized layers after leaching (McCallister 1990). Leaching of a treated soil generally takes due to the percolation of groundwater through the pores of the soil. Therefore, a more permeable soil will have a greater potential for leaching (McCallister 1990).

Leaching of calcium hydroxide from the treated layers might result in the breakdown of the soil-stabilizer system, and few studies reported leaching of stabilizers (or Ca^{2+}) to be one of the primary reasons for strength loss (McCallister 1990, Khattab *et al.* 2007, Chittoori *et al.* 2013, Aldaood *et al.* 2015). The degree of damage after leaching depends on the time duration and quantity of water percolating through the stabilized layers (Le Runigo et al. 2011).

McCallister (1990) and McAllister and Petry (1992) performed extensive leaching investigations on lime-treated soils. Lime was mixed to the soil at two different percentages. The optimum lime content determined as per Eades and Grim pH test method was 3-4%. The optimum lime was added for modification function instead of stabilization. For stabilization, a lime percentage of 7-8% was selected. The experimental results indicated that leaching had a detrimental effect on the engineering properties of post-leached specimens. As sufficient lime was not available to counteract the effects of leaching, a reduction in compressive strength was observed in the post-leached specimens.

The researchers assumed that the detrimental effect of leaching could be minimized if sufficient pozzolanic reactions occur prior to moisture intrusion. This would improve interparticle bonding and reduce permeability. With a longer curing period, it would partially minimize the loss of calcium due to leaching. The researchers also observed a much slower dissolution of the cementitious compounds formed during pozzolanic reactions. It was stated that the amount of lime obtained by the Eades and Grim test is not suitable for long-term stabilization, and a lime percentage of at least 1% above optimum is necessary for long-term stabilization reaction. Such an addition is necessary to maintain high pH, enable pozzolanic reactions, and reduce the detrimental effect of leaching.

2.3 Summary and Research Gaps

This chapter discussed existing literature related to expansive soils, chemical stabilization using Ca-based stabilizers, use of different co-additives, and durability of the treatment techniques. The present studies helped to understand the mechanism of chemical treatment and the existing efforts by the geotechnical fraternity to persistently improve the

performance of chemically treated soils. However, after the exhaustive review of the studies, certain research gaps in the existing literatures were observed as listed below:

- No major studies have been performed using silica-based co-additives (quarry fines or crystalline silica and nano-silica) with lime to treat expansive soils.
- Limited studies are available on the effects of silica-based treatment on the reaction kinetics of the high-plastic clays.
- No major studies have been performed on the application of silica-based co-additives to mitigate the problems associated with high-sulfate soils.
- The present studies using the silica-based co-additives are mostly focused on engineering properties such as strength, swell-shrink properties or Atterberg's limits. However, current knowledge to understand the effects of the silica-based co-additives on the resilient modulus properties of the treated soil matrix is limited.
- Limited research was performed on the durability aspects and long-term performance of the treated soil layers when subjected to moisture conditioning.

The next chapters focus on addressing some of these shortcomings using different engineering, chemical, and microstructural tests. The present work is expected to address some of the shortcomings of the existing literatures and consequently provide a comprehensive understanding of these novel treatment techniques.

3. MATERIALS AND TESTING METHODS

3.1 Introduction

This chapter provides an overview of the different materials and testing methodologies used in the research study. The behavior of a treated soil matrix significantly depends on the type of soil, type of stabilizer, and co-additives used for soil treatment. In particular, the macrostructural, chemical, and mineralogical composition of the materials involved in the process are essential components of chemical stabilization. Engineering characterization of the soils will help us to identify if the soil is problematic and needs chemical treatment. The engineering properties of the primary stabilizer and the co-additives are also necessary to decide the suitability of treatment. The mineralogical and microstructural studies on the geomaterials, the primary stabilizer, and the co-additives would provide an exhaustive understanding of the physical and chemical processes involved during the course of treatment.

The chapter provides detailed information on the two different soil types used in this research study having different concentrations of soluble sulfates. The basic soil characterization provides information on the problematic nature of the soil and required stabilizer properties. Subsequently, the properties of the primary Ca-based stabilizer and the two different silica-based co-additives are discussed. After the characterization of the materials, the chapter provides information on different chemical, engineering, and microstructural tests performed during the course of this research program. The next section discusses the geomaterials, chemical stabilizer, and silica-based co-additives used for this research study.

3.2 Materials

3.2.1 Geomaterials

The experimental study was conducted on two types of problematic soils collected from the state of Texas. Soil-1 was collected from a road construction site at Interstate-20 near Grand Prairie in Dallas-Fort Worth metropolitan area. Soil-2 was collected from another roadway construction site near southbound U.S. 75 Frontage Road between Randell Lake Road and State Highway 91 in Denison, Texas. Basic soil characterization studies, including specific gravity, grain-size distribution, Atterberg's limits, moisture-density relationship, and vertical free swell tests were performed in accordance with respective ASTM standards (Figure 3.1 and Table 3.1). The linear bar shrinkage test and the total sulfate content test conducted in accordance with respective TxDOT standards, are also shown in Table 3.1 below.

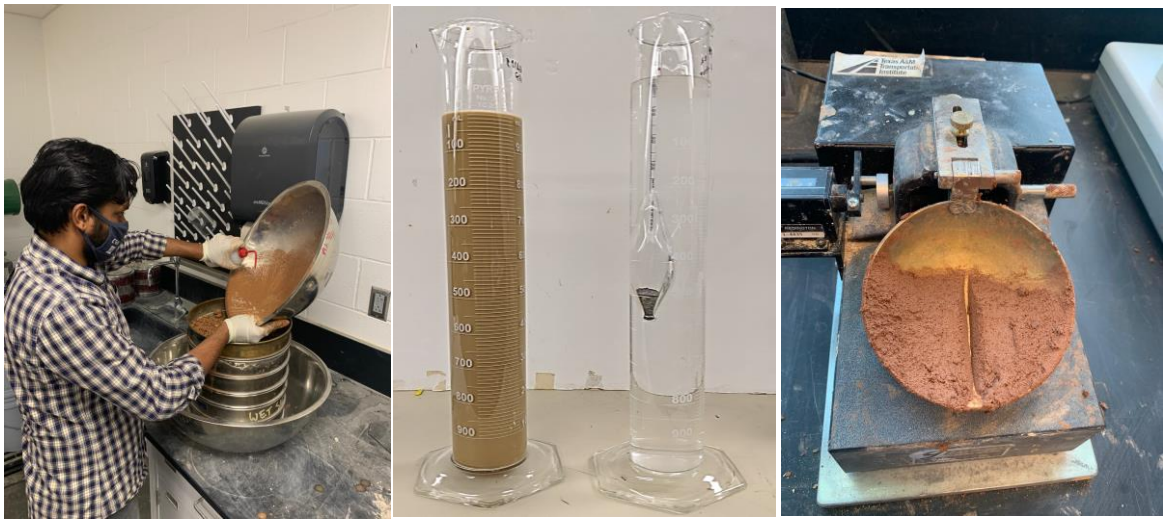

(a) (b) (c)

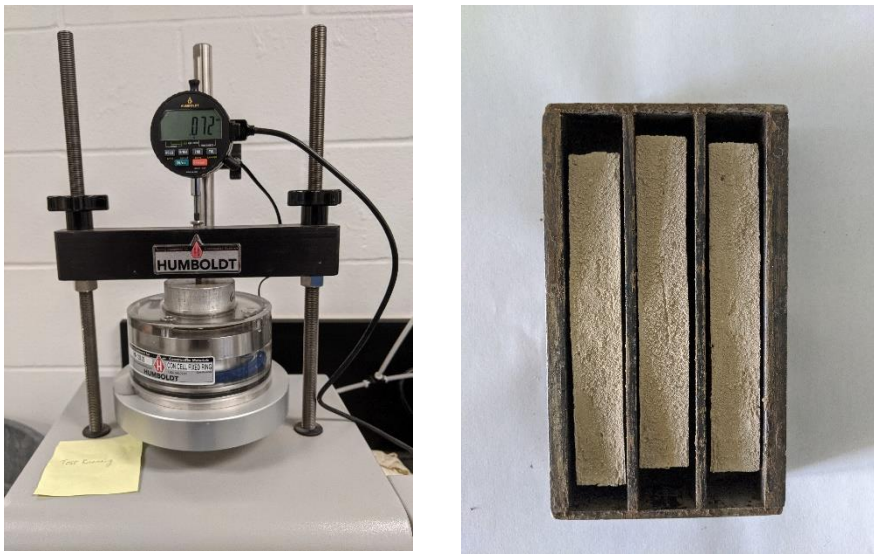

(d) (e)

Figure 3.1 Laboratory tests for soil characterization a) Grain-size distribution b) Specific gravity c) Atterberg's Limit d) Vertical free swell, and e) Linear shrinkage

The grain-size distribution of both soils indicates significant fines content (>50%), i.e., the percent amount passing #200 U.S. sieve (0.075 mm) (Figure 3.2). The maximum dry density (MDD) and optimum moisture contents (OMC) of individual soils are shown in Figure 3.3. The soil collected from Grand Prairie (Soil-1), Texas was classified as high-sulfate (HS) and high-plastic (CH) soil due to a sulfate concentration of more than 14,000 ppm as well as a high liquid limit and plasticity index based on USCS soil classification. Similarly, the soil from Paris District in Texas, USA (Soil-2) was classified as low-sulfate (LS) and high-plastic (CH) clay due to a sulfate concentration of 400 ppm. The soils were classified as high-sulfate or low-sulfate based on the TxDOT guidelines for Soil Stabilizations (Item 260). Overall, the aforementioned properties indicate that the soils are problematic in nature and should be ideal candidates for the research study. Furthermore, the high-PI value and fines content is also indicative that among different Ca-based stabilizers, lime could be considered suitable for treating these soils (Figure 2.4). The details of different basic material characterizations are provided in Table 3.1 below.

Table 3.1 Basic material characterization.

	Soil-1	Soil-2
Specific gravity (ASTM D698)	2.71	2.72
Liquid limit (LL) (ASTM D4318)	66.0	60.0
Plastic limit (PL) (ASTM D4318)	29.5	27.0
Plasticity index (PI) (ASTM D4318)	36.5	33.0
Silt (%) (ASTM D7928)	28.8	40.0
Clay (%) (ASTM D7928)	70.2	51.0
USCS soil classification (ASTM D2487)	CH	CH
Maximum dry density (MDD) (kN/m^3) (ASTM D698)	15.5	16.3
Optimum moisture content (OMC) (%) (ASTM D698)	20	20.5
Sulfate Content (ppm) (Tex-145-E of TxDOT Methods)	14,000	400
Vertical free swell strain (%) (ASTM D4546)	23	16
Linear Bar Shrinkage (%) (Tex-107-E)	16.5	14

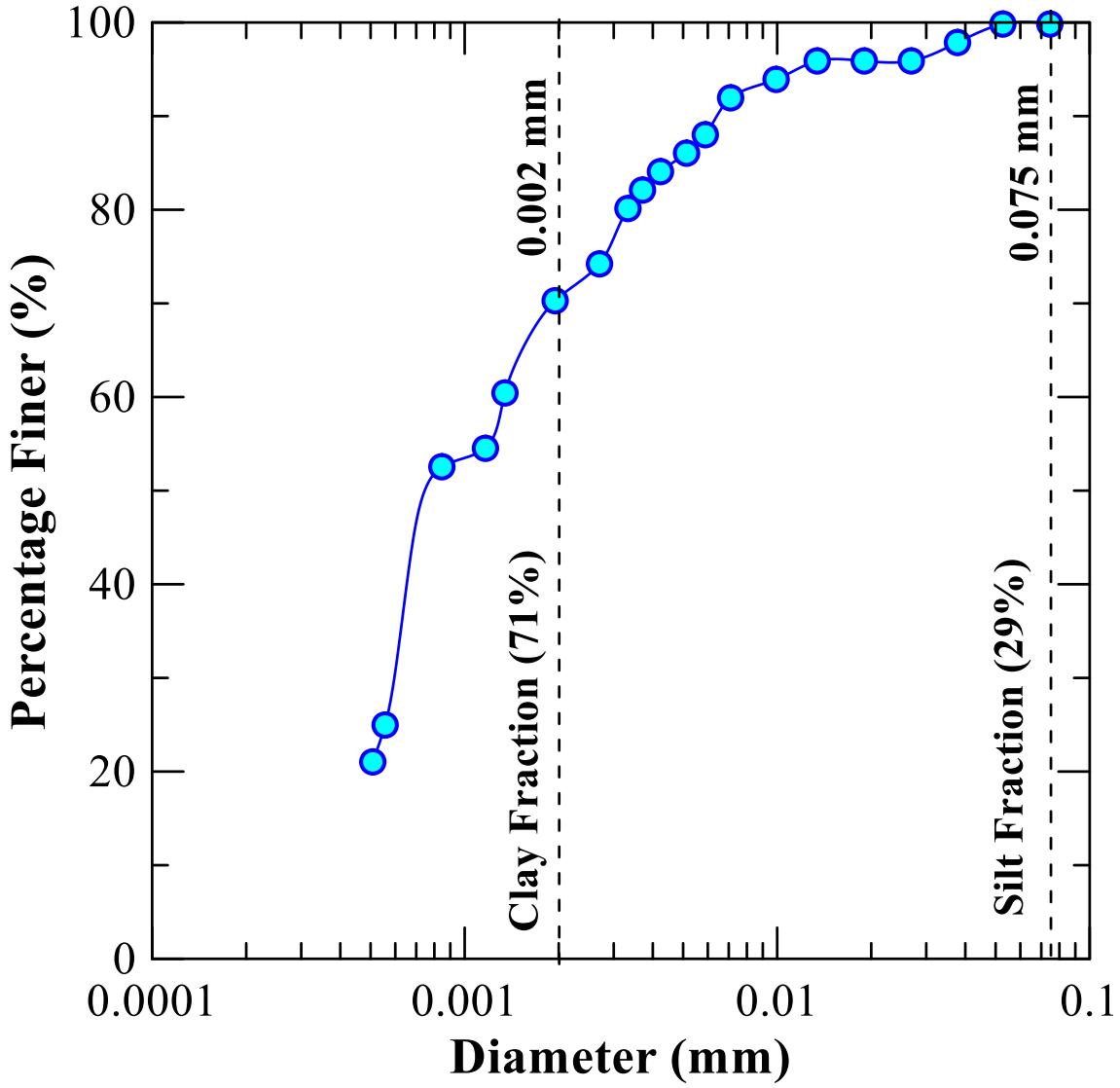
100
80
60
40
20
0
Percentage Finer (%)
0.0001
0.001
0.01
0.1
Diameter (mm)
0.002 mm
0.075 mm
Clay Fraction (71%)
Silt Fraction (29%)

(a)

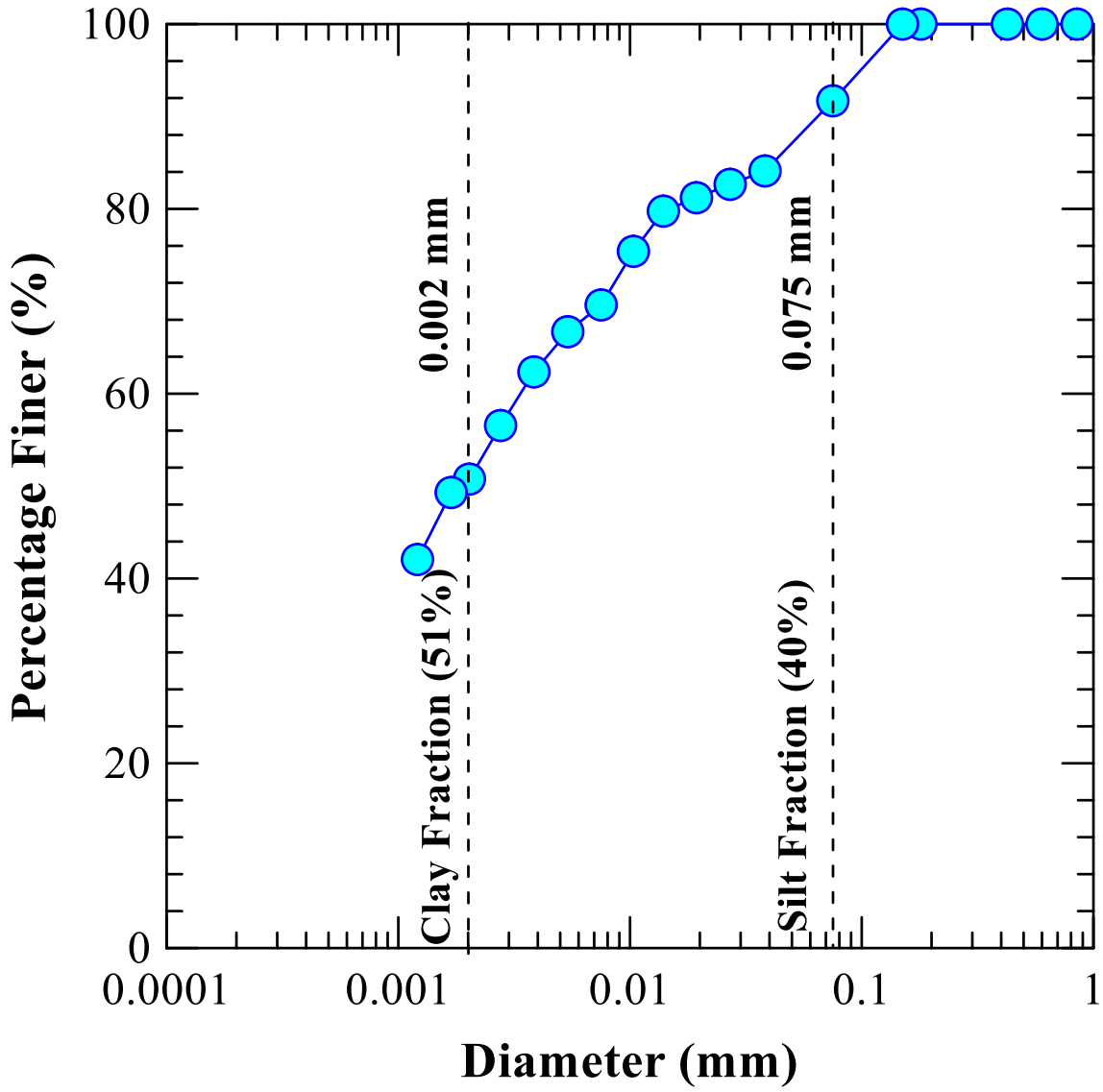

(b)

Figure 3.2 Grain Size Distribution of (a) Soil-1, and (b) Soil-2

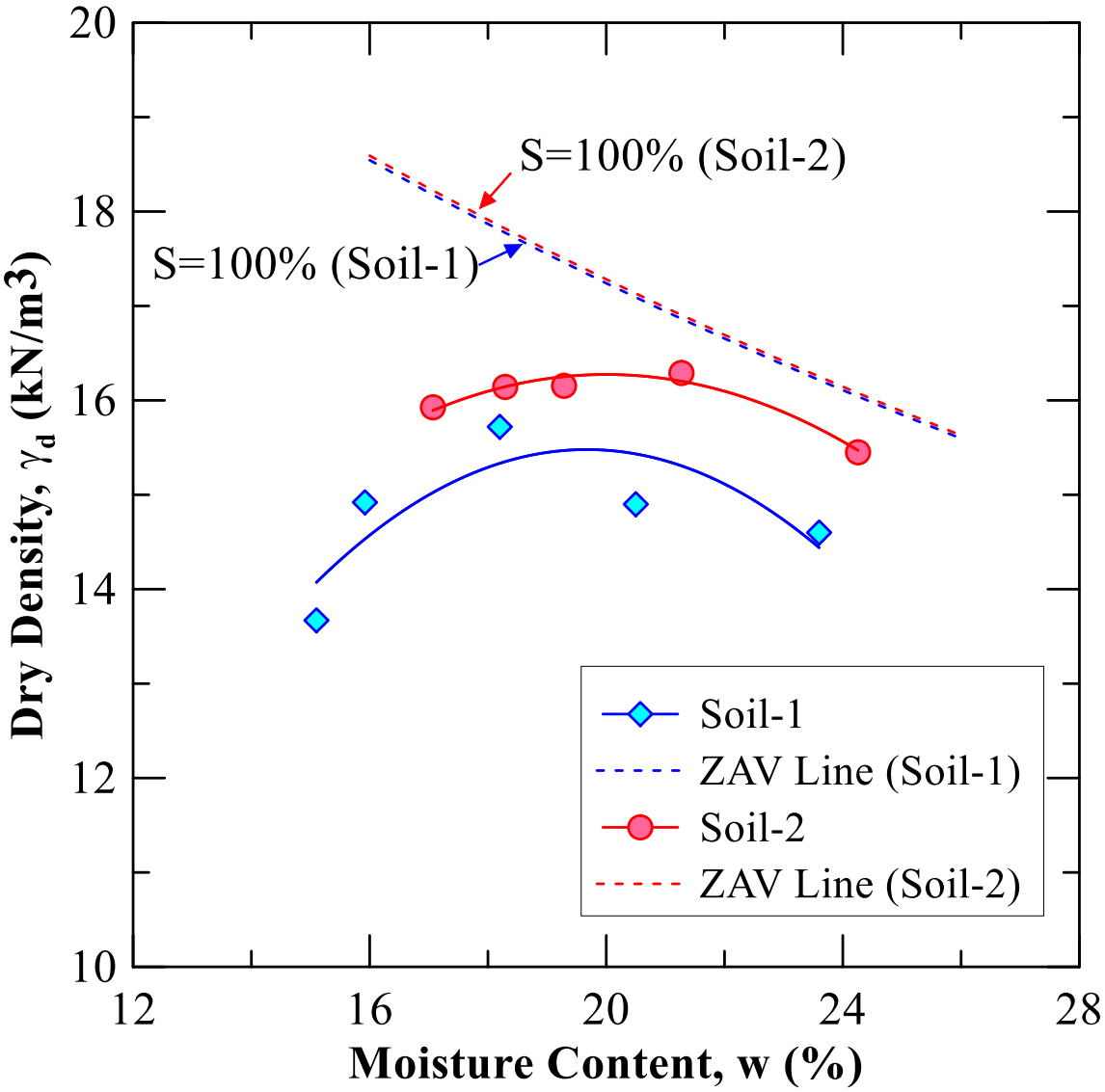

Note: ZAV Line - Zero Air Void Line

Figure 3.3 Maximum dry density and optimum moisture content of geomaterials.

The soil composition was also determined using X-ray fluorescence (XRF) Spectroscopy, as shown in Table 3.2. The XRF studies indicate that Soil-1 has a greater mass percentage of both Aluminum oxides and Silica oxides as compared to Soil-2. The mass percentage of Sulphur oxides is also higher in Soil-1. These values corroborate the

results from the colorimetric method (Tex-145-E) for determining total sulfate concentration in the geomaterials. The concentration of Calcium oxide is considerably higher in Soil-2 (more than both silica and alumina oxides), indicating the possible presence of Calcite minerals in the natural state.

Table 3.2 Chemical composition of Geomaterials.

Geomaterial type	**SiO_2**	**Al_2O_3**	**Fe_2O_3**	**CaO**	**MgO**	**SO_3**	**Na_2O**	**K_2O**
	Mass %	Mass %	Mass %	Mass %	Mass %	Mass %	Mass %	Mass %
Soil-1	39.691	35.998	14.365	2.180	1.806	1.574	0.17	1.52
Soil-2	28.771	23.482	7.247	36.959	1.682	0.111	0.029	1.683

3.2.2 Calcium-based Stabilizer

Dolomitic-hydrated lime conforming to ASTM C977 standard method was procured from a local supplier and used as a primary stabilizer for the subsequent studies. The chemical composition of the Ca-based stabilizer was determined using XRF spectroscopy, as shown in Table 3.3.

Table 3.3 Chemical composition of Ca-based stabilizer.

CaO	**SiO_2**	**Al_2O_3**	**Fe_2O_3**	**SO_3**	**MgO**	**K_2O**	**Na_2O**
Mass %	Mass %	Mass %	Mass %	Mass %	Mass %	Mass %	Mass %
51.495	4.433	9.456	0.333	0.010	28.294	0.002	0.119

3.2.3 Silica-based Co-additives

In this research study, two different silica-based co-additives have been selected to determine their overall efficacy over traditional treatment without co-additives. Subsequently, their performance was compared and their individual influence was determined when mixed with primary stabilizer (dolomitic-hydrated lime).

3.2.3.1 Crystalline Silica (CS)-based co-additives

Industrial waste products such as quarry dust is a major source of crystalline-silica rich particles. To replicate the quarry dust in the laboratory, crushed sand was used for this research study. A commercially available industrial silica sand was procured from a local supplier. The sand was washed and dried in the oven at 110ºC for 24 hours before pulverizing. The pulverized sand was wet sieved through a #200 sieve to facilitate maximum extraction of the crushed sand finer than 75 microns. The washed fine sand was allowed to settle for approximately 24 hours, and the supernatant water was siphoned out. The residual wet crushed sand was allowed to dry in the oven for 24 hours at 110ºC. The

dried crushed sand was then stored in a hermetically sealed chamber to be later used as a crystalline-silica rich co-additive for treating the expansive soils with lime (Figure 3.4).

(a) (b)

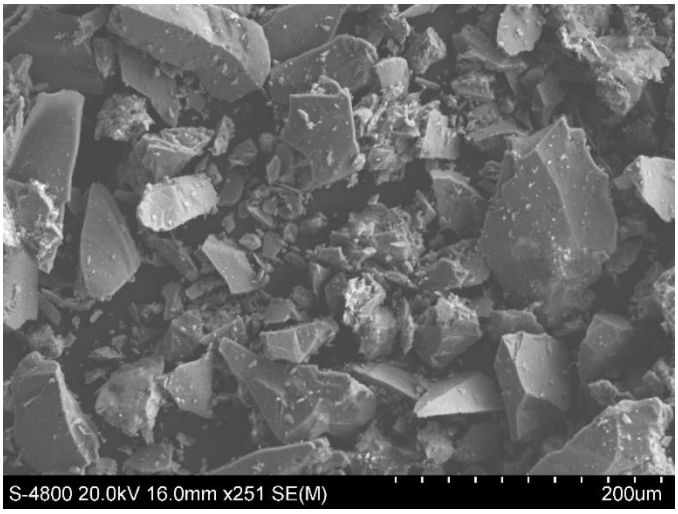

(c)

Figure 3.4 Crystalline Silica(CS)-based co-additive a) before processing (industrial sand) b) after processing (crystalline-silica rich fines) c) Scanning Electron Microscope (SEM) image of CS particles.

3.2.3.2 Nano-Silica (NS)-based co-additives

The second co-additive was an amorphous silica-based product, which is a commercially available nano-silica solute (Figure 3.5). The NS solute has a 50% weight in suspension in H_2O and has a molecular weight of 60.08 g/mol. The other properties of the co-additive are listed in Table 3.4 as obtained from the material specification sheet.

Table 3.4 Properties of laboratory-grade nano-silica (NS)-based co-additive.

Specification	**Values**
Appearance (Form)	Viscous Liquid
Appearance (Clarity)	Cloudy
pH at 25°C	8.5 - 9.5
Viscosity at 25°C	≤ 55 cps
Specific Gravity at 60°F	1.388 - 1.407
Silica	49.0 - 51.0 %
Ratio, SiO_2:Na_2O	200 – 250
Surface Area	110 - 150 m^2/g
Sulfates (SO_4) as Na_2SO_4	≤ 0.135%
Assay	≥ 20%

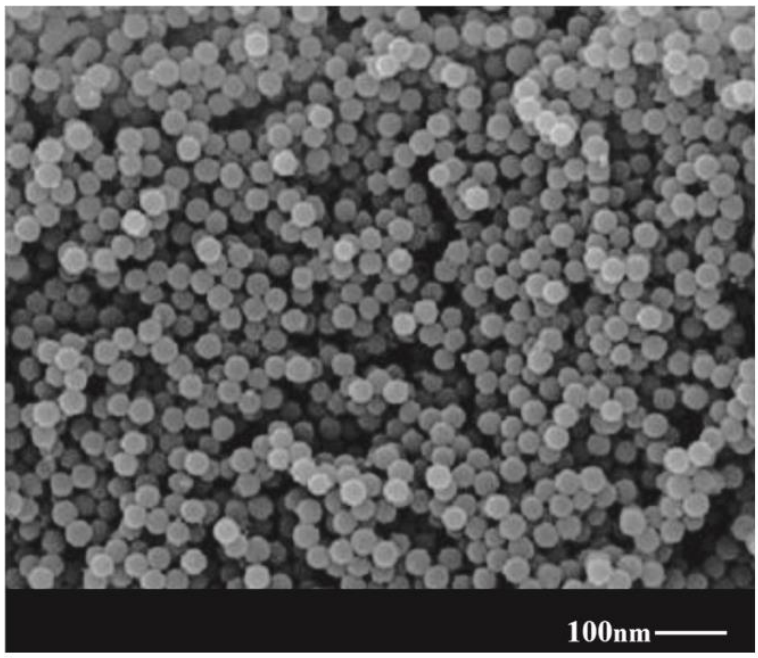

Figure 3.5 SEM image of nano-silica particles (Kutanaei and Choobbasti 2017).

The basic characterization of the materials, followed by chemical and microstructural properties, was presented in this section. These properties helped us to identify the potential problems associated with the natural soils. Furthermore, the engineering and chemical properties of stabilizers and co-additives also provide an overview of the target treatment methods needed for each type of soil and potential problems with the methods. The following section discusses the chemical, engineering, and microstructural studies performed on untreated and chemically treated soils.

3.3 Chemical Studies

3.3.1 pH

The pH of a dolomitic hydrated lime at a standard room temperature of 23±2° C is 12.4. Adding a Ca-based stabilizer to treat expansive soil immediately increases the soil pH to ≥ 12.4, due to the dissolution of oxide or hydroxides of lime into Ca^{+2} and OH^{-} ions. The increase in hydroxyl concentration increases the soil pH. (>10.5), helps in the dissolution of soil silicates and aluminates, which react with available calcium ions and water to form cementitious compounds such as C-S-H and C-A-H. During the process of pozzolanic reactions, the OH^{-} participates in the formation of reaction products and result in a decrease in soil pH. Therefore, measuring the pH of soil treated with stabilizers and co-additives could be an efficient tool to predict chemical reactions.

Therefore, the pH test was used to determine the Lime Modification Optimum (LMO) in accordance with Eades and Grim's methods (ASTM D6276) (Figure 3.6). This LMO dosage of Ca-based stabilizer determines the minimum percentage of lime, required to increase the soil pH to greater than 12.4. Furthermore, the pH of lime-soil mixture and lime-soil-co-additive mixtures were also recorded over different curing period to understand the rate of the reaction rates and develop a comprehensive knowledge on the effects of co-additives when mixed with traditional stabilizers.

In addition to the above measurements, the pH of the pore fluid obtained from the leaching test was also recorded. More details on leaching and durability studies are discussed in the later sections.

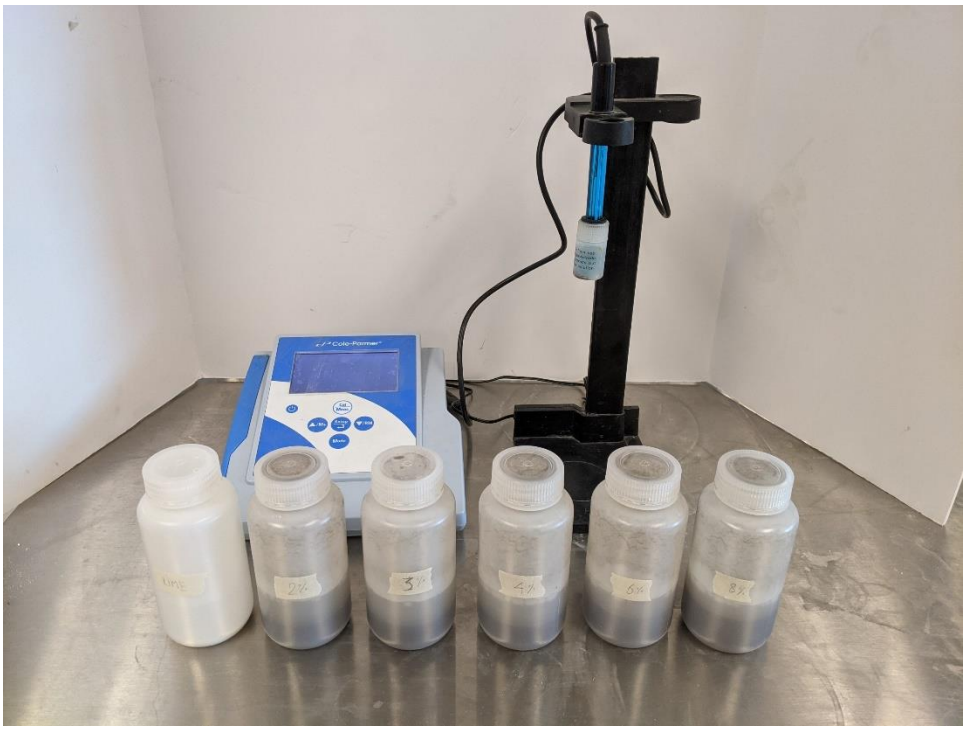

Figure 3.6 Eades and Grim pH test in accordance with ASTM D6276.

3.4 Engineering Tests

3.4.1 Strength Tests

The suitability of a stabilizer treatment in subgrade soil depends on its ability to improve both short-term and long-term performance. The traditional subgrade soil even though compacted to a maximum target density and moisture content; may still have unsatisfactory strengths to bear the design traffic loads. The loss in strength of the subsurface soils could often lead to major distresses on the top pavement layers. Therefore, determining the unconfined strength of the subgrade soils is one of the key parameters to predict the long-term pavement performance. Furthermore, the improvement in the

unconfined strength after chemical treatment is an effective tool for determining the efficacy of treatments techniques.

Sustainable use of resources has been a long-term goal of the researchers in the present century. The preparation of specimens of large diameter requires a substantial volume of soil. However, sampling restrictions often impede the collection of such a large quantity of soil. Exploration for such soils may further incur extra charges for the project. Therefore, considering the above drawbacks, miniature specimens were prepared using Harvard Miniature Compaction setup (Figure 3.7a). Cylindrical soil specimens having a diameter of 33 mm (1.3 inch) and with an aspect ratio of 2(H):1(D) (where, H = height, and D = Diameter) were prepared using static compaction in three layers.

Experimental results indicated that the mechanical performance of miniature specimens was similar to that of standard specimens prepared at the same aspect ratio. Specimen of untreated and treated soil was tested for unconfined compressive strength (UCS) in accordance to ASTM D5102 at a constant strain rate of 0.5% per min using a Universal Testing Machine as shown in Figure 3.7b.

(a) **(b)**

Figure 3.7 Unconfined compressive strength test equipment a) Harvard miniature compactor for soil specimen preparation b) Universal Testing Machine.

Another major concern for the subgrade soil is the degradation in the performance due to moisture intrusion. Subgrades being primarily composed of clay particles, as they have a major affinity to hold water molecules around them. This moisture holding capacity induces reduction in the interparticle friction and results in a significant loss in strength and long-term serviceability. Therefore, it is necessary to determine the effects of moisture intrusion on the unconfined strength for both untreated and treated specimens.

Several past studies have indicated that retained strength after the specimens are subjected to capillary soaking for 48 hours, is a good indicator of its durability. Therefore, for this research program, miniature cylindrical specimens were prepared in a similar method as described in the previous paragraph and were tested for durability when subjected to capillary soaking for 48 hours (Figure 3.8). The soaked specimens were subjected to Unconfined Compressive Strength (UCS) test (ASTM D5102) at a similar strain rate of 0.5% per minute.

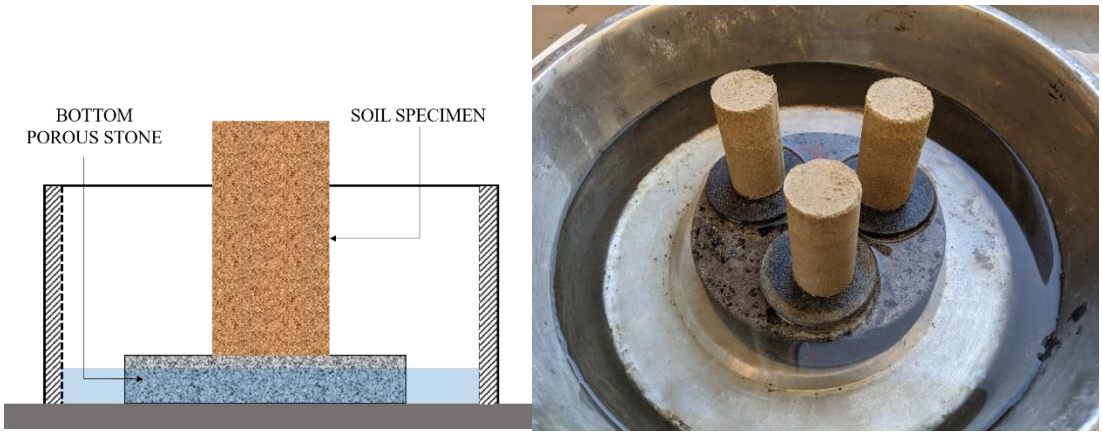

(a) (b)

Figure 3.8 Soil specimens subjected to capillary soaking a) schematic b) test setup

3.4.2 Vertical Free Swell Test

The serviceability of a pavement constructed over expansive local soils suffers significantly when subjected to seasonal moisture fluctuations. The clay minerals, especially Montmorillonite, have an affinity to absorb water molecules through the formation of double diffused layers. Due to the absorption of the water molecules, the clay particles undergo volumetric expansion. This expansion causes major distress to the pavement layers and is a major indicator of pavement performance.

The free swell test was performed on untreated and treated specimens in accordance with ASTM D4546 (Figure 3.9). The treated and untreated soil specimens were prepared by static compaction in a mold of 2.5 in diameter and 1 in height to reach the target density at target moisture content. The one-dimensional swell values were measured under a surcharge of 1 kPa using a dial gauge. The deformations readings were monitored and recorded until a constant reading for three consecutive days was obtained. The swell test was performed at a constant room temperature of 23±2°C, and proper precautions were taken to minimize the evaporation of water during the entire period of recorded data. After the final deformation data was recorded, the specimens were removed from the molds, and the final water content was recorded in accordance with ASTM D4959.

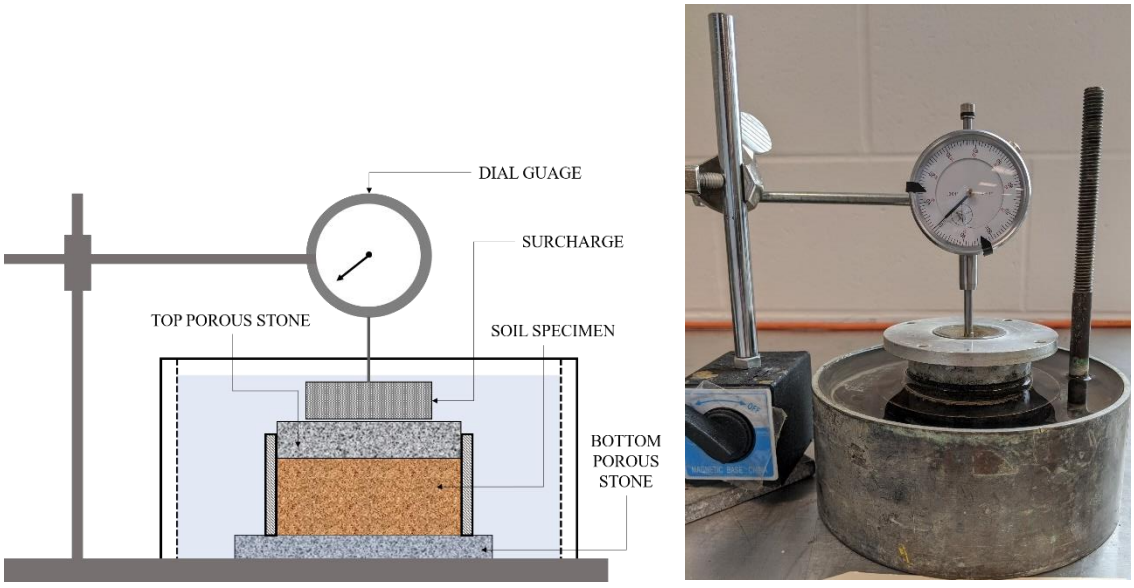

(a) (b)

Figure 3.9 Vertical free swell strain test a) schematic diagram b) specimen under test.

3.4.3 Linear Shrinkage Strain Test

Another major concern of using the high-plastic expansive soils for constructing the pavement subgrade is the issues related to shrinkage strains. Shrinkage strains occur due to the cyclic wetting and drying process, and it severely impacts the long-term pavement performance. As the subgrade soils are predominantly clay minerals, it has a major affinity to absorb water molecules, and subsequently, during the summer months, the absorbed water is dried up, and this results in major shrinkage strains in the soil. These strains induce significant cracks and fissures near the top surface of the subgrade soil. Eventually, over a longer period, these cracks propagate to the asphalt layer and reduce the serviceability

of the pavement. Therefore, it is necessary to evaluate the shrinkage properties of the subgrade soil to provide a holistic idea of pavement performance.

In general, chemical treatments tends to improve the performance of the problematic soils against shrinkage strains. Application of Ca-based stabilizers helps to reduce the moisture-holding capacity of the clay layers immediately after treatment due to phenomenon of cation exchange and reduction in the thickness of the diffused layers or positive cations and hydroxyl ions. Therefore, it was hypothesized that the application of silica-based co-additives with traditional dolomitic-hydrated lime could probably improve the performance of the high-plastic clays against shrinkage strains.

Shrinkage tests were performed for both untreated and treated soil groups at different curing periods. The linear bar shrinkage test was performed following the TxDOT guidelines outlined in Tex-107-E (Figure 3.10). For the shrinkage test, the homogenous treated soil mixtures were stored separately in a sealed chamber and cured in a similar method as other compacted soil specimens. After each target curing period, cured soils were mixed with water to reach a consistency similar to the liquid limit. Consequently, the wet soil was placed in a greased mold (19 × 19 × 127 mm) and gently jarred to assist the uniform flow of soil and remove any entrapped air. After air drying, the partially wet specimens were kept in an oven with a drying temperature of 110±5°C and monitored until a constant weight was obtained. Thereafter the specimens were removed, and the maximum linear dimension was measured to obtain the shrinkage percentage with respect to the initial dimension.

(a)

(b)

(c)

Figure 3.10 Linear bar shrinkage test a) at the beginning of the test b) after drying to a constant weight c) Linear measurements after drying to constant weight.

3.4.4 Resilient Modulus Test

Previous studies have indicated that the flexible pavement seldom fails through strength failures during its service life. 1993 AASHTO pavement design guide and the new Mechanistic Empirical Pavement Design Guide (MEPDG) developed under NCHRP Project 1-37A recommends the use of the resilient modulus parameter to determine the pavement response during the design phases. The resilient modulus of a material (M_r) is defined as the ratio of the cyclic stress (σ_d) to the recoverable strains (ε_r) as shown in the Figure 3.11 and is represented by Equation 1 below.

$$M_r = \frac{\sigma_c}{\varepsilon_r} \qquad (1)$$

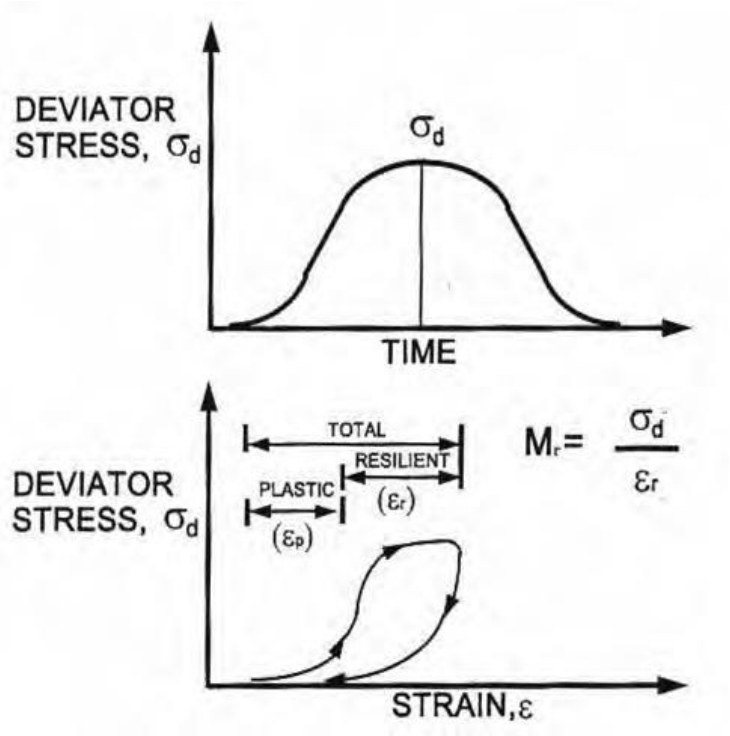

Figure 3.11 Definition of resilient modulus (Puppala 2008).

The Repeated Load Triaxial Test (RLTT) is one of the key tests primarily used to obtain the resilient modulus of the unbound geomaterial, i.e., it could be used to predict the basic mechanistic responses of a pavement when subjected to repetitive traffic loading. Laboratory studies were performed in a pneumatic controlled triaxial setup, as shown in Figure 3.12, to replicate the actual traffic loads. The major components of the test setup include a water control chamber, an air pressure control chamber, a triaxial confining chamber connected to confining pressure control cylinder to apply minor stresses, a load cell to apply normal stresses, an actuator to apply the cyclic haversine load pulse, a pair of LVDTs to measure the deformations, a monitor and an IMAC (CPU) (Figure 3.12). Duplicate specimens of diameter 71 mm and height 146 mm were prepared for all soil groups for different curing periods to evaluate their respective resilient modulus values. After each curing period, the resilient moduli of duplicate specimens from each group were determined in accordance with AASHTO T 307 method using cohesive soil testing protocol. The specimens are tested under 15 different testing conditions with three confining stresses (σ_3 = 2, 4, and 6 psi) and five deviatoric stresses (σ_d = 2, 4, 6, 8, and 10 psi), with each condition having 100 cycles of repetitive haversine pulse. At each confinement and deviatoric stress, the resilient modulus value is determined by averaging the resilient modulus values for the last 5 deviatoric loading cycles.

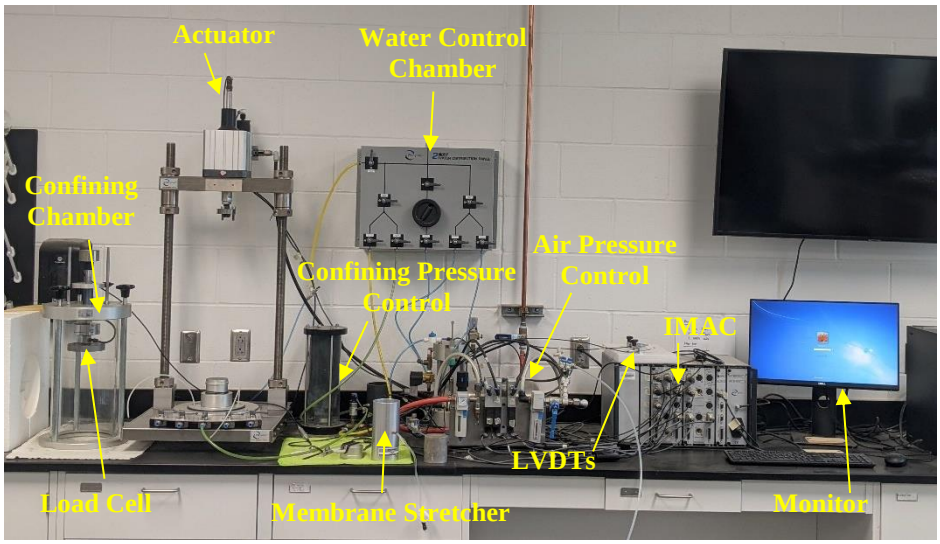

Figure 3.12 Test setup for Repeated Load Triaxial Test (RLTT).

After completion of the test, regression analyses were performed to fit the obtained test results using the universal model presented in Equation 2.

$$M_r = k_1 P_a \left(\frac{\theta}{P_a}\right)^{k_2} \left[\left(\frac{\tau_{oct}}{P_a}\right) + 1\right]^{k_3} \quad (2)$$

Where, M_r = resilient modulus; k_1, k_2 and k_3 = material specific regression coefficients; θ = bulk stress; P_a = atmospheric pressure; and τ_{oct} = octahedral shear stress

The k_1 parameters for the two groups of specimens were compared to study the improvements in the stiffness among different treated soil groups. The changes in k_2 and k_3 parameters were also studied to comprehend the influence of bulk stress and shear stress on the resilient modulus values, respectively.

3.4.5 Unsaturated Soil Tests to Determine the Pore Structure

The application of Ca-based treatment to expansive soil improves the performance of the soil through chemical reactions between the stabilizer and the soil minerals. This includes

both short-term and long-term improvements. The application of Ca-based stabilizers immediately reduces the moisture affinity through satisfying the surface charges of the clay minerals and over a long time due to pozzolanic reaction and formation of additional cementitious phases. Consequently, both these factors affect a change in the pore structure in the treated soil matrix. Due to the dissolution of clay minerals and the formation of new reaction products, there is a relative change in the pore structure of the treated soil as compared to natural soils. The cementitious compounds make the soil less moisture susceptible and more durable over the course of the curing periods.

Unsaturated soil tests could be used as a major supporting tool to predict the swelling and collapse behavior of expansive soils. The SWCC is a relationship indicating a relative change between the soil suction and moisture content at any constant temperature and stress conditions. The SWCC curves are divided into several zones, with each attributing to different features in the soil. The curves are primarily divided into three zones known as the boundary effect zone, transition zone, and the residual water content zone (Figure 3.13). The air entry value zone occurs in between the boundary effect zone and the transition zone. The air entry value in the curve represents the suction value where the expulsion of water from the soil has just started, and the air starts to fill in the largest voids. The residual determines the change in soil suction over different water contents, and the residual zone indicates the region where high suction stresses are required to remove the additional water from the soil matrix.

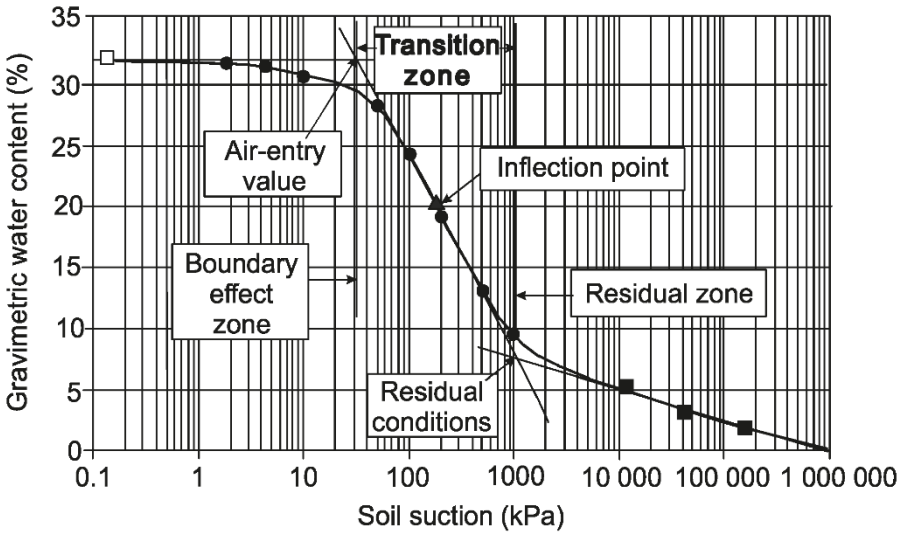

Figure 3.13 Different zones in soil water characteristic curves (Fredlund et al. 2011).

The application of chemical stabilizers is expected to change the water migration behavior, and the relative changes in the behavior of the treated soils as compared to untreated soils could be qualitatively determined from the changes in the nature of the SWCC. In this research study, the soil water retention curves were determined using axis translation techniques for suction rages below 500 kPa using the Fredlund SWCC device (Figure 3.14a). For higher suction ranges (>500 kPa), a chilled mirror hygrometer (WP4C) was used to determine the remaining retention curves (Figure 3.14b).

(a)

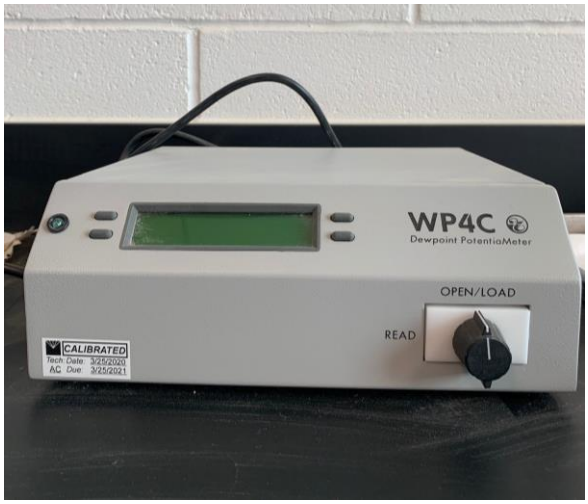

(b)

Figure 3.14 Test setup for SWCC using a) Fredlund SWCC device (axis-translation technique) b) WP4C (chilled mirror hygrometer).

3.4.6 Leaching Studies

Available lime content also plays a significant role in the behaviour of stabilized soils when exposed to moisture. Inadequate lime contents have been shown to cause significant leaching in stabilized layers. Leaching of calcium hydroxide from the treated layers might

result in the breakdown of the soil-stabilizer system. This could lead to deterioration of the engineering properties of post-leached specimens including, PI, shrinkage limit, and compressive strength.

Leaching studies were performed for untreated and chemically treated specimens after different curing periods to determine the permanency of the treatments. Cylindrical specimens of 1.4 in diameter and an aspect ratio of 2:1 were used for this study. The calcium concentration and pH of the leachate were determined in this study.to provide information on the effects on long-term soil properties.

The leaching studies were performed according to the guidelines outlined in Chittoori et al. (2013) using a tri-axial test setup as shown in Figure 3.15. The back-pressure channel was used to push the water inside the specimens from the top, and the leachate was collected from the drainage channel connected to the bottom of the specimen. Proper precautions were taken to ensure that no water movements occurred between the membrane and the soil specimens. The specimens were initially saturated (~ 90-95% saturation) by constant back pressure saturation of 5-10 kPa before running the leaching studies.

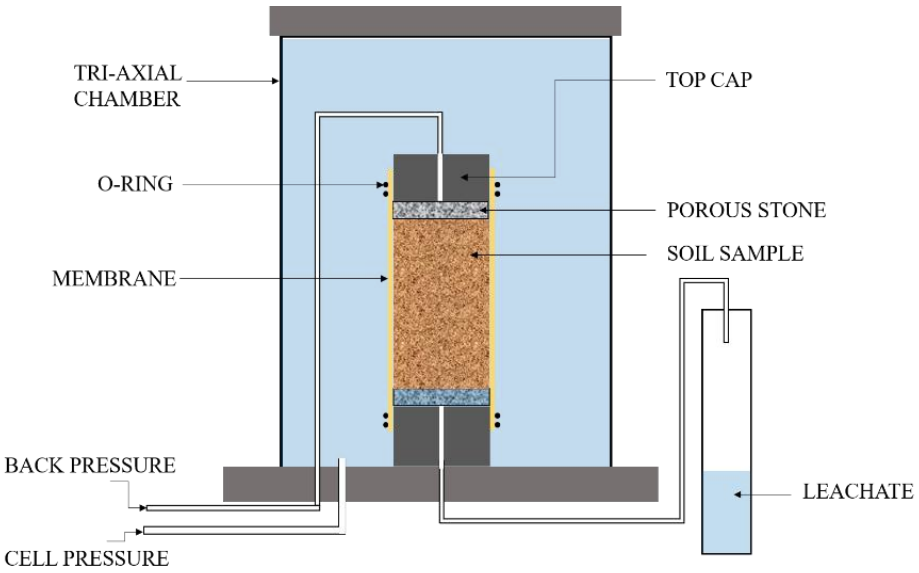

(a)

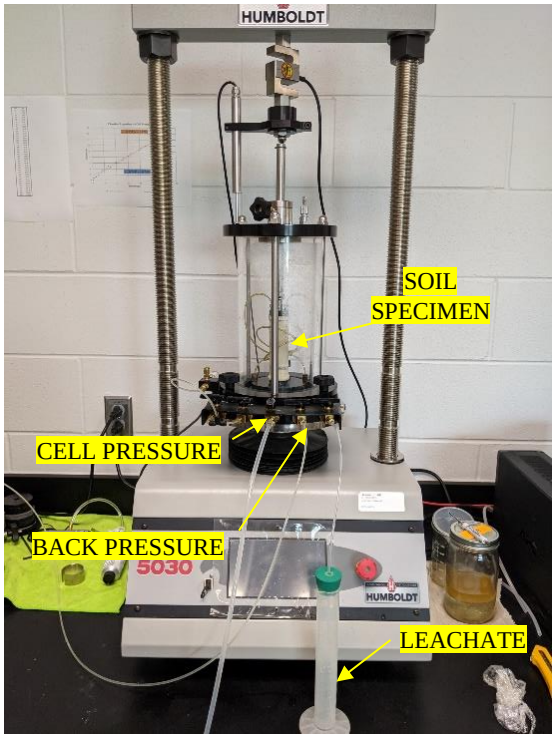

(b)

Figure 3.15 Leaching test to determine the permanency of treatment (a) Schematic diagram (b) Test setup.

Each soil specimen was subjected to 7 leaching cycles; a leaching cycle was defined as the amount of leaching volume equivalent to the total pore void volume of the soil specimen (Chittoori et al. 2013). The air and water voids present in the specimen was defined as the total pore void for any particular test. Some preliminary studies were performed, and constant backpressure ranging from 5 to 25 kPa was deemed suitable for moisture inflow in the soil. The inlet backpressure was adjusted in such a manner that the total pore void volume equivalent of leachate was collected over a time frame of 24 hrs. The advantage of using low effective confinement and low back pressures is that it would not interfere in changing the porosity of the specimens as well as the pore structure of the treated soil specimens.

3.5 Microstructural Analysis

3.5.1 X-Ray Diffraction (XRD) Studies

X-rays are short-wavelength, high-energy beams of electromagnetic radiation. The X-ray diffractions are obtained when any material is irradiated with a beam of high-energy photons. The high-energy photon is bombarded on an electron in a shell that removes the electron in the shell in the form of a photoelectron. The removal of the photoelectron creates a vacancy in the shell and a state of ionization in the atom. Electrons from outer orbits move to occupy the vacant space and, in this process, releases fluorescent X-ray photon. XRD is a non-destructive testing methodology that provides comprehensive information about the crystallographic structure, chemical composition as well as physical

properties of the tested minerals. The crystal structures and the scattered photons are correlated with the help of Braggs' Law :

$$n\lambda = 2d \sin \theta \quad (3)$$

where, the interplanar distance of crystals (d) is inversely proportional to the scattering angle (θ), n is an integer representing the order of the diffraction peaks, λ is the wavelength of the incident X-ray beam.

Microstructural studies using X-ray diffractograms were performed for analyzing the behavior of the geomaterials when treated with the Ca-based stabilizer and silica-based co-additives. The XRD studies were performed using powder specimens at different curing periods. Cu-kα radiation with a wavelength of 1.54 nm was used over the range of 5 to 60° for 2θ, with a step size of 0.02° and 0.5sec/step (Figure 3.16). International Centre for Diffraction Data was used for the identification of the minerals present in the powder based on the location of their characteristic peaks. The formation of new peaks and relative changes in the existing peak intensities of the diffractograms were used to detect the formation of new minerals and other cementitious reaction products.

(a)

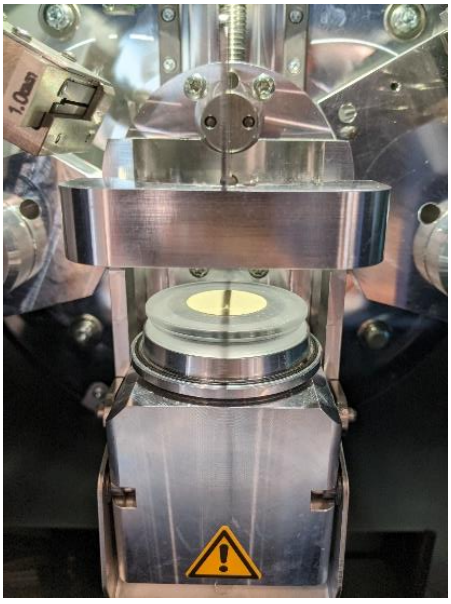

(b)

Figure 3.16 X-ray diffraction studies setup a) BRUKER D2 PHASER b) Specimen inside the chamber after loading.

3.5.2 Field Emission Scanning Electron Microscopy (FESEM)

Scanning Electron Microscopy is one of the most prevalent techniques for identifying compositional and topographical features in a material (Figure 3.17). In SEM, a low-energy electron beam scans the surface of the specimen. A typical SEM consists of a high-energy electron-gun that emits electrons, which are accelerated to high energy level (0.1-30 keV), a tungsten gun to form high-resolution images, electromagnetic lenses, and apertures, and a high-vacuum environment to prevent scattering of moving electrons due to particles in the air.

Figure 3.17 Scanning Electron Microscope (HITACHI S-4800).

3.5.3 X-Ray Fluorescence (XRF) Spectroscopy

The XRF spectrometry is a non-destructive technique used to determine the elemental composition of test specimens (Figure 3.18). Using the XRF technology, multi-elemental analysis of the specimens could be performed after subjecting the specimens to an X-ray source. The elements in the specimens emit characteristic X-ray beams, also known as 'fingerprints' when subjected to an external input wave source. After measuring the intensity of the emitted characteristic X-rays, the qualitative or quantitative characterization of the element could be performed. XRF could be extensively used for studying geomaterials to determine the presence of different chemical compounds as a percentage of mass in the tested amount of the geomaterial.

In XRF spectroscopy analysis, either a solid or a liquid specimen is irradiated with a high-energy X-ray source. The incident X-rays, when bombarded on the atoms of an element, the electrons in the inner orbital shells get dislodged. This induces instability in the atom; to balance the valency of the shell, another electron from the higher energy shell drops to the lower shell and in this process emits a characteristic fluorescent photon of energy equivalent to the difference of the energy between the two quantum states of the electron.

In this research, untreated soil, primary stabilizer, and pore fluids were tested using XRF spectroscopy. The elemental composition analysis of the untreated soils and lime were performed by preparing pellets using a static compressor, as shown in Figure 3.18a-b. The liquid specimens studied in this study were prepared from the pore fluids obtained from the leaching tests, as discussed in the previous sections.

(a)

(b)

(b)

Figure 3.18 X-ray Fluorescence testing equipment (Rigaku Supermini200).

3.5.4 Differential Scanning Calorimetry (DSC) Studies

The thermal techniques are effective tools to comprehensively study the mechanism of soil stabilization through the identification of the chemical phases involved in the process. The use of thermal techniques becomes much more significant when a relatively significant percentage of amorphous phases are involved in the chemical reactions. The use of common crystal identification techniques such as X-ray Diffractions is relatively inert in identifying amorphous phases of the cementitious reaction products due to the Ca-based stabilizations.

Differential Scanning Calorimetry (DSC) is a thermal technique that monitors the relative heat flow in or out of the specimen during the process of thermal scanning in a controlled environment. These help in the identification of the chemical reaction products and phase changes as a function of the temperature. The heat transition in the specimen is monitored with respect to a reference specimen, both of which are placed in aluminum crucibles. For this research, an empty aluminum pan was used as the reference for all studies.

At constant pressure, the heat flow is equivalent to the enthalpy changes in the specimen ($\frac{dq}{dt} = \frac{dH}{dt}$, where $\frac{dH}{dt}$ is the heat flow). The heat flow difference between the specimen and the reference ($\Delta \frac{dH}{dt}$) could be either endothermic (positive) or exothermic (negative). The endothermic reactions are primarily associated with dehydration and decomposition reactions, whereas the exothermic or heat loss reactions are attributed to crystallization reactions or oxidation processes. The schematic of the general mechanism of DSC analysis is represented in Figure 3.19.

In this research study, treated specimens were subjected to DSC analysis, and the results from the thermal plots were used to detect the formation reaction products and, in particular, the amorphous reaction phases. The thermal curves were used to complement the results obtained from X-ray diffractograms to provide comprehensive knowledge on the chemical changes occurring due to the application of silica-based co-additives to treat the problematic high-plastic soils.

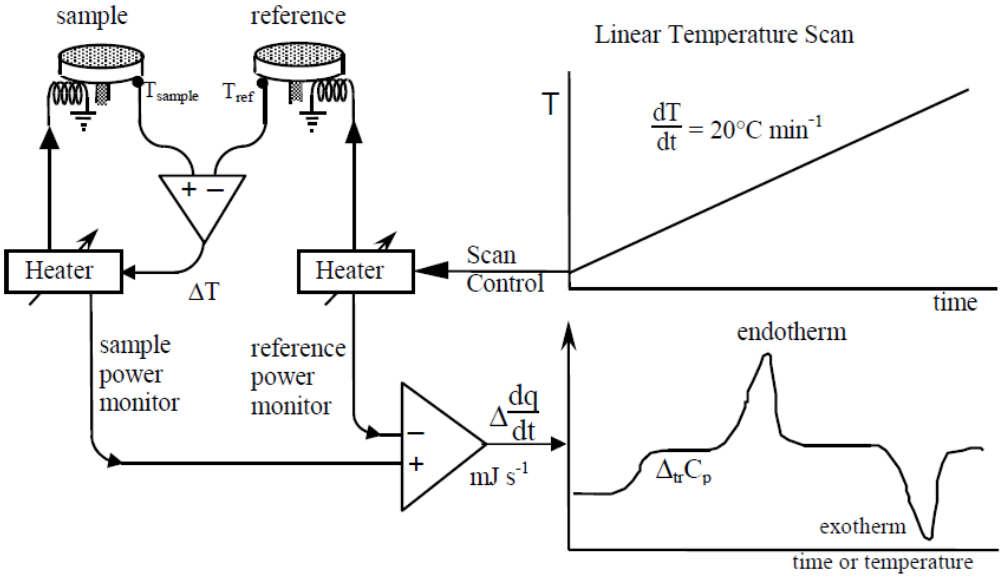

Figure 3.19 Schematic diagram of Differentia Scanning Calorimetry (https://www.colby.edu).

3.6 Summary

This chapter provided a comprehensive overview of different soil types, primary stabilizers, and silica-based co-additives used for the research study. Additionally, discussions were presented on the array of engineering, chemical, and microstructural studies. Some major conclusions from the chapters are summarized below:

- Two types of soils were where characterized in accordance with ASTM soil classification. Both soils were identified as high plastic soils (CH-soil), having significant swelling and shrinkage potential. Soil-1 was observed to have high soluble sulfate content of 14,000 ppm (high-sulfate soil), and Soil-2 had a soluble sulfate concentration level of 400 ppm (low-sulfate soil).
- The primary stabilizer used was a commercially available traditional dolomitic-hydrated lime. Two silica-based co-additives were identified as crystalline silica (CS) fines rich quarry fines and laboratory-grade nano-silica (NS).
- An array of chemical, engineering, and microstructural studies was included in the research plan to characterize the reactions involved in the treatment process. Chemical and engineering tests include pH, strength and durability, swelling and shrinkage, resilient modulus. Microstructural and mineralogical tests such as X-ray Diffraction, X-ray Fluorescence, Field Emission Scanning Electron Microscopy, and Differential Scanning Calorimetry were performed in this research study.

In the next section, the first specific objective of this research plan is investigated, where the two silica-based co-additives were used with the traditional Ca-based stabilizer to modify the reaction kinetics during the treatment of a high-plastic (CH) soil.

4. UTILIZATION OF SILICA-BASED CO-ADDITIVES WITH LIME TO ACCELERATE THE REACTION KINETICS

4.1 Introduction

This research study was undertaken to investigate and then evaluate the applicability of silica-based co-additives with traditional Ca-based lime stabilizers for rapid stabilization of problematic high-plastic soil. A comprehensive testing program including both engineering and microstructural studies was designed and performed on the lime-treated soil, lime-treated soils with crystalline silica admixture, and lime-treated soils mixed with nano-silica admixture combinations. The impacts of co-additive dosage and behavior after subjecting the soil specimens to different curing periods were addressed. Additionally, both mineralogical and microstructural analyses were performed to understand the possible reasons for observed changes in the engineering properties of the treated soils stabilized with different co-additives. A framework was developed to determine the statistical significance of different dosages of co-admixtures on the enhancements of engineering properties of the treated soils and subsequently determine the optimum stabilizer dosages.

The overall research approach outlining all tasks is presented in Figure 4.1. The steps involved in the early stabilizer mix design is organized as follows: first, the lime stabilizer optimization based on pH results with the CH soil was performed to determine the minimum lime requirement for chemical reactions. In this research study, Soil-2 was used for analysis as it has no effects of high-sulfate concentration, and detrimental effects of ettringite precipitation could be neglected. And second, a statistical optimization

analysis of engineering test results was attempted to study the optimized NS and CS levels when mixed with optimum lime dosage determined in the first step. The second approach was performed on unconfined compressive strength (UCS) and retained strength after capillary soaking of treated soil specimens after 7 days of curing.

The improvements in the UCS and the retained strength after capillary soaking of the treated soils are the key parameters to be considered as required to assess the efficacy of soil stabilization. Using the optimum dosages of both co-additives with primary lime stabilizer, other engineering tests such as swelling, shrinkage, and resilient modulus studies were performed after different curing periods of 0, 3, and 7 days. The improvements in strength and strength after capillary soaking were also analyzed over these curing periods. Final stabilization designs were made based on comprehensive analyses of engineering, chemical, and microstructural studies performed on the treated geomaterials. More details of these investigations are provided in the later sections.

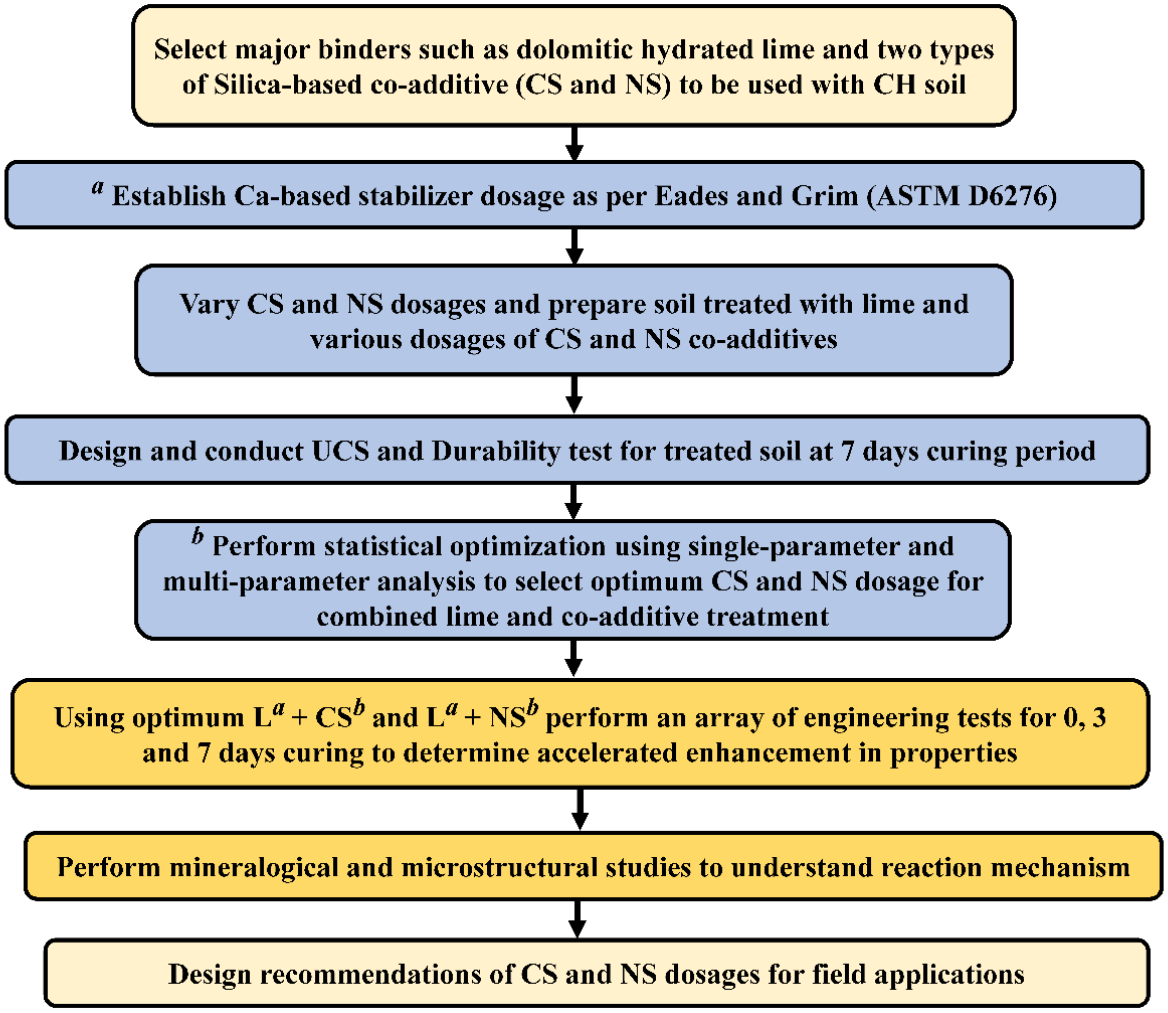

Note: CS-Crystalline Silica; NS-Nano Silica; L-Dolomitic Hydrated Lime; CH-High PI Clay; *a* = Specimens with optimum lime content; *b* = Specimens with optimum co-additive content

Figure 4.1 Research flow with tasks performed in the stabilization design.

4.2 Experimental and Statistical Analyses Studies

The Lime Modification Optimum (LMO) was determined by Eades and Grim's pH test method in accordance with the ASTM D6276 method. About 6% lime by the dry weight of the Soil-2 was required to attain a pH value of 12.4 for all treated soil groups, and this dosage was used as the LMO for this study. For the lime-treated soil and lime-CS treated soil, dry soil or dry soil with crystalline silica and lime were uniformly mixed to the desired proportions. Thereafter, water was added to the dry mixtures and blended uniformly to produce a homogeneous treated soil mixture. In the case of treatment with NS, the soil and the lime were uniformly mixed in the dry state. The NS solute was mixed with the required molding water and stirred continuously for 5 mins using a magnetic stirrer before adding the water-NS solution to the dry soil-lime mixture. This was done to ensure that the nanoparticles were uniformly distributed within the treated soil matrix.

Optimization of silica dosages was necessary considering both economic aspects and engineering performance requirements. For Crystalline Silica (CS) co-additive, four dosages were selected for the initial trials (**X%**): 5, 10, 15, and 20% of the dry weight of the soil. Similarly, for Nano-Silica (NS) co-additive, four dosages (**Y%**) of 0.25, 0.5, 1.0, and 2.0% by the dry unit weight of the soil were considered. Six cylindrical soil specimens of each treated soil groups were prepared using the static compaction method, demolded, and cured for 7 days in a hermetically sealed chamber to ensure a relative humidity close to 100% at a temperature of 23±2°C. Triplicate specimens for each soil group were tested in accordance with ASTM D5102 method for both unsoaked strength and strength after subjecting the treated soil specimens for a capillary soaking period of 48 hrs. The unsoaked

strength of the curing specimens provided insights into the extent of the pozzolanic reactions in the different treated soil groups. In contrast, the strength properties of the capillary soaked soil specimens facilitated understanding of the effects of moisture conditioning on strength properties of stabilized soil specimens, and these results also provided an indirect measure of the durability of the treated soil groups prepared after 7-day curing period.

The statistical significance of adding dolomitic-lime alone and dolomitic-lime mixed with different dosages of silica admixtures with the untreated soil on unsoaked and capillary soaked strength parameters was determined by using factorial experiments. These experiments are useful in understanding if the means of a dependent variable were significantly different from one another. The level of significance of all experimental values was chosen as 0.05 based on a 95% confidence interval. The one-factor experiments were based on the assumed null hypothesis that there is no significant difference between means of the groups. Three measures of variability were used for the analysis of variance in the one-factor test. These are:

$$SST = \sum_{i=1}^{k} \sum_{j=1}^{n} \left(y_{ij} - \bar{y}_{..}\right)^2 \quad (5)$$

$$A = \sum_{i=1}^{k} (\bar{y}_{i.} - \bar{y}_{..})^2 \quad (6)$$

$$SSE = \sum_{i=1}^{k} \sum_{j=1}^{n} \left(y_{ij} - \bar{y}_{.}\right)^2 \quad (7)$$

Where, *SST* = total sum of squares; *SSA* = treatment sum of squares; *SSE* = error sum of squares; y_{ij} = j^{th} observation from i^{th} treatment; *n* = number of specimens per treatment; *k*

= number of treatments; $\bar{y}_{..}$ = mean of *nk* observations; and $\bar{y}_{.}$ = mean of all observations in the specimen from i^{th} treatment.

After performing the single factor analysis, the statistical significance of the differences among mean UCS values of the group was determined by multiple comparison tests. Multiple comparison tests were performed when the *F*-ratio becomes statistically significant. Three tests, including Tukey HSD, Scheffe, and Bonferroni multiple parameter tests were performed in this analysis. Multiple comparison tests have been used to determine the *p*-values between the lime-treated soil group and the lime with co-additive treated soil groups. The *p*-values from multiple comparison studies provided information regarding a particular treatment that caused a significant difference between the control group (lime-treated soil) and test groups' (lime and co-additives treated soils) mean UCS values. The selection of the optimum co-additive silica dosage was based on the statistical significance of the unconfined strength of different co-additives dosages as well as retained treated soil strength after moisture conditioning.

The optimized dosages of all stabilizer groups, including dolomitic lime, crystalline silica (CS), and nano-silica (NS), were subsequently used for comprehensive evaluations of strength assessments before and after capillary soaking (ASTM D5102), vertical free swell strain (ASTM D4546), linear bar-shrinkage strain (Tex-107-E), and resilient modulus (AASHTO T 307) studies of treated soils with optimized dosages over different curing periods to understand the effects of treatment on kinetics.

Specimens of untreated and treated soils were subjected to Field Emission Scanning Electron Microscopy (FESEM) studies for visual identification of the

cementitious phases. The identification of new cementitious phases provided insights into the microstructural changes responsible for the enhancements of the macrostructural properties after the co-additive treatments. Since the primary focus of this research study was to understand the efficacy of co-additives on engineering properties, any changes in the behavior of the pure silica-based co-additives when treated with Ca-based stabilizers could help to study and understand the primary factors for the observed macrostructural changes. Therefore, additional studies, including X-ray Diffractions (XRD) studies, were undertaken on soils stabilized with silica-based co-additives and dolomitic-hydrated lime.

4.3 Analysis of Engineering Test Results

4.3.1 Optimization of CS and NS Dosages

The untreated soils have exhibited average unconfined strengths of 232 kPa and 25 kPa before and after capillary soaking periods, respectively. These results indicated that the untreated soil is not durable and crumbles when subjected to moisture intrusion during capillary soaking studies, reconfirming the need for chemical treatment.

Figure 4.2a-c presents the UCS values for both lime-treated CS and lime-treated NS specimens after curing for 7 days. For only lime-treated soils, the UCS values for the 7-days-cured specimens were 498 kPa and 147 kPa, before and after 48 hrs of capillary soaking, respectively. Figure 4.2a presents the UCS values for different dosages of CS when mixed with dolomitic lime and subjected to 7 days of curing.

Initially, with an increase in CS dosage, there was an increase in the unsoaked strength; however, beyond 15% of CS dosage, there was no considerable increase in the

strength of the treated specimens. The presence of silica co-additive source has helped in the development of additional cementitious phases, which might have been responsible for providing the additional strength to the treated soil. However, beyond an optimum dosage, CS might have replaced the original in-situ soil, which is a source of silicates and aluminates for long-term pozzolanic reactions under an alkaline environment. Therefore, over-replacement of the in-situ native soil with the crystalline silica source could potentially retard the strength gains.

Similarly, it can be observed that with an increase in NS dosage, there is an increase in the UCS values for the 7 days cured specimens. However, beyond 0.5% of NS dosage, the strength gain was small and negligible. The NS contains amorphous silica particles that are capable of uniformly mixing with the soil and providing an additional source of reactive silica for pozzolanic reactions. Mineralogical studies performed on the same treated soils were used to address these observations.

After subjecting the treated soil specimens to capillary soaking and then testing them as a part of durability studies, test results showed that there was a considerable loss of strength for the 7 days cured soil specimens (Figure 4.2b and 4.2c). In the case of lime and CS-treated soil group, the retained strength was maximum for 15% CS treated specimens. Due to the moisture intrusion in the early curing period, the cementitious bonds formed are generally weak in nature. The formation of additional cementitious phases resulted in considerable strength retention. However, it was noted that with higher replacement of in-situ native soil with CS dosages, the retained strengths were also decreased considerably. This could be primarily attributed to an increased replacement of

the cohesive soil by a cohesionless CS counterpart, and during moisture ingress, the loss of the soil bond strength occurred due to the weakening of the cementitious bonds.

For the NS-treated soils, it was noted that the 0.5% NS dosage retained maximum strength for the 7 days cured specimens. C-S-H being a hydrophilic mineral, excessive formation of C-S-H compounds could lead to an increase in water absorption when subjected to capillary soaking process (Dash and Hussain 2012, Chakraborty and Nair 2020). An increase in water absorption could possibly lead to a rapid loss of strength as compared to unsoaked treated soil specimens. It was necessary to compare the 7-days soaked strength of the treated soil using both statistical factors and engineering judgment such that together the two parameters can be used to determine the most optimized dosages of the co-additives for modifying such soils. The next section discusses the statistical approach adopted for optimization of the co-additive dosages used in this study.

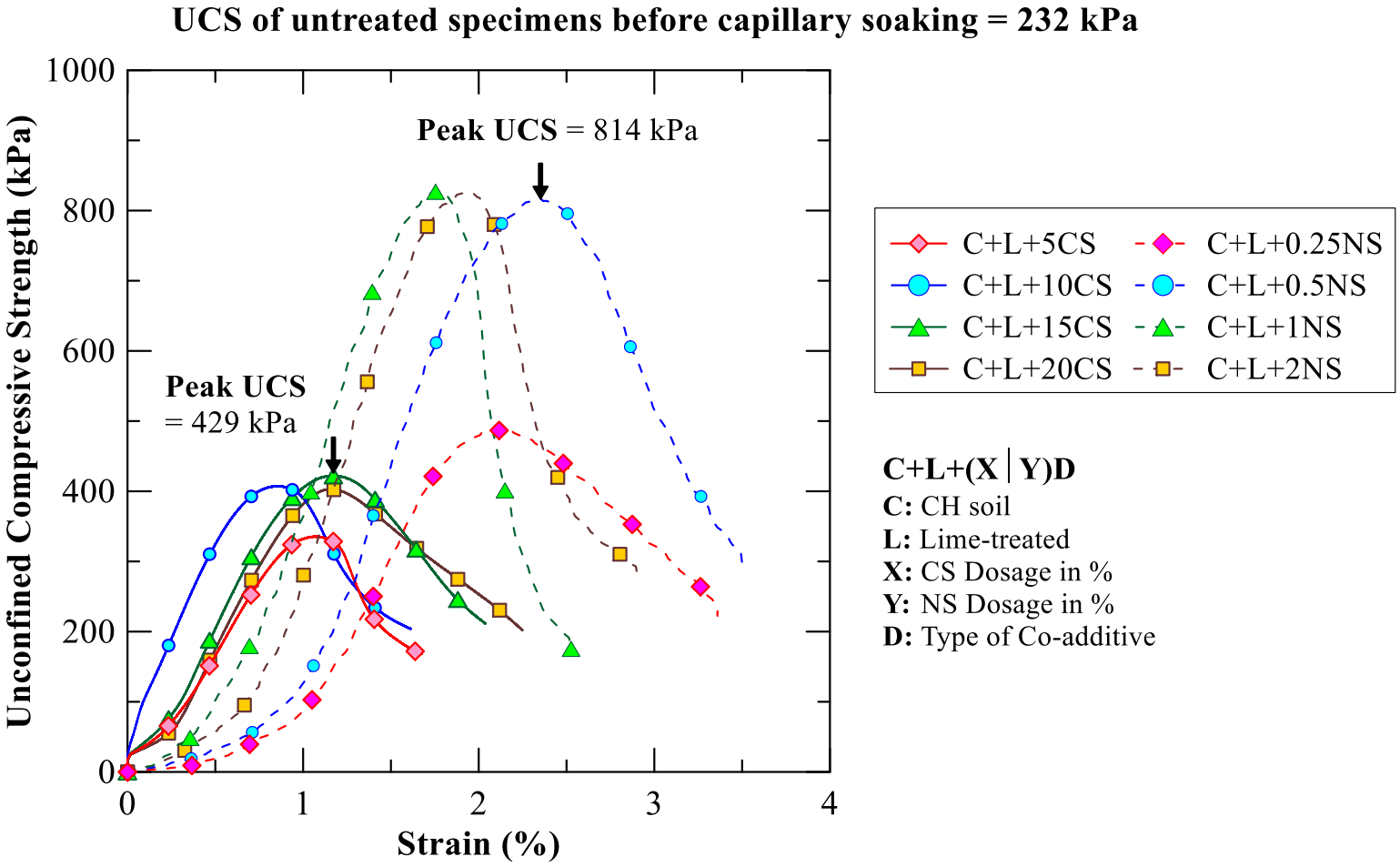
UCS of untreated specimens before capillary soaking = 232 kPa
Peak UCS = 814 kPa
Peak UCS
= 429 kPa
Unconfined Compressive Strength (kPa)
Strain (%)
0
200
400
600
800
1000
0
1
2
3
4
C+L+5CS
C+L+10CS
C+L+15CS
C+L+20CS
C+L+0.25NS
C+L+0.5NS
C+L+1NS
C+L+2NS
C+L+(X | Y)D
C: CH soil
L: Lime-treated
X: CS Dosage in %
Y: NS Dosage in %
D: Type of Co-additive

(a)

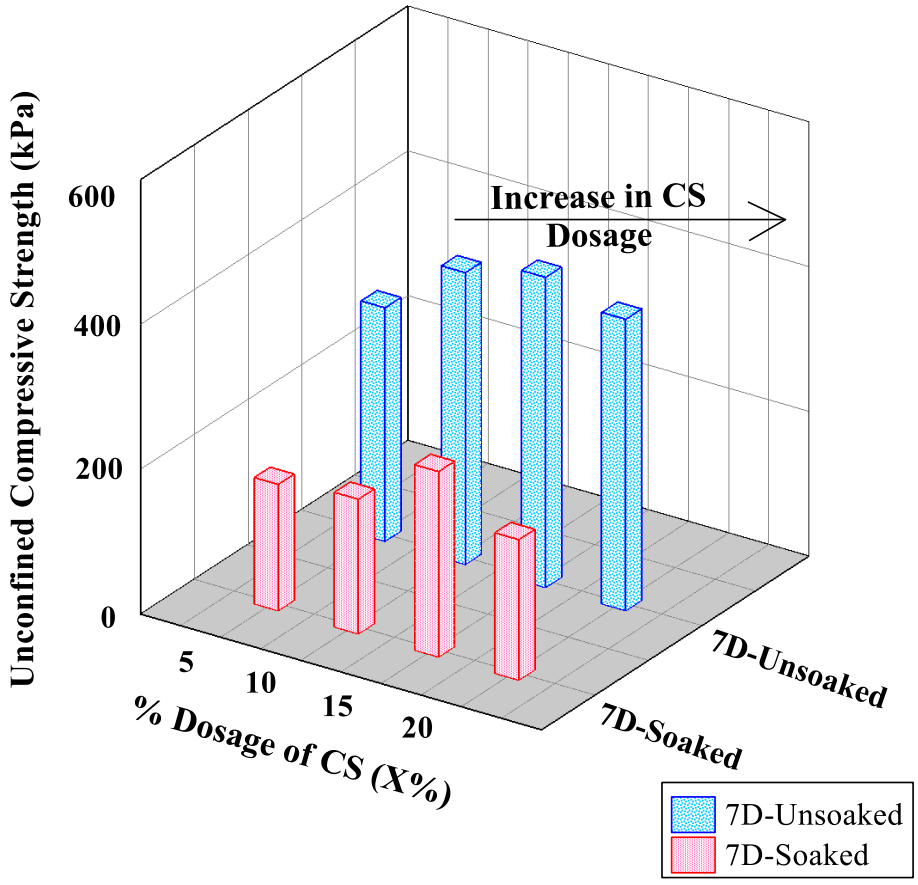
Unconfined Compressive Strength (kPa)
600
400
200
0
Increase in CS Dosage
5
10
15
20
% Dosage of CS (X%)
7D-Unsoaked
7D-Soaked
7D-Unsoaked
7D-Soaked

(b)

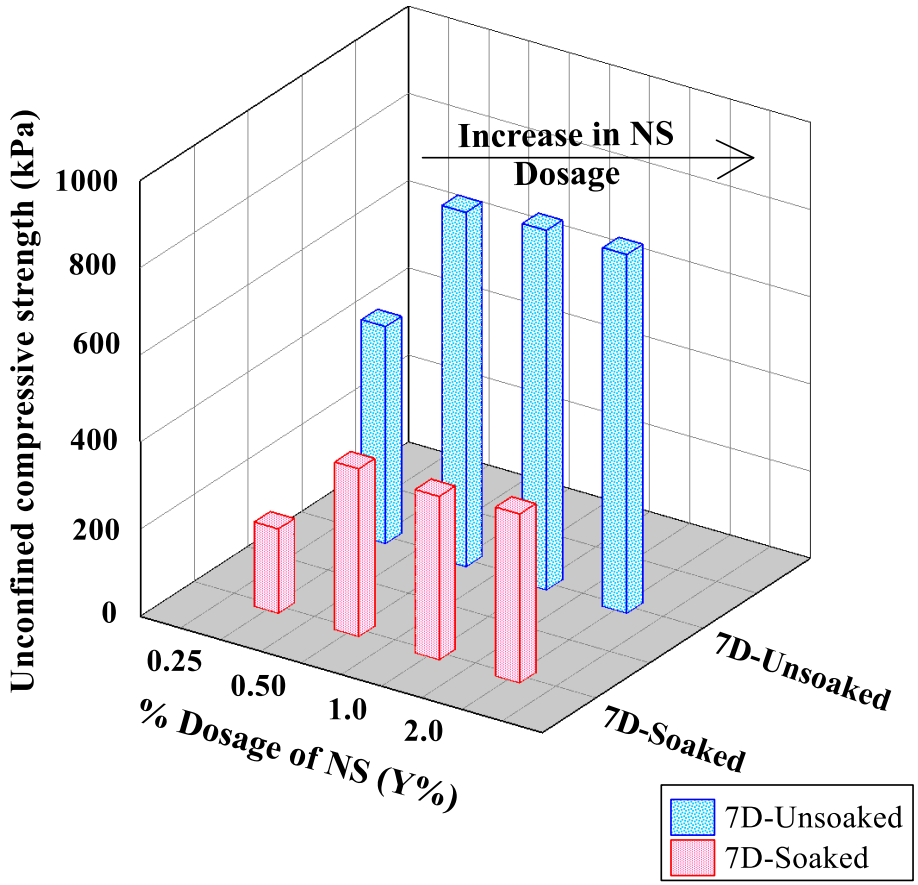

(c)

Figure 4.2 Optimization of co-additive dosage a) Unsoaked strength for different dosage after 7-day curing period; and Soaked strength after capillary soaking for b) CS treatment c) NS

4.3.1.1 One-factor Experiments

The optimization of the dosage of admixture treatment was performed using the statistical framework discussed in the earlier section. Before subjecting the data set to one-factor experiments, the initial checks of normality and homogeneity were performed on the test data (Table 4.1). After the initial assumptions were satisfied, the population data were subjected to one-factor tests, and these results are presented in Table 4.2. The one-factor tests were initially performed separately between the untreated and C+L soils (T_1), untreated and C+L+**X**CS soils (T_2), and untreated and C+L+**Y**NS soil (T_3) (where **X** and **Y** are different dosage percentages of CS and NS co-additives, respectively).

The first experiment, T_1 indicated that the *p*-value is less than the assumed level of significance (<0.05). This showed a statistically significant difference between the mean UCS values of the untreated and lime-treated group. Similar observations were noted for T_2 and T_3 experiments, indicating that at least one of the mean strengths of the treated soils (for both experiments, T_2 or T_3) was significantly different from the means of the untreated control soil group. Hence, the treatment of soil improves its strength due to the formation of cementitious products, and therefore the significant difference in mean values between the groups was noted.

Subsequently, the null hypothesis was tested on the remaining three groups of specimens, i.e., between the C+L and C+L+**X**CS soils (T_4), and C+L and C+L+**Y**NS soils (T_5). From the one-factor tests, it was noted that adding co-additives with lime has significantly affected the 7 days unsoaked strength. The *p*-values between lime-treated soil and lime and CS treated soil (T_4), even though is statistically significant, it primarily

occurred because the average strength from lime treatment was around 550 kPa, and it was significantly higher than the average strength gain of 390 kPa for the lime treated soil when mixed CS. In the case of the soil treated with lime and NS (T_5), the average strength values were much higher (740 kPa) than lime-treated soil alone (550 kPa), and hence it affected the specimen mean UCS values, and subsequently the *p*-values showing statistically significant improvements.

Table 4.1 Check for initial assumptions

Assumption	Parameter	Values	Comments
Normality	Kolmogorov–Smirnov statistic	0.201	
	p-value	0.152	Values are normally distributed
Homogeneity	Levene's statistics	1.212	
	p-value	0.341	Values are homogeneous

Table 4.2 Analysis of variance using one-factor experiments for the unsoaked strength of different soil groups

Specimen Groups	***Source of Variation***	***SS***	***D_f***	***MS***	***F***	***p-value***	***F-crit***
Untreated and C+L (T_1)	Between Groups	106667	1	106667	35.9	3.90×10^{-3}	7.708
	Within Groups	11876.7	4	2969.2			
	Total	118543	5				
Untreated and C+L+**X**CS (T_2)	Between Groups	78791.1	4	19697.77	180.2	2.85×10^{-9}	3.478
	Within Groups	1093.3	10	109.3			
	Total	79884.4	14				
Untreated and C+L+**Y**NS (T_3)	Between Groups	852878.7	4	213219.7	938.2	7.94×10^{-13}	3.478
	Within Groups	2272.6	10	227.2			
	Total	855151.3	14				
C+L and C+L+**X**CS (T_4)	Between Groups	47537.7	4	11884.4	9.9	1.64×10^{-3}	3.478
	Within Groups	11962	10	1196.2			
	Total	59499.7	14				
C+L and C+L+**Y**NS (T_5)	Between Groups	373412	4	93353	71	2.65×10^{-7}	3.478
	Within Groups	13141.3	10	1314.1			
	Total	386553	14				

4.3.1.2 Optimization of co-additive dosage

From the one-factor experiments, it was concluded that the addition of co-additives (either CS or NS) significantly improved the unsoaked strength over lime treatment alone after 7 days of curing. However, one-factor experiments failed to provide conclusive evidence regarding the optimum dosage of either CS or NS, which might have a significant influence on the differences of mean UCS values as compared to lime-treatment alone. Hence, multiple comparison experiments were performed to understand the effects from different dosages of silica co-additives (CS or NS), having significant influence over lime-treated soil results (Table 4.3 and Table 4.4).

The multiparameter analysis was initially tested on unsoaked strengths for lime and CS groups after 7 days of curing and these results are presented in Table 4.3. The Tukey HSD test was unable to provide any definitive conclusions for this set of tests and their results. However, from both Scheffe and Bonferroni *p*-values, it was observed that at 5% CS dosage, the *p*-values are less than 0.05, implying a significant difference between the means of control and test groups. This outcome was recorded because the 5% CS dosage resulted in lower strength in comparison to lime treatment. This could be primarily attributed to the partial replacement of alumino-silicate-rich clay minerals from dry soil as well as insufficient addition of crystalline counterparts to the soil. With an increase in CS dosage (10, 15, and 20%), even though there is an increase in the unsoaked strength of the soil, the difference in the means were insignificant within the groups (10, 15, and 20%). Therefore, for determining optimum dosage of CS co-additive, the effects of moisture intrusion on retained strength was also tested using multiparameter analysis as shown in

Table 5. It was observed that all retained strengths for C+L+**X**CS soils have significant difference between the means as compared to only lime-treated soil. Consequently, in addition to the statistical outcomes, engineering judgement was used to select an optimum dosage for soil treatment (Figure 4.2b). From Figure 4.2b, it could be observed that 15% CS retained the maximum strength i.e., 60% as compared to other dosages. Therefore, 15% CS dosage was considered as optimum dosage for the follow-up laboratory investigations.

In the case of NS additive studies, all three multi-parameter tests on unsoaked strengths (Table 4.3) indicated that the addition of 0.25% NS does not have any significant influence on the differences of means (p-value>0.05). However, the next higher dosage, i.e. 0.5% of NS provided the p-value less than 0.05, validating the assumption of a significant difference of mean strengths between the test groups. From the multiparameter analysis on the retained strengths after capillary soaking period, it was observed that all C+L+**Y**NS treated soil groups were able to produce significant difference of means as compared to lime-treated soils (Table 4.4). However, from the engineering judgement point of view (Figure 4.2c), it was observed that the 0.5% NS retained maximum strength (47%) after subjecting the specimen to capillary soaking. Therefore, based on engineering judgment as well as statistical analysis, 0.5%NS was deemed as the optimum dosage for further studies.

Subsequent sections present both analysis and discussion of results from other engineering tests performed on soils treated with lime and optimum silica dosages including 0.5%NS and 15% CS.

Table 4.3 Multiple comparison statistical studies on unsoaked strengths from treated and untreated soil groups

Groups		Tukey HSD p-Value	Scheffe p-Value	Bonferroni p-Value
Control Group (Mean, kPa)	Test Group (Mean, kPa)			
C+L (498.7)	C+L+5CS (323.3)	1.005×10^{-3}	9.612×10^{-4}	4.869×10^{-5}
	C+L+10CS (403)	31.955×10^{-3}	191.567×10^{-3}	55.602×10^{-3}
	C+L+15CS (429.7)	233.820×10^{-3}	607.622×10^{-3}	605.138×10^{-3}
	C+L+20CS (403)	3.195×10^{-3}	191.567×10^{-3}	55.602×10^{-3}
C+L (498.7)	C+L+0.25NS (498.3)	899.995×10^{-3}	999.897×10^{-3}	20.535
	C+L+0.5NS (812.7)	1.005×10^{-3}	8.989×10^{-9}	1.803×10^{-10}
	C+L+1NS (825.3)	1.005×10^{-3}	4.578×10^{-9}	8.976×10^{-11}
	C+L+2NS (823.3)	1.005×10^{-3}	1.789×10^{-9}	3.410×10^{-11}

Table 4.4 Multiple comparison statistical studies on soaked strengths from treated and untreated soil groups

Groups		Tukey HSD p-Value	Scheffe p-Value	Bonferroni p-Value
Control Group (Mean, kPa)	Test Group (Mean, kPa)			
C+L (148.1)	C+L+5CS (175.0)	1.613×10^{-2}	3.319×10^{-2}	2.423×10^{-2}
	C+L+10CS (182.3)	3.221×10^{-3}	7.447×10^{-3}	4.528×10^{-3}
	C+L+15CS (255.9)	1.005×10^{-3}	4.506×10^{-7}	1.939×10^{-7}
	C+L+20CS (195.7)	1.005×10^{-3}	6.400×10^{-4}	3.280×10^{-4}
C+L (148.1)	C+L+0.25NS (196.4)	8.603×10^{-3}	1.863×10^{-2}	1.254×10^{-2}
	C+L+0.5NS (385.3)	1.005×10^{-3}	2.219×10^{-8}	9.342×10^{-9}
	C+L+1NS (376.0)	1.005×10^{-3}	3.237×10^{-8}	1.365×10^{-8}
	C+L+2NS (391.3)	1.005×10^{-3}	1.715×10^{-8}	7.212×10^{-9}

4.3.2 Engineering Tests on Lime and Both Silica Treated Soils at Optimum Dosage Conditions

4.3.2.1 Strength and durability studies

Lime-treated soils continue to gain strengths even after several years of treatment, but a substantial strength gain is generally observed during the first few months after treatment (Townsend and Donaghe 1976, Little and Nair 2009c, Chakraborty and Nair 2020). Therefore, for comparison purposes, the rate of development of strength was compared to maximum strength of the treated soil at the end of 28 days curing period. The 28 days average UCS values of C+L, C+L+15CS, and C+L+0.5NS treated soil groups were 753 kPa, 823 kPa, and 889 kPa, respectively.

After 7 days of curing, the C+L, C+L+CS and C+L+NS treated soil groups showed average UCS values of 498 kPa, 429 kPa and 814 kPa, respectively. The strength gain is plotted as a percentage of the maximum strength (28-day cured strength) for different soil groups and for all three curing periods (0, 3 and 7 days) and this is presented in Figure 4.3a. For the lime-CS treated soil, it could be observed that the percentage of strength gain after 7 days is the lowest among all the treated soil groups even though it has a higher long-term strength after 28 days curing when compared to lime treated soil. This could be attributed to the partial replacement of natural soil silicates and aluminates by the CS additive during initial curing period. The crystalline counterpart from the CS co-additive might have reacted over a longer curing period and formed additional cementitious phases as compared to lime treatment alone.

For the NS-treated soil, it could be observed that there is an accelerated development of strength, and it reaches about 90% of the ultimate strength within the first 7 days of the treatment. The presence of amorphous nanoparticles provides a large specific surface area for the enhanced chemical reactions between the Ca^{+2} ions from lime and silica particles. The available nano-silica particles in NS-treated soils form the C-S-H phases immediately after the treatment, which is corroborated using microstudies in the later sections. These factors contribute to the rapid strength gain for the NS-treated soils when compared to lime-treated and lime-CS-treated soils.

The average UCS values of the treated soil groups =both before and after subjecting the specimens to capillary soaking are shown in Figure 5b and 5c. It was observed that immediately after the treatment with lime or lime plus co-additives, there is a substantial improvement in the unconfined compression strength (UCS) property (Figure 4.3a). This occurs primarily due to 'modification′ reactions among stabilizers and soil particles. Figure 5c shows the average retained strength of the treated specimens when subjected to moisture conditioning for 48 hrs.

From Figure 4.3c, it could be noted that during the early curing period, there was an appreciable loss of unconfined strength for all treated groups. The pozzolanic reactions are generally a time-dependent phenomenon, and as a result, during the early curing periods, there is no substantial development of C-S-H phases, which could provide sufficient bonding to the soil particles (Dash and Hussain 2012, Chakraborty and Nair 2020). Due to moisture intrusion of the treated soils during initial curing period, there

could be a possible weakening of the cementitious bonds, and this may have contributed to the decrease in strength values.

For the soils treated with lime and co-additives, the strength loss from moisture conditioning is 20-30% lower as compared to lime treatment alone. For the CS dosage, percentage loss is minimum because of two possible reasons, due to a partial replacement of clay by crystalline silica and the presence of a higher reactive specific surface area and broken bonds at the edges of the silica particles. Due to these two factors, less water was absorbed by the soil particles, and subsequently additional broken bonds provided active sites for the formations of cementitious phases, respectively.

For the NS treated soil, a small percentage of dosage provides a significant specific surface area of ~140 m^2/g of reactive amorphous silica particles uniformly distributed in the soil matrix. These nano-sized silica particles provide reactive surfaces and higher potential of chemical reactions with the available Ca^{+2} ions from the Ca-based stabilizer and immediately develop cementitious bonds. These additional C-S-H phases are instrumental in preventing loss of strength during a shorter curing period after treatment. Microstructural and mineralogical studies performed in the later sections have provided ample proofs of the rapid formation of cementitious phases to validate the observations recorded from the engineering properties.

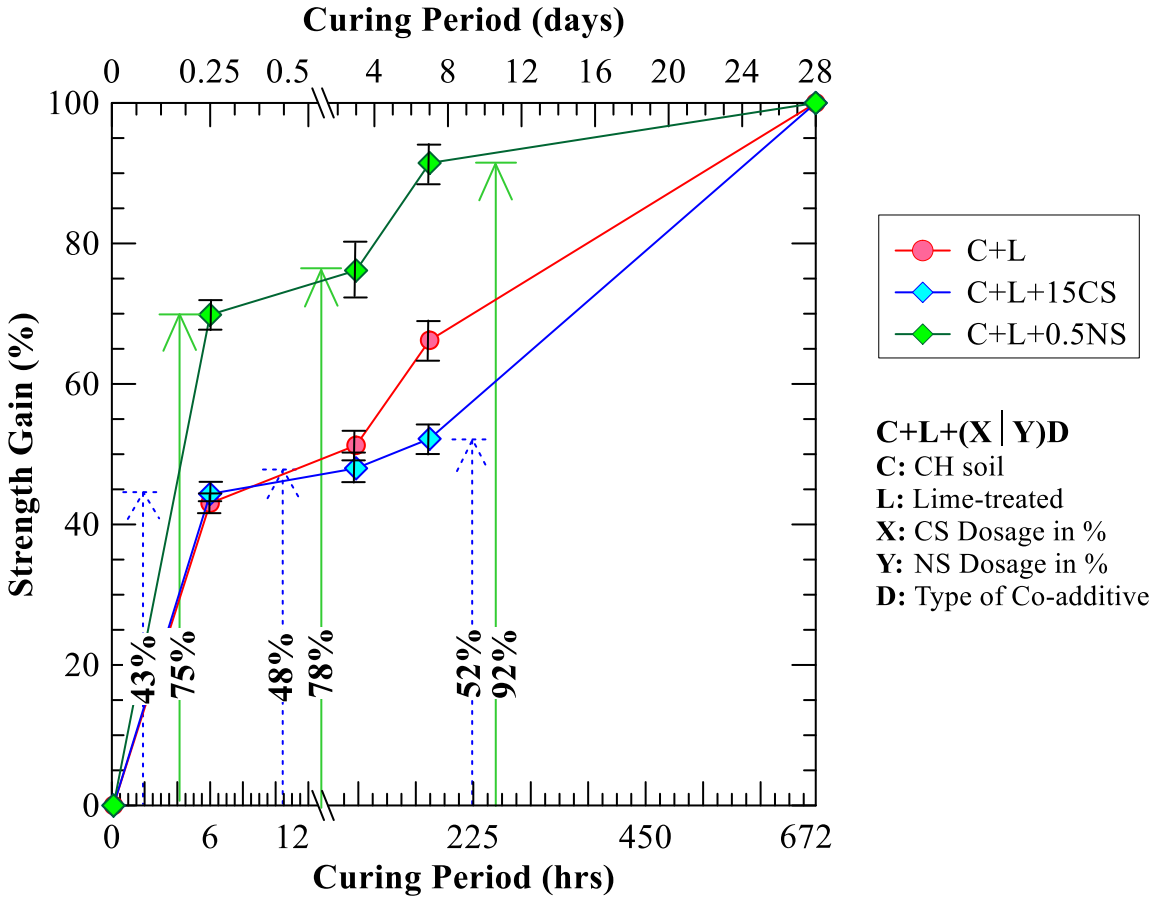
Curing Period (days)
0
0.25
0.5
4
8
12
16
20
24
28
100
80
60
40
20
0
Strength Gain (%)
43%
75%
48%
78%
52%
92%
0
6
12
225
450
672
Curing Period (hrs)
C+L
C+L+15CS
C+L+0.5NS
C+L+(X | Y)D
C: CH soil
L: Lime-treated
X: CS Dosage in %
Y: NS Dosage in %
D: Type of Co-additive

(a)

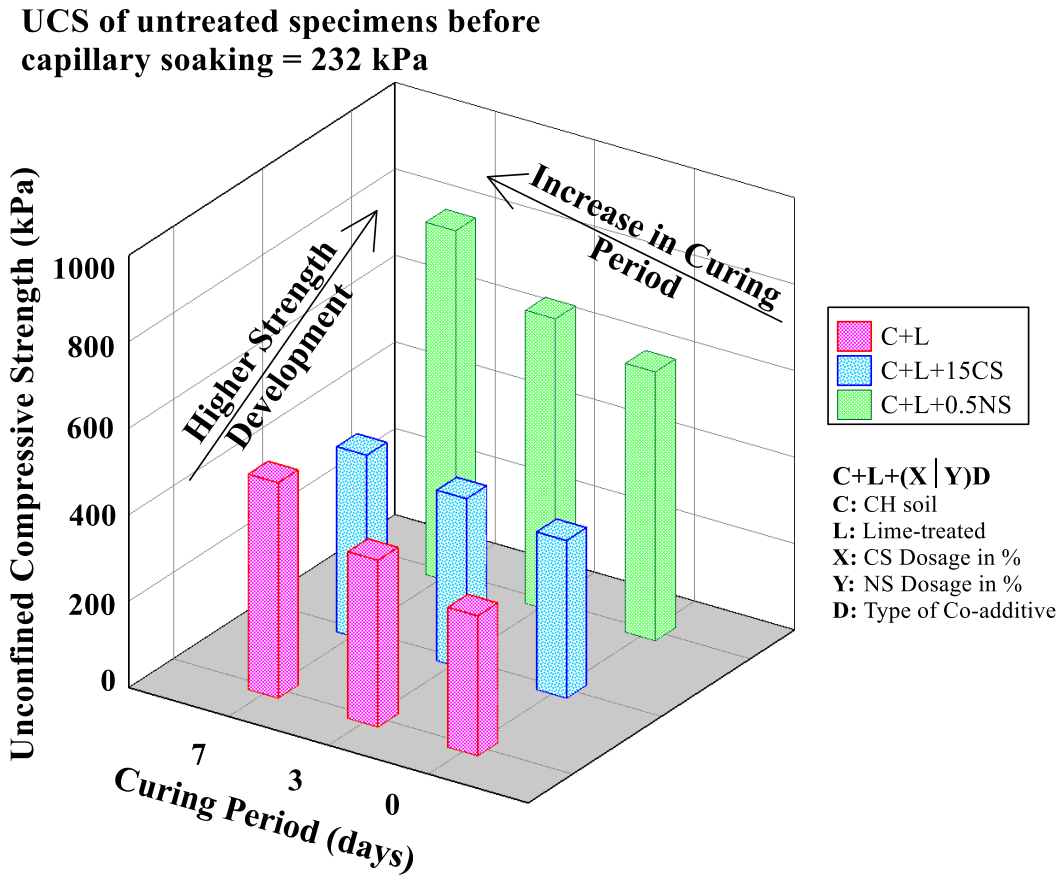
UCS of untreated specimens before capillary soaking = 232 kPa
Unconfined Compressive Strength (kPa)
1000
800
600
400
200
0
Higher Strength Development
Increase in Curing Period
7
3
0
Curing Period (days)
C+L
C+L+15CS
C+L+0.5NS
C+L+(X | Y)D
C: CH soil
L: Lime-treated
X: CS Dosage in %
Y: NS Dosage in %
D: Type of Co-additive

(b)

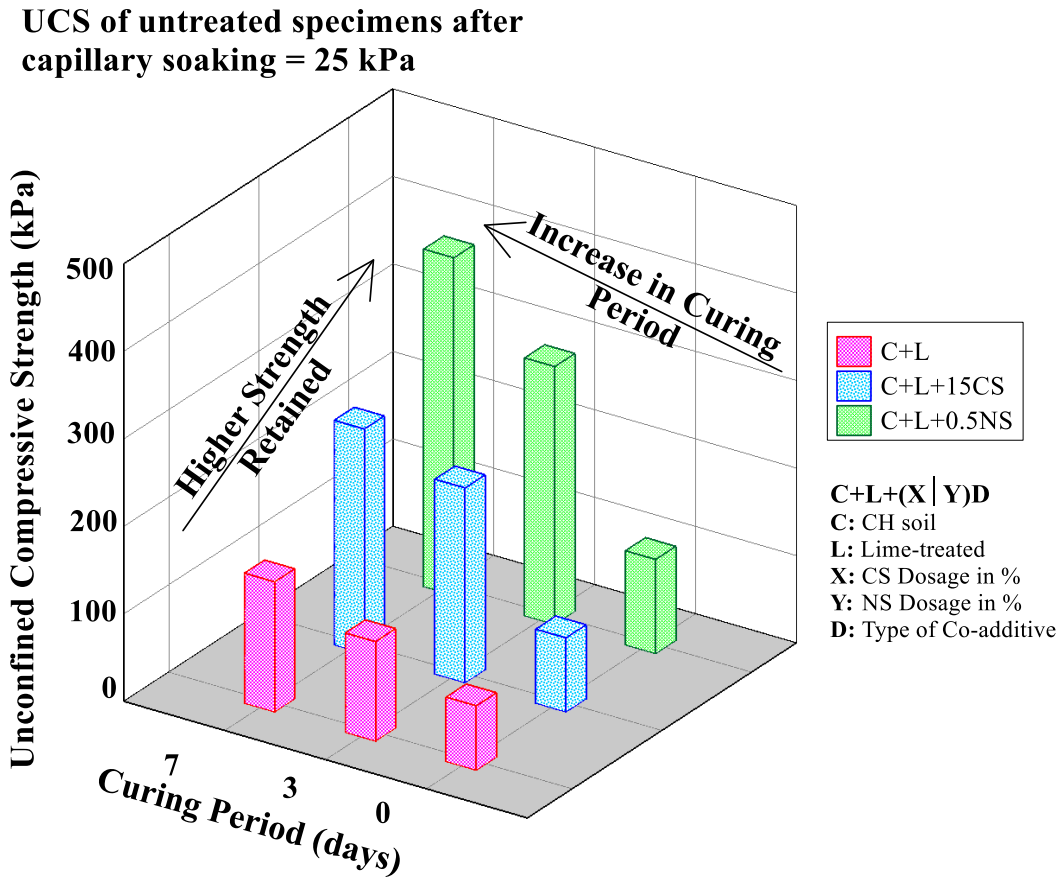

(c)

Figure 4.3 Effect of curing period of different treatments a) Percentage of strength gain with respect to 28 days strength, b) Unsoaked UCS, and c) UCS after 48 hours of capillary soaking

4.3.2.2 Free Swell Strain and Linear Shrinkage Strain Test Results

During the initial curing period (≤ 7 days), in addition to the rapid development of strength gains, the application of co-admixtures should improve other engineering properties such as free swell and shrinkage strains. Figure 4.4 shows the free swell strains for all soil groups after 0 day (6-hours), 3 and 7 days of curing period. The untreated soil has a free swell strain of 15% and could be classified as problematic high-swelling soil. For serviceability criteria, it is generally expected that after chemical treatment at a select curing period, the soil should undergo swelling less than 2-3%. Figure 4.4a shows the free swell strain curves immediately (6-hours) after treatment. In treated soil specimens, the free swelling strain was reduced as compared to untreated soil specimens. In lime-treated soil, the 'modification' reactions, including well established cation exchange and flocculation-agglomeration reactions, are known to be responsible for the observed improvements (Little 1999, Puppala et al. 2016, Chakraborty et al. 2020)

In lime and CS-treated specimens, there was a further reduction in swell strains immediately after the treatment. This could be attributed to two primary reasons, first the initiation of 'modification' reactions due to the addition of a lime binder to the soil, and second is due to the partial replacement of high swelling CH soil with a non-swelling crystalline silica counterpart. For the NS treated soil specimens, adding a small dosage of NS provides a considerable quantity of reactive silica phases which immediately reacts with the Ca^{+2} ions from lime and forms cementitious compounds. The C-S-H phases formed bonds with the soil matrix and prevented the repulsive swelling forces due to moisture intrusion during the tests.

The free swell strains of different treated soil groups after 3 and 7 days curing periods are presented in Figure 4.4b and 4.4c. Treated soils showed a lower free swell strain percentage as compared to untreated or 0 day treated soil specimens. This is attributed to the pozzolanic reactions and the formation of cementitious compounds that bond the soil particles together. In the case of the lime and CS-treated soil specimens, both partial replacement of high plasticity (PI) clays with low swelling sand and formation of additional cementitious phases on the broken edges of the admixture helped to reduce the swell strain percentage values when compared to lime treatments alone.

Since the pozzolanic reactions are slow and typically take place over a longer curing period, this slow rate of reactions has not yielded immediate reductions in free swell strains. When the NS co-additive is added to the lime-treated soil, the highly reactive surfaces immediately accelerate the reactions and produce a substantial quantity of cementitious gels. This additional C-S-H phase plus the cementitious compounds from the pozzolanic reactions might have helped to substantially decrease the free swell strain after 3 and 7 days of curing as compared to traditional treatments.

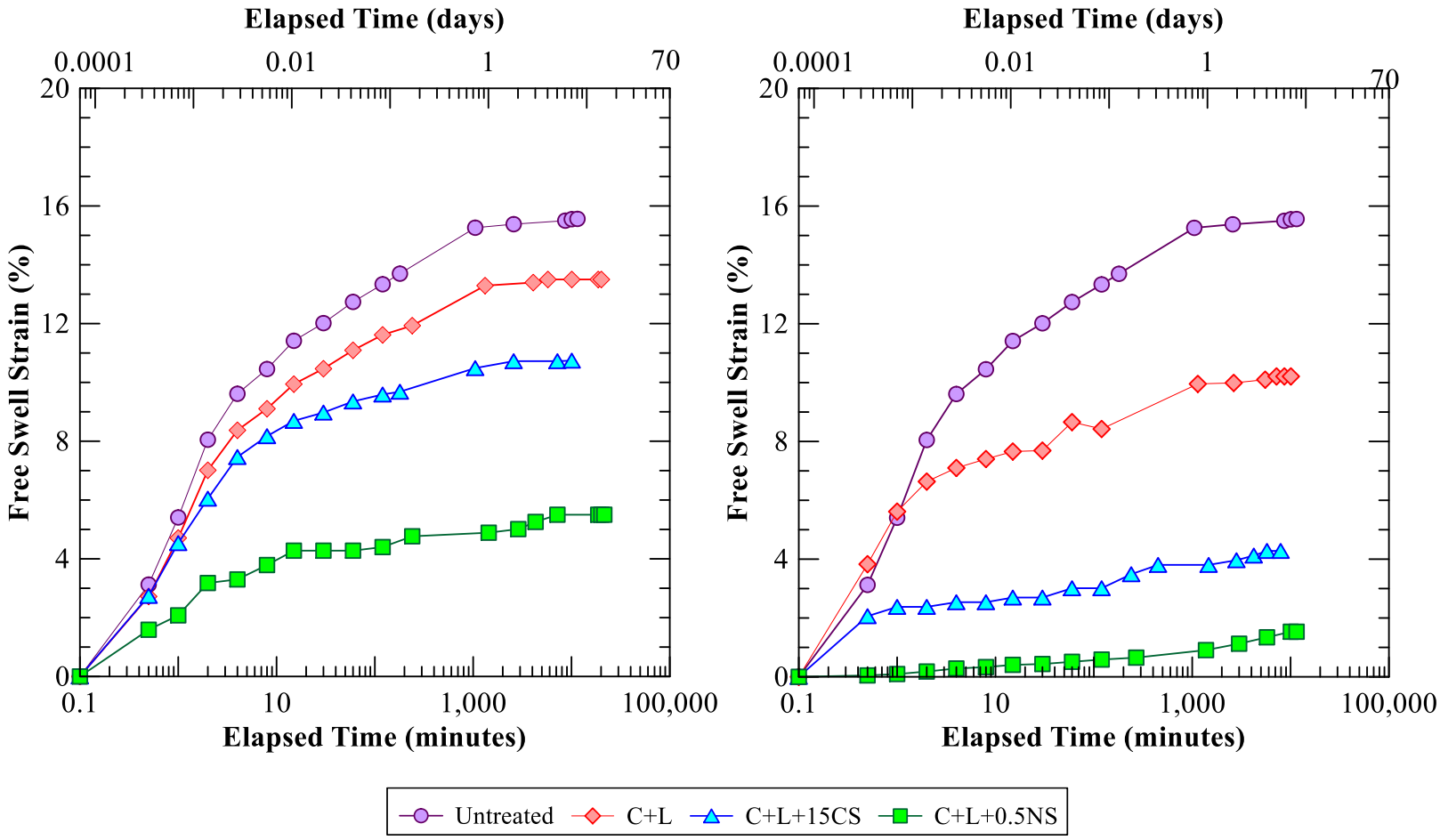
Elapsed Time (days)
0.0001
0.01
1
70
Free Swell Strain (%)
0
4
8
12
16
20
0.1
10
1,000
100,000
Elapsed Time (minutes)
Untreated
C+L
C+L+15CS
C+L+0.5NS

(a) (b)

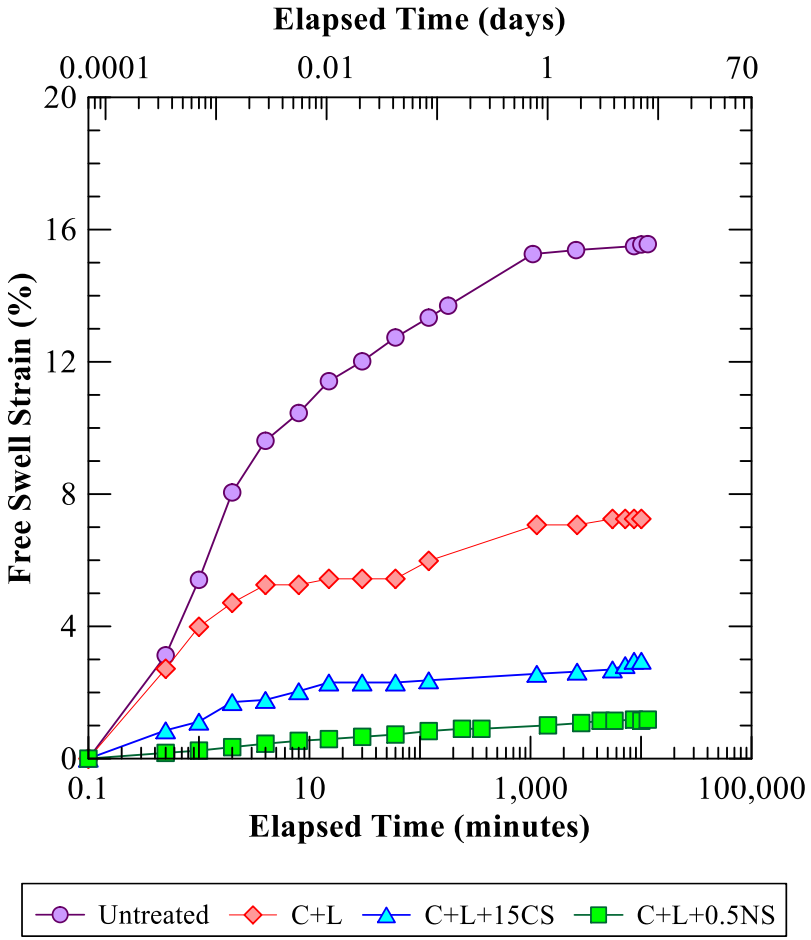

Figure 4.4 Free-swell strains of untreated and treated soils after a) 0-day (6 hrs) b) 3 days and c) 7 days

Cyclic swelling and shrinkage strains of expansive subgrade material causes a deleterious impact on pavement performance. The shrinkage of soils due to drying is a significant cause of concern for pavement infrastructure. Figure 4.5 shows the linear shrinkage strain of the untreated and treated soil groups over different curing periods. The untreated soil has a shrinkage strain of 14.5%, which is recognized as a major problematic soil condition for expansive soils. Adding Ca-based stabilizer to the untreated soil reduced the moisture affinity by neutralizing the surface charges with divalent calcium ions; the resulting treated soil absorbed less water ions and subsequently experienced lesser drying of the absorbed water, hence lower shrinkage cracks were formed in the soil.

Inclusion of the CS admixture to the high-PI clay improved the soil shrinkage cracking resistance due to partial replacement of high-plasticity clay minerals with coarse-grained CS-material. Similar to CS amendment, NS also helped to improve the linear shrinkage properties of the high PI clay by enhancing the formation of cementitious gels in the treated soil. From Figure 4.5, it is noted that the addition of NS immediately helps to reduce the soil shrinkage. Due to the presence of an appreciable quantity of nano-silica particles, the highly reactive amorphous silica forms additional C-S-H phases. This along with the filler properties of the nano-particles, helped to form bonds between the soil particles and develop a denser geomaterial matrix which subsequently prevented it from undergoing considerable shrinkage strains during drying conditions.

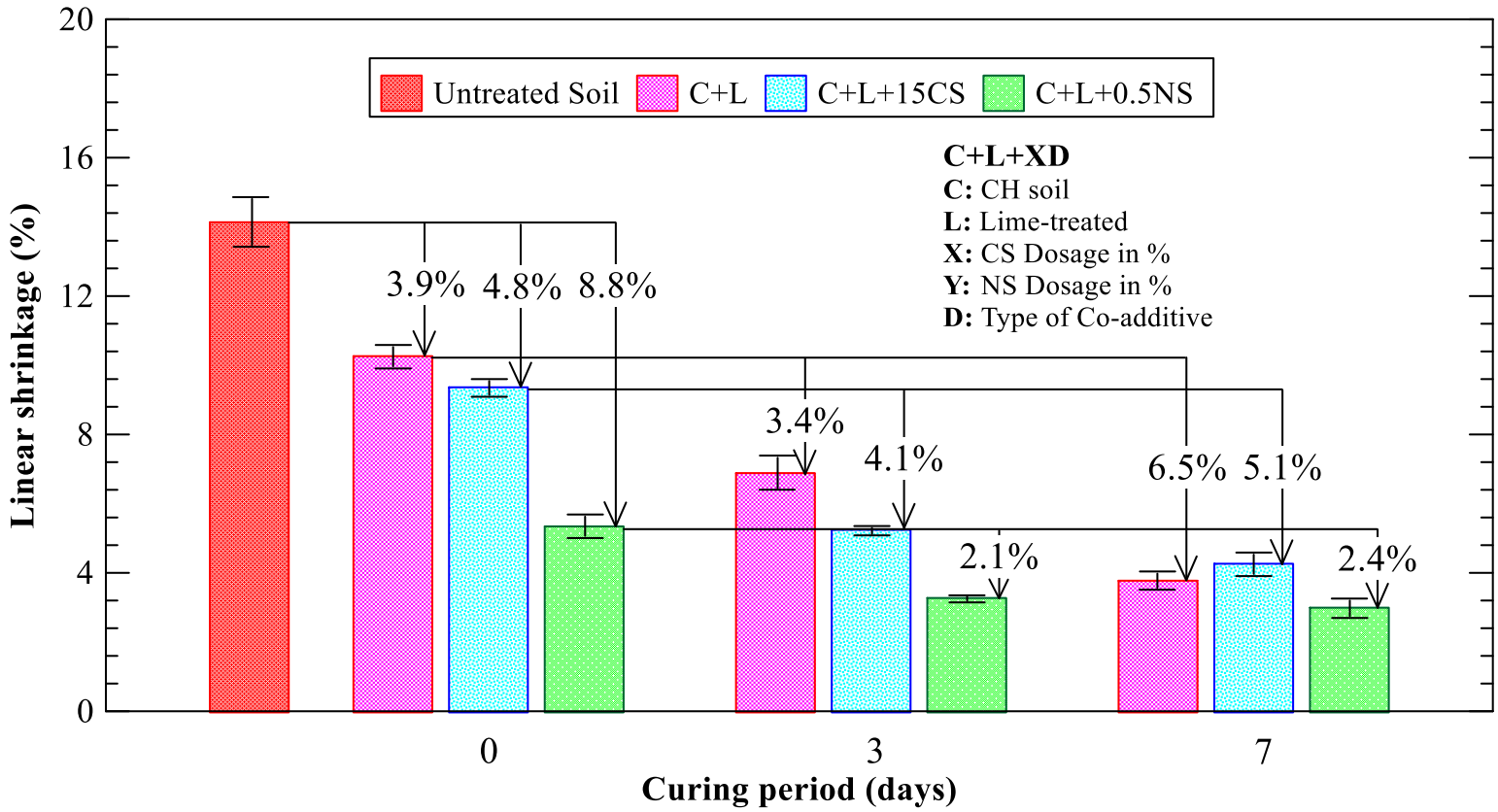

Figure 4.5 Linear shrinkage strain for untreated and treated soil specimens

4.3.2.3 Stiffness or Resilient Properties

The test consists of 15 different combinations of confining and deviatoric stresses, representing different stress conditions in the field. However, for the ease of representation of the overall influence of chemical treatment, the values are represented in the form of universal model constants (Table 4.5).

The k_1 parameter is proportional to the resilient modulus of the specimens. From Table 6, it could be noted that immediately after lime treatment, the k_1 parameter values are close for lime treated and C+L+15CS treated soil specimens. However, for the NS-treated soil specimens, there is a rapid increase in the parameter immediately after the treatment (6 hrs). With an increase in the curing period, there was a gradual increase in the resilient moduli for all treated soil groups. Overall, after 7 day curing period, the maximum increase in the elastic modulus was observed for the CS-treated soil groups. The presence of crystalline counterparts in the treated soil influenced the improvement in the moduli, whereas for NS, the additional amorphous gels within the pore structures increased the overall cohesion and reduced the inter-particular friction and subsequently affecting the elastic moduli.

The k_2 parameter represents the effect of bulk stress on the RLTT values. No definite conclusions could be drawn on the trends of the k_2 parameters in this study. The k_3 parameter, which represents the effect of the shear stress term on the soil modulus. A negative k_3 value represents a weak soil, as an increase in shear stress reduces the M_r value of the soil. A positive k_3 value with an increase in curing time period represents a strain hardening effect, a typical characteristic of treated soil materials. For the C+L and

C+L+15CS treated soil groups, the rate of increase in the k_3 value was lower when compared to those of the C+L+0.5NS soils. Therefore, at the end of 7 days of the curing period, although the overall resilient modulus of the soil groups treated with NS was lower than the rest of the treated soil groups, the improvement in strain hardening effect was significantly higher than the remaining treatment techniques.

Therefore, based on the strength studies before and after capillary soaking in the previous section, as well as the resilient modulus studies here, an important finding was noted that the NS may provide considerable strength enhancements than the moduli enhancements, and this is attributed to the size and composition of NS particles.

Many observations from previous sections on CS and NS treated soils needed further verification and validation and as a result, micro soil behavior studies were performed on the treated soils. The next section discusses microstructural studies performed to develop a holistic idea of these novel chemical treatment techniques.

Table 4.5 Universal model parameters from resilient modulus (M_r) test on treated soil groups

Curing Period (days)	k_1			k_2			k_3			R^2		
	C+L	C+L+15 CS	C+L+0.5NS	C+L	C+L+ 15CS	C+L+0.5 NS	C+L	C+L+15 CS	C+L+0.5 NS	C+L	C+L+ 15CS	C+L+0.5 NS
0	1426.34	1469.83	1746.84	0.15	0.17	0.092	-0.92	-0.75	0.13	0.92	0.95	0.94
3	1868.56	1758.51	1801.81	0.15	0.14	0.257	-0.20	0.21	0.30	0.86	0.91	0.94
7	1859.20	2088.03	1822.01	0.14	0.11	0.180	0.34	0.65	0.54	0.89	0.95	0.90

Note: k_1, k_2, and k_3 are the universal model parameters

4.3.3 Mineralogical and Microstructural analyses

The effects of co-additives when mixed with traditional stabilizer were analyzed using microstructural studies. The Field Emission Scanning Electron Microscopy (FESEM) was first performed to study the differences in the morphological changes that occurred due to different treatments, as shown in Figure 4.6. Figure 4.6a and 4.6b presents the untreated soil at 1000x and 2000x magnification, respectively. The SEM image at 1000x shows the typical honeycomb structures typically observed in clayey soils. With further magnification (2000x), it could be noted that there is a substantial amount of small flaky to rounded shaped particles with open-pore structures. Figure 4.6c and 4.6d show the images of 7 days cured C+L+15CS treated specimens under 1000x and 2700x, respectively. The addition of lime and CS additives helps to form cementitious compounds, which provide additional bonds to improve the soil properties. The SEM image at higher magnification (2700x) reveals cementitious phases formed at the edges of the soil particles. The presence of these cementitious phases helped to retain strength after being subjected to the capillary soaking process and subsequently prevented volumetric strains in the treated soil specimens, as compared to the untreated soil.

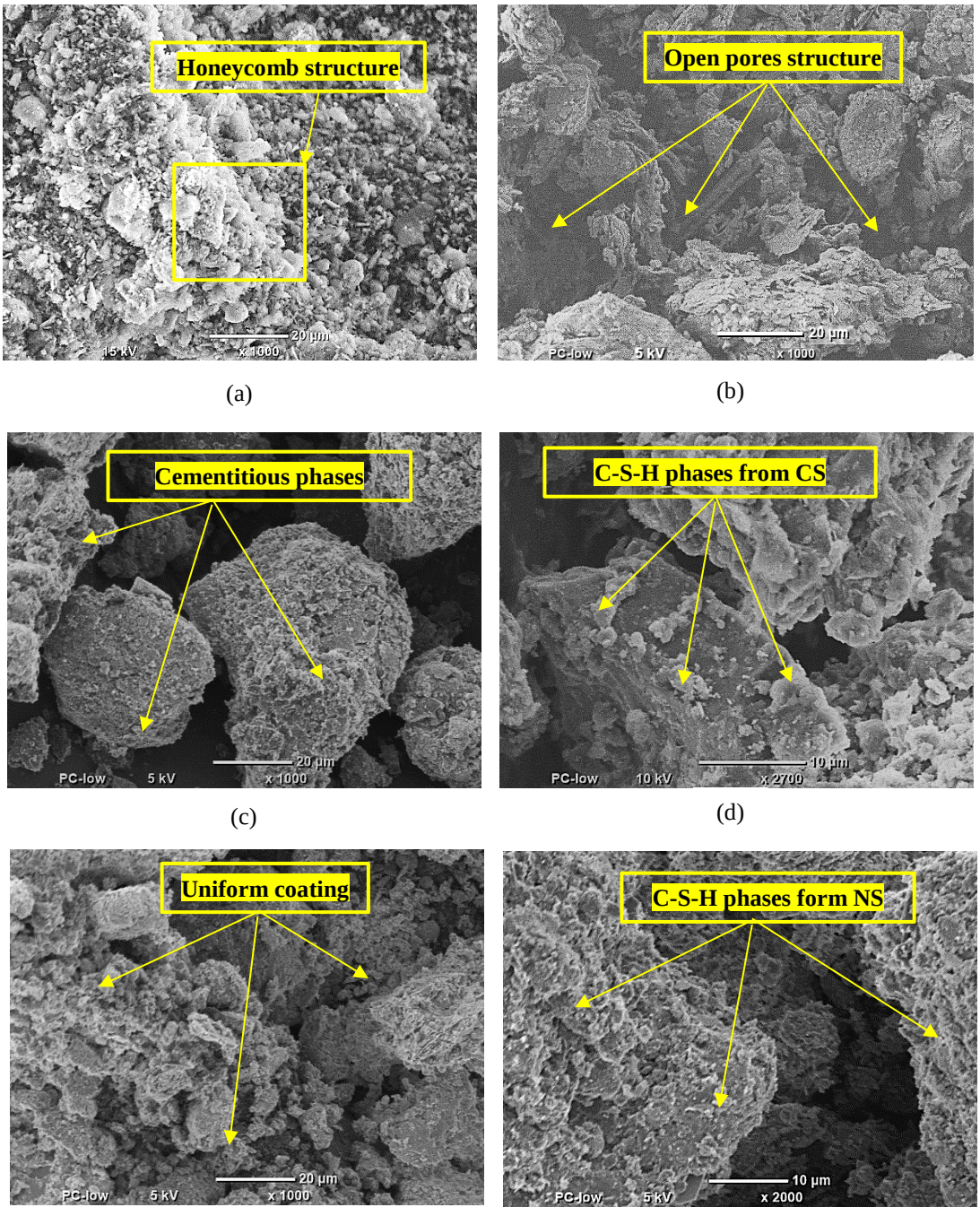

Figure 4.6 FESEM images under different magnification a) Untreated soil (1000x) b) Untreated soil (2000x) c) C+L+15CS (1000x) d) C+L+15CS (2700x) e) C+L+0.5NS (1000x) f) C+L+0.5NS (2000x)

The soil specimen treated with lime and NS binders and cured for 7 days is shown in Figure 4.6e and 4.6f. Under 2000x magnification, it could be noted that the soil particles are coated with a uniform matrix of C-S-H phases due to the NS treatment as well as the open voids are filled up due to the addition of nanoparticles. The addition of NS helps to develop cementitious products, which provides a strong soil matrix. These additional cementitious phases, along with the time-dependent pozzolanic reactions could have provided rapid enhancements in the engineering properties as observed in the previous sections. However, from the SEM images, no conclusive proofs were obtained regarding the accelerated chemical reactions. To verify the hypothesis of accelerated precipitation of C-S-H to rapidly improve the engineering properties, XRD studies on the silica-based co-additives with lime are presented in the following sections to confirm and provide conclusive evidence of accelerated chemical reactions.

Figure 4.7 represents the X-ray diffractograms for the two different co-admixtures treated with dolomitic hydrated lime. The XRD patterns of an untreated NS and CS co-additives are shown in Figure 4.7a and 4.7b. Being amorphous in nature, no definitive peak was observed in the NS powder, rather a characteristic hump associated with amorphous compounds can be observed between 2θ values of 20°-25°. The CS showed primarily the Quartz peaks at 20.84°, 26.63°, 36.51°, 39.47°, 42.41°, 50.12° and 59.91° and some K-feldspar (Orthoclase) peaks at 13.66°, 27.11° and 27.59°. Since the Quartz sand used to prepare the CS was obtained from a natural source, the presence of K-Feldspar was observed possibly due to the mineral stability and genesis from the parent rock.

Immediately after the addition of the lime dosage to the NS and CS co-additives, a number of new peaks were observed in the diffractograms. The primary peaks of Portlandite ($Ca(OH)_2$) and Brucite ($Mg(OH)_2$), were observed due to their presence in the Ca-based stabilizer. The characteristic Calcite peaks were observed due to the partial carbonation of the hydrated lime in the presence of CO_2 from the surrounding atmosphere. Since the reactions were not conducted in a nitrogen-controlled environment to simulate actual field situations, substantial Calcite formation was noted with the progress of the reactions. Immediately after the addition of lime to NS, some cementitious C-S-H phases were observed, which are visible from peaks ranging between 31° and 32° in the diffractograms. These peaks possibly developed from the immediate precipitation of C-S-H phases due to rapid reactions between the Portlandite and NS particles. The relative intensity of the amorphous hump is significantly low on 0-day because of the presence of substantial quantity of crystalline compounds from the dolomitic lime. In contrast, no immediate changes were distinctly visible in the CS and lime-treated specimen diffractogram.

After three days of curing, in the lime and NS treated specimens, none of the Portlandite peaks were visible. Portlandite being more soluble than Brucite, releases Ca^{+2} ions, which reacts with the available amorphous NS powders and form C-S-H phases. Distinct C-S-H peaks at 31.86° and 49.71° are noted after three days of treatment, corroborating the observations. Additionally, it was also observed that no relative increase in the Calcite peaks during the same period, indicating that the majority of Ca^{+2} was used to form C-S-H phases rather than carbonation reactions. With the increase in curing

period, there was a relative reduction in the Brucite peaks as compared to 3-days curing period as well as a distinct C-S-H peak is visible at 31.86° confirming the formation of C-S-H gels rapidly in the presence of NS and dolomitic hydrated lime. Furthermore, it was observed that the relative intensity of the amorphous hump increased over curing period, indicating the maximum utilization of the crystalline compounds in the stabilizer to form amorphous cementitious C-S-H phases. This rapid formation of the C-S-H phases provides additional sources of cementitious gels in addition to the pozzolanic reactions from the lime-soil reactions and helps to improve the engineering properties rapidly during the early curing period.

CS treated specimens with lime shows no rapid changes immediately during the early curing period. After 3 and 7 days of curing, most of the Portlandite and Brucite peaks were visible in the diffractogram. At the end of 7 days curing, it was observed that there was a decrease in the relative intensity of the Portlandite peaks at 18.08° and 34.11°, along with a number of amorphous peaks of C-S-H are visible between 31° and 32° in the diffractograms. This indicates chemical reactions between the crystalline silica co-additive and the calcium ions, which produces cementitious phases.

These cementitious phases are responsible for providing additional strength at the end of longer curing period (28 days). Therefore, from the microstudies it was noted that during the early curing period the precipitation of cementitious phases produced by amorphous NS was quicker in comparison to the CS co-additive. CS co-additives are crystalline in nature and have a relatively low-specific surface, whereas NS being

amorphous in nature consists of high-specific surface area of reactive silica which when treated with lime, immediately forms additional cementitious phases.

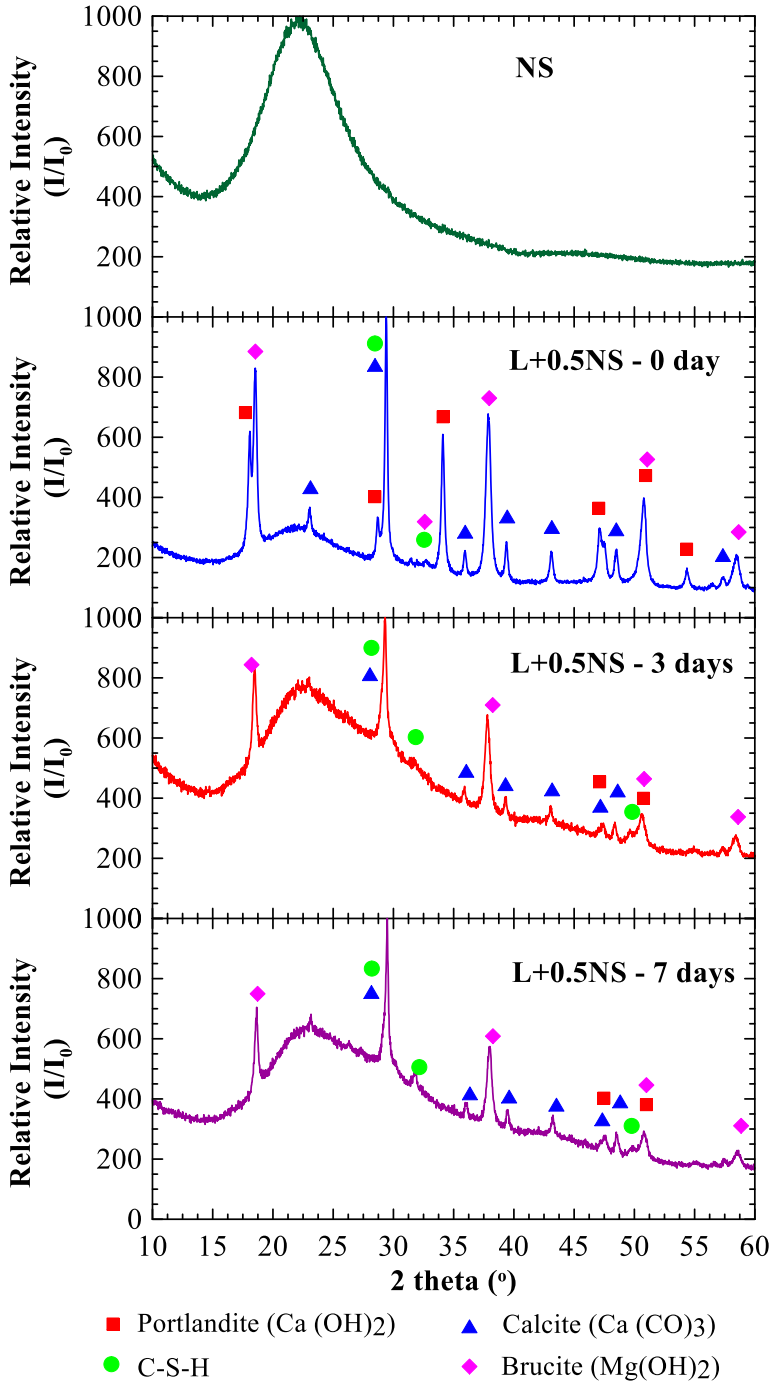

(a)

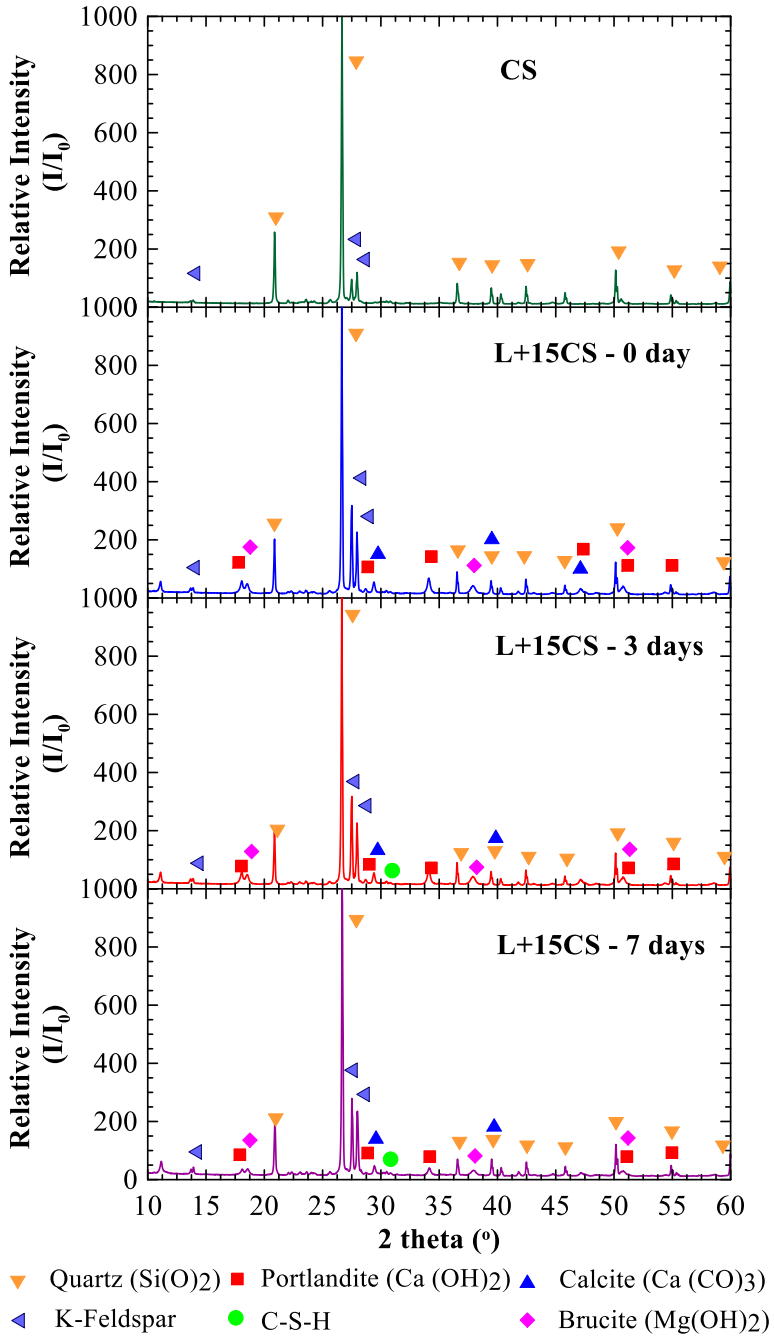

(b)

Figure 4.7 XRD pattern over different curing periods for specimens of lime mixed with silica-based co-additives a) nano-silica (NS) b) crystalline silica (CS)

4.4 Summary

A laboratory investigation was undertaken to study the effects of silica-based co-additives on accelerating the improvements in engineering properties of problematic soils when mixed with traditional Ca-based stabilizers. Two silica-based co-additives, crushed silica or CS and nano-silica or NS were studied, and their efficacy in stabilization performance was compared for early curing periods. Some major conclusions from this chapter are listed below:

- Silica-based co-additives have a significant influence on modifying the properties of expansive soils when added with dolomitic-hydrated lime.
- Based on 7-day unconfined strength, retained strength and statistical analysis using one-parameter and multi-parameter studies, dosages of 15% of CS and 0.5% of NS were determined as optimum dosages with 6% lime.
- NS co-additive has a significant influence on rapidly accelerating the strength, durability, free swell, and shrinkage of the treated soil within the first 3 days of the curing period.
- The resilient modulus properties of the CS-treated soils were observed to be moderately higher than the NS soils due to more inter-particular friction from CS materials.
- Microstructural studies indicated that both CS and NS treated soils are helpful to form additional C-S-H phases uniformly distributed in the treated soil.

Overall, the research study results in this chapter provides some insights on the effects of novel silica-based co-additives to modify the reaction kinetics.

5. APPLICATION OF SILICA-BASED CO-ADDITIVES WITH CALCIUM-BASED STABILIZER TO IMPROVE SULFATE-RICH SOILS

5.1 Introduction

Chapter 4 has provided experimental evidences that the crystalline-silica or nano-silica co-additives have the potential to enhance the cementitious reactions in the lime-treated soil matrix. However, no major studies have focused on the use of these silica-based co-additives for reducing ettringite-induced heave on Ca-based treatments. The primary objective of this chapter is to investigate the effects of the novel silica-based co-additives for treating sulfate-rich soils. Laboratory studies were performed to identify the potential of using different phases of silica base co-additives (Crystalline silica and nano-silica) as an admixture with lime. Results from this research objective evaluation are covered in this Chapter 5.

In this chapter, high-sulfate soil (Soil-1), having a soluble sulfate concentration of over 14,000 ppm, was treated with both primary stabilizers (dolomitic hydrated lime) and either of the co-additives (Crystalline silica or Nano-silica). The performance of the silica-based co-additive treatment was compared with only lime-treated and untreated soil. This chapter is divided into three subsections.

1) The first section discusses the application of crystalline silica co-additive with lime to reduce ettringite-induced heave.
2) The second section discusses the effects of crystalline silica on ettringite-induced heaving and volume change of the treated soil matrix.

3) The third section discusses the effect of nano-silica on high-sulfate soil for mitigating ettringite-induced heave

Overall, the chapter provides a comprehensive overview on the potential of using silica-based co-additive with lime to mitigate sulfate-induced heaving.

5.2 Effects of CS on Sulfate-induced Heaving

As a part of this research study, a series of engineering, mineralogical and microstructural studies were performed to determine the efficacy of crystalline silica co-additive to treat sulfate-rich soils. The engineering studies were performed to identify the macrostructural properties of the chemical treatment on sulfate-rich soils. Engineering tests included vertical free swell test, linear shrinkage test, Atterberg's limits, unconfined compressive strength test, and repetitive load triaxial test (RLTT). Free swell is one of the key parameters for treated soil, which determines the potential for the ettringite-induced volume changes and the efficacy of treatment over different curing periods. The linear shrinkage test provided a comprehensive understanding of the effects of the treatment on volumetric strains of the treated soil matrix when subjected to drying conditions. The UCS values and resilient modulus properties of the soils provide an exhaustive understanding on the development of cementitious binding matrix and ettringite in the soil and their influence on the strength and stiffness of the treated soil layers.

In addition to the engineering test, microstructural analysis using X-ray diffraction (XRD) technique, Field Emission Scanning Electron Microscopy-Energy Dispersive X-

ray Spectroscopy (FESEM-EDXS), and Differential Scanning Calorimetry were performed to detect the formation of new reaction products in the soil matrix.

5.2.1 Determination of the Optimum Dosages

The optimum dosages of lime for different test groups of this soil were determined as per the Eades and Grim's pH test (ASTM D6276) (Figure 5.1). The pH test result indicated that the lime modification optimum (LMO) was 7% by weight of dry soil is sufficient for attaining an initial pH of 12.40 for all the soil groups considered in this study. Therefore all test specimens were prepared at 7% lime dosage.

The optimum dosage of the crystalline silica (CS) was selected as 15% and 30% for this initial research purpose. The predetermined dosages of CS co-additives and the primary stabilizer were mixed to the desired proportion to make a uniform dry mixture. The specimens were mixed with water at a percentage of 20% by the dry unit weight of the soil and compacted at a dry unit weight of 14.6 kN/m^3. This dry density was considered corresponding to the dry unit weight of the compaction curve of only-lime treated soils. All treated soil groups were compacted at the same dry unit weight and moisture content to ascertain a similar zero-day strength as recommended by some previous research studies by Wild et al. (1999) and Chakraborty and Nair (2018, 2020).

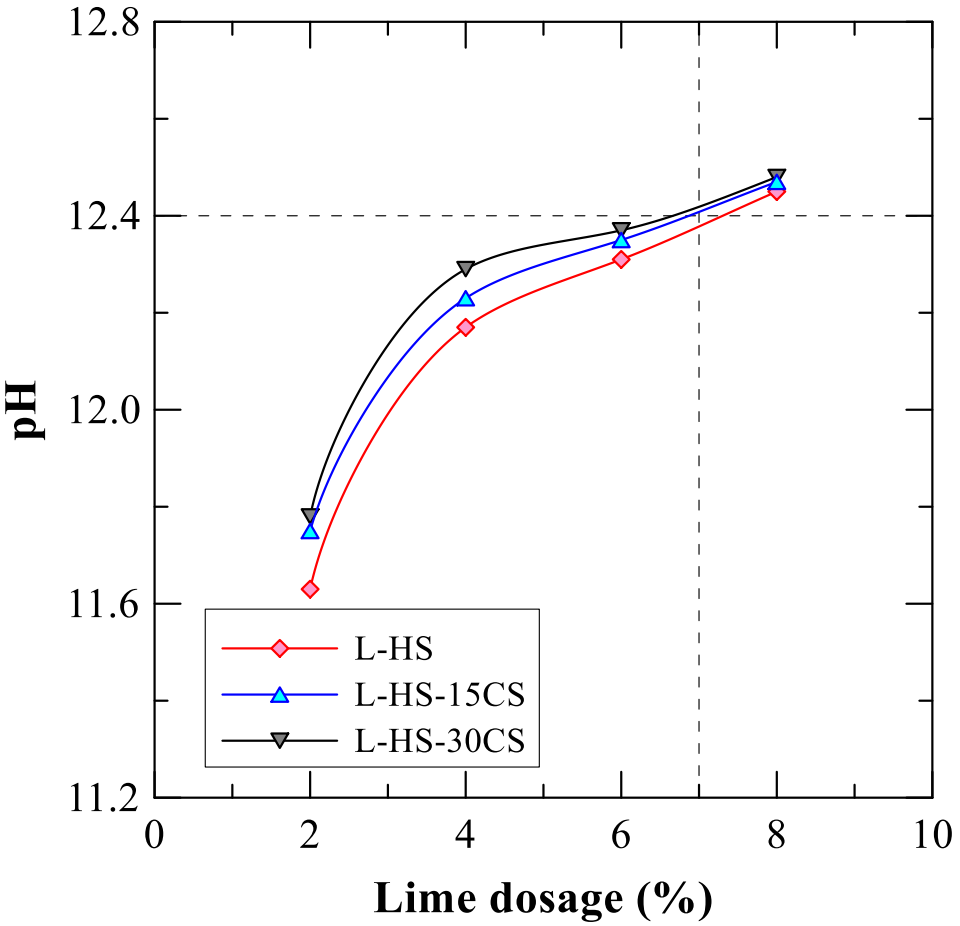

Figure 5.1 Lime Modification Optimum (LMO) for Soil-1 (High-sulfate soil).

5.2.2 Sample Preparation and Engineering Tests

Specimens for vertical-free swell tests were prepared according to the method presented in Chapter 3. The free swell strain test was performed on different soil groups of L-HS, L-HS-15CS, and L-HS-30CS, respectively. The free well test of untreated control soil was also performed to understand the preliminary expansion potential of the problematic soil. The specimens were molded at the target density and moisture content of 14.6 kN/m^3 and 20%, respectively, in a mold of dimension 2.5 in diameter and 1 in height using static compaction. The specimens were cured in a hermetically sealed plastic chamber to ensure

100% relative humidity during the process of curing at a standard room temperature of 23±2℃. Five curing periods of 0 (8-hrs), 3, 7, 14, and 28 days were considered for this research study. The specimens were tested in accordance with ASTM-4546, as discussed earlier.

Linear bar shrinkage test was performed on L-HS and L-HS-30CS. Dry soil, lime, and co-additives were mixed in the desired dosage with 20% moisture content and stored in hermetically sealed plastic bags for different curing periods (0, 3, 7, 14, and 28 days) at a standard room temperature of 23±2℃. At the end of each curing period, the cured soil was removed from the sealed bags, and extra water was added until the specimens reached a consistency close to the liquid limit. Subsequently, the specimens were tested for shrinkage limit in the 5 in. x 0.75 in. mold according to the procedure outlined in Tex-107-E (Chapter 3). The cured soils were also tested for Atterberg's limit in accordance with ASTM D4318 to understand the changes in soil plasticity over different curing periods.

Unconfined strength test was performed to assess the improvements in the engineering properties of the chemically treated soil groups. Strength tests were performed on L-CS, L-HS, L-HS-15CS, and L-HS-30CS specimens for all curing periods. For each curing period, 6 specimens were prepared in a mold of diameter 33 mm with an aspect ratio of 2:1 (H:D) (Figure 5.2). The UCS test was performed on three specimens, and the remaining three specimens were subjected to moisture conditioning to assess the efficacy of the treatment due to capillary soaking as an indirect measure of durability. Details of

the moisture conditioning tests will be discussed under the durability section in Chapter 6. The UCS testing was conducted at a strain rate of 0.5%/min, as per ASTM D5102.

UCS testing using miniature specimens not only saves the quantity of material required for testing but also reduces the effort required to prepare the specimens. Several past researchers have performed UCS testing using miniature specimens and have found it to be an effective way of studying the performance of chemically treated soil specimens (Wild et al. 1999, Sivapullaiah et al. 2000, Al-Amoudi et al. 2010, Bahmani et al. 2014, Bandara et al. 2015, Chakraborty and Nair 2018, 2020). Furthermore, the authors also tested the UCS of both large specimens (71 mm diameter with 2:1 aspect ratio) and miniature specimens (33 mm diameter with 2:1 aspect ratio) and have observed that the UCS results obtained from both the specimens are comparable (Figure 5.3).

Figure 5.2 Specimen mold, a typical miniature specimen after compaction and after UCS testing.

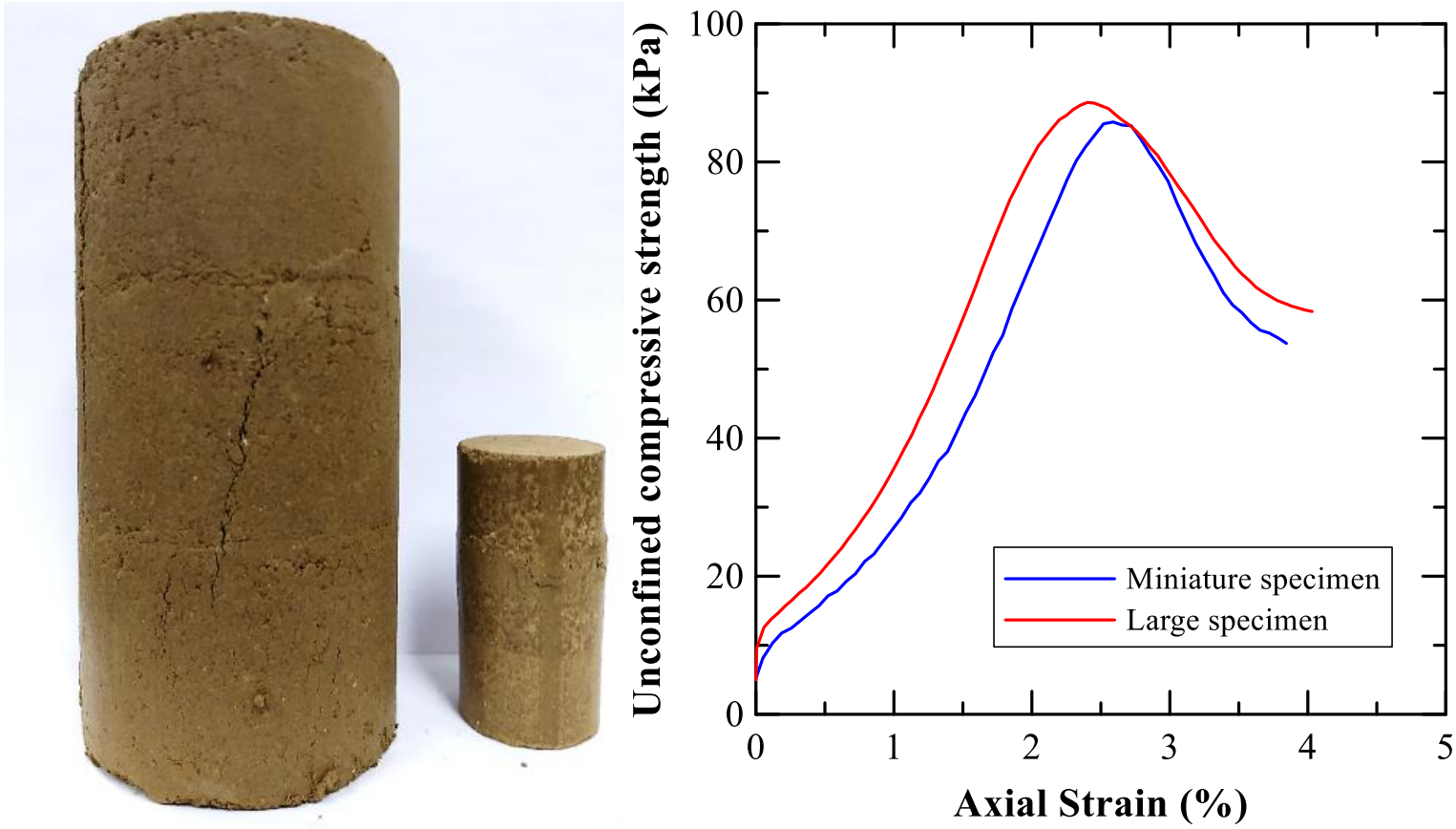

(a) (b)

Figure 5.3 Comparison of (a) Specimen sizes (b) UCS data obtained for specimens of different sizes.

The resilient modulus test was performed on L-HS and L-HS-30CS specimens for all the curing periods. Duplicate specimens with 71 mm diameter and 2:1 aspect ratio were tested for each curing period. The results of the test were analyzed in accordance with AASHTO T 307. A multi-parameter regression model was developed to determine three independent parameters correlating to the stiffness, bulk stress, and shear stress of the treated soils.

5.2.3 Microstructural and Mineralogical Tests

The untreated soil specimens were oven-dried overnight and crushed in a mortar and pestle before testing. The lime/lime-CS treated specimens were prepared as slurries, in accordance with the recommendations made by Puppala et al. (2005) and Chakraborty and Nair (2018, 2020). This was done to ensure homogeneity and reduce the chances of sampling error while collecting subsamples for testing. The treated specimens were cured for 14 days at 25±1°C. Prior to testing, the specimens were dried in an oven at 40°C for 8 hours and lightly crushed.

XRD studies were performed on different test groups of specimens, including CS, L-CS, HS, L-HS, and L-HS-30CS. Cu-kα radiation with a wavelength of 1.54 nm was used over the range of 5 to 60° for 2θ, with a step size of 0.02° and 0.5sec/step. ICDD database was used for the identification of the minerals from the location of their characteristic peaks on the diffractogram. Relative changes in the intensity of the crystal peaks and the identification of the new peaks helped to determine the chemistry of the reaction process. The diffractogram results between CS and L-CS enabled us to identify the potential of the chemical reaction between crystalline silica phases and the calcium

stabilizer to form new C-S-H phases. The XRD studies between HS, L-HS, and L-HS-30CS helped to detect the possible formation of ettringite and additional phases of C-S-H formed due to treatment with CS co-additives.

Several literary works in the past have argued that the C-S-H phases formed are usually amorphous in nature, and hence identification using XRD studies are sometimes not adequate (Glenn 1970, Sivapullaiah and Moghal 2011, Bahmani et al. 2014, Chakraborty and Nair 2018, 2020). Therefore, additional analyses using FESEM-EDXS and DSC were performed to identify the possible formation of new cementitious products.

FESEM studies were performed on CS, L-CS, L-HS, and L-HS-30CS specimens. Subsamples of the powdered specimens were placed on the double-sided carbon tape and silver sputter-coated before testing. SEM studies were performed to visually detect the formation of new reaction products. In addition to visual identification, the elemental composition of the C-S-H phases was determined using EDXS. DSC is a suitable tool for determining the presence of cementitious phases in treated specimens (Glenn 1970, Harris et al. 2009, Chakraborty and Nair 2018, 2020). In this research study, cured soil specimens of L-CS and L-HS-30CS were tested in DSC. Approximately 20mg of the specimens were placed in an inert alumina crucible and tested in temperatures ranging from 28°C to 1000°C at a heating ramp of 10°C/min. A constant nitrogen purge of 20 ml/min was maintained during the test.

5.2.4 Chemical Tests

The pH of a specimen during any chemical reaction provides significant information about the progress of the reaction. When lime is added to the soil at the optimum dosage (7%),

it increases the soil pH to more than 12.40. However, due to the progress of the reaction and the formation of the cementitious phases, the available hydroxyl ions (OH^-) ions are utilized to form the C-S-H phases (Hunter 1988). Due to this, there is a reduction in the soil pH level, which serves as an ideal indicator to predict the progress of the reaction. For this research study, specimens including lime (L), lime-treated sand (L-S), and lime-treated crushed sand/crystalline silica (L-CS) in a solution form to determine the pH over different curing periods. 10 gm of dry specimens of each mixture were mixed with 500 ml of water and stored in a burette at standard room temperature. The pH values were monitored after each curing period of 0, 3, 7, 14, and 28 days. The results and analyses from these tests are summarized in the next section.

5.2.5 Analysis and Discussion of Tests Results

5.2.5.1 Engineering Tests

Two dosages of crystalline silica (CS), 15% and 30%, were used along with lime for stabilizing the HS soil. Figure 5.4 presents the total swell strain of the specimens of L-HS, L-HS-15CS, and L-HS-30CS groups. At 0-day curing, specimens of both the lime-CS treated HS soils (L-HS-15/30CS) showed an immediate decrease in the swell strain when compared to the L-HS group without CS amendment. The beneficial effect of the presence of crystalline silica is evident after a short curing period of 3 days. The final vertical swell strain decreased below 3% for the L-HS-15CS and below 2% for the L-HS-30CS group soil specimens cured for 14 days and above. This reduction in swell may be attributed to (i) the replacement of a part of the soil with crushed sand, (ii) tendency of the crushed

sand to suppress the dissolution of reactive alumina, which is an important ingredient of ettringite formation and (iii) formation of some weak CSH bonds during the swell test. Introducing crystalline silica in the treatment might have suppressed the availability of reactive alumina from the clay particles, as reported by McKennon et al. (1994) and Little and Nair (2009c). A reduction in available alumina might be partially responsible for deterring the formation of ettringite and thereby suppressing the associated heaving.

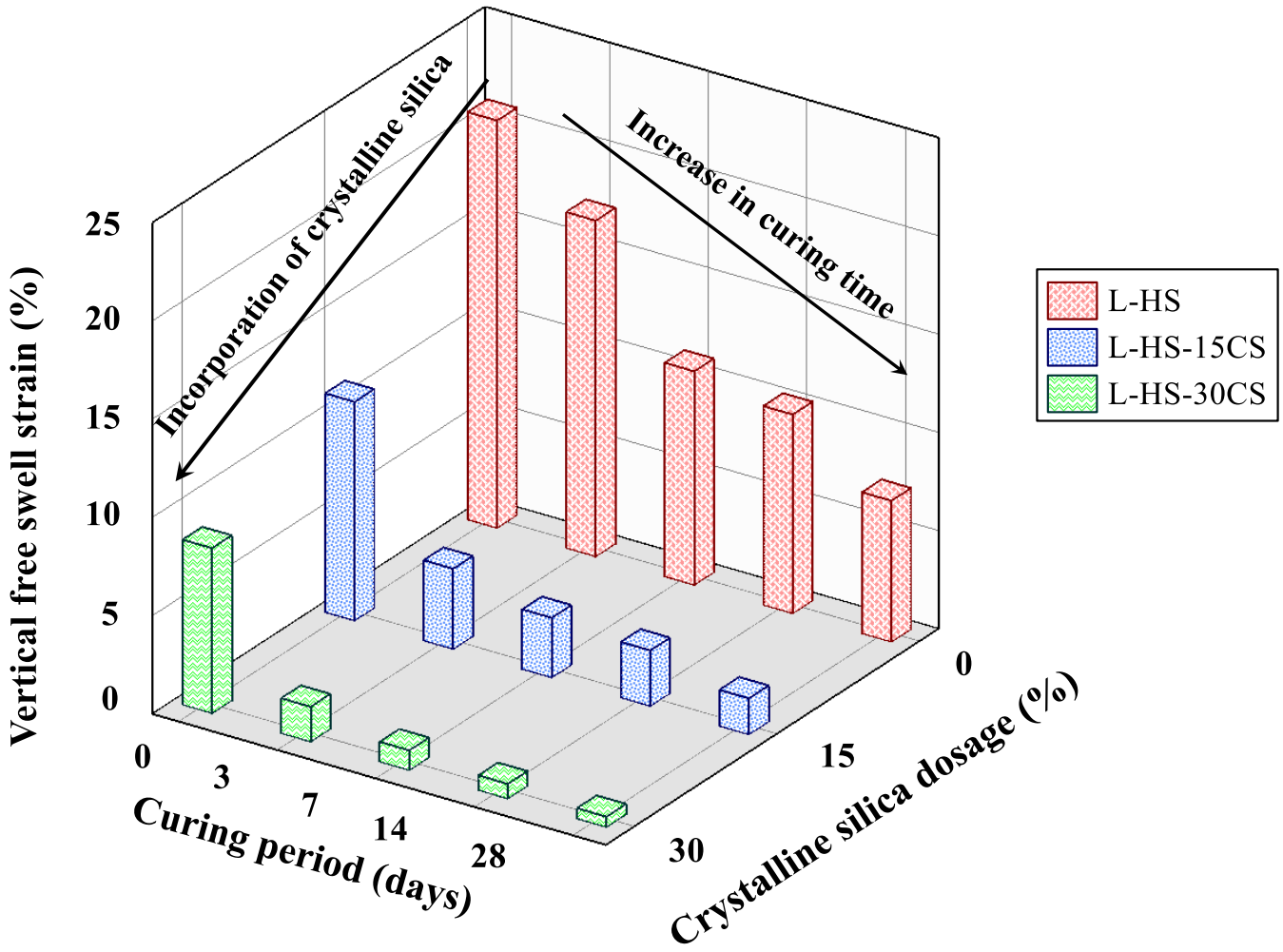

Figure 5.4 Free swell values of L-HS, L-HS-15CS and L-HS-30CS over different curing periods.

The linear bar shrinkage test results of untreated soil (HS), L-HS and L-HS-30CS are shown in Figure 5.5. The shrinkage test was performed with 30% CS amendment since the free swell test indicated that 30% CS has a major influence on reducing ettringite induced heave and also considering the environmental aspects, maximum utilization of the quarry dust would help to reduce the problems associated with their disposal in landfills. The specimens of L-HS-30CS showed a considerable higher reduction in linear shrinkage after 3 day of curing as compared to lime treatment alone. The modification reactions and the partial replacement of high plastic clay with non-plastic crushed sand have helped to reduce the plasticity immediately, and subsequently, lower shrinkage strain was observed.

Over a longer curing period of 28 days, it was noted that no major difference in the shrinkage strain in percentage between only lime-treated and lime and CS treated soil mixtures. After a long curing period, the formation of C-S-H phases probably helped to reduce the moisture affinity by reducing the active surfaces of clay surfaces to absorb the water molecules. The hypothesis of reduction in plasticity was further verified by performing Atterberg's limit tests on the treated specimens over different curing periods.

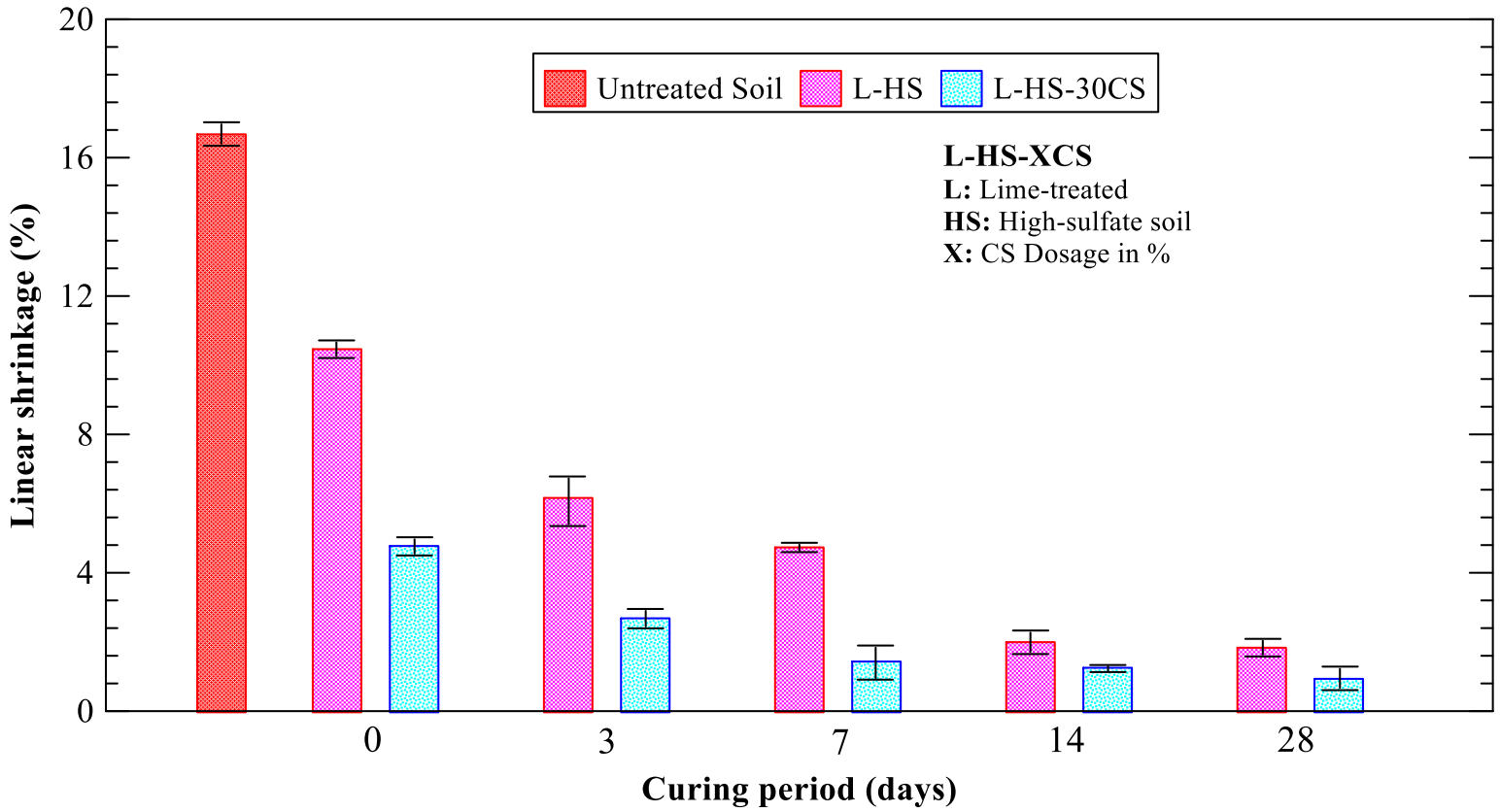

Figure 5.5 Linear shrinkage over different curing periods for HS soils treated with lime or lime and CS.

The variation of the Liquid Limit (LL), Plastic Limit (PL), and the Plasticity Index (PI) of soil is shown in Figure 5.6. The LL, PL and the PI for the untreated HS soil were observed to be 66, 29.5, and 36.5, as provided in Chapter 3. The application of the Ca-based stabilizer was able to reduce the plasticity index immediately by reducing the moisture affinity through modification reactions in L-HS specimens. The modification reactions make the soil more workable and friable and help to develop flocculated structures similar to the granular soils.

During the curing phase, lime-treated soils showed more than 10% reduction in soil LL after 3 days of curing, which remained almost constant over a longer curing period. However, the PL recorded an increase significantly (> 5%) after 14 days of curing. The reduction in the LL and an increase in PL affected the overall soil plasticity or made the soil more granular in nature and consequently modified the soil behavior from high plastic to medium plastic clay.

In CS amended soils, an additional reduction in the LL was observed due to partial replacement of the high plastic clay particles with non-plastic inert crushed sand particles. Similar to the L-HS specimens, no major changes in the PL were noted during the entire curing period after 3 days of curing. Overall, the reduction in soil plasticity was higher than the L-HS specimens rendering the behavior of the soil to be granular and non-plastic. Therefore, the addition of CS co-additive has a major influence in reducing the soil plasticity by reducing the moisture affinity and thereby improving the durability of the treated layers.

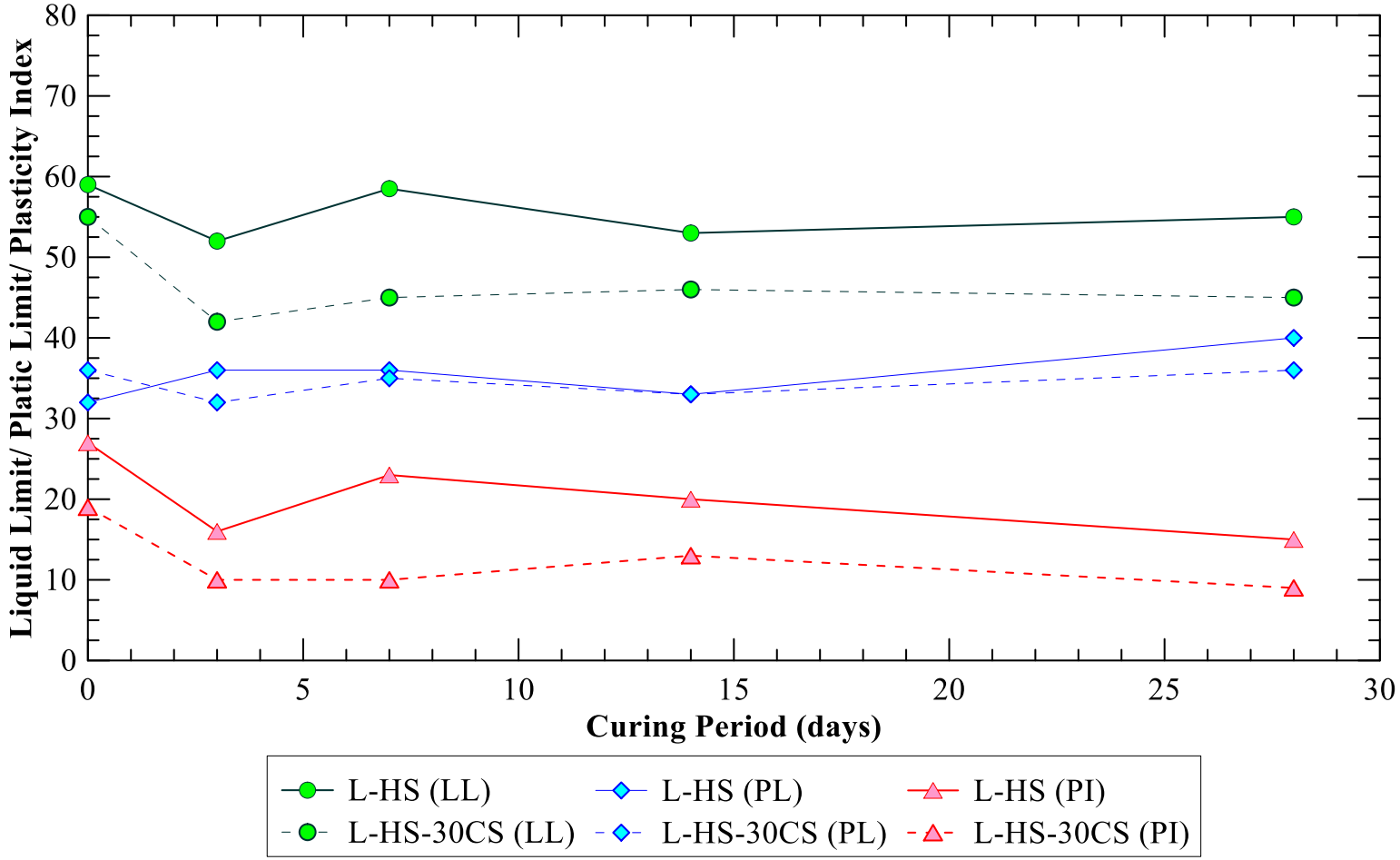

Figure 5.6 Variation of Atterberg's Limits over different curing periods for HS soil.

Figure 5.7 presents the UCS test results of different groups of treated specimens before moisture conditioning by capillary soaking. And additional test group of geomaterials, i.e. lime with only CS was tested to determine the possibility of pozzolanic reactions due to the presence of crystalline particles. The lime-treated crystalline silica (L-CS) specimen group had a UCS value close to 180 kPa immediately after the specimen preparation (0-day curing). Since crushed sand does not have cohesive properties, the 0-day UCS value can be attributed to the effect of suction stresses existing in the unsaturated L-CS specimen. However, with an increase in the curing time, the UCS value of the L-CS specimen increased by three-fold (≈ 560 kPa) after four weeks of curing. The UCS data suggests that the lime reacted chemically with the available silica of the crushed sand to form cementing C-S-H phases that are capable of binding the particles and subsequently imparting strength to the specimens.

The untreated HS soil had UCS of 184 kPa and 5 kPa, before and after capillary soaking, respectively. An immediate improvement in the UCS value can be observed in all lime-treated soil specimens for 0 days curing (Figure 5.7). This immediate improvement after lime treatment can be attributed to soil modification from cation-exchange, flocculation-agglomeration, and change in soil texture. The strength results of the L-HS-15CS and L-HS-30CS groups indicate that the addition of crystalline silica as an admixture is beneficial in enhancing the UCS of the soil prior to capillary soaking, especially with the increase in curing period.

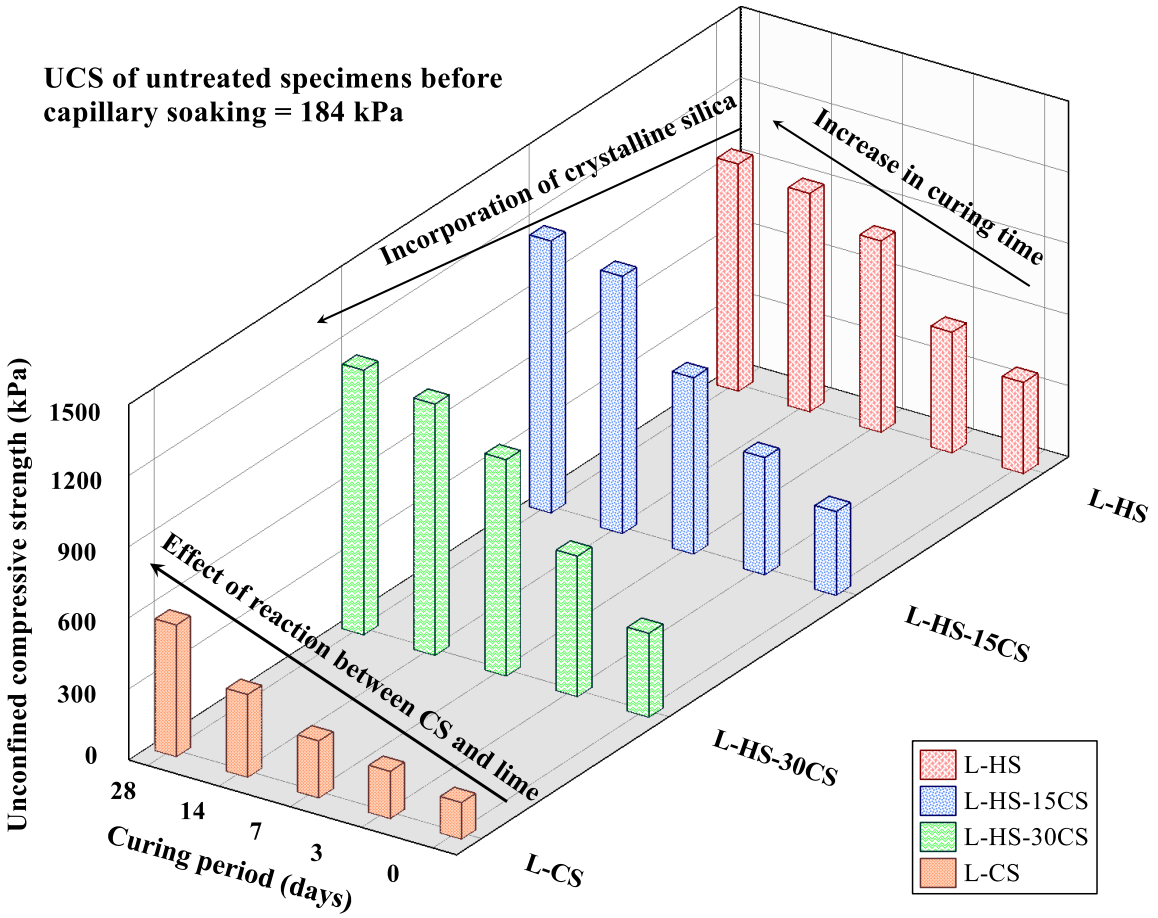

Figure 5.7 Unconfined strength of different treated soil groups.

Table 5.1 presents the regression coefficients of the universal model used to fit the respective RLTT data. For this research study, the changes in coefficient k_1 are used to detect improvements in the stiffness (elastic modulus) of the L-HS-30CS, over the L-HS group. The k_1 value of a lime-CS treated specimen can be observed to be less than that of the lime treated specimen for 0-day curing. This may be due to the usage of same water content for preparing both the groups of specimens. Since 30% of the untreated CH soil is replaced by the crushed sand, the water content probably shifted beyond the optimum moisture content of the soil-crushed sand mixture.

An increase in moisture content beyond optimum value is usually associated with a decrease in the M_r value for any given bulk stress. However, the difference in the 0-day cured k_1 is not appreciable possibly due to the positive influence of the presence of crushed sand, which is expected to enhance the stiffness in the presence of confining pressure. Nonetheless, the k_1 values of both the groups are nearly comparable, which is similar to that observed for the unsoaked UCS results of the two groups of specimens, for 0-day curing (Figure 5.7).

With an increase in curing time, the k_1 values of both the groups are observed to increase, due to the progressive pozzolanic reaction and formation of CSH phases. For any of the curing periods (3, 7, 14, or 28), the k_1 values of the L-HS-30CS group is greater than that of the L-HS group. The addition of crushed sand probably resulted in the formation of additional CSH phases in lime-admixture treated specimen, causing an increase in the

stiffness. Moreover, as mentioned before, the presence of crushed sand is expected to provide a higher stiffness or moduli when subjected to confining pressure.

Table 5.1 Regression coefficients of the universal model for L-HS and L-HS-30CS group for different curing periods.

Curing Period (days)	k_1		k_2		k_3		R^2	
	L-HS	*L-HS-30CS*	*L-HS*	*L-HS-30CS*	*L-HS*	*L-HS-30CS*	*L-HS*	*L-HS-30CS*
0	1473	1449	0.128	0.175	0.161	0.358	0.90	0.94
3	1676	1684	0.131	0.171	0.233	0.383	0.97	0.96
7	1877	1920	0.169	0.138	0.310	0.413	0.94	0.93
14	2002	2136	0.127	0.169	0.499	0.505	0.91	0.91
28	2049	2147	0.151	0.152	0.562	0.797	0.90	0.93

Note: k_1, k_2, and k_3 are the universal model parameters

5.2.5.2 Microstructural and Mineralogical Tests

XRD studies were performed to qualitatively determine the presence of different constituent minerals in a specimen and detect the formation of new products after chemical

treatment. Figure 5.8 presents the XRD data of crushed sand (CS) and lime-treated crushed sand (L-CS), cured for 14 days at 23±2°C. The diffractogram for the crushed sand specimen shows the presence of predominant Quartz peaks. The lime-treated crushed sand specimen also showed Quartz peaks at the same 2-theta angles after 14 days of curing. However, the relative intensity of the peaks reduced appreciably, indicating the utilization of silica from the crushed sand due to reaction with lime. Some additional minor peaks also emerged on the XRD results on the lime-treated sand specimen, at 2-theta of 31°, due to the formation of CSH phases. The CSH formed at room temperature conditions is usually amorphous, and hence the intensity of the CSH peak is weak as compared to the Quartz peak. However, this formation of CSH phases resulted in an increase in UCS value of L-CS specimen with curing time

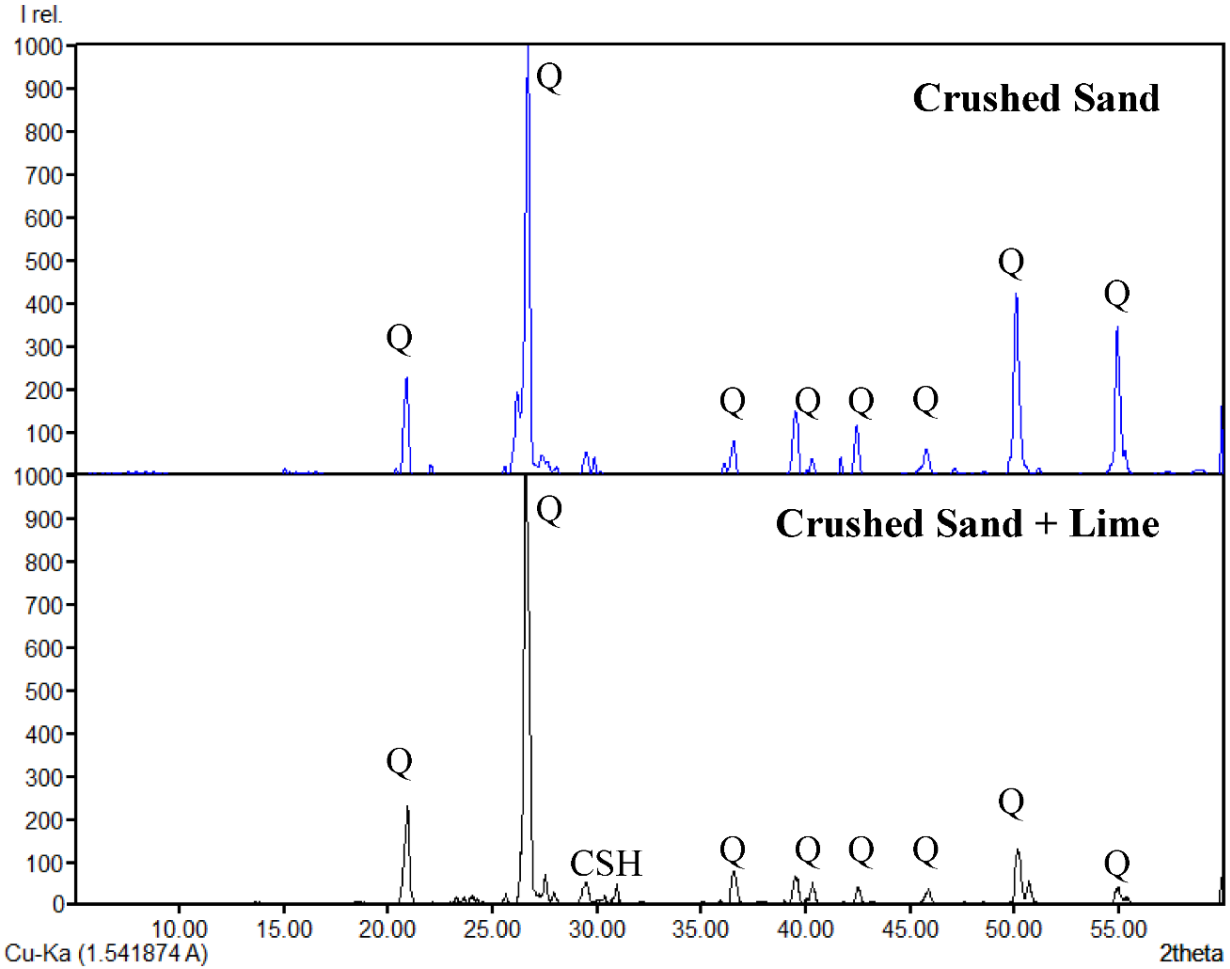

Figure 5.8 X-ray diffractogram of CS and L-CS.

XRD study was also used to study and confirm the presence of sulfate salts in the untreated soil, and formation of ettringite in the lime-treated soil. Figure 5.9 presents the diffractograms for the untreated soil (HS), lime-treated soil (L-HS), and lime treated crushed sand (L-HS-30CS). The presence of Calcite, Quartz, and different clay minerals such as Illite, Kaolinite, and Montmorillonite is apparent from the diffractogram of the untreated soil Figure 5.9a). In addition, gypsum peaks were also present in the untreated soil, which acted as the source of sulfate in the untreated soil.

The lime treated soil specimens exhibited a similar diffractogram as the untreated soil (Figure 5.9b). The primary gypsum peak (G) present in the untreated soil was absent after lime treatment, and additional broad peaks were formed close to 2-theta of 16º due to the formation of ettringite. Moreover, the formation of ettringite resulted in an increase in the intensity of some peaks (marked as E) that were originally present in the untreated soil but corresponded to other minerals that have peaks at same 2-theta angles as ettringite. An increase in the peak intensity at 2-theta of 29º was observed in the lime treated soil possibly due to carbonation of lime to form calcium carbonate (Calcite) and due to formation of CSH phases, which have XRD peaks at the similar 2-theta angle. Formation of CSH phases is also detected through the presence of new additional peaks in the treated soil specimens. However, it should be noted that the intensity of the CSH peaks is not significantly strong owing to the non-crystalline/amorphous nature of the CSH formed under ambient temperature used for curing.

XRD studies of the lime-crushed sand treated soil were also performed to identify potential reasons behind the observed improvements in engineering properties with regard

to addressing ettringite-induced heave in the lime treated soil. A significant decrease in the intensity of the ettringite peak can be observed in Figure 12c, which suggests that the use of crushed sand as an admixture has the potential to suppress the quantity of ettringite formed. This is in agreement with the observations made by McKennon et al. (1994) and Little and Nair (2009c).

The intensity of the CSH peaks decreased when compared to the lime treated specimen. The formation of additional CSH phase due to the reaction of lime with silica available from the crushed sand is not apparent from the diffractogram presented in Figure 5.9c. However, it is important to realize that the diffractogram presented in Figure 5.9c corresponds to a specimen with 30% crushed sand, which provided a significant source of a highly crystalline mineral, Quartz. The ordinate of the diffractogram is presented in terms of relative intensity, normalized with respect to the intensity of the most prominent peak at 2-theta of 26º (Quartz). Hence, the intensity of the CSH phases is expected to be reduced substantially in the lime-CS treated soil, as compared to the diffractogram of lime-treated soil (Figure 5.9b). The hypothesis regarding the formation of additional CSH phases due to chemical reaction between lime and crushed sand was further tested by means of FESEM-EDXS and DSC data, details of these results are provided in the following sections.

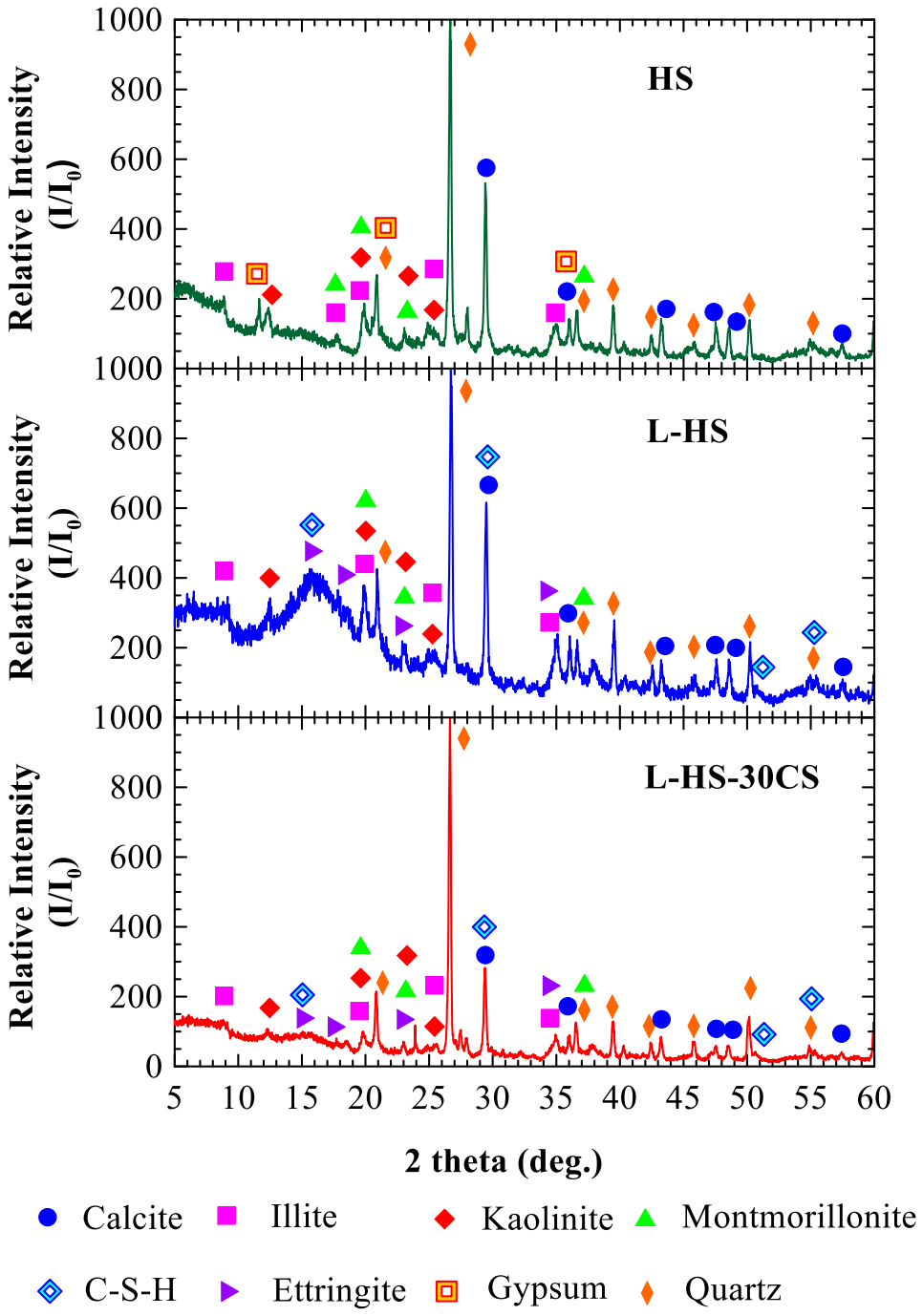

Figure 5.9 X-Ray diffractogram for (a) HS, (b) L-HS, and (c) L-HS-30CS specimen groups.

Figure 5.10a presents a typical SEM image of the crushed sand which shows the presence of granules of the pulverized sand, at a magnification of 250x. A stark difference in the surface morphology can be observed for lime-treated crushed sand in Figure 5.10b and 5.10c, which were also captured at 250x. A higher magnification (at 500x) shows the formation of some amorphous compounds on the surface of all the granules of crushed sand (Figure 5.10b). Three such typical images are shown to highlight the uniform distribution of the reaction product formed in the lime-treated crushed sand.

The surface morphology of the lime-treated sand particles was also studied at 1000x, and 15000x, and the presence of new reaction products are better observed a higher magnification (Figure 5.10c and 5.10d). The reaction products appear to be round-shaped amorphous globules that are present all along the surface of the sand particles. the elemental composition of these globules was estimated using the EDXS (Figure 5.11a). EDXS data confirmed the precipitated products to be CSH I phase having a Ca/Si molar ratio of 0.68. These CSH phases played a vital role in binding the crushed sand particles to impart strength to the soil matrix and resulted in an increase in the UCS value due to the progressive pozzolanic reaction.

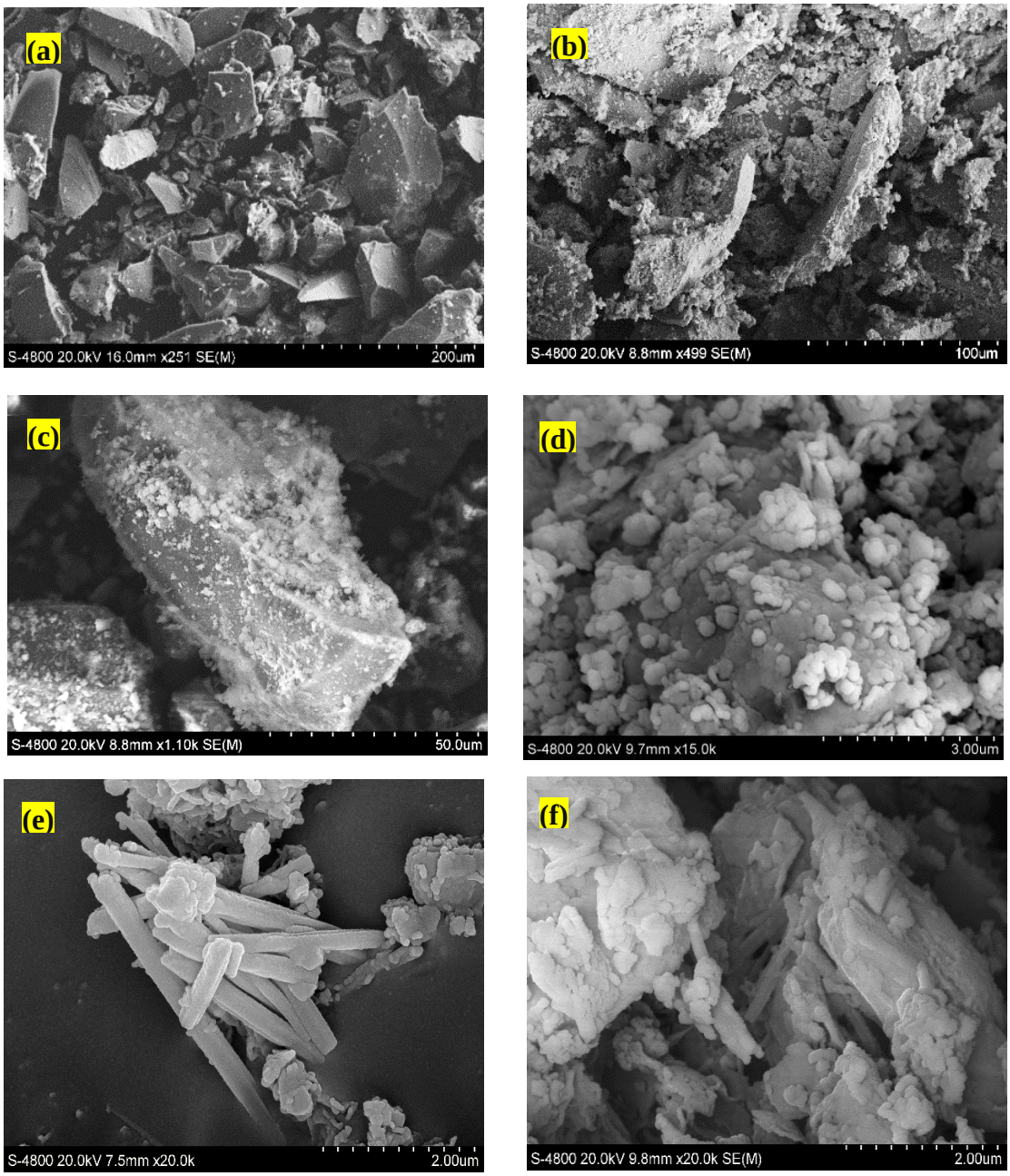

Figure 5.10 SEM images of a) Crushed Sand (CS) b) L-CS (500x) c) L-CS (1,000x) d) L-CS (15,000x) e) L-HS f) L-HS-30CS.

The lime-treated soil was also scanned to detect the presence of ettringite minerals. Clusters of elongated, rod-like crystals were observed in the 14-days cured lime-treated

soil specimens (Figure 5.10e). The elemental composition of the crystals was determined using EDXS, which suggests the crystals to be composed of Ca, Al, and S, the key ingredients of ettringite (Figure 5.11b). The shape of the crystals, along with the EDXS data confirm the presence of ettringite in the lime-treated specimens. Similar rod-like crystals were observed in the lime-CS treated soil specimen (Figure 5.10f). However, the crystal size apparently seems to be smaller than that observed in the lime-treated specimen (Figure 5.10e). Abundant lumps of amorphous C-S-H phases, similar to that shown in Figure 5.10d, are also visible in Figure 5.10f. The presence of additional C-S-H phases produced by the reaction of lime and crushed sand particles resulted in the reduction in swell strain and consequent increase in UCS properties.

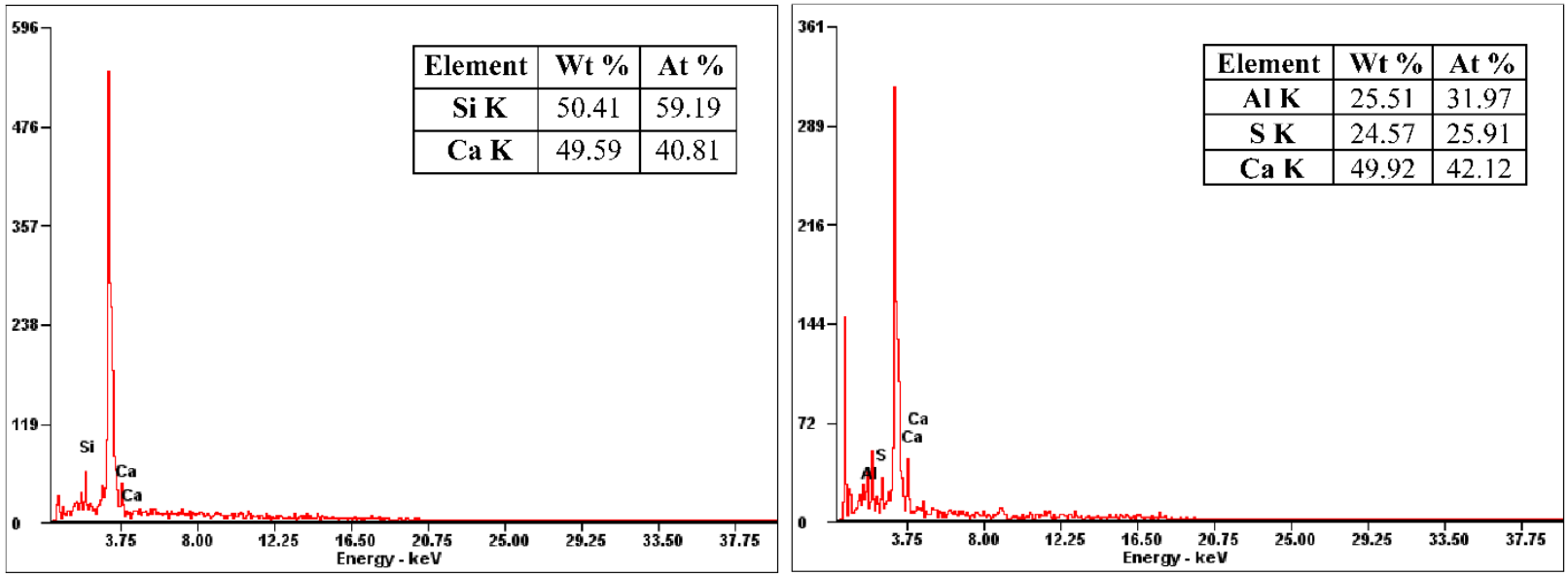

Figure 5.11 EDXS data for (a) amorphous globules and (b) rod-like crystals.

Figure 5.12a-b present the DSC thermograms obtained for the lime-treated crushed sand and lime-CS treated soil specimens, respectively. Strong endothermic peaks can be observed around (i) 380ºC, (ii) 570ºC and (iii) 690ºC due to absorption of heat and decomposition of (i) $Mg(OH)_2$ to MgO and H_2O, (ii) $Ca(OH)_2$ to CaO and H_2O, and (iii) $CaCO_3$ to CaO and CO_2, respectively. A weak endothermic peak was observed around 200ºC, and re-crystallization exothermic peaks were present at 850ºC, which is typical of CSH gel, especially CSH I phase (Figure 5.12a). This is in agreement with Ca/Si ratio estimated from the EDXS, for the amorphous CSH phases.

The locations of the endothermic decomposition peaks of $Mg(OH)_2$, $Ca(OH)_2$ and $CaCO_3$ in the lime-CS treated soil specimen are very much similar to those observed for lime-treated crushed sand (Figure 5.12). The exothermic peaks at 850ºC and 920ºC are observed in the lime-CS treated specimens due to re-crystallization of both CSH I and CSH II phases. The CSH I phase may have formed in the vicinity of the crushed sand particles where the concentration of available silica is expected to be higher. CSH II phase might have precipitated near the clay particles, where the available silica is expected to be less as compared to that provided by the crushed sand.

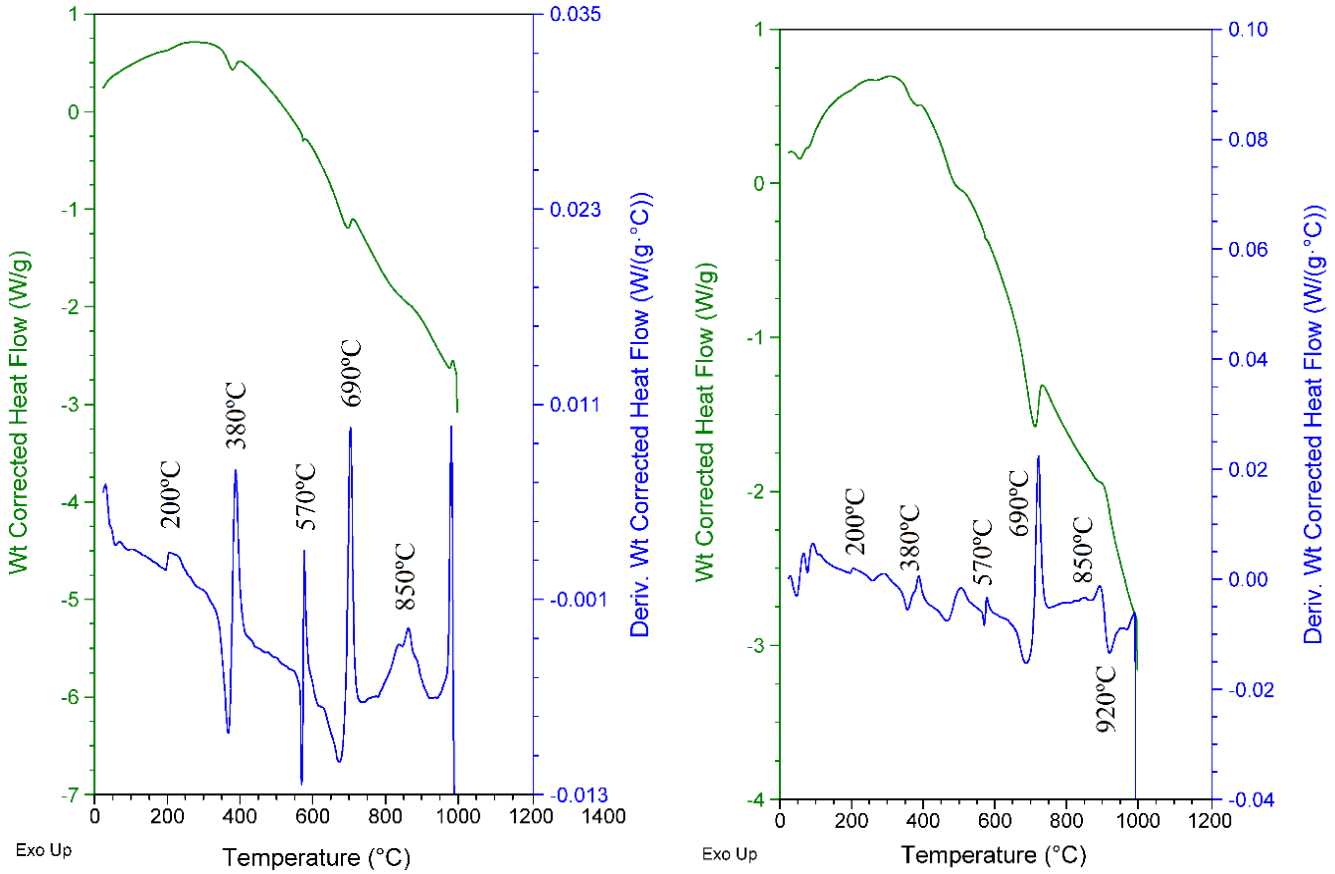

200ºC - Dehydration of C–S–H; 380ºC - Dehydration of magnesium hydroxide; 570ºC - Dehydration of calcium hydroxide

690ºC - Decarbonation of calcium carbonate; 850ºC - Recrystallisation of C–S–H

Figure 5.12 DSC thermogram of a) L- CS b) L-HS-30CS specimen.

5.2.5.3 Chemical Tests

The potential for the chemical reaction between lime and crystalline silica was assessed by analyzing the pH of various specimen groups, including lime (L), lime-treated sand (L-S), and lime-treated crushed sand/crystalline silica (L-CS) (Figure 5.13). The pH of the lime solution (L) decreased from 12.4 to 12.3 in four weeks, possibly due to partial carbonation of lime additive. A similar variation in pH was also observed for the L-S specimens. This indicates that the coarse sand (before pulverization) did not react chemically with lime, and the decrease in pH was also attributed to the carbonation of lime. The pH of the L-CS specimen decreased from 12.4 to 12.1, and this indicates a potential chemical reaction between lime and CS admixture, owing to an increase in surface area of the sand particles after pulverization.

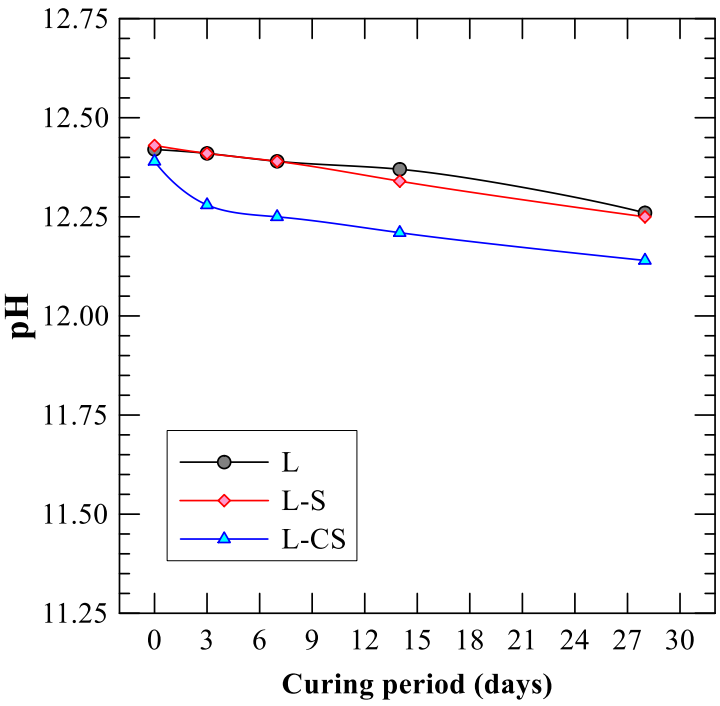

Figure 5.13 Change in the pH over time.

5.3 Effects of CS on the Void Ratio of Treated Sulfate-rich Soil

The HS soil exhibited swelling characteristics due to the water absorption by the clay minerals (Figure 5.14). This clay-mineral-induced swelling resulted in a vertical strain of 23%, and majority of this swelling took place immediately within a day of moisture exposure. Lime treatment of the problematic soil suppressed the immediate clay-mineral-induced swelling in the L-HS specimens due to cation exchange, and flocculation-agglomeration reactions as well as formation of pozzolanic cementitious products. However, a substantial increment in swell strain was recorded for the L-HS specimens after a day of submergence, and this can be attributed to the ettringite-induced soil heaving. The ettringite-induced swelling was not apparent immediately after submerging the L-HS specimens in water due to the dormant ettringite nucleation phase, which is then followed by crystal growth and hydration.

The ettringite-induced heaving was more prominent in the 3 days cured specimen as compared to that cured for 28 days (Figure 5.14). During the initial curing stages, a higher concentration of unreactive lime, coupled with an elevated pH environment, facilitated ettringite crystal formation. In the later curing stages, the soil-C-S-H matrix partially counteracted ettringite's disruptive force, resulting in lower swell strain than the 3-days cured specimen. However, even after 28 days of curing, the L-HS specimens experienced a considerable swell strain of 7%, which can be classified as high-swelling material. Therefore, these results indicate that lime treatment was ineffective for the present high-sulfate soil.

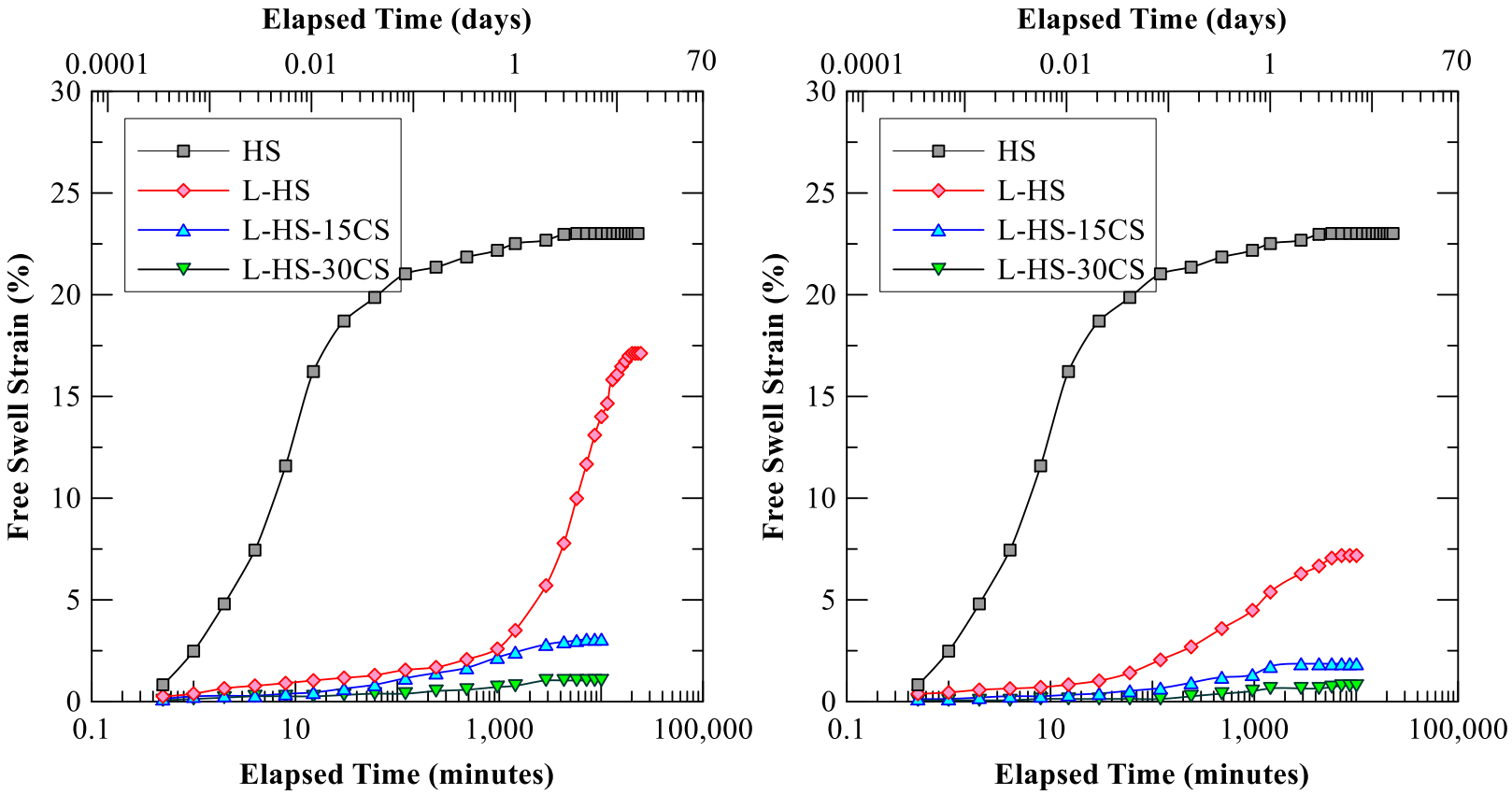

Figure 5.14 Swell test results for (a) 3 days cured and (b) 28 days cured specimens.

The reduction in ettringite-induced heaving is apparent in both L-HS-15CS and L-HS-30CS specimen groups for both the curing periods and this could be primarily attributed to three factors. Firstly, the partial replacement of high-sulfate soil by CS admixture in the L-HS-15/30CS groups reduced the sulfate level as compared to the L-HS group. Secondly, the presence of silica-rich compounds like CS suppressed the formation of ettringite crystals. Finally, the chemical reaction between lime and CS resulted in the formation of additional cementitious phases that formed a strong matrix and partially resisted ettringite-induced heaving.

The effects of the first two factors were studied by analyzing the ettringite-induced swelling interpreted from the swell test results and comparing those with the values estimated from stoichiometric analysis. The ettringite-induced swelling was segregated from the clay-mineral-induced swelling based on the location of the sudden slope change observed for the lime-treated specimens in Figure 5.14. The time of slope change indicates the possible initiation of ettringite crystal growth and subsequent hydration after the initial dormant nucleation phase. The swell strain incurred before the initiation of the ettringite-induced swelling could be attributed to the clay-mineral-induced swelling. The clay-mineral-induced and ettringite-induced swell strains for different specimen groups were interpreted from swell test results and these are reported in Table 5.2.

Table 5.2 Clay mineral-induced and ettringite-induced swell strains interpreted from swell tests.

Specimen group (sulfate content in ppm)	Curing period (days)	Clay mineral-induced swell strains interpreted (%)	Ettringite-induced swell strains interpreted (%)	Normalized clay mineral-induced swell strains interpreted (%)	Normalized ettringite-induced swell strains interpreted (%)
HS (14,000)	N/A	23.0	0.0	23.0	0.0
L-HS (14,000)	3	2.6	14.5	2.6	14.5
	28	0.6	6.6	0.6	6.6
L-HS-15CS (11,900)	3	0.6	3.5	0.7	4.1
	28	0.2	1.7	0.2	2.0
L-HS-30CS (9,800)	3	0.4	1.4	0.6	2.0
	28	0.2	0.3	0.3	0.4

Table 5.2 results show that utilization of crystalline silica admixture with lime resulted in a significant reduction in the ettringite-induced swelling even after a short curing period of 3 days. The beneficial influence of CS admixture is more pronounced with high admixture dosage and a longer curing period. The disproportionate reduction in ettringite-induced swelling with an increase in CS dosage is evident from the swell strains normalized with respect to the proportion of clay present in the different specimen groups. This suggests that the decrease in the sulfate content due to partial replacement of HS soil

with CS material might not be the only reason for the observed improvements. This hypothesis was tested by estimating the ettringite-induced volume increase using stoichiometric analysis.

Little et al. (2010) and Talluri et al. (2020) computed the expected ettringite content and associated volume increase in a sulfate soil using stoichiometric analysis. The analysis assumes soluble sulfate as the limiting reagent, and availability of ample water from external sources. The molar volume calculations were performed using chemical Equation 8, and Equation 9 was used to estimate the proportion of ettringite formed for a sulfate content of 10,000 ppm.

$$6Ca^{2+} + 2Al(OH)_4^- + 4(OH)^- + 3SO_4^{2-} + 26H_2O \rightarrow Ca_6[Al(OH)_6]_2.(SO_4)_3.26H_2O$$

(ettringite) (8)

- 10,000 ppm is equivalent to 1 g SO_4 in 100 g of dry soil
- 1 mol SO_4 is equivalent to 96 g of SO_4
- 1 mol ettringite (E) forms from 3 mol SO_4
- 1 mol ettringite (E) is equivalent to 1,254 g of ettringite (E)
- Volume increase from ettringite formation in presence of external source of wate r = 137%

$$\frac{1 \text{ g of } SO_4}{100 \text{ g of soil}} \text{ x } \frac{1 \text{ mol } SO_4}{96 \text{ g of } SO_4} \text{ x } \frac{1 \text{ mol E}}{3 \text{ mol } SO_4} \text{ x } \frac{1{,}254 \text{ g of E}}{1 \text{ mol E}} = 4.36\% \text{ E} \quad (9)$$

Overall, lime treatment of soil with sulfate content of 10,000 ppm is expected to form 4.36% ettringite (by weight of dry soil), which will result in a volume increase of 5.97% (= 4.36×1.37). The sulfate contents of L-HS-15CS and L-HS-30CS specimen groups were computed based on the proportion of HS soil replaced by CS admixture, and

unitary method was used to estimate the ettringite-induced heaving. Based on stoichiometric analyses, the L-HS, L-HS-15CS, and L-HS-30CS specimens are expected to experience ettringite-induced swell strains of 8.4%, 7.1%, and 5.9%, respectively.

The ettringite-induced swell strain interpreted from swell test results for 3-days cured L-HS specimen is higher than that estimated from the stoichiometric analysis. It should be noted that the volume expansion computed from stoichiometric analysis presents the volume expansion due to the formation of the ettringite crystals and does not account for any changes in the void ratio of the specimen due to ettringite formation. The ettringite formation and hydration in the 3-days cured specimen possibly increased the void ratio as the soil-C-S-H bonds were possibly not strong enough to resist the disruptive forces of ettringite. It should be noted that the free swell tests were performed under vertical stress of 1kPa, which was inadequate for preventing the expansion. The 28-days cured L-HS specimen exhibited slightly less ettringite-induced swelling as compared to that computed stoichiometrically. The stronger soil-C-S-H bonds developed after a longer curing time might have partially counteracted the ettringite heaving.

To address the impact of sulfate heaving on the void ratios of lime-treated materials, one of the earlier sulfate heave field case study on the damaged subbase reported by Hunter (1988) was reexamined. (Hunter 1988)reported that the severely affected lime-treated subbase at Stewart Avenue in the City of Las Vegas, Nevada had dry unit weights of 15.1 kN/m^3 (96.2 pcf), and 9.3 kN/m^3 (59.3 pcf), before and after ettringite-induced damage, respectively. Hunter (1988) also reported that ettringite heaving resulted in 100% increase in volume; that is 1 ft^3 (0.028 m^3) of stabilized layer increased in volume to 2 ft^3

(0.057 m^3) after heaving. The native geomaterials consisted of sandy silts and sandy clays with Quartz, Sepiolite, Montmorillonite, Kaolinite, Calcite, and Gypsum as the predominant constituent minerals. The native soil was classified as moderately expansive and was not capable of exhibiting clay mineral-induced swelling of 100%.

Using the abovementioned information, the void ratios of the lime-treated subbase before and after ettringite-induced damage were estimated using mass-volume relationships. The specific gravity of soil solids and ettringite crystals were assumed as 2.60 and 1.77, respectively. Based on the initial dry unit weight reported by Hunter (1988), 1 ft^3 (0.028 m^3) of stabilized material was made up of 0.59 ft^3 (0.017 m^3) of solids and 0.41 ft^3 (0.011 m^3) of voids, and the initial void ratio of the stabilized material was 0.68.

Different volumetric combinations of remaining soil solids, ettringite formed, the volume of voids, and void ratios, which satisfy the target dry unit weight of 9.31 ± 0.05 kN/m^3 and heaved volume of 2 ft^3 (0.057 m^3), were estimated (Table 5.3). Analytical calculations indicate that the void ratio of the damaged subbase should range between 1.13 and 1.47 to satisfy the observed volumetric expansions and post-heaving dry unit weights. The estimated void ratio of the damaged subbase reported in Table 5.3 is substantially higher than the initial void ratio of 0.68. These results indicate that ettringite mineral formation and hydration can increase the volume of voids and disintegrate the treated matrix. Results presented in Table 5.2, in particular for L-HS material, will lead to similar distresses in the field, especially if the overburden pressure and extent of cementitious reactions are not sufficient to counteract the heaving.

The ettringite-induced swell strains interpreted for the L-HS-15CS/30CS specimens are less than those estimated from stoichiometric analyses, and this indicates that the inclusion of crystalline silica might have suppressed the availability of alumina and utilized lime to form additional cementitious phases. This phenomenon potentially made alumina or calcium the limiting reagent instead of sulfate, which ultimately suppressed the ettringite formation. Similar observations were reported by McKennon et al. (1994). Overall, the comprehensive analyses of the swell test results in this Chapter highlight the disruptive effects of ettringite induced heaving and affirm the beneficial influence of utilizing crystalline silica fines as a co-additive with lime.

Table 5.3 Estimated void ratio of damaged lime-treated subbase at Stewart Avenue

V_s (m^3)	V_e (m^3)	V_v (m^3)	V_{total} (m^3)	Void ratio	Dry unit weight (kN/m^3)
0.016	0.007	0.034	0.057	1.47	9.25
0.014	0.009	0.033	0.057	1.40	9.27
0.013	0.012	0.032	0.057	1.32	9.30
0.011	0.014	0.032	0.057	1.26	9.32
0.010	0.016	0.031	0.057	1.19	9.34
0.008	0.018	0.030	0.057	1.13	9.36

Where, V_s = volume of remaining soil solids, V_e = volume of ettringite crystals formed, V_v = volume of voids, void ratio = $V_v/(V_s+V_e)$ and V_{total} = total volume.

5.4 Effects of NS Treatment with Lime in Mitigating Problems from Ettringite-induced Heaving

In this section, nano-silica particles were used as a co-additive with lime to treat sulfate-rich soils. Similar to the studies of the crystalline silica, an array of engineering tests, such as vertical free swell, linear bar shrinkage, Atterberg's limits, strength, and resilient modulus studies, were performed on the treated soil at five curing periods (0 (6 hrs), 3, 7, 14, and 28 days). The free swell and shrinkage tests would help to comprehend the efficacy of amorphous phases of nano-silica in mitigating the ettringite induced heave of the sulfate-rich soils when subjected to moisture intrusion from external sources. The strength and the stiffness properties of the chemically treated soil would provide an overview of the formation of new cementitious reaction products for the development of a stronger soil matrix.

Microstructural studies, including XRD, FESEM, and DSC studies, were performed in addition to engineering tests to develop a comprehensive understanding of the chemical reactions and reaction products formed when treating high-sulfate soil with nano-silica co-additives and dolomitic-hydrated lime.

5.4.1 Determination of the Optimum Dosages

The optimum dosage of lime with Soil-1 was determined in a similar method as discussed in the earlier sections (Eades and Grim test method: ASTM D6276). The optimization of nano-silica co-additives was performed based on the unconfined strength of treated specimens mixed with an optimum dosage of lime (7%) and different dosage percentages of NS. It was necessary to optimize the dosage of nano-silica since the cost of nano-

materials is significantly high, and it might increase the overall project cost. Furthermore, the extensive formation of cementitious reaction products has a detrimental impact on the stabilized soil matrix. C-S-H being a hydrophilic material, when subjected to moisture intrusion, may absorb excess moisture and undergo a significant reduction in the engineering properties.

The trial dosages of NS co-additive were selected as 0.5, 1, 2, and 4% by the dry unit weight of the soil. Dry soil and 7% lime were blended together to prepare a uniform mixture. The NS aqueous solution was mixed to desired proportion to the molding water and subsequently stirred in a magnetic stirrer for 5 mins to form a consistent solution of water and NS co-additive. The solution of water and NS was thereafter mixed with the dry soil-lime mixture and uniformly mixed to form a homogenous molding soil. Cylindrical specimens of diameter 33 mm (1.3 in) and aspect ratio 2:1 (H:D) were prepared by static compaction. Triplicate specimens were prepared for each dosage of NS and cured in a hermetically sealed chamber at 100% relative humidity for 7 days at a standard temperature of 23±2℃ before testing them for unconfined strengths.

After testing the specimens for UCS, their peak values are plotted in Figure 5.15. It was noted that, at a lower dosage of 0.25% NS, there was no significant improvement in the strength as compared to only lime-treated specimens. However, with a higher dosage of 1%, the strength increased 1.35 times more than that obtained after 7 day curing of only lime-treated soils. With further higher dosage, i.e. 2% and 4%, the maximum strength developed was 1.37 and 1.45 times the unconfined strength of lime-treated soils. Therefore, considering the economic aspect of including a co-additive and the engineering

performance of higher dosages of NS, 1% NS was considered optimum for this research study. The remaining engineering and microstructural tests are performed using the optimum dosage of NS mixed with an optimum dosage of lime and dry soil, as discussed in the following section.

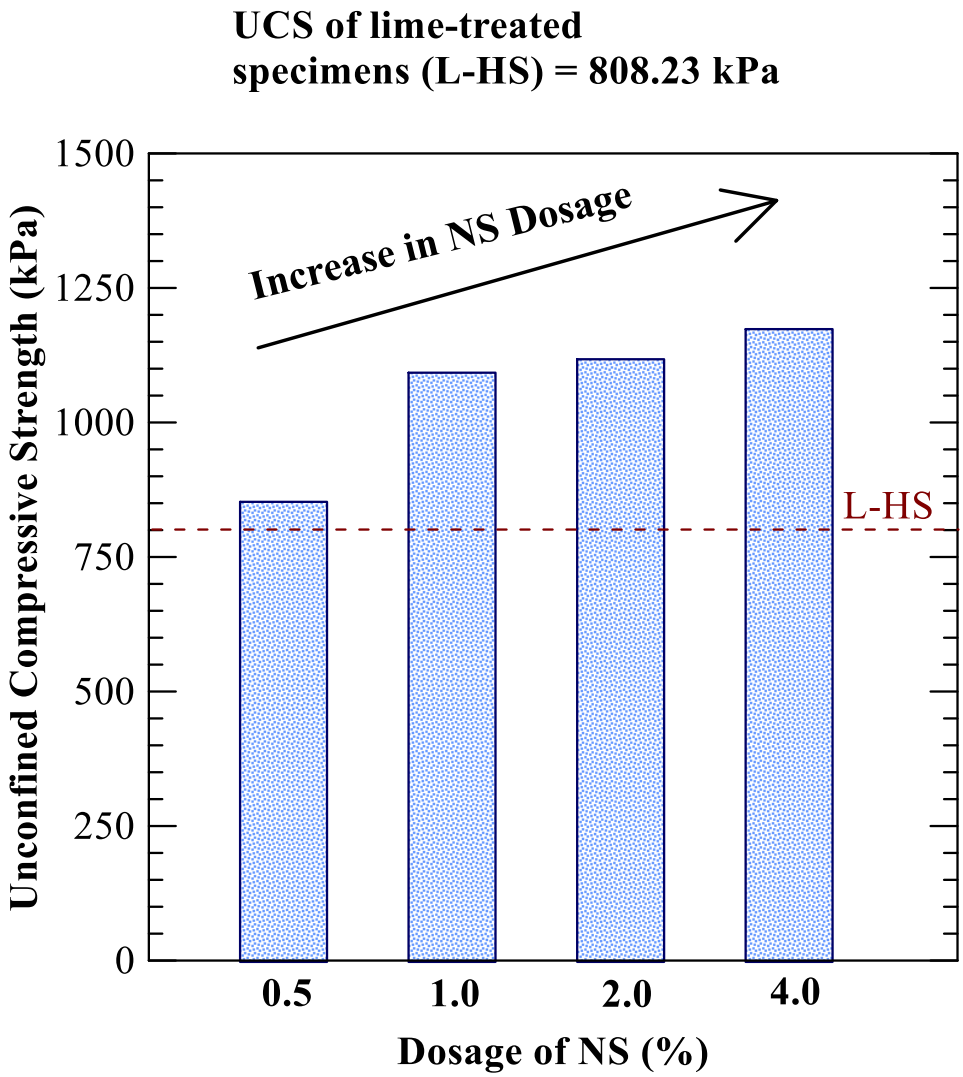

Figure 5.15 Optimum dosage of NS with lime to treat HS soil after 7 day curing.

5.4.2 Engineering Tests

The optimization of the dosages of the nano-silica indicated that 1%NS by dry weight of the soil was optimal to develop the necessary enhancement of the unconfined strength properties as compared to untreated or only lime-treated specimens. Therefore, the remaining engineering tests were performed using the optimum dosages of both lime (7%) and nano-silica (NS) (1%) by the dry unit weight of the soil. The specimens of high-sulfate soil treated with lime and 1% NS (L-HS-1NS) were tested for vertical free swell, linear bar shrinkage, unconfined strength, and stiffness properties over five curing periods of 0 (6 hrs), 3, 7, 14, and 28 days.

The vertical free swell tests were performed in accordance with ASTM 4546. The soil mixing procedures were similar to the methodology discussed in the optimization section. The homogeneously mixed soil was compacted using static compaction in molds of size 2.5 in diameter and 1 in height. After preparing the specimens, all other testing conditions were similar to the one discussed under Section 5.2.2 (crystalline silica 1D-free swell tests). Similarly, the shrinkage tests were also performed in accordance with Tex-145-E. The soil mixing for shrinkage test was done similar to the procedure as discussed in the optimization section (Section 5.4.1). The homogeneously mixed soil was stored in hermetically sealed chambers before testing the shrinkage potential. The specimens for the UCS test for different curing periods were prepared in a similar fashion, as discussed in Section 5.4.1 (optimization of NS dosage). The duplicate specimens for RLTT tests were molded in 71 mm diameter molds with an aspect ratio of 2:1 (H:D) using static compaction and tested for different curing periods in accordance with AASHTO T 307.

In addition to macrostructural engineering tests, microstructural and mineralogical studies were also performed, as discussed below.

5.4.3 Mineralogical and Microstructural Tests

Powder X-ray diffraction analysis was performed on the nano-silica (NS), untreated soil (HS), lime-treated high-sulfate soil (L-HS), and lime and nano-silica treated high-sulfate (L-HS-1NS) specimens. The lime-treated specimens were prepared as slurries, in accordance with the recommendations made by Puppala et al. (2005) and Chakraborty and Nair (2018, 2020), to ensure homogeneity and reduce chances of sampling error while collecting subsamples for XRD. Treated specimens were cured at 23±2°C, and prior to testing, air-dried in an oven at 40°C for 4 hours, lightly crushed, and placed in the powder XRD specimen holder. Cu-kα radiation with a wavelength of 1.54 nm was used over the range of 5 to 60° for 2θ, with a step size of 0.02° and 0.5sec/step.

ICDD database was used for the identification of the minerals from the location of their characteristic peaks on the diffractogram. As discussed in some previous sections, identification of amorphous phases of cementitious reactions products is often difficult in soil mixture due to the presence of other distinct crystal peaks of constituent minerals. Hence additional studies using FESEM and DSC were also performed to identify the new reaction products formed in the treated soil matrices.

Specimens of L-HS, and L-HS-1CS were scanned using FESEM. The specimens were cured in a similar procedure as those used for the XRD specimens. The FESEM imaging was performed with the aim to visually detect the formation of cementitious reaction products and the presence of ettringite crystals in the different specimens. DSC

was performed on specimens of L-HS and L-HS-1NS after 14 days of curing. Approximately 50 mg of the specimens were placed in an inert alumina crucible and tested in temperatures ranging from 50°C to 1000°C, at a heating ramp of 10°C/min. A constant nitrogen purge of 20 ml/min was used during the heating process.

The microstructural test results were used to comprehend the characteristics exhibited by the different specimens at a macro scale. The following section presents a detailed analysis and discussion of the test results and highlights the salient findings of this research.

5.4.4 Analysis and Discussion of Results

5.4.4.1 Engineering Tests

The vertical free swell test results of HS, L-HS, and L-HS-1NS specimens are presented in Figure 5.16 after different curing periods of 0, 3, 7, 14, and 28 days. The untreated soil (HS) has a free swell percentage of 23.5%. Due to the application of Ca-based stabilizers, the swelling percentage reduced to around 20% immediately after treatment with lime. This immediate improvement is attributed to the cation exchange and flocculation-agglomeration reactions, collectively known as modification reactions.

After 3-day curing, the L-HS specimens exhibited a swell strain percentage of 17.1%, and as discussed in the previous section when treating with CS, this typical nature of the S-Shaped curve could be attributed to ettringite induced swelling. Over longer curing periods of 7, 14, and 28-days, the specimens treated with only lime exhibited swell strain percentages of 10.9%, 10.1%, and 7.2%, respectively (Figure 5.16a). The swell

curves of the L-HS specimens are typically associated with the formation and precipitation of ettringite, as discussed in the previous sections.

The specimens treated with both lime and NS accumulated a swelling strain of 16% immediately after treatment. The presence of additional amorphous phases of the co-additives provided the active sites for Ca^{+2} ions to react with the silica and form C-S-H phases. These cementitious phases, in addition to modification reactions, helped to reduce the swell in these NS-treated specimens. Over the longer curing period of 3 days and onwards, there was a general reduction in the swell percentage. The free swell percentage reduced gradually to 8.3%, 8.1%, 6.5%, and 5.1% after curing for 3, 7, 14, and 28 days (Figure 5.16b).

The swelling observed in the NS treated specimens is comparatively lower than the swelling observed in only lime treated specimens. However, it should be noted that the treating the HS soil with both 7% lime and 1% NS was unable to reduce the swelling percentage below 2-3% even after a longer curing period (unlike the CS co-additives). Swelling of expansive soils more than 2-3% is considered detrimental to any structures supported by the expansive soil. Therefore, further rationales are discussed below for determining the reasons for the failure of the NS augmentation in mitigating the heaving problems of sulfate-rich soils.

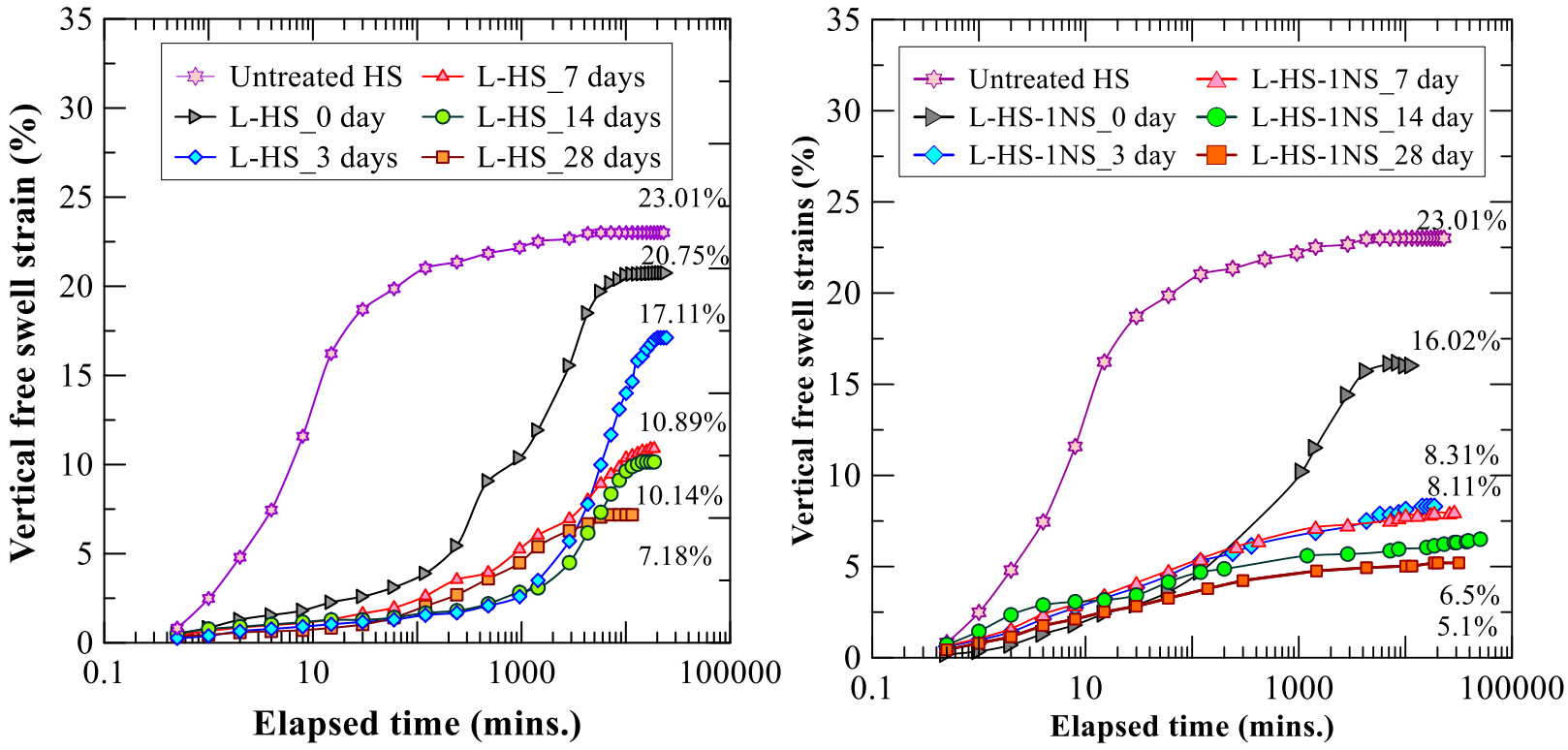

Figure 5.16 1D free vertical swell over different curing periods for a) L-HS b) L-HS-1NS.

Comparing the swelling behavior of L-HS soils and L-HS-1NS soils, a stark difference in the behaviors was noted, which are discussed below. Immediately after treatment (6 hrs), when the L-HS-1NS specimens were subjected to free swell test, the specimens swelled more than 15%. Even though the percentage swelling was less than L-HS specimens, the S-shaped swelling curve was observed for the specimens. During this early curing period, the behavior of the NS-treated soil showed similarity to that of only lime-treated soils. This primarily occurred because immediately after soaking the specimen during the swell test, the modification reactions and the partial C-S-H gels formed from the reaction between co-additive and lime. These gels bonded the soils, which was able to resist the swelling in the soils from hydration.

Ettringite precipitation and nucleation might be in the nascent state and enough crystals have not precipitated to exhibit immediate swelling. However, as the test proceeded over the next 25 days, there was an ample time to nucleate and precipitate a substantial proportion of ettringite due to the dissolution of the alumina from the soil and the available Ca-ions from the lime treatment. Furthermore, the ettringite crystals formed absorbed the moisture from submerged water and underwent swelling to develop the repulsive forces in the crystals. As the specimen was constantly submerged underwater, the bonding gels formed in the specimen probably could not develop enough anchoring forces between them or within the soil matrix to resist the repulsive forces. As a result, more than 16% of final swelling was observed in the 0-day treated specimens.

The L-HS-1NS treated specimens after 3 days of curing did not show the behavior atypical to only lime-treated soils (L-HS). The curves do not have the typical S-shaped

nature as the lime-treated specimens and probable causes could be explained as follows. The treated soil specimens showed an immediate swelling as soon as they were subjected to moisture intrusion. The high-sulfate soil, when treated with lime and NS and subjected to a longer curing period experienced three distinct chemical reactions. First, due to dissolution of soil silicates and soil aluminates under alkaline environment and results in the formation of cementitious compounds such as C-S-H and C-A-H, next in the presence of additional reactive silica phases in the form of nanoparticles, partial Ca^{+2} ions from the dissolution of $Ca(OH)_2$ reacts with nano-silica particles to form cementitious gels of C-S-H. Finally, due to the presence of high-sulfate concentration in the soil, partial Ca^{+2} ions react with the dissolved alumina and soluble sulfates to precipitate ettringite crystals.

As the temperature of the reaction is controlled at 23±2℃, the probability of formation of thaumasite by isostructural substitution could be easily neglected. The treated soils at different stages of curing possess different percentages of the three major reaction products. The percentage of each reaction product and their behavior due to water absorption during the swell test influence the overall behavior of the specimens.

After the lime-treated specimens have been subjected to curing, it is expected that partial Ca^{+2} has been utilized to precipitate ettringite within the soil matrix. When added to the soil, NS co-additives provide additional reactive surfaces, and concurrently, the nano-sized particles have the potential to develop a filler effect and develop a denser matrix, making the soil less porous compared to lime treatment alone. Due to the development of a very dense matrix, there is a reduction in soil porosity, and consequently, there is a reduction in the available voids in the treated matrix.

As moisture intrusion in the soil matrix takes place, the ettringite crystals absorb the water and result in crystal growth. Due to the dense matrix, the cured soil cannot accommodate the swelling crystals within the pores, and as a result, it immediately starts to swell. This behavior is different from that of lime-treated soil specimens where, first the ettringite would be accommodated inside the available pores and subsequently, further swelling of the crystals would increase the overall swelling of the treated soil (or increase in the overall void ratio). As a result, in the case of L-HS specimens, a typical S-shaped swelling curve was observed, where the initial part accommodated the growing ettringite crystals within the available voids and after a particular time undergoes an overall increase in the void ratio. However, it was observed that 1% NS was not able to resist the swelling, which could be either due to excessive growth of ettringite crystals or the inability of the C-S-H phases to resist the moisture-induced repulsive forces. These factors were further analyzed in the microstructural analysis to determine predominant minerals that affect the soil swelling behavior. In addition to the swell behavior, the effects of moisture extrusion from the soil are also analyzed using shrinkage test as discussed below.

The specimens of L-HS and L-HS-1NS were tested for linear bar shrinkage tests (Figure 5.17). The untreated specimen of the high-sulfate soils has a shrinkage potential of more than 15%. The high shrinkage percentage might have a damaging effect on the overlying structure when subjected to drying conditions in the summer seasons. Treatment of the soil with lime immediately reduces the shrinkage strain to about 9%, and with the increase in curing period, the shrinkage strain is reduced to 1.9% for all L-HS specimens. The presence of Ca ions for lime induces cation exchange with monovalent ions on the

clay surface. Due to the presence of divalent ions on the clay surface, the surface charges are neutralized, and it reduces the potential to absorb bipolar water molecules. Over a longer curing period, the pozzolanic reactions form cementitious gels in the soil induce chemical bonds between reactive clay surfaces and thus leading to newly formed cementitious bonding. This reduces the overall affinity of the high-plastic clay to undergo water absorption. As a result, the soils become workable and less plastic. As the plasticity reduces, the shrinkage potential will also go down.

L-HS-1NS specimens experienced low shrinkage strain almost immediately after treatment. In comparison to the lime treatment alone, the reduction in shrinkage was 2% more after 3 days of curing. The final shrinkage strain in percentage after 28 days of curing was almost negligible and less than 1%. The presence of additional phases of C-S-H in the treated soil possibly helped to develop neutral clay surfaces, thereby reducing the affinity to absorb water molecules. In order to verify the changes in the soil plasticity, Atterberg's Limit tests were performed on the treated soil specimen after different curing periods. The results from Atterberg's limit tests are discussed below.

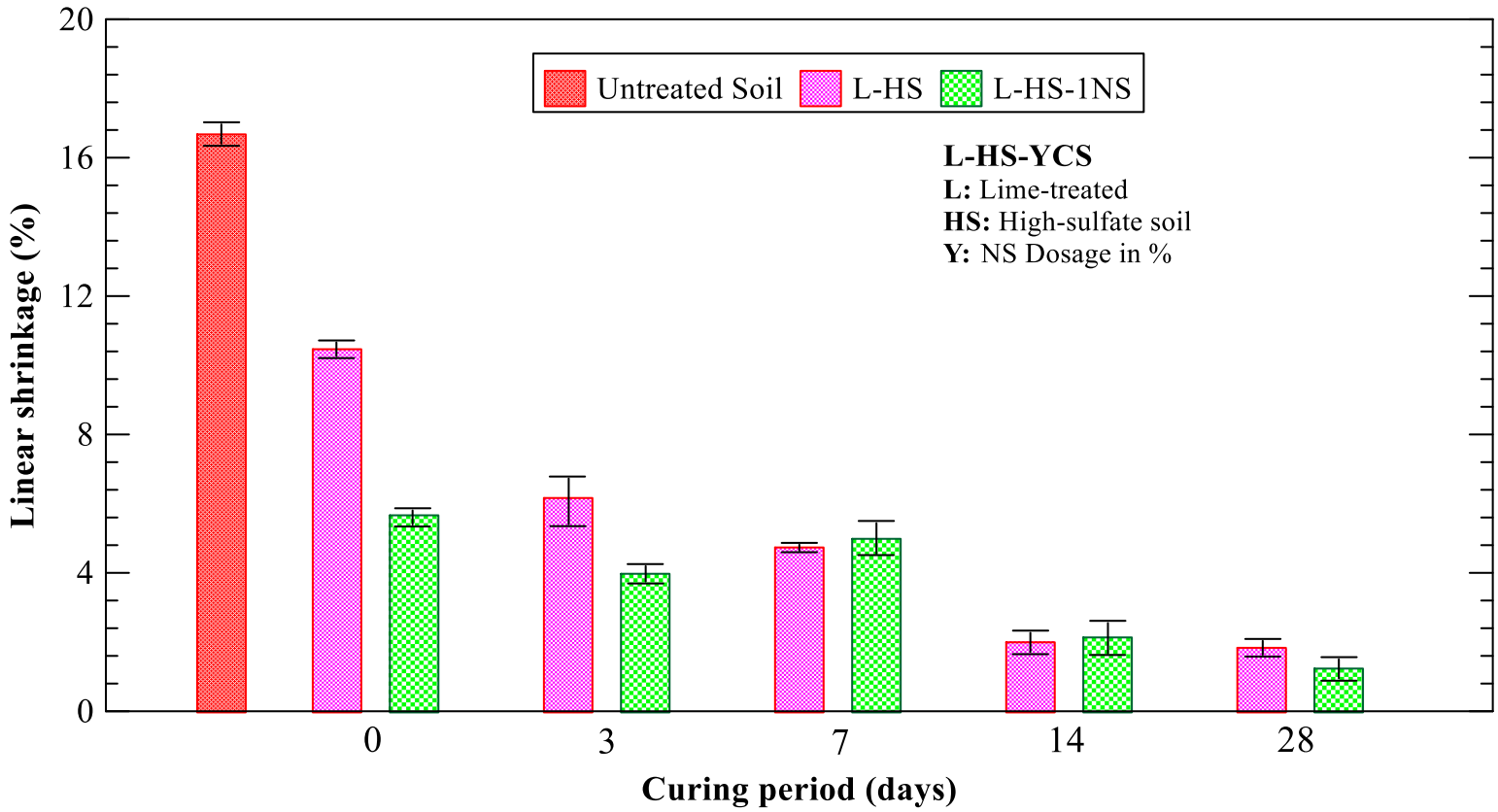

Figure 5.17 Linear shrinkage of NS treated specimens over different curing periods.

The L-HS-1NS specimens were tested for Atterberg's limits over different curing periods and the values are compared with traditional lime treatment (Figure 5.18). Similar to the CS co-additive, the addition of NS with lime immediately helped to reduce the soil plasticity as compared to only lime treatment. The immediate modification reactions coupled with the additional cementitious phases helped to neutralize the surface charges and reduced the moisture affinity of the soil.

Furthermore, with the progress of the curing period, the NS treated soils develop a granular nature with lower moisture affinity compared to only lime treatment. This helps to further reduce the plasticity in NS-treated soils, as compared to only lime treatments. However, over an extended curing period, it was observed that there is a significant increase in the both LL and PL due to NS addition. Therefore, the results indicate that more water is needed for the loss of shear strength, verifying that the reaction products have a tendency to develop a strong soil matrix and require more water molecules to develop repulsive forces. In addition to the volumetric strains due to moisture migrations, the treated soil was tested for unconfined strengths over five different curing periods, as discussed below.

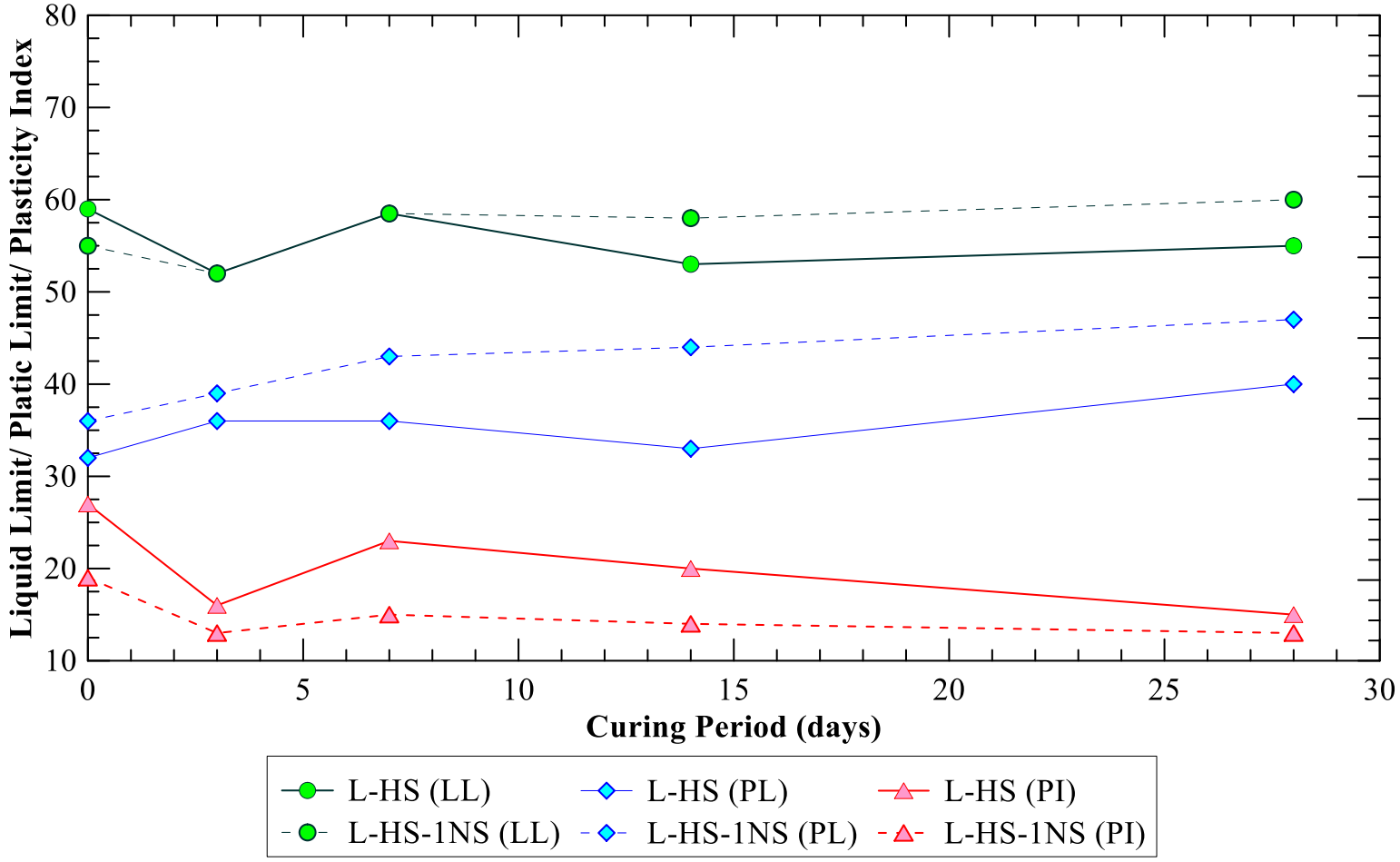

Figure 5.18 Atterberg's limit tests on lime-treated and lime and NS-treated high-sulfate soil.

Specimens of L-HS-1NS were subjected to unconfined strength tests after 5 curing periods. Triplicate specimens were tested for each curing period and the results reported here are an average of all three values. Efforts were made to minimize the errors in the strength values among the tested specimens (Standard Deviation, $\sigma <\pm 10\%$). Application of the NS co-additive with lime accelerated the formation of peak strengths as compared to only lime-treated specimens (L-HS). Figure 5.19 shows the unconfined strength test results of L-HS and L-HS-1NS specimens over different curing periods.

In addition to accelerated strength gains immediately after 3days of curing, the overall strength of the treated specimens at the end of 28 days is 1.42 times higher than only lime-treated specimens. Over a longer curing period, the formation of cementitious phases due to pozzolanic reactions, additional C-SH phases occurred from the presence of nan-silica particles and its reaction with available Ca^{+2}, and the formation of needle-shaped ettringite crystals helped in the development of the overall strengths of the specimens. In order to address the efficacy of using the stabilizer for supporting pavement infrastructure, it is necessary to study the stiffness property strength behavior for a comprehensive understanding of the material behavior. The next section discusses the resilient moduli properties of the treated soil specimens tested in accordance with AASHTO T 307.

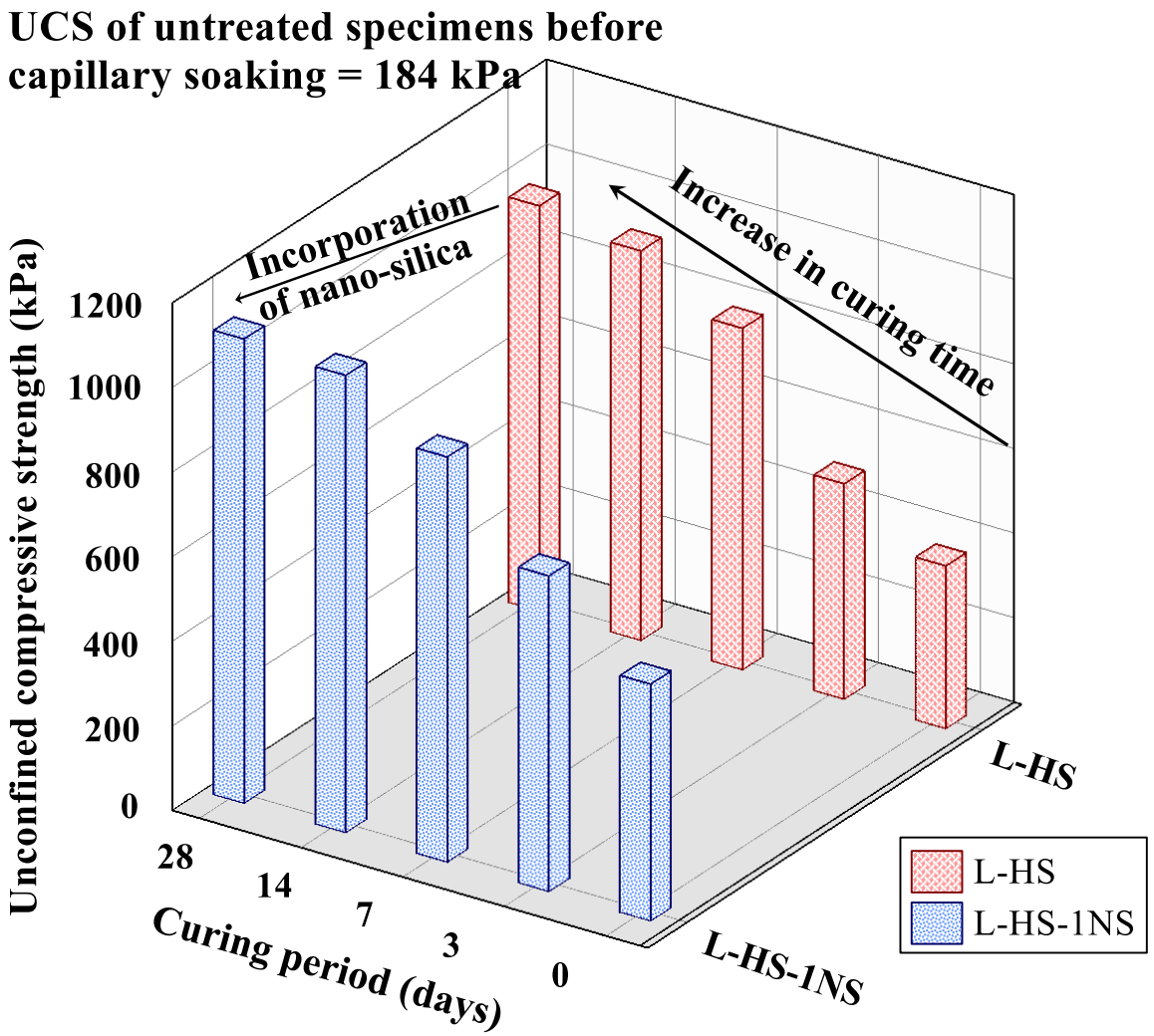

Figure 5.19 UCS values of L-HS and L-HS-1NS over different curing periods.

In order to understand the effects of lime and NS co-additive treatments on high-sulfate soils, the analysis of the RLTT is presented in terms of universal model parameters k_1, k_2, and k_3. The discussion on the universal model and its parameters are already presented in the previous sections. Table 5.4 shows the universal model parameters for the L-HS soil and the L-HS-1NS soil over different curing periods. The k_1 parameter is generally indicative of the dynamic elastic modulus magnitude of the soil under consideration. From the table, it could be noted that the application of NS co-additive with lime has significantly accelerated the elastic modulus after 3 day of curing as compared to lime treatment. This primarily occurs due to the additional sources of silica in the soil.

Over a longer period, the elastic stiffness parameters are observed to be lower than L-HS soils. As previously discussed, the application of NS co-additives helps to develop a uniform coating of C-S-H around the surface of the soil particles. Even though the cementitious gels form a bonding gel with the soil, due to their amorphous nature, reduce the inter-particular friction and increase the cohesion among soil solids. This could be one of the primary reasons for the lower stiffness properties as compared to lime-treated soils. There was no particular trend noted for k_2 parameter in the treated soil. The k_3 parameter value gradually increases from 0.071 to higher values with the progress of the curing period, except for 28 days. A negative value of the k_3 parameter indicates a softening effect, which is noted in untreated soil and soil during the early curing period (0-day). A positive value of k_3 indicates the strain hardening effect typical of any treated soil, and similar results were noted in this study.

Table 5.4 Regression coefficients of universal model for L-HS and L-HS-1NS specimens over different curing periods

Curing Period (days)	k_1		k_2		k_3		R^2	
	L-HS	*L-HS-1NS*	*L-HS*	*L-HS-1NS*	*L-HS*	*L-HS-1NS*	*L-HS*	*L-HS-1NS*
0	1473	1465	0.128	0.103	0.161	0.071	0.90	0.82
3	1676	1681	0.131	0.257	0.233	0.308	0.97	0.94
7	1877	1822	0.169	0.180	0.310	0.541	0.94	0.90
14	2002	1831	0.127	0.137	0.499	0.693	0.91	0.90
28	2049	2113	0.151	0.204	0.562	0.434	0.90	0.93

Note: k_1, k_2 and k_3 are universal model parameters

5.4.4.2 Microstructural and Mineralogical Tests

The FESEM studies were performed on L-HS and L-HS-1NS cured for 14 days to observe the changes in the morphological properties of the treated soil specimens. Figure 5.20a shows the SEM image of the lime-treated soil at a magnification of 5,000x and 10,000x. The specimens are observed to contain a combination of soil particles and reaction products which has formed at the surface of the particles. Further magnification of around 25,000x indicates the presence of needle-shaped crystals of ettringite in the soil (Figure 5.20c). The presence of calcium, alumina, and sulfate in the soil helped in the nucleation and precipitation of the ettringite crystals in the lime-treated soils.

The SEM images of L-HS-1NS specimens are shown in Figure 5.21a-e. At lower magnifications 250x and 1,000x, the material is observed to be coated with some uniform reaction products. After increasing the magnification to 2,000x and 2,500x, it was observed that the soil particles were coated with uniform materials of cementitious phases as well as some evidence of needle-shaped ettringite crystals were also noted. Therefore, after the treatment of NS to high sulfate soils, there was evidence of both additional phases of C-S-H that forms a uniform coating on the surfaces of the particles as well as in some locations ettringite crystals has also precipitated. The ettringite crystals possibly precipitated at the location where the concentration of dissolved alumina is high than the concentration of silica for both clay dissolution and nano-silica phases. In the locations where the concentration of silica compounds was higher, the Ca^{+2} from lime has reacted to form the cementitious bonding phases. Therefore, the ettringite crystals formed have the potential to develop disruptive repulsive forces, which can induce the expansion of

stabilized layer when subjected to moisture intrusion. This could be one of the reasons for the observed swelling in the treated soils even after longer curing periods.

Although, the NS treated soil specimens have the potential to swell similar to only L-HS specimens due to ettringite, the presence of additional phases of C-S-H restricts the repulsive forces from ettringite and helps to reduce the overall swelling as compared to lime-treated specimens. The theory of the efficacy of additional silica-based phases in reducing ettringite heave was verified with DSC studies and XRD studies as discussed below.

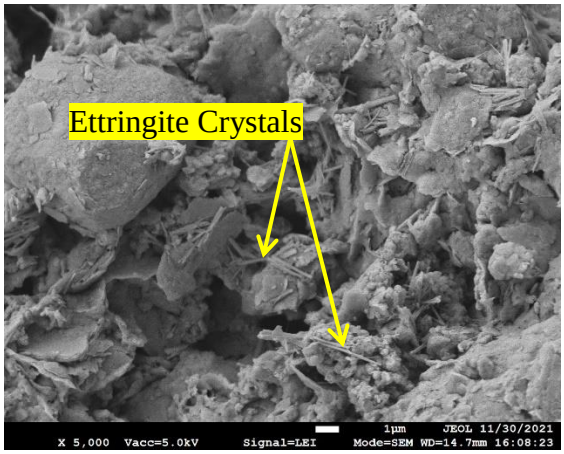

(a)

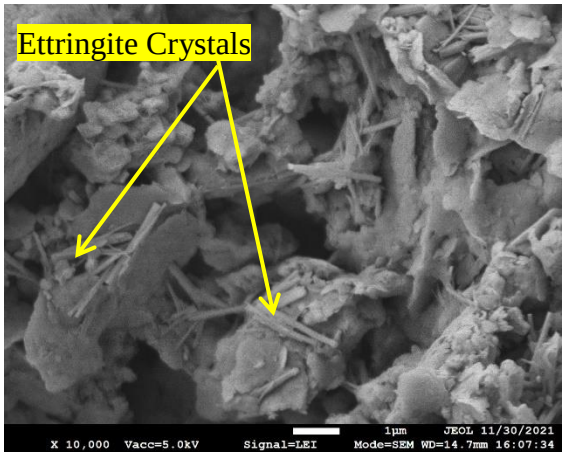

(b)

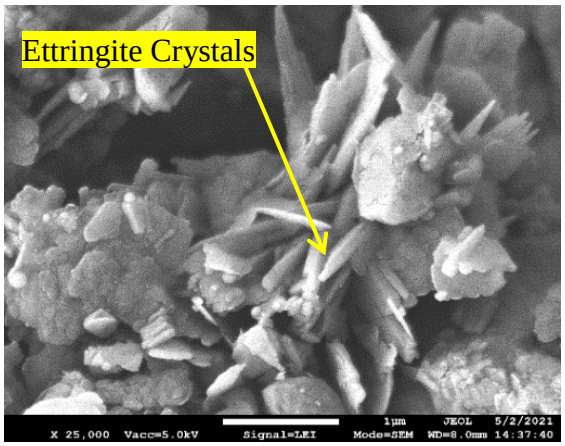

(c)

Figure 5.20 SEM images of L-HS at different magnification a) 5000x b)10,000x and c) 25,000x.

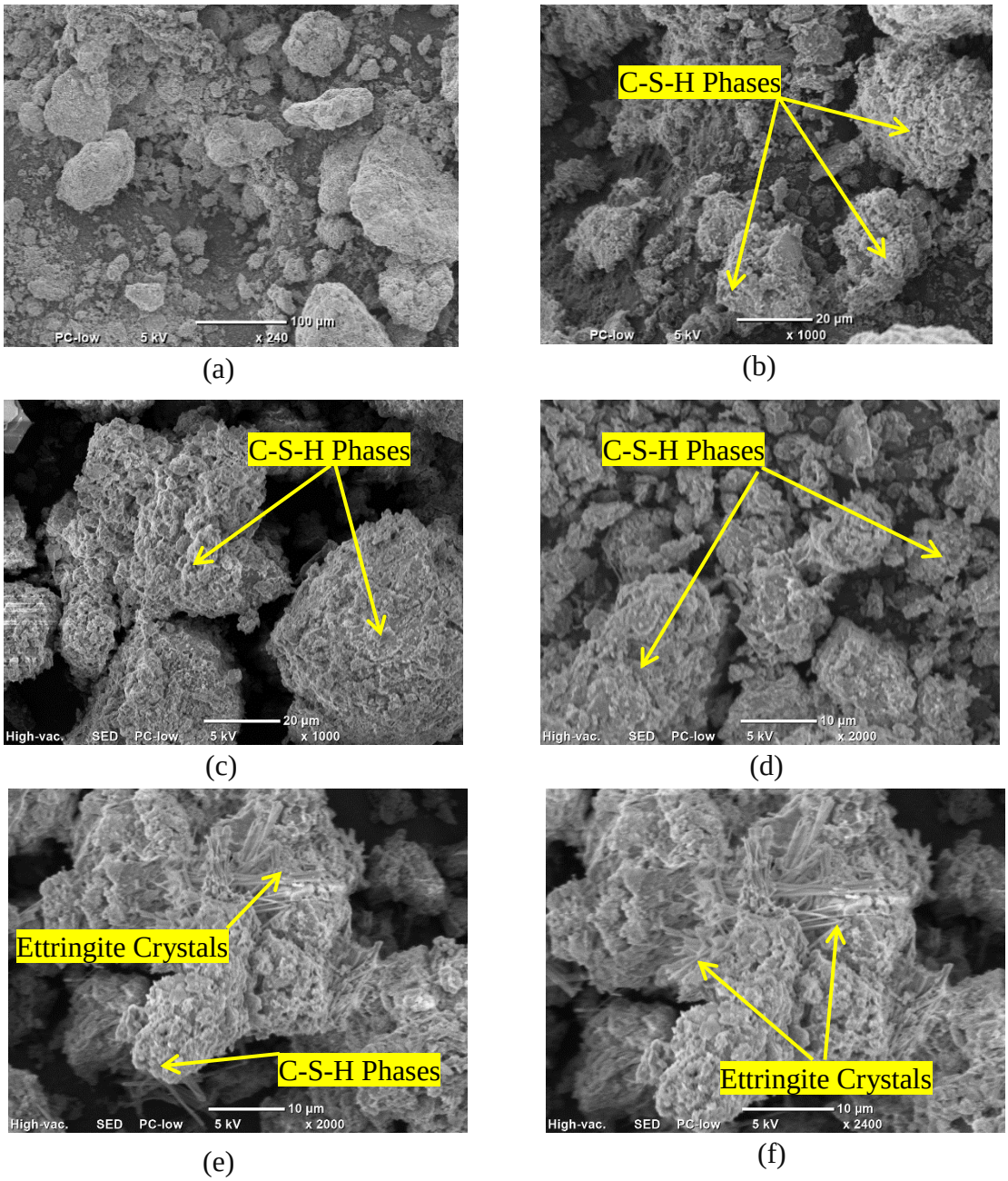

Figure 5.21 SEM images of L-HS-1NS after 14 days of curing at different magnifications a) 250x b) 1000x c) 1,000x d) 2,000x e) 2,000x and f) 2,500x.

Figure 5.22a and 22b present the DSC thermograms of the lime-treated HS soil specimens and the lime and nano-silica treated HS soil specimens, respectively. For the

purpose of easy identification of the endothermic or exothermic thermal peaks, the plot is shown in terms of weight corrected heat flow, as well as derivative of weight, corrected heat flow. In Figure 5.22a, strong endothermic peaks are noted at 386ºC, 500ºC and 760ºC. These endothermic peaks are formed due to absorption of heat and thermal decomposition of $Mg(OH)_2$ to MgO and H_2O, $Ca(OH)_2$ to CaO and H_2O, and $CaCO_3$ to CaO and CO_2, respectively. A strong endothermic peak was observed at 135ºC, which is associated with the dehydration of ettringite.

In addition to the ettringite dehydration, a weak endothermic peak was observed at around 154ºC, which is associated with the first dehydration stage of $CaSO_4.2H_20$ to $CaSO_4.0.5H_20$. A weak exothermic peak was observed between 850ºC and 890ºC, which is generally associated with the re-crystallization peaks of C-S-H phases with Ca/Si ratio between 1.0-1.33 (Rodriguez et al. 2017). This C-S-H phase probably formed in the soil where the concentration of Ca^{+2} ions was comparable to the SiO_2^{-4}, and part of available calcium has been used for the formation of calcium-alumino-sulfate phases resulting in a higher Ca/Si ratio.

Figure 5.22b shows the DSC peaks of lime and nano-silica treated high sulfate soils. The endothermic peaks corresponding to the decomposition of $Mg(OH)_2$, $Ca(OH)_2$, and $CaCO_3$ were observed to be similar to the lime-treated soil. Strong endothermic peaks were also observed between 50ºC -110ºC, corresponding to the dehydration of C-S-H phases and some ettringite phases. These strong peaks are formed due to the additional phases of C-S-H from the addition of NS co-additive to the soil. A strong endothermic peak at 154ºC corresponding to dehydration of gypsum shows that due to the presence of

NS, the amount of gypsum utilized is significantly reduced and indirectly validates that less ettringite has precipitated in the treated soil.

Furthermore, the absence of ettringite dehydration peaks in this thermogram shows the utility of adding additional source of silica to lime. In the case of lime-treated soils, the gypsum peak was weak, whereas the NS addition increased the intensity of gypsum dehydration, indicating a higher concentration of residual gypsum concentration. Therefore, the addition of nano-silica has resulted in the utilization of the available calcium from lime to form additional phases of C-S-H and subsequently reducing the availability of Ca^{+2} ions to form the calcium-alumino-sulfate phases, or ettringite. This strongly supports the efficacy of using the silica-based source to mitigate the formation of ettringite-induced heaving.

In addition, exothermic peaks at 830ºC and 915ºC were observed corresponding to the re-crystallization of C-S-H I (Ca/Si = 1) and C-S-H II (Ca/Si > 1.5) phases in the lime and NS treated soils. The C-S-H II phases have precipitated in the regions where the available concentration of Ca^{+2} was more than the nano-silica or silica dissolved from the clay layers. Whereas the C-S-H I phases might have precipitated in the vicinity of the nano-silica particles, which have increased the concentration of Si as compared to available lime resulting in a lower Ca/Si ratio. From the thermal studies, it was evident that adding NS co-additive to lime has a beneficial effect on mitigating ettringite-induced heave for high-sulfate soils. This theory was further validated by performing XRD studies on the treated soil specimens, as represented in the following paragraphs.

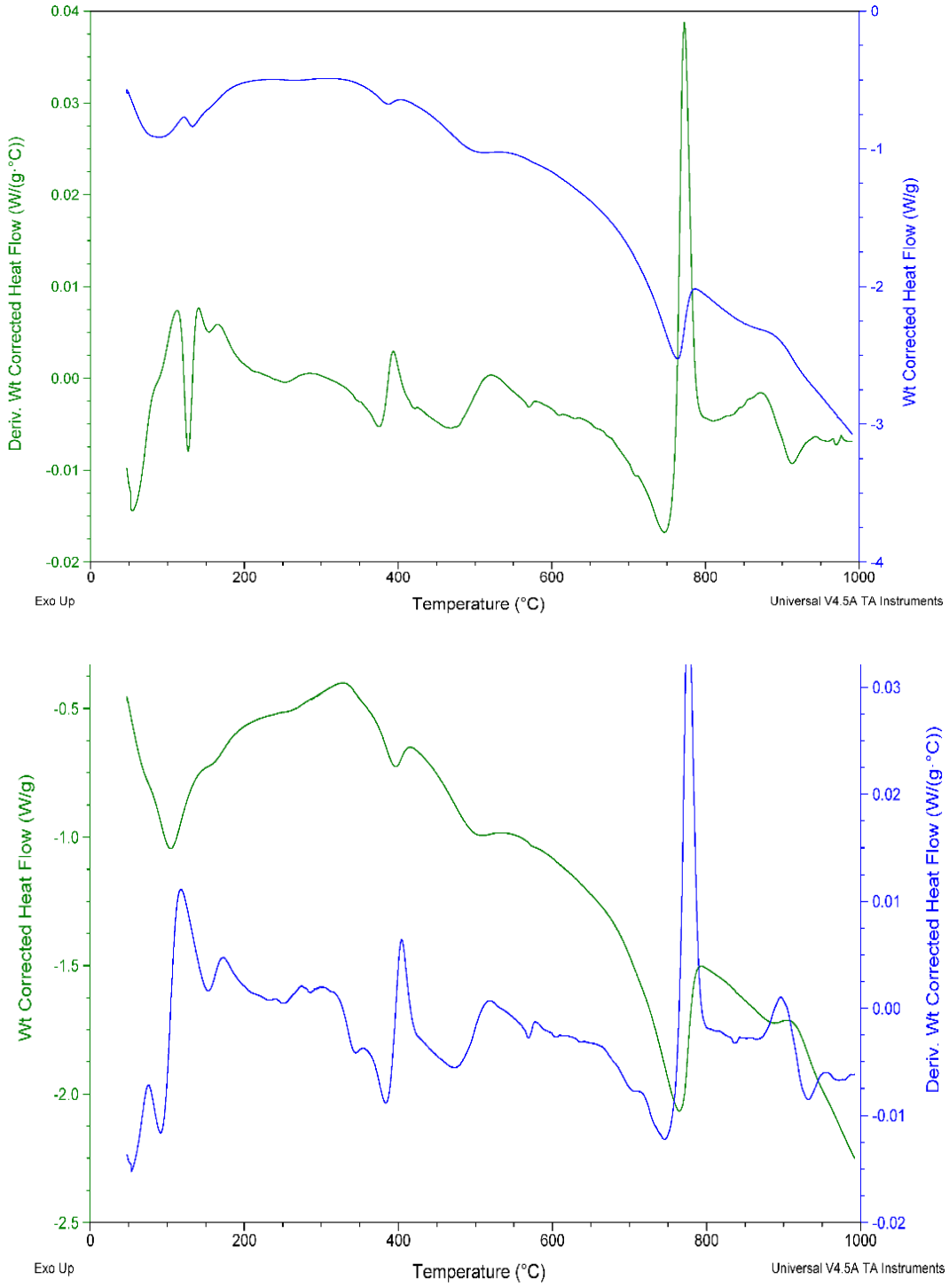

Figure 5.22 DSC curves of a) L-HS and b) L-HS-1NS.

XRD studies were performed on HS, L-HS and L-HS-1NS soil specimens to determine the efficacy of NS treatment in mitigating the sulfate-induced heave problems (Figure 5.23). The treated soils were tested after 14 days of curing period. Figure 5.23 represents the XRD diffractograms of all untreated soil. As mentioned earlier, characteristic peaks of Calcite, Quartz and several other clay minerals, including Illite, Kaolinite, and Montmorillonite, were observed in the specimen. Furthermore, the characteristic gypsum peak was also present, indicating the presence of the deleterious source of sulfate ions in the soil.

Treating the soil with lime exhibited similar characteristic peaks as the untreated soil of the majority of the minerals. However, it was noted that broad peaks of ettringite were formed in the region of the 2θ peak of 16°, and another characteristic peak was observed at 18°. Furthermore, there was an absence of the gypsum peak in the diffractogram, indicating the utilization of gypsum as a reactant to form the tri-sulfate phases of alumino-sulfate compounds. Similar observations were also made using the DSC analysis. No significant peaks of C-S-H were observed in the soil even though it has precipitated due to the amorphous nature of the cementitious bonding gels.

In the NS treated soils, the characteristic peaks of dominant clay minerals were visible in the diffractogram. There is an increase in the relative intensity of the peaks at 29° as compared to untreated soil; this could be attributed to carbonation reactions as well as the formation of C-S-H phases. Small peaks observed in the region of 2θ = 31° are due to C-S-H precipitation from pozzolanic reactions as well as Ca^{+2} and nano-silica reactions. Since amorphous in nature, the C-S-H peaks were distinctly not visible in the

diffractogram. Unlike the L-HS specimens, no major hump of amorphous ettringite was observed at 2θ = 16°. Characteristic ettringite peaks were observed at 18°, 23°, and 35º; however, the relative intensity was significantly lower as compared to only lime-treated soils. This verifies the previous observation of SEM and DSC analysis which shows that the presence of additional sources of silica reduces the potential of formation ettringite, either by reducing the dissolution of alumina in the soil matrix or by reducing the percentage of available Ca^{+2}-ions for forming the alumino-sulfate compounds.

Therefore, from the series of engineering and the microstructural and mineralogical studies, it could be concluded that the presence of additional silica phases in the form of NS co-additive while treating sulfate-rich soils with lime have a strong potential to mitigate the precipitation of ettringite and consequently reduce the damages from ettringite-induced heave.

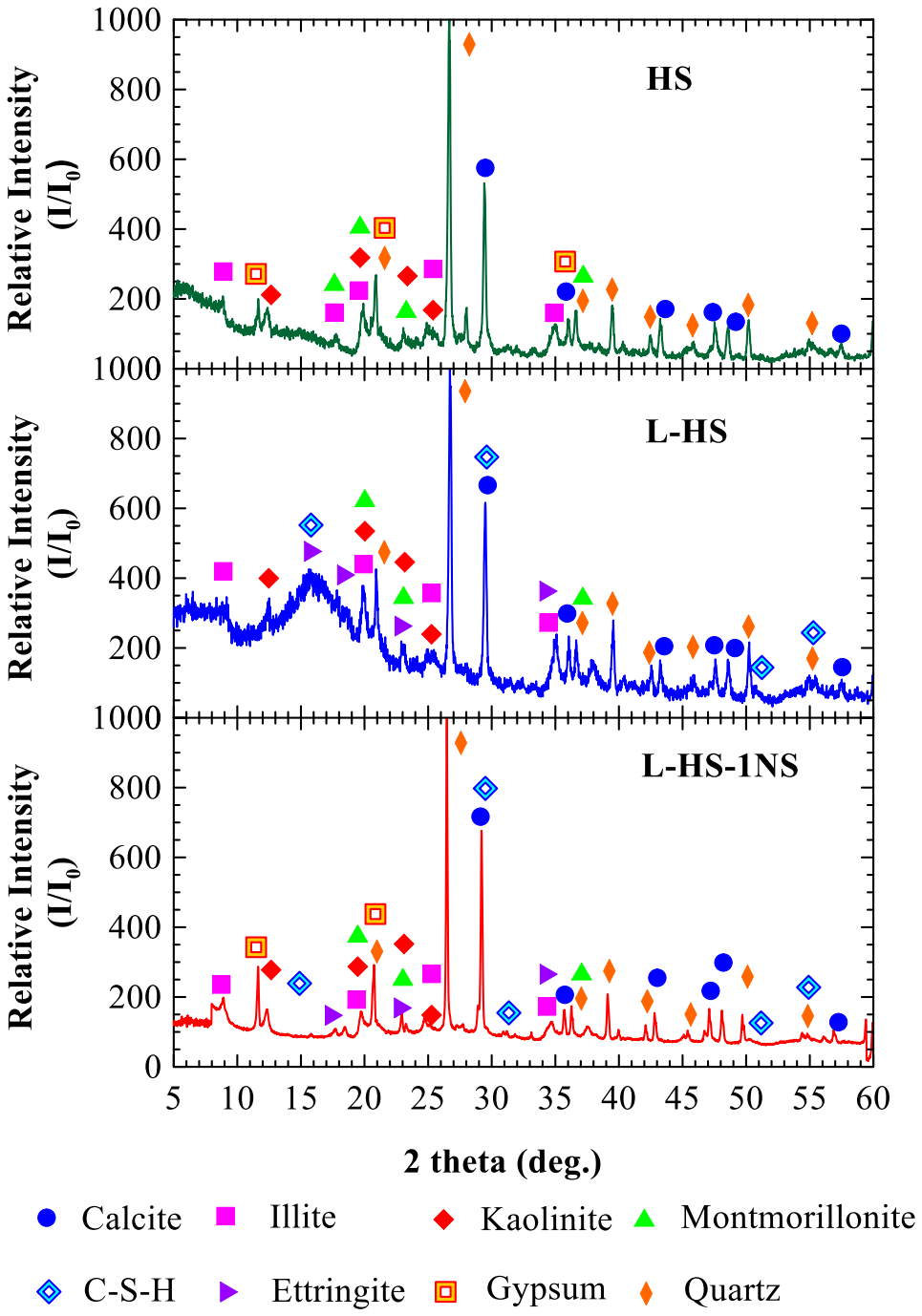

Figure 5.23 X-ray diffractogram of HS, L-HS, and L-HS-1NS.

5.5 Summary

In this Chapter, the crystalline silica (CS) and nano-silica (NS) based co-additives were mixed with traditional lime to treat and stabilize high-sulfate soil. A series of engineering and microstructural test were performed to understand the efficacy of each co-additive to mitigate ettringite-induced damages. Some major conclusions from this Chapter are stated below:

- The addition of crushed sand, a crystalline silica-rich admixture, has substantially reduced the ettringite-induced heave in high-sulfate soils. It also helped to improve the shrinkage, strength and stiffness properties of the treated specimens, as compared to lime treatment alone.

- The presence of new products, formed by the reaction of lime and silica available from crushed sand, was evident from the XRD data and SEM images. The EDXS data and DSC thermograms confirmed the reaction products to be the strength contributing C-S-H phases. The engineering test results, supplemented by the mineralogical and microstructural analyses results, indicate that the silica admixtures can potentially suppress the formation of ettringite.

- The swelling characteristics were substantially reduced by introducing crystalline silica fines as co-additive with lime. The beneficial influence of crystalline silica increased with dosage and curing time. Comparison of ettringite-induced swell strains interpreted from swell tests and those estimated using stoichiometric models indicates that the presence of crystalline silica can potentially suppress the availability of alumina. Moreover, the crystalline silica fines reacted with lime to

form cementitious compounds that prevented the ettringite-induced heaving and increase in void ratio. This characteristic is expected to prevent ettringite-induced damage and wreaking of the treated soil and the pavement infrastructure.

- Similar to crystalline silica, the addition of nano-silica also reduces the swelling potential of treated soils as compared to lime treatment alone. Furthermore, the nano-silica particles being amorphous in nature with highly reactive surfaces accelerate the development of strength and stiffness and rapidly reduce the shrinkage properties.
- Microstructural studies validated that the nano-silica has effectively reduced the precipitation of ettringite by suppressing the availability of alumina or calcium for forming the calcium-alumino-sulfate hydrate compounds. Therefore, the development of a denser matrix due to the filler effect of nano-silica and reduction of soil porosity to accommodate ettringite crystals could be attributed as a primary reason for swelling of the cured specimens when subjected to moisture intrusion.

6. DURABILITY AND PERMANENCY OF TREATMENTS WITH SILICA-BASED CO-ADDITIVES

6.1 Introduction

In the previous chapters, detailed discussions have been provided on the efficacy of the two new novel co-additives to improve the performance of lime treatments in high-plasticity clayey soil. However, research studies have indicated that a comprehensive knowledge of the long-term performance of the treated soil layers is necessary before recommending the stabilizers for the geotechnical practitioners. During the process of pozzolanic reactions, excess moisture infiltration into the soil layers from external sources could potentially cause damage to the stabilized layers. Additionally, research studies have suggested that the migrating water has the potential to remove unreacted or partially reacted calcium through the leaching process. Permanency of stabilizer dosage is, therefore, a cause of concern, as removal of Ca^{+2} ions, could result in appreciable lower final target strength and subsequently could impact the serviceability performance of the infrastructure.

A research task was developed to address the issues regarding the durability and permanency of the co-additive treatment when commixed with a traditional Ca-based stabilizer. The performance of these novel co-additives was compared with the traditional treatment technique involving only dolomitic-hydrated lime as stabilizer. Engineering tests, including unconfined strength after subjecting the specimens to capillary soaking for 48 hours, measurement of volumetric swell, and determining the water absorption potential of the treated specimens after capillary soaking were performed to predict the

durability of the stabilized soils after different curing periods. Unsaturated studies using soil water retention curves were performed to understand the pore structural changes after a 28 days of curing period that would help us to interpret the relation between the moisture retention capacity of the treated soils and its probable effects on durability. Leaching studies were performed on the treated specimens over different curing periods to understand the efficacy of the co-additives in preventing the loss of primary stabilizer. The general flow of the chapter is as follows:

a) In the first section, the durability of the treatment techniques when used as a co-additive with lime is analyzed and these results are compared with only lime-treated soil test results. This section provides an exhaustive overview of the effects of moisture intrusion through capillary soaking in the treated soil layers. Additionally, the effects of the silica treatments on the pore structure were investigated. This helped to identify the probable causes for the moisture-induced damages and efficacy of different treatment techniques.
b) In the second section, the permanency of the stabilizer and co-additive treatments, when subjected to continuous moisture intrusion through leaching, was analyzed. The ionic concentrations in the collected pore solutions provided an overview of the efficacy of co-additive application with the traditional Ca-based stabilizer.

The analysis of the durability of the stabilizers provides an effective tool for predicting the overall efficacy of silica-based treatments and therefore is necessary before it could be recommended for practicing professionals. The following sections discuss the

moisture susceptibility related durability, pore structural changes, and effects of leaching due to the chemical treatments.

6.2 Durability in terms of moisture susceptibility

In this study, the durability of the chemically treated specimens was analyzed at different curing periods of 0, 3, 7, 14, and 28 days. The engineering tests were performed on Soil-1, which was noted to be more problematic as compared to the Soil-2 due to an appreciable sulfate concentration, plasticity index (PI), and vertical free swell strain percentage. The durability studies were first performed on the lime and CS-treated soil specimens, and their performance was compared with only lime-treated soils. The lime-treated soil specimens were prepared at optimum lime content at a dosage of 7% by the dry unit weight of the soil. Similar to the studies in the previous chapter, the two CS dosage percentages used were 15% and 30% by the dry unit weight of the soil.

After studying the CS-treated soils, the comparative studies of engineering performance when subjected to moisture intrusion were also performed between lime-treated and lime and NS-treated specimens over different curing periods. The optimum NS dosage used for this study was 1% by the dry unit weight of the soil, as determined in Chapter 5. As previously discussed in Chapter 5, each soil-stabilizer mixture was molded into cylindrical specimens or 33 mm diameter, and 6 specimens were prepared for each curing period. Three specimens were used for strength testing, as discussed in chapter 5, and the remaining three specimens were used for moisture-induced durability studies.

The triplicates used for durability testing were cured in a similar fashion as the specimens for strength testing (i.e., hermetically sealed plastic chamber at a relative humidity of 100% and at room temperature of 23±2°C). The cured specimens were subjected to moisture intrusion through capillary soaking for 48 hours or until the specimens collapsed. The capillary soaked specimens were subjected to an unconfined compressive strength (UCS) test in accordance with ASTM D5102 at a constant strain rate of 0.5%/min. Before subjecting the soil specimens for strength tests, the dimensions of the specimens were precisely measured in both lateral and vertical directions to determine the volumetric changes after 48 hours of capillary soaking.

The linear dimensions were measured using a Vernier caliper, and the radial dimensions were carefully measured using pi-tapes. The weights of the capillary soaked specimens were also recorded after testing them for UCS. Subsequently, the tested specimens were dried in an oven at 110±5°C to determine the dry weight. The measurement of the UCS, volumetric swell, and weight increase due to absorption of moisture would help to understand the efficacy of treatments and provide insights into the behavior of the new co-additives when subjected to moisture intrusion.

6.2.1 Unconfined Compressive Strength after Capillary Soaking

Figure 6.1 presents the UCS values of the different groups of soil specimens after exposure to 2-days of capillary soaking. The UCS values of the 0-day cured L-HS, L-HS-15CS, and L-HS-30CS were close to 10 kPa when exposed to capillary soaking. The absence of cementitious bonds and probable nucleation and growth of ettringite formed during the 48

hours of capillary soaking resulted in this 98% drop in UCS values (Figure 6.1). The addition of crystalline silica was ineffective in preventing the strength loss in the 0-day cured specimens as the reaction between lime and crystalline silica present in crushed sand is not a spontaneous process.

The capillary soaked L-HS specimens incurred a strength loss close to 80%, even after 28 days of curing. This shows that the extent of moisture-induced damage is significant in lime-treated sulfate-rich soil even after 28 days of curing. The disruptive nature of the ettringite crystals is strong enough to break some of the C-S-H bonds, leading to strength loss after capillary soaking. The beneficial effect of using crystalline silica as an admixture is apparent in Figure 6.1. The post-soaking UCS and the rate of increase in retained UCS of the L-HS-15CS and L-HS-30CS specimens were significantly higher than that of the L-HS specimens.

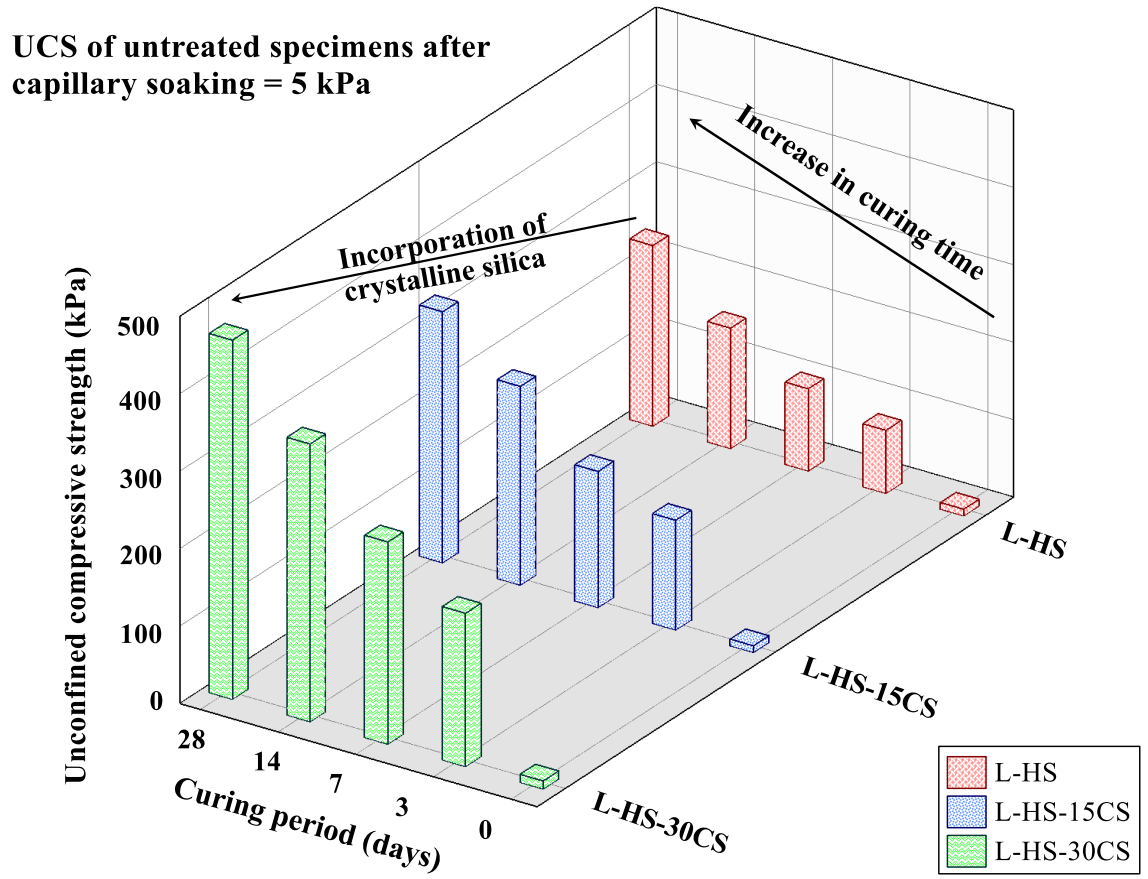

Figure 6.1 Unconfined strength of CS-treated specimens after capillary soaking for 48 hrs.

Table 6.1 shows the calculation for the retained strength after capillary soaking, which can be expressed as following Equation 10,

$$\text{Retained Strength (\%)} = \frac{UCS\ after\ capillary\ soaking\ for\ 48\ hrs}{UCS\ before\ capillary\ soaking} \times 100\% \qquad (10)$$

The retained strength is very low for early curing periods due to the absence of sufficient cementitious phases developed during this short duration. However, it could be noted that with the progress of the curing period, the percentage strength retained is much more for CS-treated soils as compared to only lime-treated soil specimens. At the end of 28 days of curing, the retained strength of L-HS-15CS and L-HS-30CS specimens is about 1.15 and 1.7 times higher than that of the L-HS specimens.

The capillary soaking substantially increased the degree of saturation (S_r > 89%) for all the specimens of different experimental groups (Table 6.2). The S_r data provided in Table 6.2 have been calculated assuming a specific gravity (G_s) of 2.65 for the treated soil solids. The higher retained strength for the CS-treated groups can be attributed to the lower water absorption resulting in a low degree of saturation (S_r), as shown in Table 6.2. The additional cementitious phases formed due to the reaction of lime and crystalline silica might be responsible for binding the matrix together (Figure 6.1 and Table 6.1). The efficacy of CS amendment in reducing the degree of saturation after capillary soaking and its consequent effects in reducing the soaked weight and volumetric strain will be discussed in the next section.

Table 6.1 Comparison of retained strength after capillary soaking for L-HS, L-HS-15CS and L-HS-30CS specimens

Curing period (Days)	Before Capillary Soaking (kPa)			After Capillary Soaking (kPa)			Retained Strength (%)		
	L-HS	L-HS-15CS	L-HS-30CS	L-HS	L-HS-15CS	L-HS-30CS	L-HS	L-HS-15CS	L-HS-30CS
0	385.43	354.54	355.09	9.06	9.07	10.84	2.35	2.56	3.05
3	510.00	495.41	593.72	81.93	142.15	198.39	16.06	28.69	33.42
7	808.23	745.28	913.31	106.64	176.25	261.56	13.19	23.65	28.64
14	921.45	1086.03	1060.93	155.93	257.14	359.07	16.92	23.68	33.85
28	958.41	1148.22	1116.99	233.58	324.46	464.14	24.37	28.26	41.55

Table 6.2 S_r (%) of different L-HS, L-HS-15CS and L-HS-30CS group of specimens after capillary soaking

Group		L-HS	L-HS-15CS	L-HS-30CS
Curing period (days)	**0**	94.8	94.9	92.9
	3	93.6	93.6	92.9
	7	93.2	93.4	93.6
	14	93.4	92.3	90.4
	28	94.1	91.9	91.4

The UCS values for the lime and NS treated specimens over different curing periods when subjected to capillary soaking for 48 hours are shown in Figure 6.2. Similar to the CS treated specimens, the values of the retained strength of the capillary soaked specimens are shown in Table 6.3. From Figure 6.2., it was observed that, as compared to lime-treated specimens, the percentage retained strength is higher for all curing periods.

In the 0-day cured specimens, a strength loss of more than 85% was observed in lime and NS-treated specimens as compared to 90% in only lime-treated. Although the strength loss is significant, the presence of additional phases of silica enhanced the bonding of the soil through the development of additional phases of C-S-H gels. Over longer curing periods, due to the presence of NS, the retained strength increased gradually until 14 days of curing. No major changes in retained strength values were noted between 14 days cured and 28 days cured specimens (Figure 6.2).

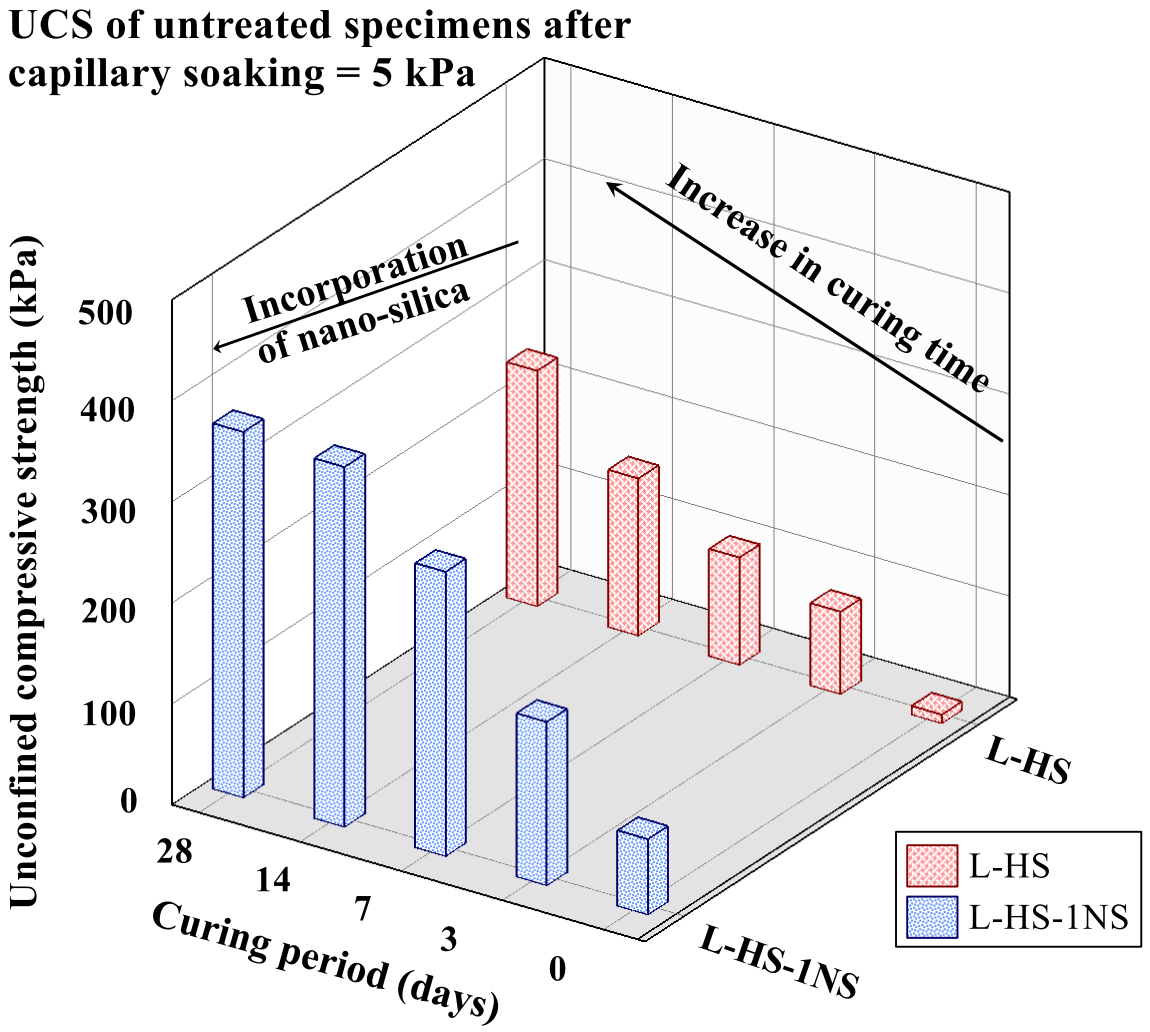

Figure 6.2 Unconfined strength of NS-treated specimens after capillary soaking for 48 hrs.

Chemically treated soils should retain a significant strength to perform satisfactorily over a longer curing period (Thompson 1970, Little and Nair 2009). In the case of lime and NS treated soil, although the absolute value of the strength retained after 28 days of curing was more than the minimum strength required after moisture intrusion as recommended by NCHRP-145, the percentage loss of strength was significantly high, and retained strength percentage was correspondingly lower than CS-treated soils (Table 6.1 and Table 6.3). The percentage of retained strengths for CS and NS co-additive treatment over different curing periods are compared with only lime-treated specimens in Figure 6.3.

Previous engineering and microstructural studies in Chapter 5 have established that the presence of additional amorphous silica phases has the potential to reduce the nucleation and precipitation of ettringite. Therefore, the strength loss of this proportion could not be only attributed to the ettringite precipitation. The degree of saturation (S_r) for the lime and NS-treated specimens are compared with only those of lime-treated specimens in Table 6.4. It was observed that the degree of saturation was more than lime-treated specimens for all curing periods. Furthermore, it was also noted that the degree of saturation increased partially over a longer curing period, indicating more water was absorbed in the specimens with the progress of the pozzolanic reactions.

Table 6.3 Comparison of retained strength after capillary soaking for L-HS, and L-HS-1NS specimens

Curing period (Days)	Before Capillary Soaking (kPa)		After Capillary Soaking (kPa)		Retained Strength (%)	
	L-HS	L-HS-1NS	L-HS	L-HS-1NS	L-HS	L-HS-1NS
0	385.43	560.17	9.06	75.11	2.35	13.41
3	510.00	746.67	81.93	162.15	16.06	21.72
7	808.23	1058.33	106.64	281.87	13.19	26.56
14	921.45	1081.67	155.93	356.62	16.92	32.97
28	958.41	1098.15	233.58	362.32	24.37	32.99

Table 6.4 S_r (%) of different L-HS and L-HS-1NS group of specimens after capillary soaking

Group		L-HS	L-HS-1NS
Curing period (days)	**0**	94.8	95.16
	3	93.6	95.09
	7	93.2	95.89
	14	93.4	97.42
	28	94.1	96.58

The presence of additional amorphous phases of NS material helps to develop C-S-H phases immediately after treatment. These C-S-H phases enhance the engineering performance in the treated soils by rapidly forming bonds among the soil particles and developing a strong soil matrix. For the HS soils, the presence of NS also reduces the potential for the precipitation of ettringite due to partial utilization of available Ca^{+2} ions and reducing the solubility of alumina from clay minerals. However, when subjected to moisture intrusion, there is an appreciable loss of strength in the specimens. C-S-H being a hydrophilic mineral, has the potential to absorb water molecules.

The absorption of water molecules reduces the bonding strength of the cementitious gels. Therefore, for a longer curing period, the culmination of three factors, i) formation of additional C-S-H phases from pozzolanic reactions, ii) presence of additional C-S-H gels from NS treatment, and iii) partial precipitation of ettringite, collectively results in the significant loss of strength in the treated soils.

The following section discusses the effects of the silica-based co-additives on the volumetric swell and weight increase in capillary soaking and the overall efficacy of adding these novels stabilizers to traditional lime treatment techniques.

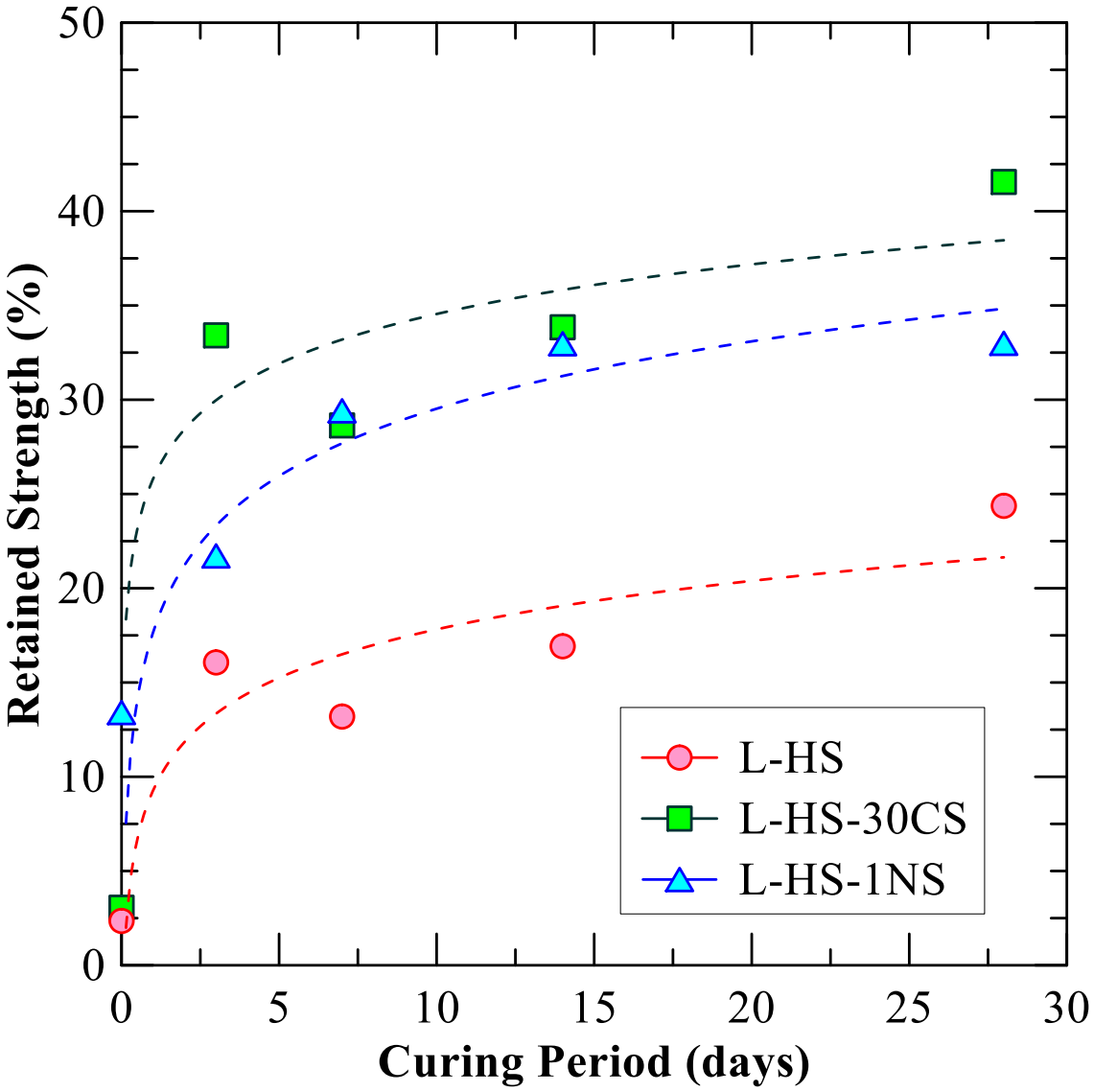

Figure 6.3 Percentage retained strength for different curing periods for L-HS, L-HS-30CS and L-HS-1NS specimens.

6.2.2 Volumetric Swell Strain and Weight after Capillary Soaking

The capillary soaked specimens after each curing period were used to measure the change in linear and radial dimensions as well as total weight increase due to moisture intrusion before subjecting them to unconfined strength tests (durability studies) as discussed in the previous section. Figure 6.4 and Figure 6.5 provide information on the volumetric swell and corresponding weight increase in the L-HS, L-HS-15CS, and L-HS-30CS specimens after different curing periods, respectively.

The L-HS specimens incurred a volumetric strain close to 45% and a weight increase of around 35% due to the absorption in the 0-day cured specimens, which is in consonance with the high swell strain exhibited by the 0-day cured L-HS specimen. Numerically, the 1D swell strain is less than the 3D volumetric strain because of the restraining effect of the metallic ring, which confines a swell test specimen.

The volumetric strain and weight increase in the 0-day cured lime-CS treated soil specimens were marginally less than the same of L-HS specimens due to partial replacement of the clayey soil with crystalline silica. This behavior is considerably different from that observed from the swell test results of 0-day cured specimens. The rationale for this apparent anomaly is attributed to the difference in duration of moisture exposure. The swell tests lasted over two weeks, whereas the capillary soaking for strength testing lasted for two days. Unlike the capillary-soaked strength testing specimens, the swell testing specimens got ample time and water for the complete crystal growth and hydration of ettringite crystals.

Over a longer curing period, the volumetric strains and corresponding water absorption in the L-HS specimens were 5% and 15%, respectively. The values are notably lower than 0-day cured specimens. However, the retained strength of less than 25% accompanied by a volumetric swell of 5% show the detrimental effects of ettringite in sulfate-laden soils (Figure 6.4 and 6.5, and Table 6.1). The addition of CS shows the beneficial effects of significantly reducing the volumetric swell strains immediately after 3 days of curing and overall less than 2% at the end of 28 day curing period. The higher retained strength can be attributed to the lower water absorption and subsequent reduction in the weight and volumetric strain (Figure 6.1). The partial replacement of high plastic sulfate-laden soils and the formation of additional cementitious phases due to the reactions between lime and CS additives might have contributed for the observed improvements.

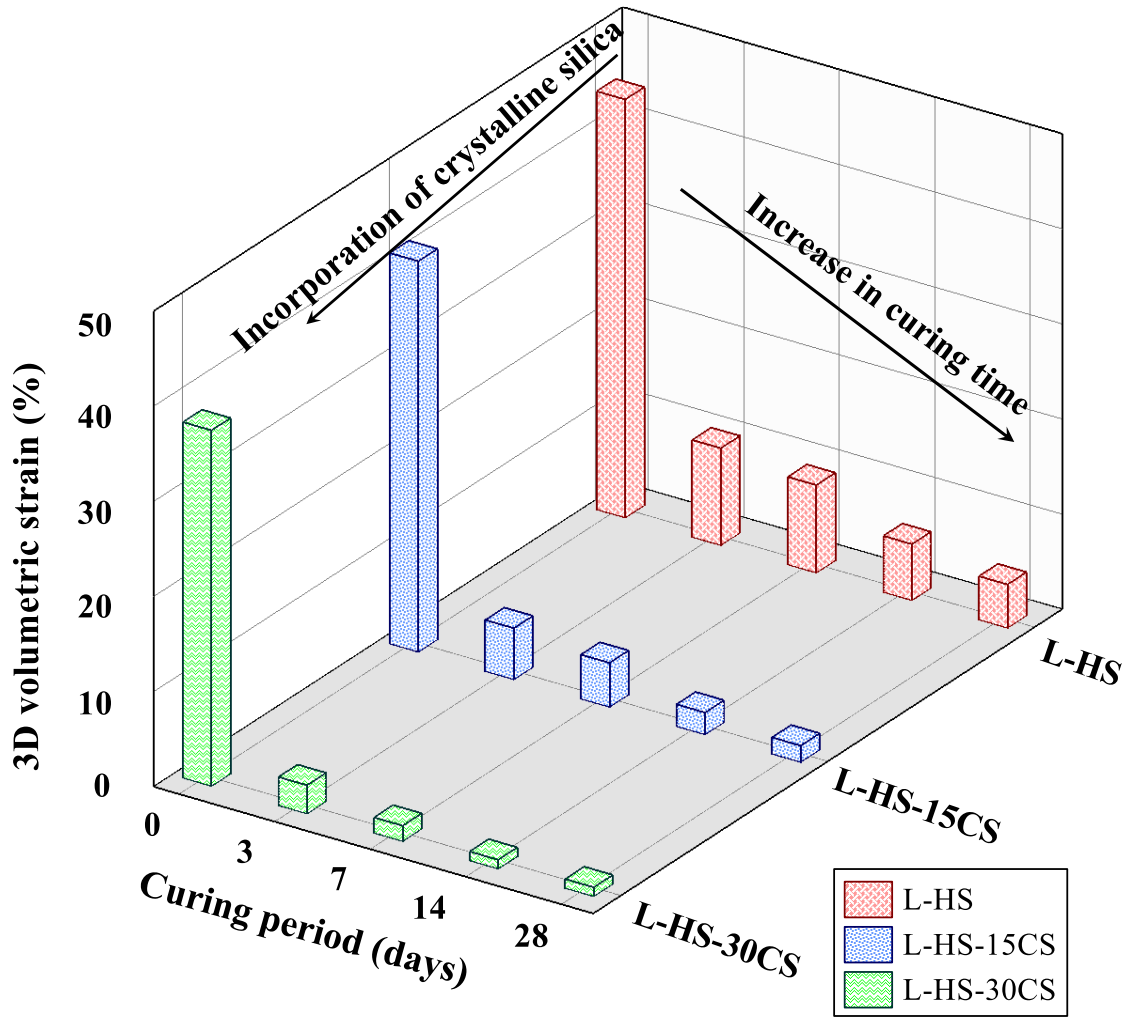

Figure 6.4 3D Volumetric strains after capillary soaking in L-HS, L-HS-15CS, and L-HS-30CS specimens.

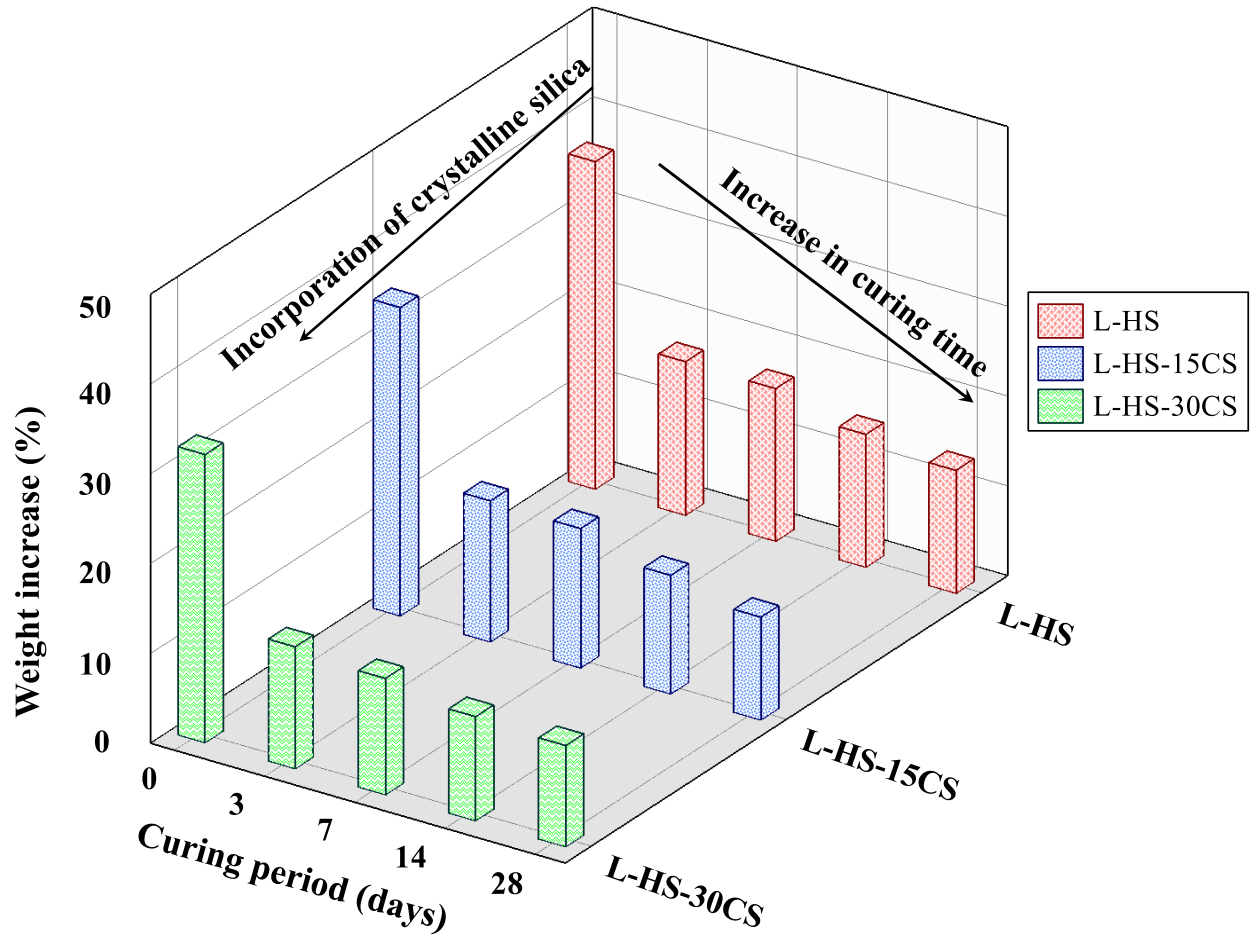

Figure 6.5 3D Weight increase after capillary soaking in L-HS, L-HS-15CS and L-HS-30CS specimens.

The volumetric swell and the weight increase in the capillary soaked specimens when subjected to 1%NS treatment are shown in Figure 6.6 and Figure 6.7, respectively. The values are compared with traditional lime treatment for all the curing periods. Application of NS to the soil immediately affected the volumetric swell and the percentage of water absorbed in the treated specimens, reducing the values by approximately 30% and 20% as compared to L-HS specimens. This indicates the beneficial effects of adding the NS and rapidly improving the moisture affinity of the soils. This reduction in moisture affinity helps to rapidly increase the retained strength as compared to only lime-treated soils.

Over a longer curing period, different behavior of the NS-treated specimens was observed as compared to lime-treated specimens. There was no appreciable reduction in either volumetric swell or weight of the capillary soaked specimens. These values indicate that the treated specimens have a strong potential to absorb and retain moisture even after 28 days of curing. The moisture-holding capacity severely influences the retained strength of the soils, and therefore, a significant reduction in retained strengths was recorded in Table 6.3. The presence of nano-silica restricted the precipitation of ettringite phases and instead enhanced the formation of additional C-S-H phases. The absorption of water due to the additional C-S-H phases could be attributed as one of the major reasons for the loss in the durability of the NS treated specimens.

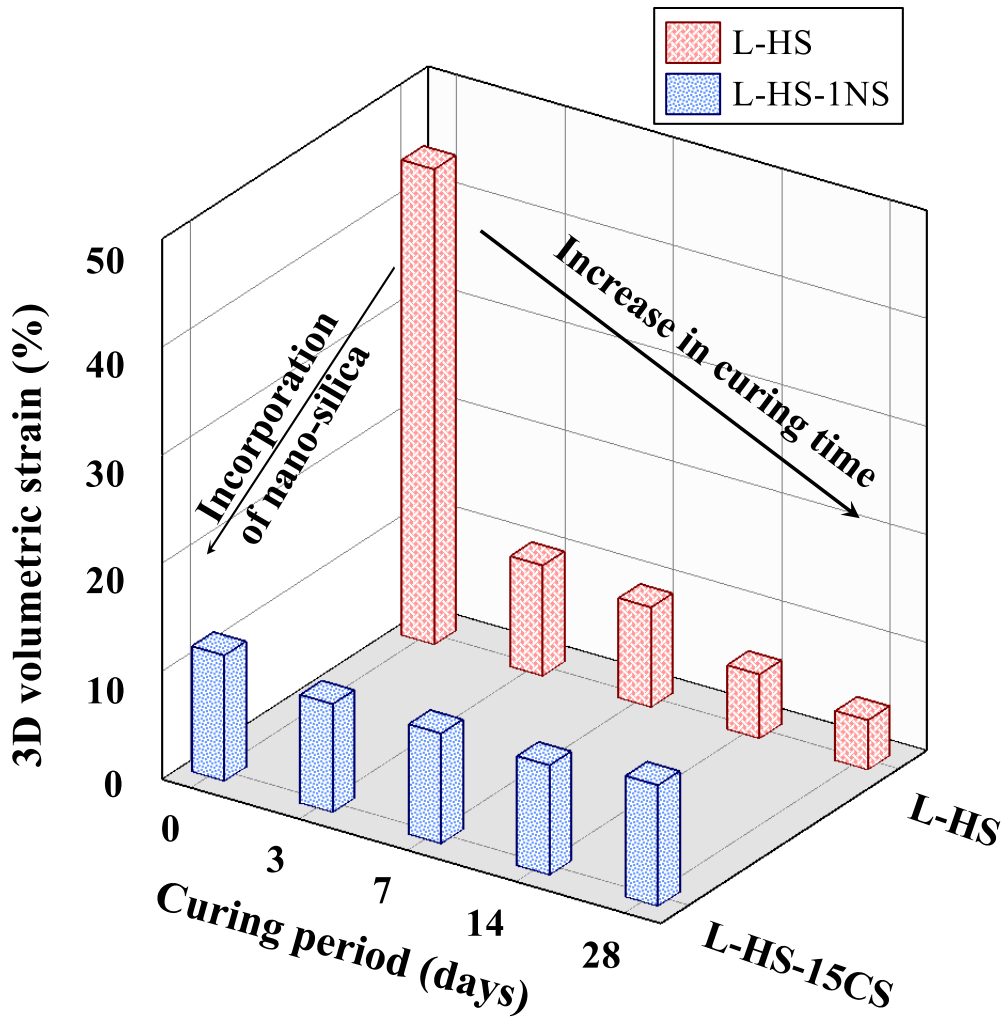

Figure 6.6 3D Volumetric strains after capillary soaking in L-HS, and L-HS-1NS specimens.

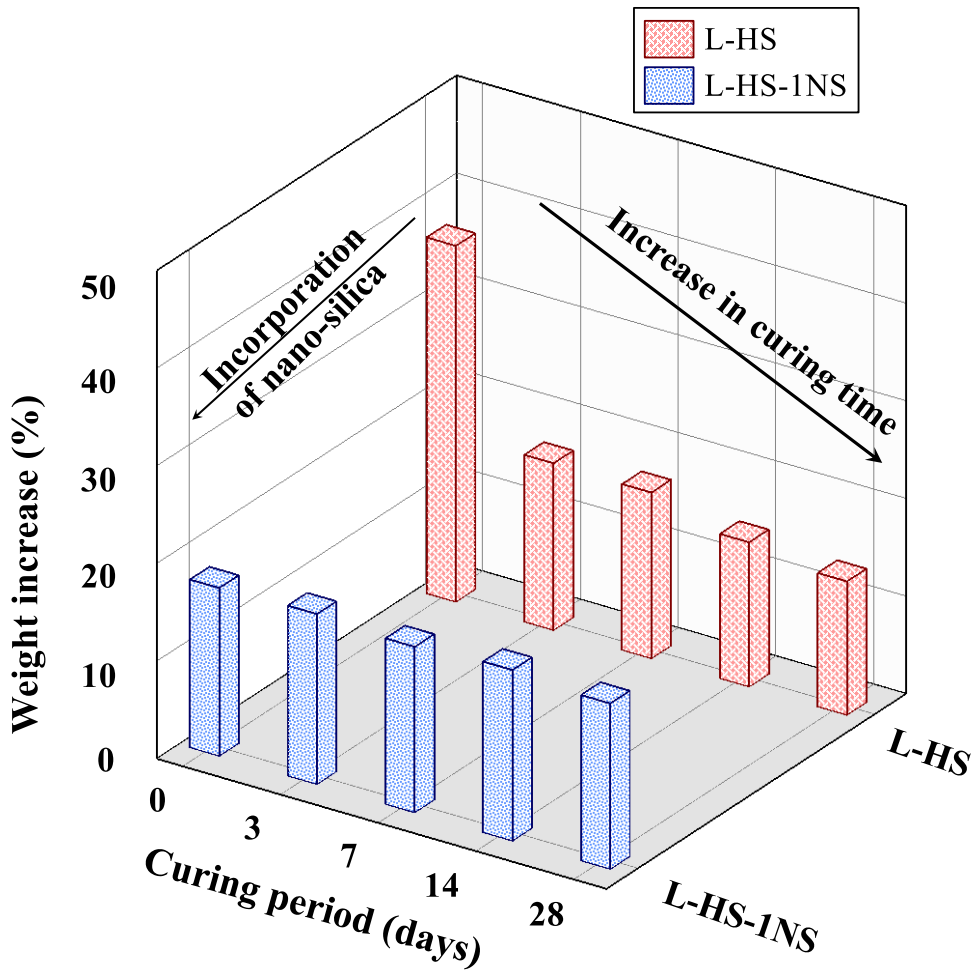

Figure 6.7 Weight increase after capillary soaking in L-HS, and L-HS-1NS specimens.

6.2.3 Analysis of the Soil Pore Structure

The ability of the treated soil to retain water after saturation affects the long-term durability of the treatment. The addition of Ca-based stabilizers reduces the moisture affinity and enhances the performance of the treated soil layers. The addition of silica-based co-additives is expected to influence the moisture retention ability of the treated soils. The changes in the pore structure with and without silica-based co-additives will help to develop a comprehensive understanding on the behavior of the treated soils.

This section discusses the effects of this co-additive on the soil pore structure. This study was performed using the unsaturated soil testing using axis translation techniques and chilled mirror hygrometer, and subsequently developing soil water retention curves for treated specimens. Specimens of untreated soil (HS), lime-treated soil (L-HS), lime and nano-silica treated soil (L-HS-1NS), and lime and crystalline silica treated soil (L-HS-30CS) were tested for the unsaturated behavior. The specimens were prepared using molds of dimension 2.5 in diameter and 1 in height in a similar methodology as discussed in the vertical free swell test. The treated specimens were cured for 28 days in a hermetically sealed chamber at 23±2℃. The untreated and treated specimens were soaked in a water chamber to saturate the soil before beginning of the unsaturated soil testing using the Fredlund SWCC device. The specimens were saturated using vacuum saturation in the water chamber until a constant weight, and subsequently, the specimens were removed and subjected to unsaturated testing. The dimensions and the weight of the specimens were recorded before and after the tests. After the soil specimens were removed from the Fredlund SWCC device, a small proportion of the tested specimen was used to

determine the final water content in the test soil. The remaining soil was used to determine the water retention curves at higher suction using the chilled mirror hygrometer (WP4C).

Figure 6.8 and Figure 6.9 show the SWCC curves for all soil groups and the best-fit curves using the Fredlund and Xing (1994)) equation. The curves were plotted after multiple regressions analyses and most models yielded parameters with an adjusted R-squared value of more than 0.95, indicating a very good fit. The Fredlund and Xing (1994) model could be represented as the following equation 11:

$$\theta_v = \frac{\theta_s}{\left[ln\left\{e+\left\{\frac{\psi}{a}\right\}^n\right]^m} \quad (11)$$

Where, θ_v = volumetric water content; θ_s = volumetric water content at saturation (or, suction = 0); e = void ratio; ψ = soil suction (kPa); and a, n and m = model parameters. The a parameter correlates to the air-entry value, n is related to the pore-size distribution in the soil, and m is correlated to the symmetry in the model curve. The model parameters from any curve could be used to predict the behavior of the tested soils. It should be noted that, at higher suctions, the values measured by chilled mirror hygrometer are a combination of both osmotic suction as well as matric suction. However, in this study, the effects of osmotic suction were neglected, and the suction values from chilled mirror hygrometer were assumed equal to only matric suction.

Table 6.5 presents the model parameters for the untreated soil and all treated soil groups at the end of 28 days of curing. The application of lime to the high plastic soil was able to partially reduce the air entry value as well as volumetric moisture holding capacity

at saturation (Figure 6.8a). This behavior was expected as the application of Ca-based stabilizers reduces the thickness of double diffused layers in the clay particles by satisfying the negative charges on the clay surface. This helps the fine clay particles to form large agglomerated treated soil lumps, similar to coarser-grained materials. The reduction in moisture holding affinity and an increase in grain size make the soil drainable as subsequently a partial reduction in the air entry value.

The *n*-parameter of the L-HS specimens was partially higher than untreated soils. A higher *n*-parameter indicates a more uniform pore size. The application of the lime treatment helped to develop a uniform pore size as compared to untreated soil. The *m*-parameter value of 0.5 or less indicates a moderate slope, and the value of 1.2 or higher indicates a steeper slope. In the case of both untreated and lime-treated soils, the *m* values were observed to be higher than 1.2. A partial reduction in the *m* value of the treated soil represents a milder slope as compared to untreated soils.

Application of coarse-grained silica particles in the form of CS significantly reduces the air entry value as compared to untreated and lime-treated soils (Figure 6.8b). The final volumetric moisture content at saturation before the start of the test in the Fredlund SWCC device (i.e., ψ = 2 kPa) was observed to be 0.33 as compared to 0.35 for the untreated soils. The presence of CS particles with lime helped to reduce the moisture affinity and increase the soil pore sizes resulting in a lower air entry value. Therefore, it could be interpreted that the CS particles help the treated soil to drain out water easily as compared to untreated or lime-treated soils. The reduction in the *n*-parameter and

corresponding increase in the *m*-parameter represents that in the treated soil due to the presence of coarser particles (CS co-additives) reduces the uniform distribution of the pore sizes and also increases the slope of the symmetry curve.

In the specimens treated with both lime and nano-silica, there is an increase in the volumetric moisture content at $\psi = 0$ kPa (at saturation), as well as the air entry value (*a*-parameter) (Figure 6.8c). The application of fine particles of NS has made the soil matrix dense and, therefore, significantly reduced the soil pore sizes (and possibly reduced the soil permeability). This dense soil matrix, when subjected to saturation, has a higher tendency to retain moisture as compared to lime-treated soils, making the soil more prone to lose strength and stiffness. As compared to the untreated soil, the pore size distribution was more uniform due to the application of amorphous nano-particles, which helped to fill in the voids and also helped to develop additional cementitious gels in the soils. The *m*-parameter increased as compared to untreated soils, and therefore it represents a steeper slope as compared to lime treated or untreated soil.

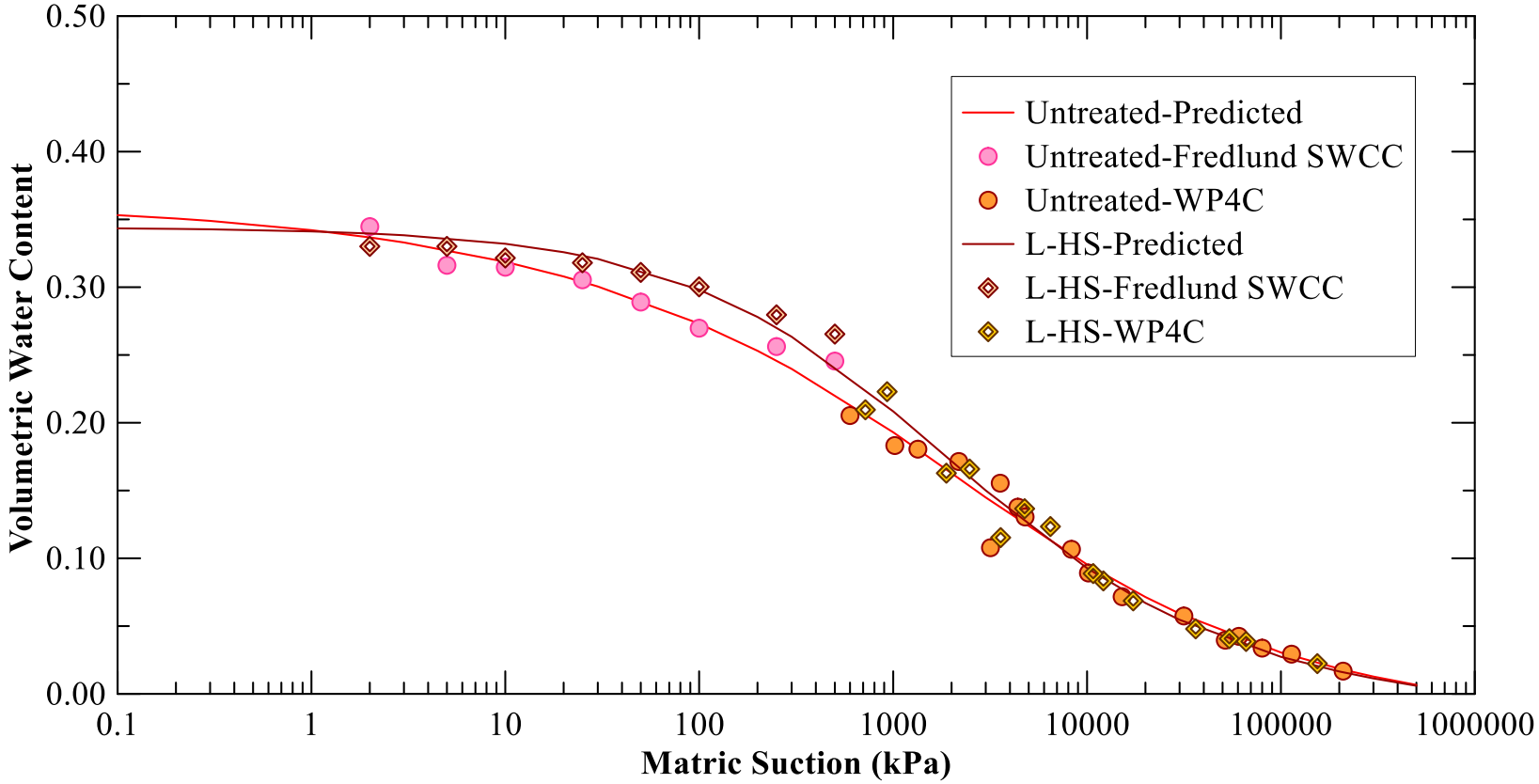
0.50
0.40
0.30
0.20
0.10
0.00
Volumetric Water Content
0.1
1
10
100
1000
10000
100000
1000000
Matric Suction (kPa)
Untreated-Predicted
Untreated-Fredlund SWCC
Untreated-WP4C
L-HS-Predicted
L-HS-Fredlund SWCC
L-HS-WP4C

(a)

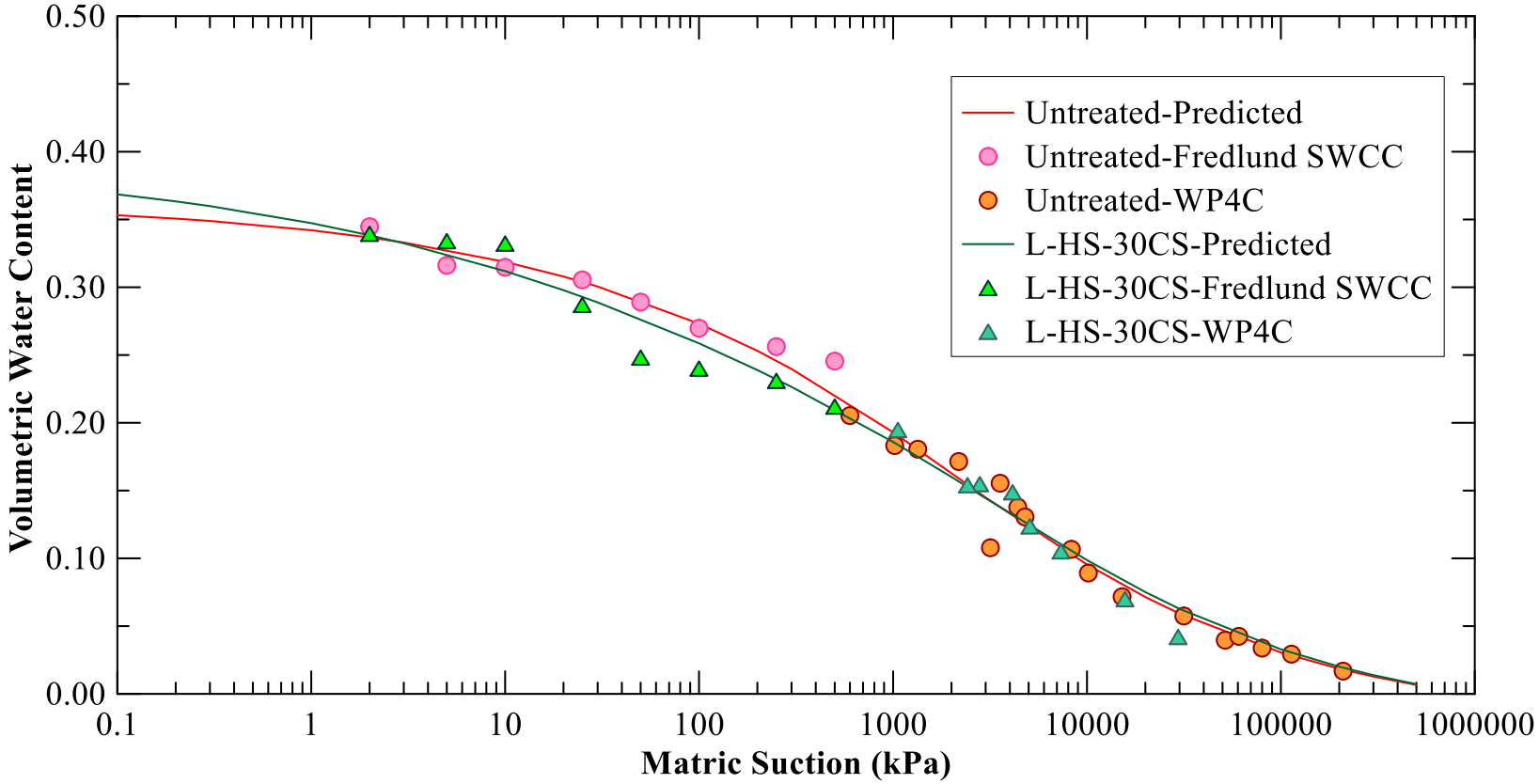
0.50
0.40
0.30
0.20
0.10
0.00
Volumetric Water Content
0.1
1
10
100
1000
10000
100000
1000000
Matric Suction (kPa)
Untreated-Predicted
Untreated-Fredlund SWCC
Untreated-WP4C
L-HS-30CS-Predicted
L-HS-30CS-Fredlund SWCC
L-HS-30CS-WP4C

(b)

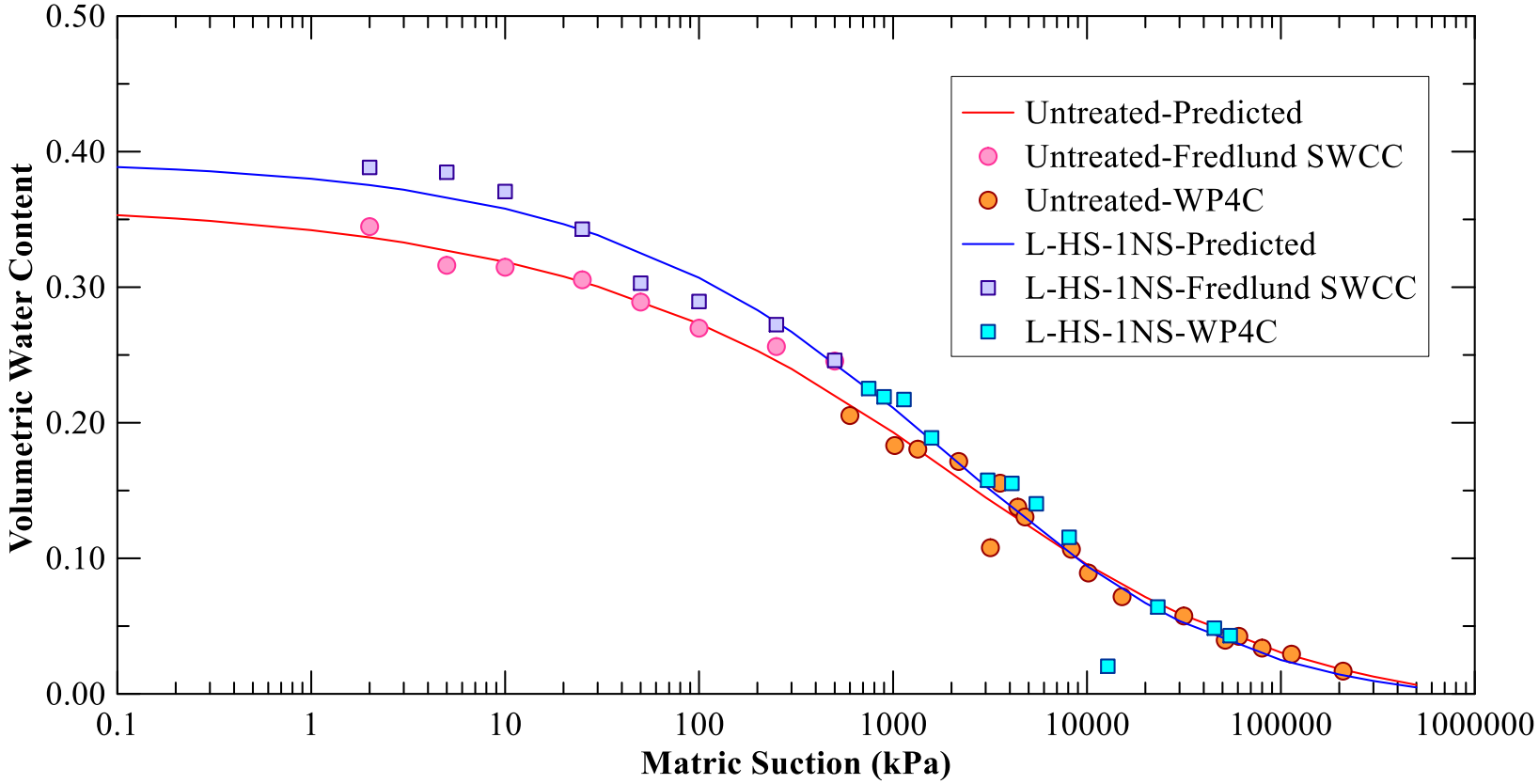

(c)

Figure 6.8 SWCC curves between a) Untreated and L-HS b) Untreated and L-HS-30CS c) Untreated and L-HS-1NS.

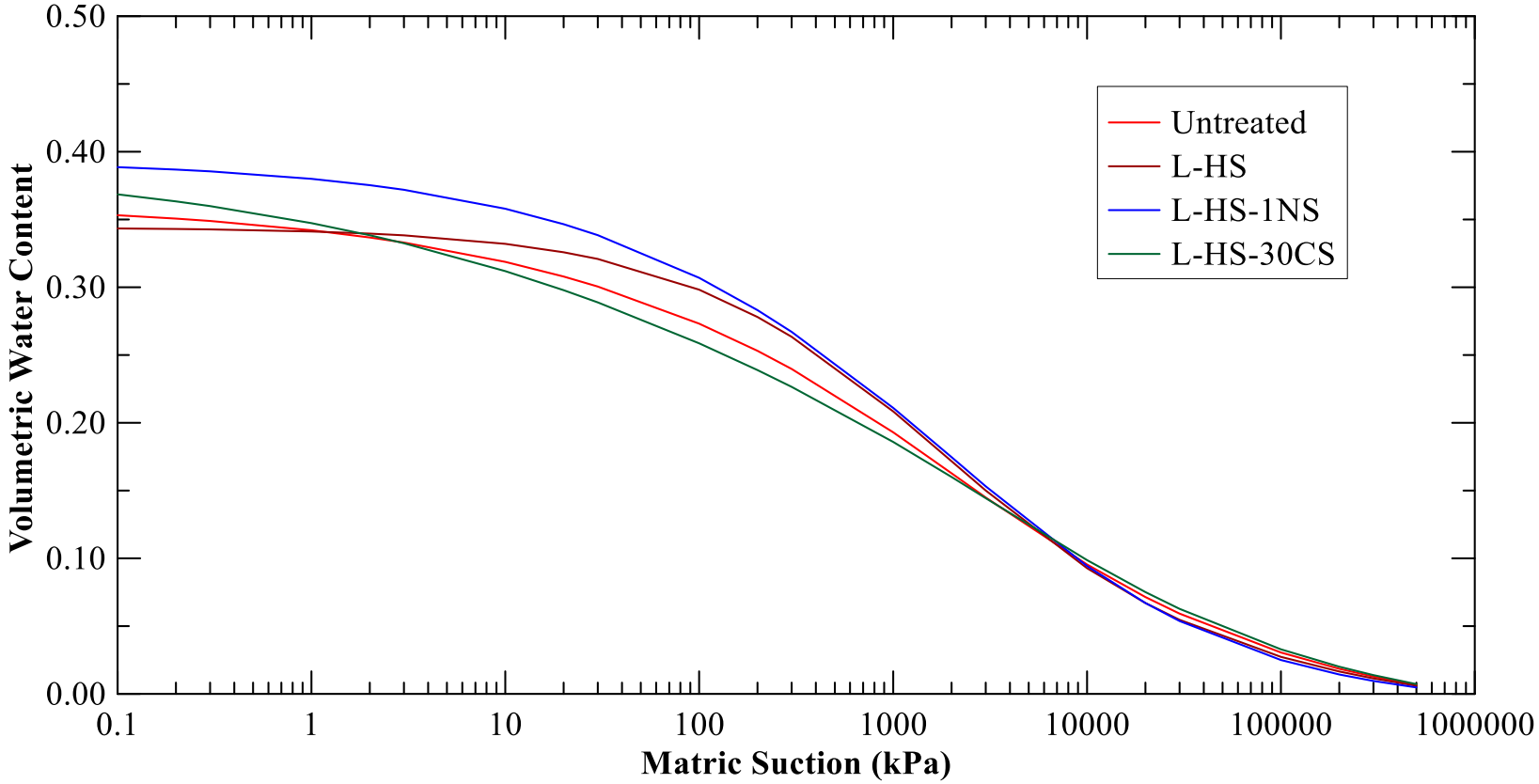

Figure 6.9 Predicted SWCC curves using Fredlund and Xing (1994) model for Untreated, L-HS, L-HS-30CS and L-HS-1NS

Table 6.5 Soil-water characteristic curve parameters for different soil groups after 28 day curing period

Soil Type	*a*	*n*	*m*	R^2
Untreated	745	0.36	1.77	0.98
L-HS	632	0.62	1.29	0.97
L-HS-30CS	491	0.29	2.18	0.99
L-HS-1NS	1110	0.43	2.12	0.97

6.3 Leaching Studies

The previous section discussed the susceptibility of the treated specimens when subjected to moisture intrusion through capillary soaking. The studies indicated that the lime and CS treated specimens retained maximum strength and recorded minimum volumetric strains and weight increase as compared to both lime-treated and lime-NS treated specimens. Furthermore, it was also observed that the lime and NS treated specimens underwent a substantial loss in strength, though microstudies suggested the NS has a potential to reduce ettringite formation. Therefore, further analysis of the pore water chemistry was performed using the leaching studies. The leaching studies are instrumental in determining the permanency of the chemical treatment and consequently provide an indirect measure of the durability of the treatment.

Specimens of L-HS, L-HS-30CS, and L-HS-1NS were tested using the leaching setup as described in Chapter 3. The methodology for the leaching test was obtained from

the studies of Chittoori et al. (2013). In this research study, the specimens were tested after two curing periods of 7 and 28 days. The two curing periods were selected to predict the overall nature of the permanency of chemical treatment during early as well as longer curing periods. The leachates collected from the specimens were analyzed for concentrations of Ca^{+2} and Na^{+1} using X-ray fluorescence spectroscopy. The pore fluid of the untreated soil was also extracted by leaching and the Ca^{+2} and Na^{+1} concentrations were recorded as 962 ppm and 489 ppm, respectively. Such high concentrations of sodium ions indicate the soil is primarily composed of Sodium (Na) Montmorillonite. This could be one of the major reasons for the high plasticity index, free swell, and shrinkage potential in its natural state.

The Ca^{+2} concentrations over different leaching cycles for the 7 days and 14 days cured specimens are shown in Figure 6.10a and 6.10b. In lime-treated specimens (L-HS), the leaching of Ca^{+2} was observed to be of intermediate concentration as compared to either silica-treated specimens. After 7 days of curing, the concentration of Ca^{+2} was approximately 400 ppm during the first leaching cycle. Furthermore, no reduction in concentration was observed over longer leaching. Similar concentrations of Ca^{+2} were also observed in the leachate after 14 days of curing in L-HS specimens (Figure 6.10b). The leaching of Na^{+1} in the L-HS specimens is presented in Figure 6.11. The concentrations of Na^{+1} during the first cycle were higher, which reduces over longer leaching cycles for both curing periods. This rapid washout could be attributed to the high solubility of Na^{+1} and the initial permeability of the soil structure, which declines over cycles due to

clogging. Furthermore, after 14 days, the concentration of Na^{+1} leaching reduced in L-HS specimens indicating its probable presence in the clays structure and participation with calcium in chemical reactions. The pH of the L-HS specimens for both curing periods was observed to be in the range of 11.0-11.5, having a depreciation of 0.90-1.50 as compared to the initial Eades and Grim test pH of 12.40 (Figure 6.12). However, pH greater than 10.5 is considered adequate to induce pozzolanic reactions, and therefore, the leaching of Ca^{+2} could have been induced due to initial calcium cation concentrations in the pore water of the control soil. Excess cations might have diffused away from the clay surface and been easily removed by the excess water.

In the lime and CS treated specimens, the concentration of Ca^{+2} leached out was significantly low for both the curing periods as compared to L-HS and L-HS-1NS specimens (Figure 6.10). Furthermore, with the progress in leach cycles, a general trend in the reduction of concentrations was also observed. Due to the presence of CS in the lime-treated soil, there is an enhancement in the tendency to retain higher concentrations of calcium cations. This retention of calcium ions helps to enhance long-term engineering properties as compared to only lime-treated specimens. The pH of the leachate in the CS treated specimens for both curing periods was measured as 12.0 - substantial alkalinity to sustain long-term pozzolanic reactions, making the treatment highly durable (Figure 6.12). The concentrations of Na^{+1} leached out during the first cycle for both curing periods are significantly high, indicating high cationic exchanges between the divalent and monovalent ions (Figure 6.11). This occurred due to the presence of coarse-grained

crystalline phases in the treated soils that enhanced the permeability and subsequently improved the divalent cation migration within the soil matrix.

The specimens of L-HS-1NS leached about 500 ppm of Ca^{+2} ions for all leaching cycles for both the curing periods. The concentration of Ca^{+2} ions leached out during every leaching cycle was higher as compared to both L-HS and L-HS-30CS (Figure 6.10). The concentrations of sodium ions (Na^{+1}) during the same leaching cycles are presented in Figure 6.11. The sodium ion concentration was comparable to L-HS treated specimens during the early curing period but decreased further as compared to other treatment techniques over a longer curing period. Therefore, as compared to other treatments, low cationic exchange between the divalent and monovalent ions has occurred with the addition of NS with lime. In addition to the ionic concentrations, the pH measured in the leachate showed a significant reduction in the value for both curing periods, the values of which are close to the pH of nano-silica solute (pH = 8.53) (Figure 6.12). Such a low value of pH indicates the unavailability of sufficient hydroxyl ions in the leachate.

The engineering tests such as strength, stiffness, swelling, and shrinkage presented an immediate improvement in the properties of the NS-treated soil matrix even though it leaches out a higher concentration of Ca^{+2} ions and has a lower pH as well as sodium ion concentration as compared to the lime-treated specimens. This possibly occurs due to the low permeability and filler effect of the nano-silica co-additives resulting in a denser matrix. The atomic radius of Na^{+} ions is higher than the Ca^{+2} ions, and therefore as the NS reduces the soil permeability, the leaching of the sodium ions is lower as compared to

calcium ions. Furthermore, this low permeability probably restricts the water from migrating into the inner pores of the soils during the leaching test and primarily flows in between the boundary between the membrane and the soil, and subsequently, a low pH similar to the source water was observed.

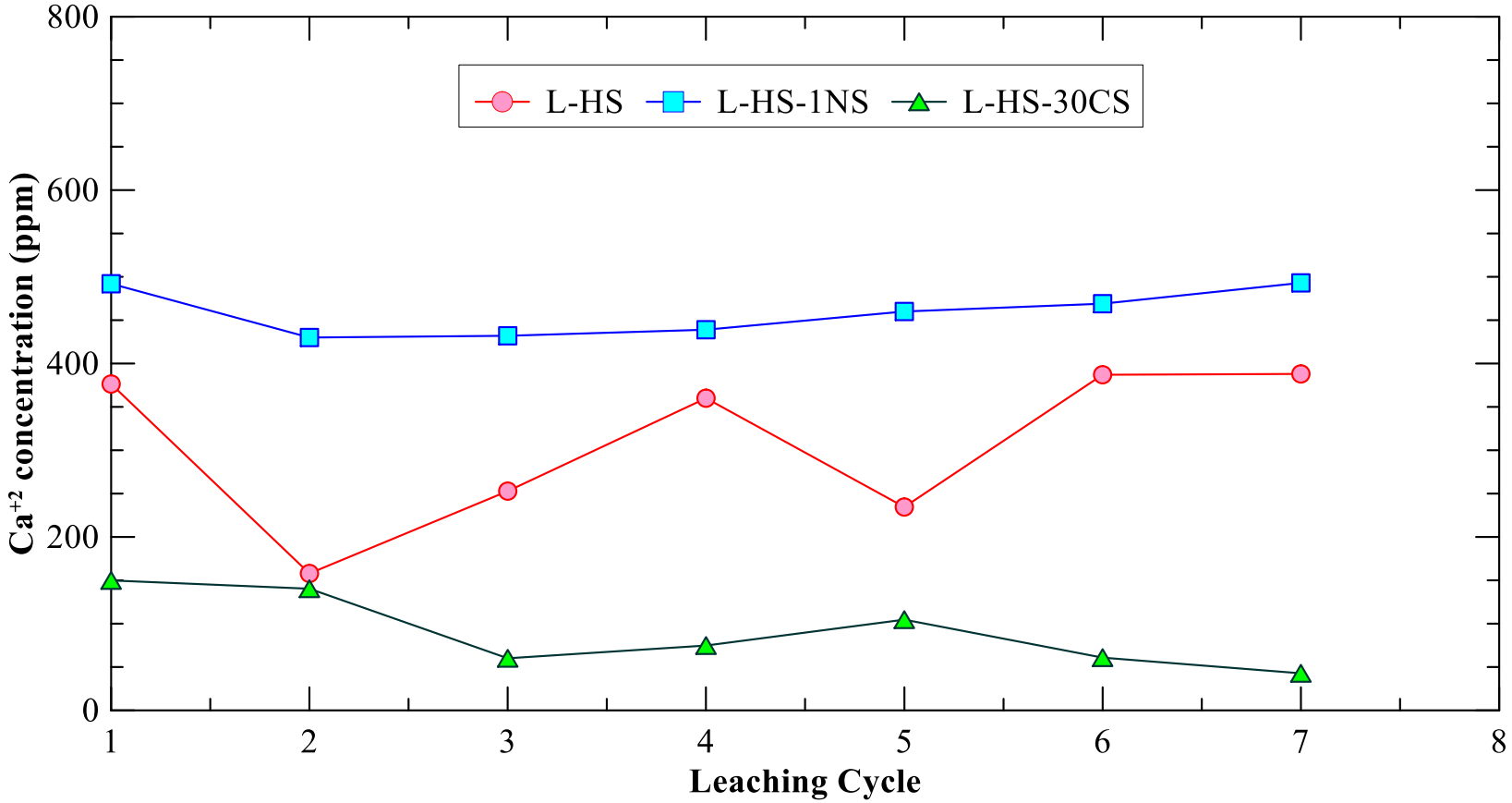
L-HS
L-HS-1NS
L-HS-30CS
Ca+2 concentration (ppm)
Leaching Cycle
0
200
400
600
800
1
2
3
4
5
6
7
8

(a)

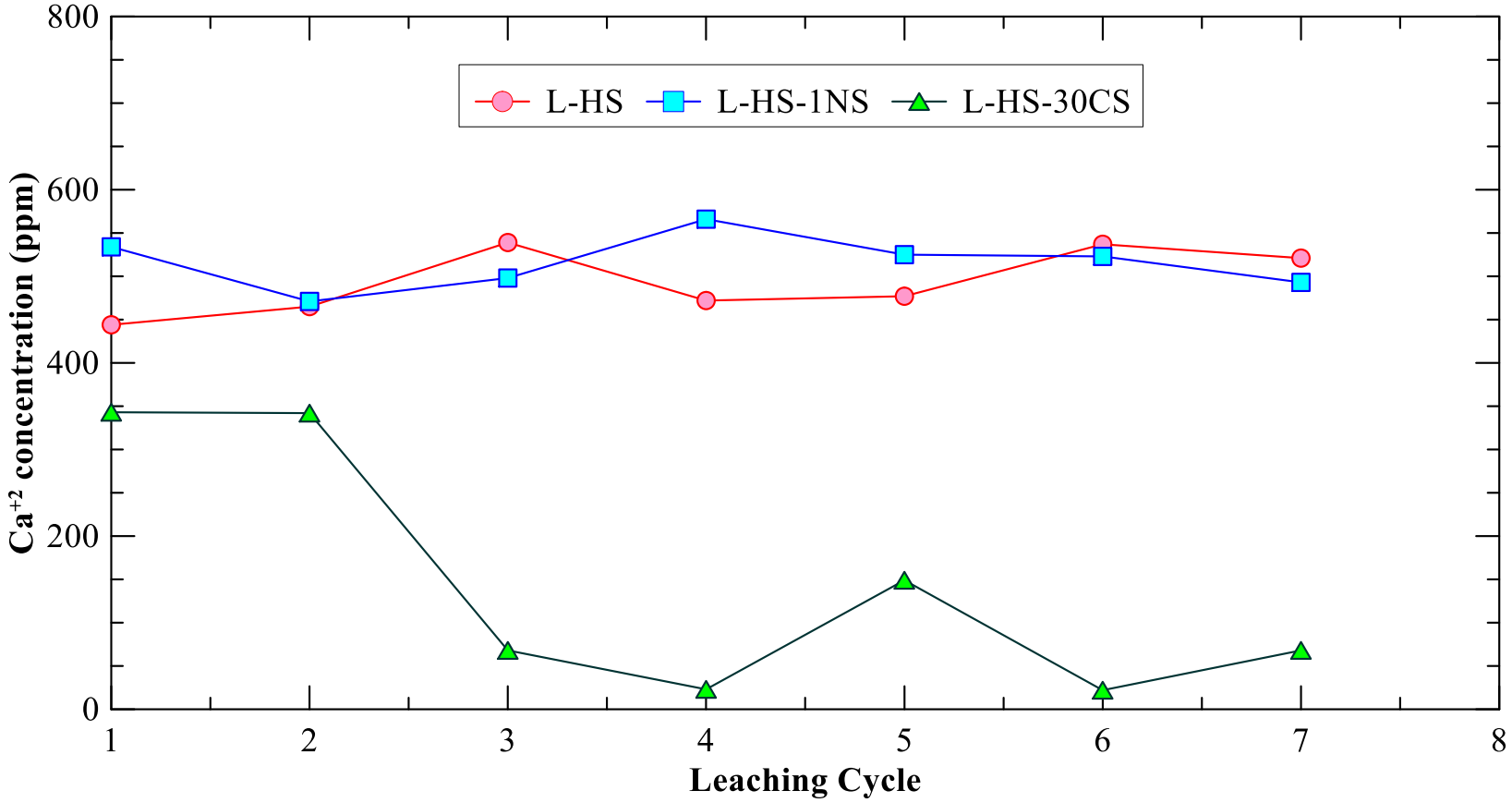

(b)

Figure 6.10 Ca^{+2} concentration in pore fluid after different leaching cycles a) 7 day cured b) 28 day cured specimens

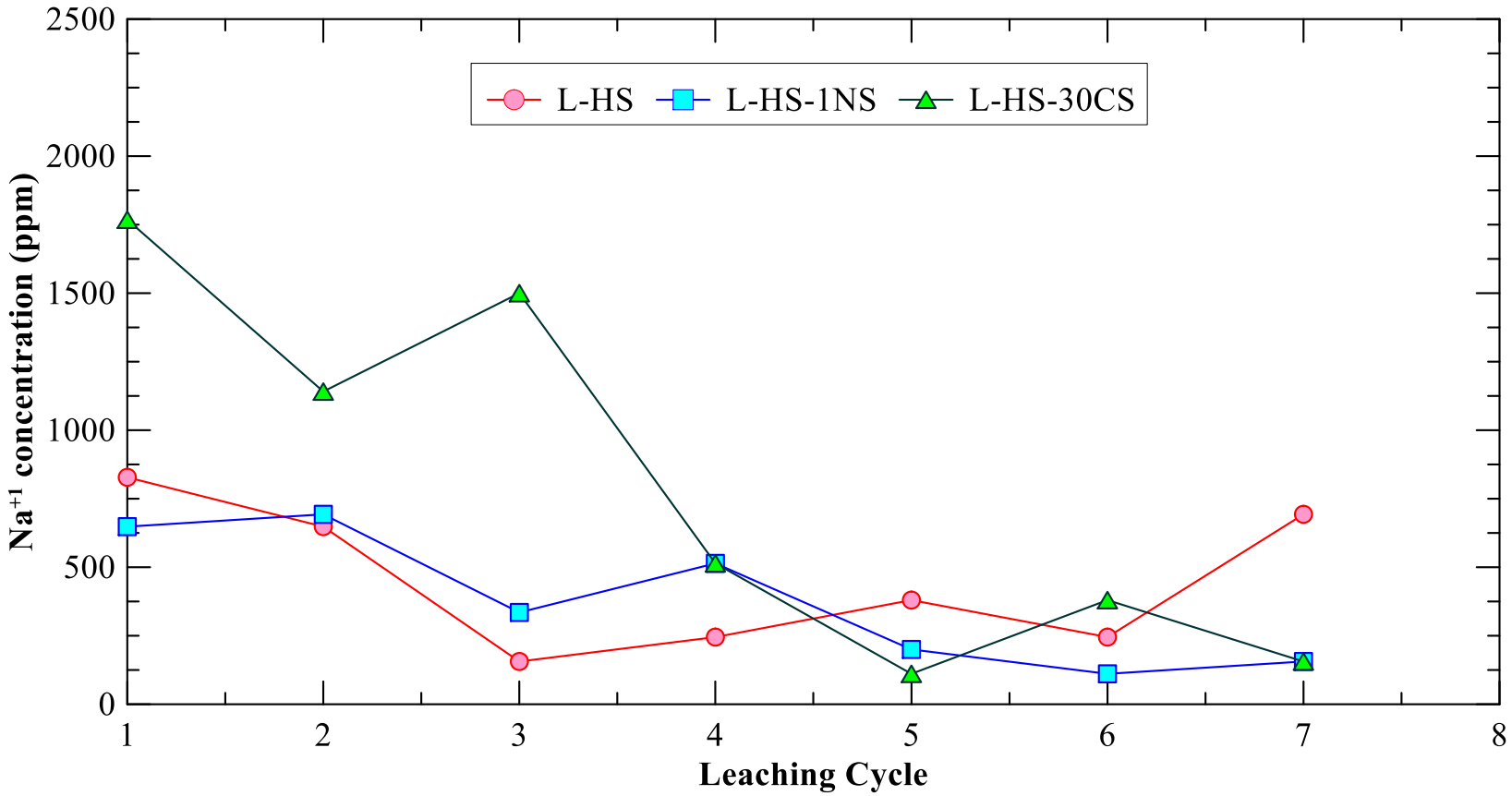
L-HS
L-HS-1NS
L-HS-30CS
Na+1 concentration (ppm)
Leaching Cycle
0
500
1000
1500
2000
2500
1
2
3
4
5
6
7
8

(a)

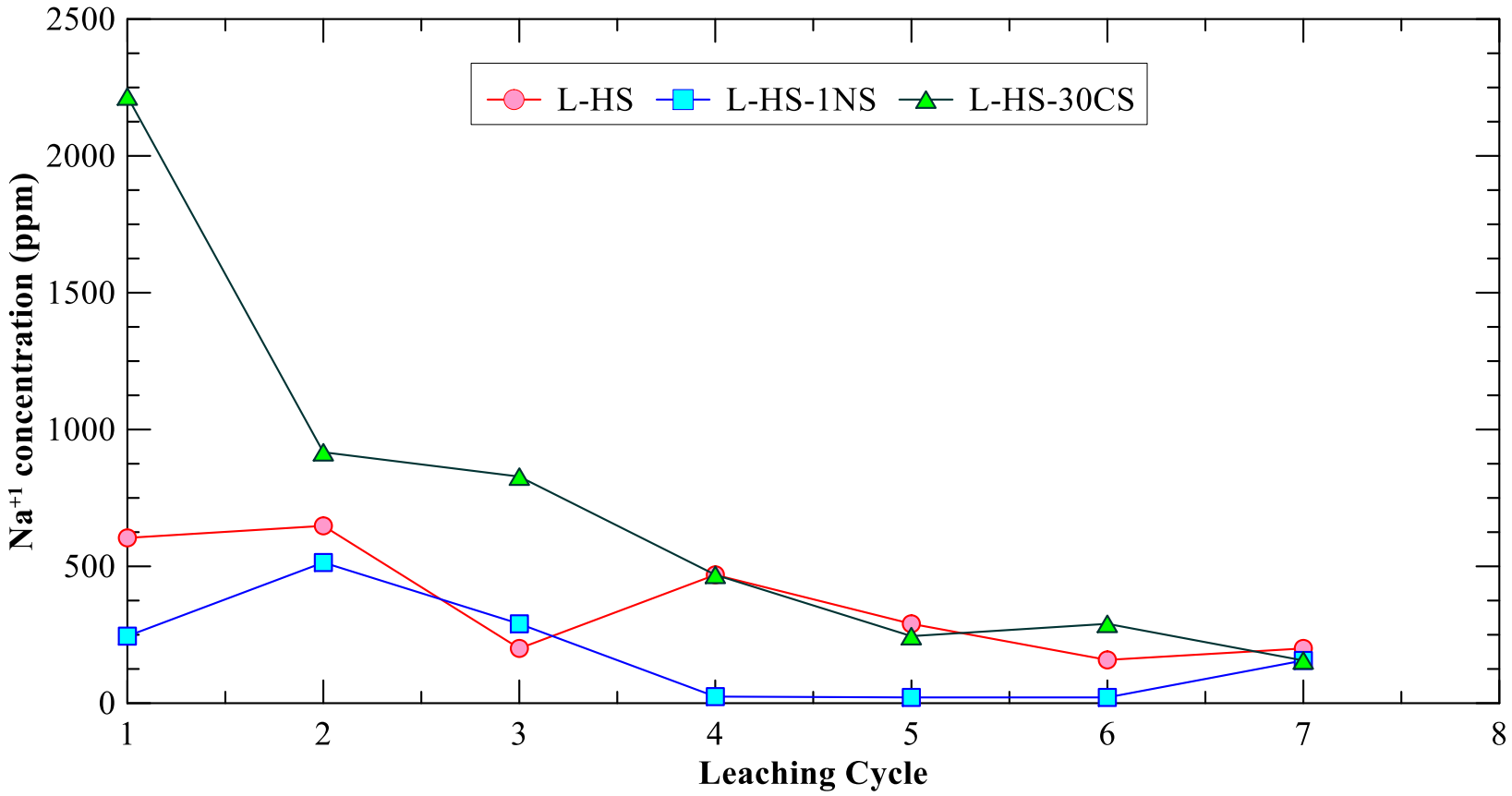

(b)

Figure 6.11 Na^{+1} concentration in pore fluid after different leaching cycles a) 7 day cured b) 28 day cured specimens

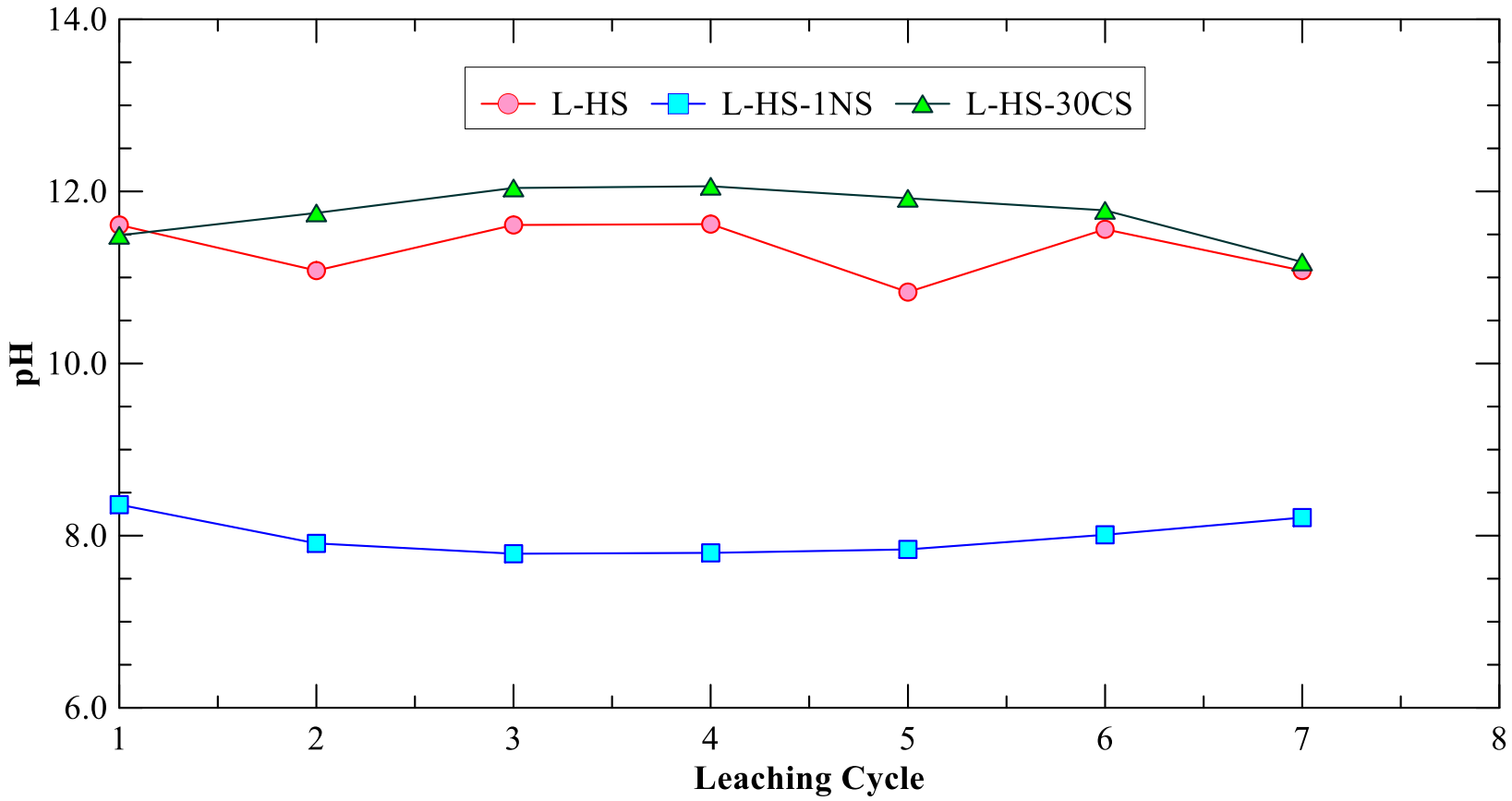
14.0
12.0
10.0
8.0
6.0
pH
1
2
3
4
5
6
7
8
Leaching Cycle
L-HS
L-HS-1NS
L-HS-30CS

(a)

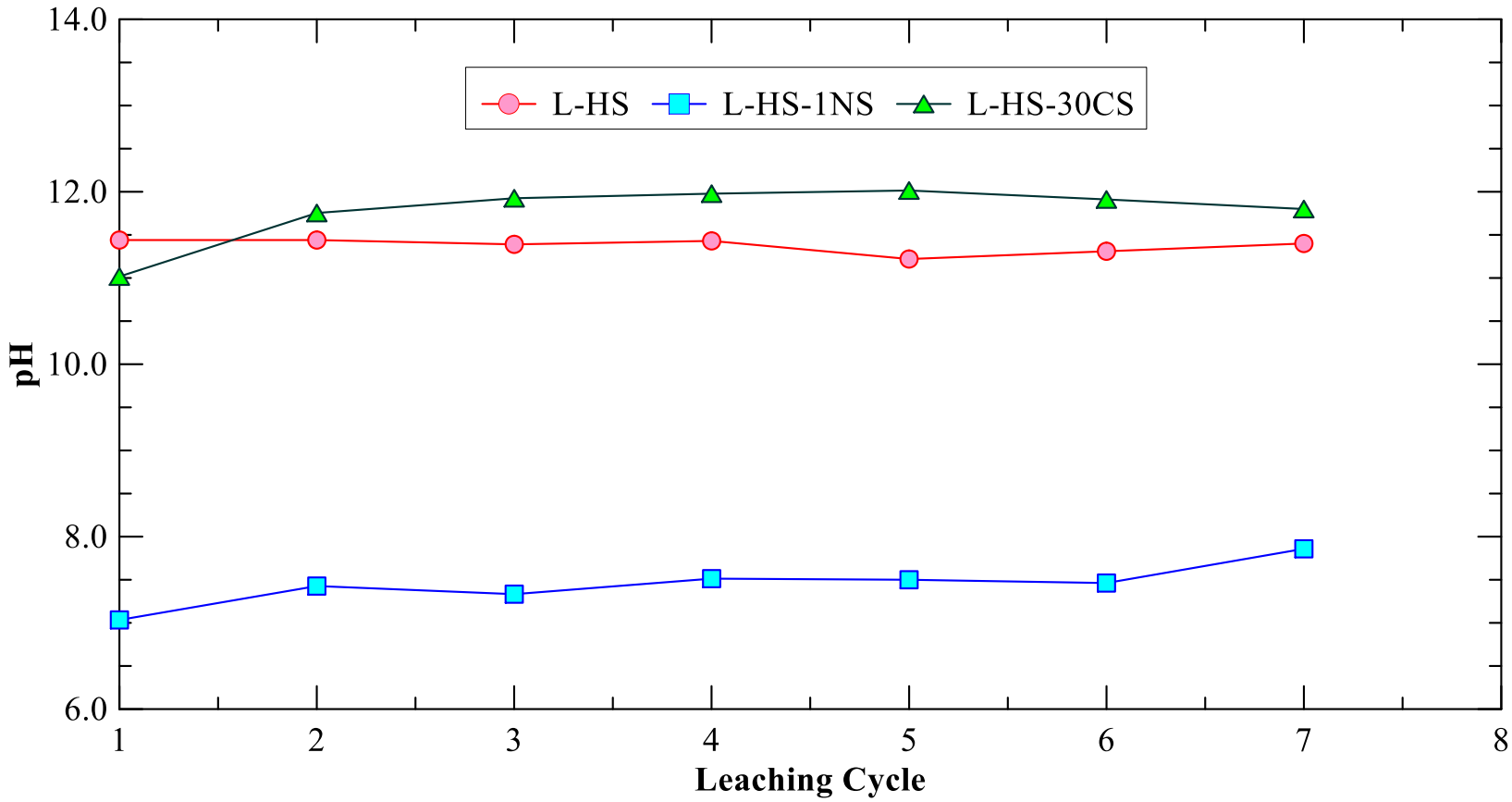

(b)

Figure 6.12 pH of pore fluid after different leaching cycles a) 7 day cured b) 28 day cured specimens

6.4 Summary

In this chapter, the durability and permanency of the stabilizers were analyzed, and the effects of silica-based co-additives on these properties were studied. Specimens of untreated, lime-treated, lime and CS treated and lime and NS treated soils were subjected to moisture conditioning test using capillary action for 48 hours, leaching studies after different curing periods, and finally unsaturated tests to develop a comprehensive understanding of the behavior of the treatments and long-term performance of the treated soil matrix. Some of the major conclusions from this chapter are as follows:

- The application of silica-based co-additives with lime to treat high plastic problematic soil significantly affects the durability of the treated soils against moisture intrusion. Both CS and NS co-additive improve the unconfined strength of the treated soils as compared to only lime treatment. However, the percentage strength loss in NS treated specimens was higher than in the CS treated soils. Additionally, a higher degree of saturation in the capillary soaked specimens treated with NS indicated its moisture-holding capacity, which possibly resulted in higher strength loss.
- The SWCC curves verified the assumption on the moisture-holding ability in different treated soils. The CS co-additive reduced the saturation moisture content and correspondingly lowered the air entry value as compared to only lime treatment. In contrast, the presence of fine nano-particles increased the moisture-holding capacity of the treated soil, which validated the significant loss in strength when subjected to moisture conditioning.

- The leaching test indicated that the application of CS significantly reduced the leaching of divalent Ca^{+2} ions as compared to only lime-treated soils while maintaining sufficient alkalinity in the treated soil. This proves that the CS co-additive has a higher potential to sustain long-term pozzolanic reactions and subsequently make the soil more durable. A significant loss in the Ca^{+2} concentration was observed in NS treated specimens followed by a low pH in the pore solution or leachate. Compounded by low leaching concentration of Na^{+2} ions, this indicates that the available Ca^{+2} ions are not fully utilized, part of the available ions developed C-S-H gels with nano-silica particles; however, the remaining particles probably could not participate in the pozzolanic reactions due to the filler and coating effect of the nano-silica and C-S-H gels, respectively.

7. SUMMARY, CONCLUSIONS AND FUTURE RECOMMENDATIONS

7.1 Summary

The longevity and performance of infrastructure depend on the shear strength, stiffness, stability, and durability of the underlying soils. Most of the distress on infrastructure in western and southwestern USA is attributed to the presence of expansive soils. These expansive soils exhibit a high affinity for water due to the presence of a problematic clay mineral, Smectite/Montmorillonite. The swell-shrink behavior of expansive soils causes extensive damage to pavements and highway embankment slopes. Besides the swelling and shrinking characteristics, these problematic soils also incur significant strength loss and soften in the presence of water. Since replacing the entire problematic soil is not an economically feasible option, soil stabilization is preferred as a viable alternative to enhance the engineering properties of the problematic soils that are not suitable in their natural state.

Calcium-based stabilizers, such as commercially available dolomitic-hydrated lime, have been predominantly used to treat problematic expansive soils over the past several decades. The addition of lime immediately causes the clay particles to flocculate and agglomerate, which results in an immediate change in texture, gradation, and plasticity. In the presence of sufficient lime that elevates the pH of the soil-water system, the clay particles start dissociating to release silicates and aluminates. The silicates and aluminates react with the Ca^{2+} ions, in the presence of water to form Calcium Silicate

Hydrate and Calcium Aluminate Hydrate phases. These amorphous phases produced during this time-dependent pozzolanic reaction bind the soil particles in a strong matrix

However, the time-dependent benefits of lime-treated soils are often encountered with problems such as slow construction or maintenance and long-traffic delays that culminate into social sustainability red flags. Although stabilization improves engineering properties of soils under normal conditions, water intrusion, leaching, and other environmental conditions like freeze-thaw and wet-dry cycles can influence the long-term performance and durability of stabilized layers. Additionally, treatments using lime are quite effective if there is a presence of a significant concentration of soluble sulfates in the soil. The soluble sulfates present in the soil react with available calcium ions, and soil aluminates to form different phases of calcium-alumino-sulfate compounds. The tri-sulfate phase of the reaction product, also known as ettringite, is significantly deleterious in nature and in the presence of an external water source, causes major damage to the treated soil layers.

A research study was planned to address some of the shortcomings of the use of a calcium-based stabilizer to treat high-plastic clays having different levels of sulfate concentrations. In this research study, two novel silica-based co-additives were used with traditional dolomitic-hydrated lime to mitigate the problems associated with the traditional techniques. The two stabilizers used were classified as crystalline silica or CS, from quarry dust and laboratory-grade nano-silica or NS. A series of engineering, chemical and microstructural and mineralogical studies were performed on two different soils to address

multiple issues over the course of this study. The following sections present the major conclusions derived from engineering and microstructural studies undertaken in this research program.

7.1.1 Engineering Studies

The conclusions from the engineering test results and analyses are presented in this section. The engineering test results helped us to identify the overall behavior of the chemically treated soils with and without silica-based co-additives. The major conclusions are presented in the following:

- Silica-based co-additives have a major influence on modifying the engineering properties of expansive high-plastic soils (CH) when added with dolomitic-hydrated lime.
- In soil with a low concentration of soluble sulfate, the optimum dosages of NS and CS with lime were determined using strength tests before and after moisture conditioning for 48 hrs. The optimum dosages were also verified using a statistical framework, and subsequently, the final dosages were selected considering both engineering and statistical judgment.
- Among both co-additives, a very low dosage of NS has a major influence in rapidly accelerating the strength, durability, free swell, and shrinkage of the treated soil within the first 3 days of the curing period. CS additive, on the other hand, has shown to provide higher strength, moduli, and durable properties over a longer duration. CS co-additives improve the long-term performance of the treated soil as

compared to lime treatment alone; however, it has a negligible influence on rapidly developing the engineering properties during the first 7 days of curing process. The particle size and the available specific reaction surfaces of the individual co-additives could be attributed as some of the reasons for these changes in soil behaviors. The resilient modulus properties of the CS-treated soils were observed to be moderately higher than the NS soils due to more inter-particular friction from CS materials.

- Lime treatment reduced the immediate clay-mineral-induced swelling in the expansive high-sulfate soil. However, the soluble sulfates reacted with calcium ions from lime and available alumina from clay minerals in the presence of water to form ettringite. The progressive pozzolanic reaction was partially effective in counteracting the ettringite heaving. Nevertheless, the high swell strain experienced by the cured lime-treated high-sulfate soil proved that traditional calcium-based stabilizers are ineffective for stabilizing high-sulfate soils.
- The CS and NS co-additives effectively reduced the precipitation of ettringite when used with lime to treat high-sulfate soil. The engineering test results, including vertical free swell strain, soil strength test with and without capillary soaking, and resilient moduli test, affirm the beneficial influence of using silica-based co-additives as an admixture to address the deleterious impact of ettringite formation in lime-treated high sulfate soils. The presence of additional silica co-additives possibly prevented the dissolution of soil aluminum and concurrently

formed additional C-S-H phases with the available Ca^{+2} ions, consequently reducing the precipitation of ettringite in the treated soil matrix.

- The moisture conditioned durability of the lime and CS treated soils were considerably higher than the lime and NS treated soils or only lime-treated soils. The moisture susceptibility of the treated specimens could be attributed to the nature of the reaction products in the treated soil and the soil pore structure. The presence of ettringite or excess C-S-H phases interfered with the strength retention ability of the treated geomaterials. Additionally, the leaching studies also provided evidence that among the two co-additives, the application of CS has a higher potential to sustain long-term pozzolanic reactions as compared to NS-treated soils.

7.1.2 Microstructural Studies

Microstructural studies provided valuable evidence to understand the physical and chemical processes involved in the treatment processes with and without silica-based co-additives. Some major conclusions from the micro studies are presented below:

- The Field Emission Scanning Electron Microscope images provided valuable information on the morphology of the chemically treated soils. The SEM and Energy Dispersive X-ray Spectroscopy studies verified the presence of tubular-shaped ettringite crystals in sulfate-rich soils. Additionally, globular-shaped C-S-H phases, typical of Ca/Si ≈ 0.68, were detected in CS-treated specimens. The crystalline silica (CS) rich quarry dust fines possess a higher specific surface and

significantly broken bonds near the edges due to their micro-particle size. These enhance the development of additional cementitious phases when mixed with traditional stabilizers. In NS treated soils, the particles were observed to be coated with uniform networks of different phases of C-S-H. Laboratory grade nano-silica (NS) based co-additive consists of nanoparticles, which provide substantial reactive surfaces to form additional bonding gels when added along with lime.

- The X-ray Diffraction studies provided evidence on the formation of additional cementitious phases when the silica-based co-additives were mixed with lime. These C-S-H formed due to the presence of additional reactive silica surfaces, along with the C-S-H phases formed due to pozzolanic reactions, bonded the admixture-clay system, and enhanced both strength and resilient moduli properties. The XRD studies also provided additional evidence on the reduction in ettringite minerals formed upon the addition of silica admixture during the lime treatment.
- Thermal analyses using the Differential Scanning Calorimetry (DSC) presented valuable information on the reaction products formed after treatment. The DSC established that the CS fines have the potential to react with calcium from the primary stabilizer to form multiple phases of C-S-H depending on the availability of Ca or Si in a given location. The broken bonds near the edges due to their micro-particle size could act as reactive sites for such chemical reactions. Furthermore,

the thermal analysis also verified the ability of additional silica phases to suppress the precipitation of ettringite when added with lime to treat a sulfate-rich soil.

Overall, this research study helped us to develop a comprehensive understanding of the behavior of the traditional lime treatment techniques and the effects of the crystalline silica or nano-silica co-additives. Finally, to compare the performance of the three treatment techniques, radar charts were developed, as shown in Figure 7.1. These charts represent the comprehensive stabilization performance immediately after treatment (<7 days) and for longer curing periods. For the representation purpose, the performance parameters were assigned values based on the studies in this research study (Best Performance = 1.0, Optimum Performance = 0.75, and Poor Performance = 0.5).

During the early curing period, the application of NS with lime stabilizer significantly improved the soil strength, swelling, and shrinkage performance in the plastic clays as compared to only lime or lime and CS-treated soils. However, the lime and CS treated soils performed better in the stiffness and durability aspects of the treatment. However, both sources of additional silica significantly performed better than only lime-treated specimens. Over a longer curing period, the lime and CS-treated soils performed considerably better than other treatment techniques. Additionally, the lime and NS treated soils performed almost similar to only lime-treated specimens. Therefore, from these charts, it was observed NS co-additives could be suitable for accelerating the reaction kinetics but may fail to perform over a longer curing period in durability. The CS co-

additives may not be suitable for accelerated improvement of properties but has a better long-term performance than lime with NS-treated and only lime-treated soils

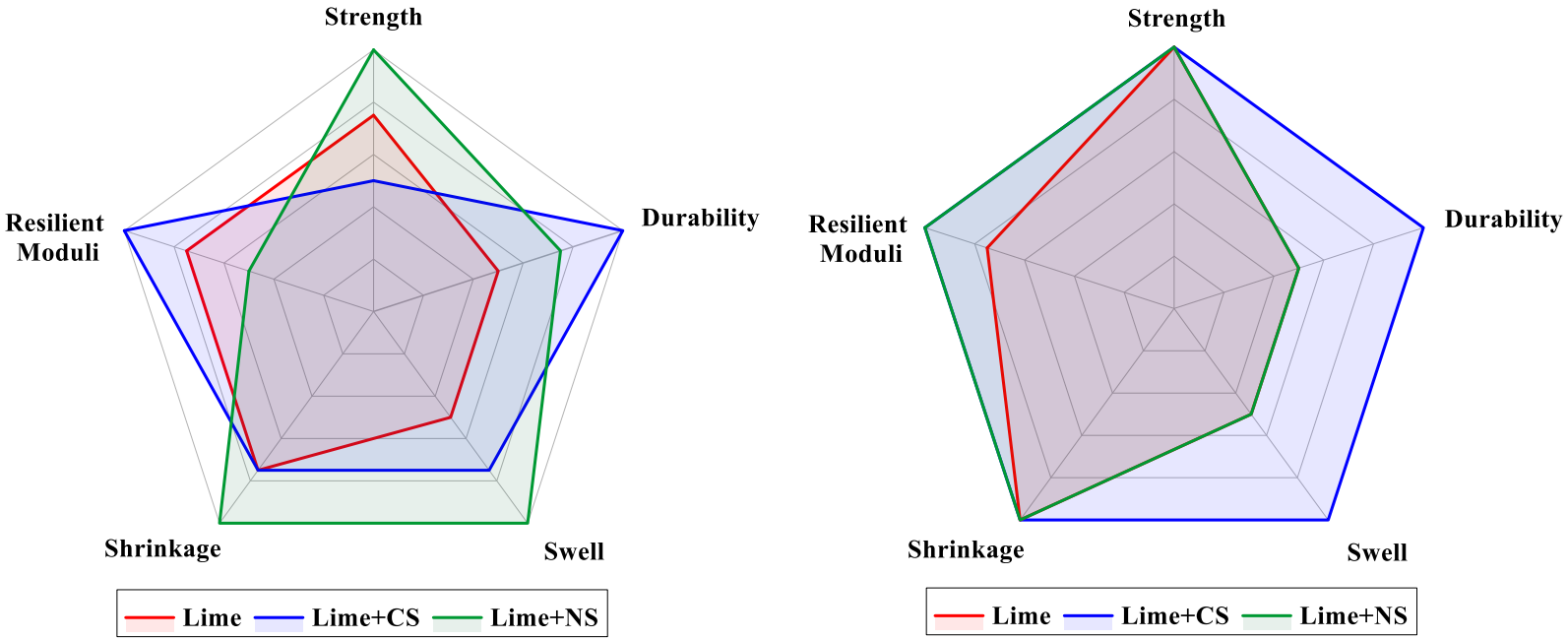

Figure 7.1 Comparison of performance between CS and NS co-additives when used with Ca-based stabilizer

a) Immediately at 7 days b) After 28 days of curing

7.2 Scope for Future Studies

Overall, this study showed a successful application of silica-based co-additives for the effective treatment of high plastic soils by contributing to strengthening reactions by forming C-S-H phases that enhance the bonding among soil particles. However, the beneficial outcomes of using silica-based admixtures with lime for the construction and rehabilitation of transportation infrastructures need to be further studied. Some future recommendations of this work are listed below:

- It is the responsibility of the engineers to design a sustainable system that can offset socio-economic consequences and environmental impacts of the developing new technologies for the transportation infrastructures. Furthermore, the designs for the infrastructures should be resilient to sustain extreme environmental impacts and be verified through a sustainability framework.
- The present study was performed with only high-plastic clays. Further research and analyses are necessary to understand the effects of these co-additives on other types of soils before providing a comprehensive guideline.
- Other aspects of the durability, such as effects of carbonation, presence of organic matters, wet-dry and freeze-thaw durability studies, need to be verified in future studies.

REFERENCES

Abbasi, N., Farjad, A., and Sepehri, S. 2018. The Use of Nanoclay Particles for Stabilization of Dispersive Clayey Soils. Geotechnical and Geological Engineering, **36**(1): 327–335. doi:10.1007/s10706-017-0330-9.

Al-Amoudi, O.S.B., Khan, K., and Al-Kahtani, N.S. 2010. Stabilization of a Saudi calcareous marl soil. Construction and Building Materials, **24**(10): 1848–1854. doi:10.1016/j.conbuildmat.2010.04.019.

Al-Mukhtar, M., Lasledj, A., and Alcover, J.-F. 2010. Behaviour and mineralogy changes in lime-treated expansive soil at 50°C. Applied Clay Science, **50**(2): 199–203. doi:10.1016/j.clay.2010.07.022.

Al-Rawas, A.A., and Goosen, M.F.A. 2006. Expansive soils: recent advances in characterization and treatment. Taylor & Francis.

Aldaood, A., Bouasker, M., and Al-Mukhtar, M. 2015. Effect of long-term soaking and leaching on the behaviour of lime-stabilised gypseous soil. International Journal of Pavement Engineering, **16**(1): 11–26. doi:10.1080/10298436.2014.893329.

Ali, H., and Mohamed, M. 2019. Assessment of lime treatment of expansive clays with different mineralogy at low and high temperatures. Construction and Building Materials, **228**: 116955. doi:10.1016/j.conbuildmat.2019.116955.

Amulya, G., Moghal, A.A.B., and Almajed, A. 2021. A State-of-the-Art Review on Suitability of Granite Dust as a Sustainable Additive for Geotechnical Applications. Crystals, **11**(12): 1526. doi:10.3390/cryst11121526.

Arabi, M., and Wild, S. 1986. Microstructural development in cured soil-lime composites. Journal of Materials Science, **21**(2): 497–503. doi:10.1007/BF01145514.

Baghdadi, Z.A., Fatani, M.N., and Sabban, N.A. 1995. Soil Modification by Cement Kiln Dust. Journal of Materials in Civil Engineering, **7**(4): 218–222. doi:10.1061/(ASCE)0899-1561(1995)7:4(218).

Baghdadi, Z.A., and Rahman, M.A. 1990. The potential of cement kiln dust for the stabilization of dune sand in highway construction. Building and Environment, **25**(4): 285–289. doi:10.1016/0360-1323(90)90001-8.

Bahmani, S.H., Farzadnia, N., Asadi, A., and Huat, B.B.K. 2016. The effect of size and

replacement content of nanosilica on strength development of cement treated residual soil. Construction and Building Materials, **118**: 294–306. doi:10.1016/j.conbuildmat.2016.05.075.

Bahmani, S.H., Huat, B.B.K., Asadi, A., and Farzadnia, N. 2014. Stabilization of residual soil using SiO2 nanoparticles and cement. Construction and Building Materials, **64**: 350–359. doi:10.1016/j.conbuildmat.2014.04.086.

Bahoria, B.V., Parbat, D.K., and Nagarnaik, P.B. 2018. XRD Analysis of Natural sand, Quarry dust, waste plastic (ldpe) to be used as a fine aggregate in concrete. Materials Today: Proceedings, **5**(1): 1432–1438. doi:10.1016/j.matpr.2017.11.230.

Bakharev, T., Sanjayan, J.G., and Cheng, Y.-B. 1999. Effect of elevated temperature curing on properties of alkali-activated slag concrete. Cement and Concrete Research, **29**(10): 1619–1625. doi:10.1016/S0008-8846(99)00143-X.

Bandara, N., Binoy, T.H., and Aboujrad, H.S. 2015. Freeze-Thaw Durability of Subgrades Stabilized with Recycled Materials. *In* Cold Regions Engineering 2015. American Society of Civil Engineers, Reston, VA. pp. 135–145.

Baston, G.M.N., Clacher, A.P., Heath, T.G., Hunter, F.M.I., Smith, V., and Swanton, S.W. 2012. Calcium silicate hydrate (C-S-H) gel dissolution and pH buffering in a cementitious near field. Mineralogical Magazine, **76**(8): 3045–3053. doi:10.1180/minmag.2012.076.8.20.

Behnood, A. 2018. Soil and clay stabilization with calcium- and non-calcium-based additives: A state-of-the-art review of challenges, approaches and techniques. Transportation Geotechnics, **17**: 14–32. doi:10.1016/j.trgeo.2018.08.002.

Bell, F.G. 1996. Lime stabilization of clay minerals and soils. Engineering Geology, **42**(4): 223–237. doi:10.1016/0013-7952(96)00028-2.

Bensted, J. 2000. Mechanism of thaumasite sulphate attack in cements, mortars and concretes. ZKG international, **53**(12): 704–709.

Biswas, N., Chakraborty, S., Puppala, A.J., and Banerjee, A. 2021a. A Novel Method to Improve the Durability of Lime-Treated Expansive Soil. *In* Proceedings of the Indian Geotechnical Conference 2019: Lecture Notes in Civil Engineering. *Edited by* S.S.K. Patel S., Solanki C.H., Reddy K.R. Springer, Singapore. pp. 227–238.

Biswas, N., Puppala, A.J., Chakraborty, S., and Khan, M.A. 2021b. Utilization of Silica-Based Admixture to Improve the Durability of Lime-Treated Expansive Soil. *In* IFCEE 2021. pp. 233–242.

Biswas, N., Puppala, A.J., Khan, M.A., Congress, S.S.C., Banerjee, A., and Chakraborty, S. 2021c. Evaluating the Performance of Wicking Geotextile in Providing Drainage for Flexible Pavements Built over Expansive Soils. Transportation Research Record: Journal of the Transportation Research Board, **2675**(9): 208–221. doi:10.1177/03611981211001381.

Brough, A.., and Atkinson, A. 2002. Sodium silicate-based, alkali-activated slag mortars. Cement and Concrete Research, **32**(6): 865–879. doi:10.1016/S0008-8846(02)00717-2.

Burkart, B., Goss, G.C., and Kern, J.P. 1999. The Role of Gypsum in Production of Sulfate-Induced Deformation of Lime-Stabilized Soils. Environmental & Engineering Geoscience, **V**(2): 173–187. doi:10.2113/gseegeosci.V.2.173.

Cabrera, J.G., and Nwakanma, C.A. 1979. Pozzolanic activity and mechanism of reaction of red tropical soil-lime systems. Transportation research record, (702).

Chakraborty, S., and Nair, S. 2018. Impact of different hydrated cementitious phases on moisture-induced damage in lime-stabilised subgrade soils. Road Materials and Pavement Design, **19**(6): 1389–1405. doi:10.1080/14680629.2017.1314222.

Chakraborty, S., and Nair, S. 2020. Impact of curing time on moisture-induced damage in lime-treated soils. International Journal of Pavement Engineering, **21**(2): 215–227. doi:10.1080/10298436.2018.1453068.

Chakraborty, S., Puppala, A.J., and Biswas, N. 2020. Role of crystalline silica admixture in mitigating ettringite-induced heave in lime-treated sulfate-rich soils. Géotechnique,: 1–17. doi:10.1680/jgeot.20.p.154.

Changizi, F., and Haddad, A. 2017. Improving the geotechnical properties of soft clay with nano-silica particles. Proceedings of the Institution of Civil Engineers-Ground Improvement, **170**(2): 62–71. Thomas Telford Ltd.

Chen, R., Drnevich, V.P., and Daita, R.K. 2009. Short-Term Electrical Conductivity and Strength Development of Lime Kiln Dust Modified Soils. Journal of Geotechnical and Geoenvironmental Engineering, **135**(4): 590–594. doi:10.1061/(ASCE)1090-0241(2009)135:4(590).

Chen, X., and Peng, Y. 2018. Managing clay minerals in froth flotation—A critical review. Mineral Processing and Extractive Metallurgy Review, **39**(5): 289–307. doi:10.1080/08827508.2018.1433175.

Chesner, W.H., Collins, R.J., MacKay, M.H., and Emery, J. 2002. User Guidelines for

Waste and By-Product Materials in Pavement Construction. Recycled Materials Resource Center.

Chittoori, B., Puppala, A., Wejrungsikul, T., and Hoyos, L. 2013a. Experimental Studies on Stabilized Clays at Various Leaching Cycles. Journal of Geotechnical and Geoenvironmental Engineering, **139**(10): 1665–1675. doi:10.1061/(ASCE)GT.1943-5606.0000920.

Chittoori, B.C.S., Puppala, A.J., and Pedarla, A. 2018. Addressing Clay Mineralogy Effects on Performance of Chemically Stabilized Expansive Soils Subjected to Seasonal Wetting and Drying. Journal of Geotechnical and Geoenvironmental Engineering, **144**(1): 04017097. doi:10.1061/(ASCE)GT.1943-5606.0001796.

Chittoori, B.C.S., Puppala, A.J., Wejrungsikul, T., and Hoyos, L.R. 2013b. Experimental Studies on Stabilized Clays at Various Leaching Cycles. Journal of Geotechnical and Geoenvironmental Engineering, **139**(10): 1665–1675. doi:10.1061/(ASCE)GT.1943-5606.0000920.

Christopher, B.R., Schwartz, C.W., and Boudreau, R.L. 2006. Geotechnical aspects of pavements, Rep. No. FHWA NHI-05-037. *In* NHI Course No.132040. Washington, D.C.

Ciardi, G., Vannucchi, G., and Madiai, C. 2021. Effects of Colloidal Silica Grouting on Geotechnical Properties of Liquefiable Soils: A Review. Geotechnics, **1**(2): 460–491. doi:10.3390/geotechnics1020022.

Çokça, E. 2001. Use of Class C Fly Ashes for the Stabilizationof an Expansive Soil. Journal of Geotechnical and Geoenvironmental Engineering, **127**(7): 568–573. doi:10.1061/(ASCE)1090-0241(2001)127:7(568).

Consoli, N.C., Bittar Marin, E.J., Quiñónez Samaniego, R.A., Scheuermann Filho, H.C., Miranda, T., and Cristelo, N. 2019. Effect of Mellowing and Coal Fly Ash Addition on Behavior of Sulfate-Rich Dispersive Clay after Lime Stabilization. Journal of Materials in Civil Engineering, **31**(6): 04019071. doi:10.1061/(ASCE)MT.1943-5533.0002699.

Consoli, N.C., Lopes, L. da S., Prietto, P.D.M., Festugato, L., and Cruz, R.C. 2011. Variables Controlling Stiffness and Strength of Lime-Stabilized Soils. Journal of Geotechnical and Geoenvironmental Engineering, **137**(6): 628–632. doi:10.1061/(ASCE)GT.1943-5606.0000470.

Consoli, N.C., Prietto, P.D.M., Carraro, J.A.H., and Heineck, K.S. 2002. Behavior of Compacted Soil-Fly Ash-Carbide Lime Mixtures. Journal of Geotechnical and

Geoenvironmental Engineering,. doi:10.1061/(asce)1090-0241(2001)127:9(774).

Consoli, N.C., da Silva Lopes, L., and Heineck, K.S. 2009. Key Parameters for the Strength Control of Lime Stabilized Soils. Journal of Materials in Civil Engineering, **21**(5): 210–216. doi:10.1061/(ASCE)0899-1561(2009)21:5(210).

Correia, A.A.S., Casaleiro, P.D.F., and Rasteiro, M.G.B.V. 2015. Applying Multiwall Carbon Nanotubes for Soil Stabilization. Procedia Engineering, **102**: 1766–1775. doi:10.1016/j.proeng.2015.01.313.

Correia, A.A.S., and Rasteiro, M.G. 2016. Nanotechnology Applied to Chemical Soil Stabilization. Procedia Engineering, **143**: 1252–1259. doi:10.1016/j.proeng.2016.06.113.

Crammond, N.. 2003. The thaumasite form of sulfate attack in the UK. Cement and Concrete Composites, **25**(8): 809–818. doi:10.1016/S0958-9465(03)00106-9.

Czerewko, M.., Cripps, J.., Reid, J.., and Duffell, C.. 2003. Sulfur species in geological materials—sources and quantification. Cement and Concrete Composites, **25**(7): 657–671. doi:10.1016/S0958-9465(02)00066-5.

Das, J.T. 2018. Assessment of Sustainability and Resilience in Transportation Infrastructure Geotechnics. University of Texas at Arlington.

Das, J.T., Banerjee, A., Puppala, A.J., and Chakraborty, S. 2019. A Unified Approach for Assessment of Sustainability and Resilience in Pavement Infrastructure. Environmental Geotechnics,: 1–13. doi:10.1680/jenge.19.00035.

Dash, S.K., and Hussain, M. 2012. Lime Stabilization of Soils: Reappraisal. Journal of Materials in Civil Engineering, **24**(6): 707–714. American Society of Civil Engineers. doi:10.1061/(ASCE)MT.1943-5533.0000431.

Dempsey, B.J., and Thompson, M.R. 1968. Durability properties of lime-soil mixtures. Highway Research Record, (235).

Deng, Y., Dixon, J.B., and White, G.N. 2006. Adsorption of polyacrylamide on smectite, illite, and kaolinite. Soil Science Society of America Journal, **70**(1): 297–304. Wiley Online Library.

Dermatas, D. 1995. Ettringite-Induced Swelling in Soils: State-of-the-Art. Applied Mechanics Reviews, **48**(10): 659. doi:10.1115/1.3005046.

Dhar, S., and Hussain, M. 2019. The strength and microstructural behavior of lime

stabilized subgrade soil in road construction. International Journal of Geotechnical Engineering,. Taylor and Francis Ltd. doi:10.1080/19386362.2019.1598623.

Diamond, S., and Kinter, E.B. 1966. Adsorption of calcium hydroxide by montmorillonite and kaolinite. Journal of colloid and interface science, **22**(3): 240–249. Elsevier.

Dumbleton, M.J. 1962. Investigations to assess the potentialities of lime for soil stabilisation in the United Kingdom. Road Research Technical Paper 64. Transport Research Laboratory, Crowthorne, Berks,.

Estabragh, A.R., Pereshkafti, M.R.S., Parsaei, B., and Javadi, A.A. 2013. Stabilised expansive soil behaviour during wetting and drying. International Journal of Pavement Engineering, **14**(4): 418–427. doi:10.1080/10298436.2012.746688.

Fredlund, D.G., Sheng, D., and Zhao, J. 2011. Estimation of soil suction from the soil-water characteristic curve. Canadian Geotechnical Journal, **48**(2): 186–198. doi:10.1139/T10-060.

Fredlund, D.G., and Xing, A. 1994. Equations for the soil-water characteristic curve. Canadian Geotechnical Journal, **31**(4): 521–532. doi:10.1139/t94-061.

Gaudette, H.E., Eades, J.L., and Grim, R.E. 1964. The nature of illite. Clays and clay minerals, **13**(1): 33–48. Springer.

Givi, A.N., Rashid, S.A., Aziz, F.N.A., and Salleh, M.A.M. 2013. Influence of 15 and 80 nano-SiO 2 particles addition on mechanical and physical properties of ternary blended concrete incorporating rice husk ash. Journal of Experimental Nanoscience, **8**(1): 1–18. doi:10.1080/17458080.2010.548834.

Glenn, G.R. 1970. Differential Thermal and Thermogravimetric Analysis of Reacted Bentonite-Lime-Water Mixtures. Highway Research Record, (315): 122–132.

Gohari, G., Mohammadi, A., Akbari, A., Panahirad, S., Dadpour, M.R., Fotopoulos, V., and Kimura, S. 2020. Titanium dioxide nanoparticles (TiO2 NPs) promote growth and ameliorate salinity stress effects on essential oil profile and biochemical attributes of Dracocephalum moldavica. Scientific Reports, **10**(1): 912. doi:10.1038/s41598-020-57794-1.

Harris, A.W., Manning, M.C., Tearle, W.M., and Tweed, C.J. 2002. Testing of models of the dissolution of cements—leaching of synthetic CSH gels. Cement and Concrete Research, **32**(5): 731–746. doi:10.1016/S0008-8846(01)00748-7.

Harris, P., Harvey, O., Puppala, A., Sebesta, S., Chikyala, S.R., and Saride, S. 2009. Mitigating the Effects of Organics in Stabilized Soils. *In* Technical Report: Rep. No. FHWA/TX-09/0-5540-1.

Hilbig, H., and Buchwald, A. 2006. The effect of activator concentration on reaction degree and structure formation of alkali-activated ground granulated blast furnace slag. Journal of Materials Science, **41**(19): 6488–6491. doi:10.1007/s10853-006-0755-7.

Ho, C., and Handy, R.L. 1963. Characteristics of lime retention by montmorillonitic clays. Highway Research Record, (29).

Horpibulsuk, S., Phojan, W., Suddeepong, A., Chinkulkijniwat, A., and Liu, M.D. 2012. Strength development in blended cement admixed saline clay. Applied Clay Science, **55**: 44–52. doi:10.1016/j.clay.2011.10.003.

Horpibulsuk, S., Rachan, R., and Raksachon, Y. 2009. Role of Fly Ash on Strength and Microstructure Development in Blended Cement Stabilized Silty Clay. Soils and Foundations, **49**(1): 85–98. doi:10.3208/sandf.49.85.

Horpibulsuk, S., Rachan, R., and Suddeepong, A. 2011. Assessment of strength development in blended cement admixed Bangkok clay. Construction and Building Materials, **25**(4): 1521–1531. doi:10.1016/j.conbuildmat.2010.08.006.

Hoyos, L.R., Laikram, A., and Puppala, A.J. 2006. Assessment of seasonal effects on engineering behavior of chemically treated sulfate-rich expansive clay. Expansive Soils: Recent Advances in Characterization and Treatment,: 483. Taylor & Francis.

Hoyos, L.R., Puppala, A.J., and Chainuwat, P. 2004. Dynamic Properties of Chemically Stabilized Sulfate Rich Clay. Journal of Geotechnical and Geoenvironmental Engineering,. doi:10.1061/(ASCE)1090-0241(2004)130:2(153).

https://www.generatorsource.com/. (n.d.). Generator Modifications for Rock Crushing Plants | Industrial Rock Crusher Generators | Blog. Available from https://www.generatorsource.com/blog/February-2018/Rock-Crushing-Plant-Generator-Modifications.aspx. [accessed 3 February 2022].

Hunter, D. 1988. Lime-Induced Heave in Sulfate-Bearing Clay Soils. Journal of Geotechnical Engineering, **114**(2): 150–167.

Ingalkar, R.S., and Harle, S.M. 2017. Replacement of Natural Sand by Crushed Sand in the Concrete. Landscape Architecture and Regional Planning, **2**(1): 13–22. doi:10.11648/j.larp.20170201.12.

Ingles, O.G., and Metcalf, J.B. 1972. Soil stabilization principles and practice.

Jafari, N.H., Puppala, A., Boluk, B., Cadigan, J.A., Chakraborty, S., Bheemasetti, T., and Pleasant, J.E. 2019. Predicting the Performance of Highway Embankment Slopes. *In* MATEC Web of Conferences. *Edited by* H. Sadek. p. 02007.

James, R., Kamruzzaman, A.H.M., Haque, A., and Wilkinson, A. 2008. Behaviour of lime–slag-treated clay. Proceedings of the Institution of Civil Engineers - Ground Improvement, **161**(4): 207–216. doi:10.1680/grim.2008.161.4.207.

Janek, M., and Lagaly, G. 2001. Proton saturation and rheological properties of smectite dispersions. Applied Clay Science, **19**(1–6): 121–130. Elsevier.

Jang, J., Puppala, A.J., Biswas, N., Chakraborty, S., and Radovic, M. 2022. Utilization of Metakaolin-Based Geopolymers for Stabilization of Sulfate-Rich Expansive Soils. *In* Geo-Congress 2022. American Society of Civil Engineers, Reston, VA. pp. 222–231.

Jang, J., Puppala, A.J., Chakraborty, S., Biswas, N., Huang, O., and Radovic, M. 2021. Eco-Friendly Stabilization of Sulfate-Rich Expansive Soils Using Geopolymers for Transportation Infrastructure. *In* Tran-SET 2021. American Society of Civil Engineers, Reston, VA. pp. 223–231.

Jewell, R., Rathbone, R., Duvallet, T., Robl, T., and Mahboub, K. 2015. Fabrication and Testing of Low-Energy Calcium Sulfoaluminate-Belite Cements that Utilize Circulating Fluidized Bed Combustion By-Products. Coal Combustion and Gasification Products, **7**(1): 9–18. doi:10.4177/CCGP-D-15-00001.1.

Jung, C., Bobet, A., Siddiki, N.Z., and Kim, D. 2011. Postconstruction Evaluation of Subgrades Chemically Treated with Lime Kiln Dust. Journal of Materials in Civil Engineering, **23**(7): 931–940. doi:10.1061/(ASCE)MT.1943-5533.0000251.

Kakrasul, J.I., Parsons, R.L., and Han, J. 2017. Lime kiln dust for treated subgrades. Kansas. Dept. of Transportation.

Kalhor, A., Ghazavi, M., Roustaei, M., and Mirhosseini, S.M. 2019. Influence of nano-SiO2 on geotechnical properties of fine soils subjected to freeze-thaw cycles. Cold Regions Science and Technology, **161**: 129–136. doi:10.1016/j.coldregions.2019.03.011.

Kalkan, E. 2011. Impact of wetting–drying cycles on swelling behavior of clayey soils modified by silica fume. Applied Clay Science, **52**(4): 345–352. doi:10.1016/j.clay.2011.03.014.

Kampala, A., Horpibulsuk, S., Prongmanee, N., and Chinkulkijniwat, A. 2014. Influence of Wet-Dry Cycles on Compressive Strength of Calcium Carbide Residue–Fly Ash Stabilized Clay. Journal of Materials in Civil Engineering, **26**(4): 633–643. doi:10.1061/(ASCE)MT.1943-5533.0000853.

Kehew, A.E. 2021. Geology for engineers and environmental scientists. Waveland Press.

Keller, W.D. 1964. Processes of origin and alteration of clay minerals. Soil clay mineralogy, **3**. University of North Carolina Press Chapel Hill.

Kennedy, T.W., Smith, R., Holmgreen Jr, R.J., and Tahmoressi, M. 1987. An evaluation of lime and cement stabilization. Transportation Research Board, (1119): 11–25.

Keramatikerman, M., Chegenizadeh, A., and Nikraz, H. 2016. Effect of GGBFS and lime binders on the engineering properties of clay. Applied Clay Science, **132**–**133**: 722–730. doi:10.1016/j.clay.2016.08.029.

Khan, M.A., Nripojoyti, B., Banerjee, A., and Puppala, A.J. 2020. Performance of geocell-reinforced recycled asphalt pavement (rap) bases in flexible pavements built on expansive soils. *In* Geotechnical Special Publication. American Society of Civil Engineers (ASCE). pp. 488–497.

Khattab, S.A., Al-Mukhtar, M., and Fleureau, J.-M. 2007. Long-Term Stability Characteristics of a Lime-Treated Plastic Soil. Journal of Materials in Civil Engineering, **19**(4): 358–366. American Society of Civil Engineers. doi:10.1061/(ASCE)0899-1561(2007)19:4(358).

Khoury, N., Brooks, R., Boeni, S.Y., and Yada, D. 2013. Variation of Resilient Modulus, Strength, and Modulus of Elasticity of Stabilized Soils with Postcompaction Moisture Contents. Journal of Materials in Civil Engineering, **25**(2): 160–166. doi:10.1061/(ASCE)MT.1943-5533.0000574.

Kloprogge, J.T., Komarneni, S., and Amonette, J.E. 1999. Synthesis of smectite clay minerals: a critical review. Clays and Clay Minerals, **47**(5): 529–554. Springer.

Köhler, S., Heinz, D., and Urbonas, L. 2006. Effect of ettringite on thaumasite formation. Cement and Concrete Research, **36**(4): 697–706. doi:10.1016/j.cemconres.2005.11.006.

Kolias, S., Kasselouri-Rigopoulou, V., and Karahalios, A. 2005. Stabilisation of clayey soils with high calcium fly ash and cement. Cement and Concrete Composites, **27**(2): 301–313. doi:10.1016/j.cemconcomp.2004.02.019.

Konan, K.L., Peyratout, C., Bonnet, J.-P., Smith, A., Jacquet, A., Magnoux, P., and Ayrault, P. 2007. Surface properties of kaolin and illite suspensions in concentrated calcium hydroxide medium. Journal of colloid and interface science, **307**(1): 101–108. Elsevier.

Kota, P.B.V.S., Hazlett, D., and Perrin, L. 1996. Sulfate-Bearing Soils: Problems with Calcium-Based Stabilizers. Transportation Research Record: Journal of the Transportation Research Board, **1546**(1): 62–69. doi:10.1177/0361198196154600107.

Kufre Etim, R., Ufot Ekpo, D., Christopher Attah, I., and Chibuzor Onyelowe, K. 2021. Effect of micro sized quarry dust particle on the compaction and strength properties of cement stabilized lateritic soil. Cleaner Materials, **2**: 100023. doi:10.1016/j.clema.2021.100023.

Kukko, H. 2000. Stabilization of Clay with Inorganic By-Products. Journal of Materials in Civil Engineering, **12**(4): 307–309. doi:10.1061/(ASCE)0899-1561(2000)12:4(307).

Kumar, A., and Gupta, D. 2016. Behavior of cement-stabilized fiber-reinforced pond ash, rice husk ash–soil mixtures. Geotextiles and Geomembranes, **44**(3): 466–474. doi:10.1016/j.geotexmem.2015.07.010.

Kumar, A., Walia, B.S., and Bajaj, A. 2007. Influence of Fly Ash, Lime, and Polyester Fibers on Compaction and Strength Properties of Expansive Soil. Journal of Materials in Civil Engineering, **19**(3): 242–248. doi:10.1061/(ASCE)0899-1561(2007)19:3(242).

Kutschera, M., Nicoleau, L., and Bräu, M. 2011. Nano-optimized Construction Materials by Nano-seeding and Crystallization Control. *In* Nanotechnology in Civil Infrastructure. Springer Berlin Heidelberg, Berlin, Heidelberg. pp. 175–205.

Lamb, M.J. 2005. Design guide for applications of sandstone quarry sand in South Wales, Viridis Report VR8. TRL Limited.

Lerch, W., Ashton, W., and Bogue, H. 1925. The sulphoaluminates of calcium. Soil Science, **19**: 125.

Little, D., Males, E., Prusinski, J., and Stewart, B. 2000. Cementitious stabilization. *In* Transportation in the Millenium.

Little, D., and Nair, S. 2009a. Recommended Practice for Stabilization of Subgrade Soils and Base Materials. *In* Transportation Research Board. Transportation Research

Board, Washington, D.C.

Little, D.N. 1995. Handbook for stabilization of pavement subgrades and base courses with lime. National Lime Association, Kendall/Hunt Publishing Company, Iowa.

Little, D.N. 1996. Evaluation of resilient and strength properties of lime-stabilized soils for the Denver, Colorado area. Colorado.

Little, D.N. 1999. Evaluation of structural properties of lime stabilized soils and aggregates - Volume 1: Summary of findings. National Lime Association,. doi:09.04.2015.

Little, D.N., Herbert, B., and Kunagalli, S.N. 2005. Ettringite formation in lime-treated soils establishing thermodynamic foundations for engineering practice. Transportation Research Record, **5**(1936): 51–59. doi:10.3141/1936-07.

Little, D.N., and Nair, S. 2009b. Validation of Sensitivity of Sulfate-Bearing Soils to Ettringite Growth by Differential Scanning Calorimetry. Transportation Research Record: Journal of the Transportation Research Board, (2104): 63–70.

Little, D.N., and Nair, S. 2009c. Recommended Practice for Stabilization of Sulfate-Rich Subgrade Soils, NCHRP 145. Transportation Research Board, Washington, D.C.

Little, D.N., Nair, S., and Herbert, B. 2010. Addressing Sulfate-Induced Heave in Lime Treated Soils. Journal of Geotechnical and Geoenvironmental Engineering, **136**(1): 110–118. doi:10.1061/(ASCE)GT.1943-5606.0000185.

Little, D.N., and Yusuf, M. 2001. Example Problem Illustrating the Application of the National Lime Association Mixture Design and Testing Protocol (MDTP) to Ascertain Engineering Properties of Lime Treated Subgrades for Mechanistic Pavement Design/Analysis.

McCallister, L.D. 1990. The effects of leaching on lime-treated expansive clay. University of Texas at Arlington, Texas.

McCallister, L.D., and Petry, T.M. 1992. Leach tests on lime-treated clays. Geotechnical testing journal, **15**(2): 106–114. ASTM International.

McCarthy, G.J., Swanson, K.D., Keller, L.P., and Blatter, W.C. 1984. Mineralogy of western fly ash. Cement and Concrete Research, **14**(4): 471–478. doi:10.1016/0008-8846(84)90121-2.

McKennon, J.T., Hains, N.L., and Hoffman, D.C. 1994. Method for producing enhanced

sol stabilization reactions between lime and clay soils due to the effect of silica addition. United States Patents, USA.

Mehta, P.K. 1973. Mechanism of expansion associated with ettringite formation. Cement and Concrete Research, **3**(1): 1–6. doi:10.1016/0008-8846(73)90056-2.

Miller, G.A., and Azad, S. 2000. Influence of soil type on stabilization with cement kiln dust. Construction and Building Materials, **14**(2): 89–97. doi:10.1016/S0950-0618(00)00007-6.

Min, D., and Mingshu, T. 1994. Formation and expansion of ettringite crystals. Cement and Concrete Research, **24**(1): 119–126. doi:10.1016/0008-8846(94)90092-2.

Misra, A. 1998. Stabilization Characteristics of Clays Using Class C Fly Ash. Transportation Research Record: Journal of the Transportation Research Board, **1611**(1): 46–54. doi:10.3141/1611-06.

Mitchell, J., and Dermatas, D. 1992. Clay Soil Heave Caused by Lime-Sulfate Reactions. *In* Innovations and Uses for Lime. ASTM International, 100 Barr Harbor Drive, PO Box C700, West Conshohocken, PA 19428-2959. pp. 41–64.

Mitchell, J.K. 1981. Soil improvement-state of the art report. *In* Proc., 11th Int. Conf. on SMFE. pp. 509–565.

Mitchell, J.K., and Soga, K. 2005. Fundamentals of soil behavior. John Wiley & Sons New York.

Mooney, M.A., and Toohey, N.M. 2010. Accelerated curing and strength-modulus correlation for lime-stabilized soils. Colorado Department of Transportation, DTD Applied Research and Innovation.

Moore, A., and Taylor, H.F.W. 1968. Crystal Structure of Ettringite. Nature, **218**(5146): 1048–1049. doi:10.1038/2181048a0.

Morris, P.H., Graham, J., and Williams, D.J. 2011. Cracking in drying soils. https://doi.org/10.1139/t92-030, **29**(2): 263–277. NRC Research Press Ottawa, Canada . doi:10.1139/T92-030.

Myneni, S.C.B., Traina, S.J., and Logan, T.J. 1998. Ettringite solubility and geochemistry of the Ca(OH)2–Al2(SO4)3–H2O system at 1 atm pressure and 298 K. Chemical Geology, **148**(1–2): 1–19. doi:10.1016/S0009-2541(97)00128-9.

Nahlawi, H., and Kodikara, J.K. 2006. Laboratory experiments on desiccation cracking

of thin soil layers. Geotechnical and Geological Engineering, **24**(6): 1641–1664. doi:10.1007/s10706-005-4894-4.

Nair, S., and Little, D.N. 2009. Water as the Key to Expansion of Ettringite in Cementitious Materials. Transportation Research Record: Journal of the Transportation Research Board, **2104**(1): 55–62. doi:10.3141/2104-06.

Nakarai, K., and Yoshida, T. 2015. Effect of carbonation on strength development of cement-treated Toyoura silica sand. Soils and Foundations, **55**(4): 857–865. doi:10.1016/j.sandf.2015.06.016.

Nelson, J.D., and Miller, D.J. 1992. Expansive soils : problems and practice in foundation and pavement engineering. J. Wiley.

Nidzam, R.M., and Kinuthia, J.M. 2010. Sustainable soil stabilisation with blastfurnace slag – a review. Proceedings of the Institution of Civil Engineers - Construction Materials, **163**(3): 157–165. doi:10.1680/coma.2010.163.3.157.

Niroumand, H., Zain, M.F.M., and Alhosseini, S.N. 2013. The Influence of Nano-clays on Compressive Strength of Earth Bricks as Sustainable Materials. Procedia - Social and Behavioral Sciences, **89**: 862–865. doi:10.1016/j.sbspro.2013.08.945.

O'Rourke, T.D., McGinn, A.J., Dewsnap, J., and Stewart, H.E. 1998. Case history of an excavation stabilized by deep mixing methods. *In* Design and construction of earth retaining systems. ASCE. pp. 41–62.

Odler, I., and Gasser, M. 1988. Mechanism of Sulfate Expansion in Hydrated Portland Cement. Journal of the American Ceramic Society, **71**(11): 1015–1020. doi:10.1111/j.1151-2916.1988.tb07573.x.

Odom, I.E. 1984. Smectite clay minerals: properties and uses. Philosophical Transactions of the Royal Society of London. Series A, Mathematical and Physical Sciences, **311**(1517): 391–409. The Royal Society London.

Ogawa, K., and Roy, D.M. 1982. C4A3S hydration, ettringite formation, and its expansion mechanism: II. Microstructural observation of expansion. Cement and Concrete Research, **12**(1): 101–109. doi:10.1016/0008-8846(82)90104-1.

Okamura, H., and Ouchi, M. 1998. Self-compacting high performance concrete. Progress in Structural Engineering and Materials, **1**(4): 378–383. doi:10.1002/pse.2260010406.

Ormsby, W.C., and Kinter, E.B. 1973. STRENGTH DEVELOPMENT AND

REACTION-PRODUCTS IN LIME-MONTMORILLONITE-WATER SYSTEMS. Public Roads, **37**(4): 136–148. US GOVERNMENT PRINTING OFFICE SUPT OF DOCUMENTS, WASHINGTON, DC 20402-9325.

Ouhadi, V.R., and Yong, R.N. 2008. Ettringite formation and behaviour in clayey soils. Applied Clay Science, **42**(1–2): 258–265. doi:10.1016/j.clay.2008.01.009.

Ozyildirim, H.C. 1990. Admixtures and ground slag for concrete. Transportation Research Board, **365**: 33–43.

Pedarla, A., Chittoori, S., and Puppala, A. 2011. Influence of Mineralogy and Plasticity Index on the Stabilization Effectiveness of Expansive Clays. Transportation Research Record: Journal of the Transportation Research Board,. doi:10.3141/2212-10.

Peethamparan, S., and Olek, J. 2008. Study of the Effectiveness of Cement Kiln Dusts in Stabilizing Na-Montmorillonite Clay. Journal of Materials in Civil Engineering, **20**(2): 137–146. doi:10.1061/(ASCE)0899-1561(2008)20:2(137).

Peethamparan, S., Olek, J., and Diamond, S. 2008a. Physicochemical Behavior of Cement Kiln Dust–Treated Kaolinite Clay. Transportation Research Record: Journal of the Transportation Research Board, **2059**(1): 80–88. doi:10.3141/2059-09.

Peethamparan, S., Olek, J., and Lovell, J. 2008b. Influence of chemical and physical characteristics of cement kiln dusts (CKDs) on their hydration behavior and potential suitability for soil stabilization. Cement and Concrete Research, **38**(6): 803–815. doi:10.1016/j.cemconres.2008.01.011.

Petry, T.M., and Little, D.N. 1992. Update on sulfate-induced heave in treated clays; problematic sulfate levels. Transportation research record,: 51–55. NATIONAL ACADEMY OF SCIENCES.

Petry, T.M., and Little, D.N. 2002. Review of Stabilization of Clays and Expansive Soils in Pavements and Lightly Loaded Structures—History, Practice, and Future. Journal of Materials in Civil Engineering, **14**(6): 447–460. doi:10.1061/(ASCE)0899-1561(2002)14:6(447).

Pham, H., and Nguyen, Q.P. 2014. Effect of silica nanoparticles on clay swelling and aqueous stability of nanoparticle dispersions. Journal of Nanoparticle Research, **16**(1): 2137. doi:10.1007/s11051-013-2137-9.

Phetchuay, C., Horpibulsuk, S., Arulrajah, A., Suksiripattanapong, C., and Udomchai, A.

2016. Strength development in soft marine clay stabilized by fly ash and calcium carbide residue based geopolymer. Applied Clay Science, **127**–**128**: 134–142. doi:10.1016/j.clay.2016.04.005.

Puppala, A., Hoyos, L., Viyanant, C., and Musenda, C. 2008a. Fiber and Fly Ash Stabilization Methods to Treat Soft Expansive Soils. : 136–145. doi:10.1061/40552(301)11.

Puppala, A., Mohammad, L., and Allen, A. 1996. Engineering Behavior of Lime-Treated Louisiana Subgrade Soil. Transportation Research Record: Journal of the Transportation Research Board,. doi:10.3141/1546-03.

Puppala, A., Viyanant, C., Kruzic, A., and Perrin, L. 2002. Evaluation of a Modified Soluble Sulfate Determination Method for Fine-Grained Cohesive Soils. Geotechnical Testing Journal, **25**(1): 85. doi:10.1520/GTJ11083J.

Puppala, A.J. 2008. Estimating Stiffness of Subgrade and Unbound Materials for Pavement Design. Transportation Research Board, Washington, D.C.

Puppala, A.J. 2016. Advances in ground modification with chemical additives: From theory to practice. Transportation Geotechnics,. doi:10.1016/j.trgeo.2016.08.004.

Puppala, A.J. 2021. Performance Evaluation of Infrastructure on Problematic Expansive Soils: Characterization Challenges, Innovative Stabilization Designs, and Monitoring Methods. Journal of Geotechnical and Geoenvironmental Engineering, **147**(8): (ASCE)GT.1943-5606.0002518. doi:10.1061/(ASCE)GT.1943-5606.0002518.

Puppala, A.J., and Cerato, A. 2009. Heave distress problems in chemically-treated sulfate-laden materials. Geo-Strata, **10**(2): 28.

Puppala, A.J., Chittoori, B.C.S., Talluri, N., Le, M., Bheemasetti, T., and Thomey, J. 2013. Stabilizer selection for arresting surficial slope failures: A sustainability perspective. 2013 Congress on Stability and Performance of Slopes and Embankments III, Geo-Congress 2013, (231 GSP): 1472–1481.

Puppala, A.J., Intharasombat, N., and Vempati, R.K. 2005. Experimental Studies on Ettringite-Induced Heaving in Soils. Journal of Geotechnical and Geoenvironmental Engineering, **131**(3): 325–337. doi:10.1061/(ASCE)1090-0241(2005)131:3(325).

Puppala, A.J., and Pedarla, A. 2017. Innovative ground improvement techniques for expansive soils. Innovative Infrastructure Solutions,. doi:10.1007/s41062-017-0079-2.

Puppala, A.J., Pedarla, A., Chittoori, B., Ganne, V.K., and Nazarian, S. 2017a. Long-term durability studies on chemically treated reclaimed asphalt pavement material as a base layer for pavements. *In* Transportation Research Record : Journal of the Transportation Research, **2657**: 1–9. doi:10.3141/2657-01.

Puppala, A.J., Pedarla, A., Gaily, A., and others. 2016. Implementation: Mitigation of High Sulfate Soils in Texas: Development of Design and Construction Guidelines. : 1–39.

Puppala, A.J., Punthutaecha, K., and Vanapalli, S.K. 2006a. Soil-Water Characteristic Curves of Stabilized Expansive Soils. Journal of Geotechnical and Geoenvironmental Engineering, **132**(6): 736–751. doi:10.1061/(ASCE)1090-0241(2006)132:6(736).

Puppala, A.J., Saride, S., and Chomtid, S. 2009. Experimental and Modeling Studies of Permanent Strains of Subgrade Soils. Journal of Geotechnical and Geoenvironmental Engineering, **135**(10): 1379–1389. doi:10.1061/(ASCE)GT.1943-5606.0000163.

Puppala, A.J., Saride, S., Sirigiripet, S.K., Williammee, R., and Dronamraju, V.S. 2008b. Evaluation of Cemented Quarry Fines as a Pavement Base Material. *In* GeoCongress 2008. American Society of Civil Engineers, Reston, VA. pp. 312–319.

Puppala, A.J., Saride, S., Yenigalla, R. V., Chittoori, B.C.S., and Archeewa, E. 2017b. Long-Term Performance of a Highway Embankment Built with Lightweight Aggregates. Journal of Performance of Constructed Facilities, **31**(5): 04017042. doi:10.1061/(ASCE)CF.1943-5509.0001043.

Puppala, A.J., Wattanasanticharoen, E., and Porbaha, A. 2006b. Combined lime and polypropylene fiber stabilization for modification of expansive soils. Expansive soils: recent advances in characterization and treatment, **1**: 349–367.

Puppala, A.J., Wattanasanticharoen, E., and Punthutaecha, K. 2003. Experimental evaluations of stabilisation methods for sulphate-rich expansive soils. Proceedings of the Institution of Civil Engineers - Ground Improvement,. doi:10.1680/grim.2003.7.1.25.

Rajasekaran, G., and Narasimha Rao, S. 1997. The microstructure of lime-stabilized marine clay. Ocean Engineering, **24**(9): 867–878. doi:10.1016/S0029-8018(96)00041-8.

Rao, S.M., and Shivananda, P. 2005. Role of curing temperature in progress of lime-soil

reactions. Geotechnical and Geological Engineering, **23**(1): 79–85. doi:10.1007/s10706-003-3157-5.

Reid, J.M., Crabb, G., Temporal, J., and Clark, M. 2006. A study of water movement in road pavements. *In* Published Project Report PPR082.

Le Runigo, B., Ferber, V., Cui, Y.J., Cuisinier, O., and Deneele, D. 2011. Performance of lime-treated silty soil under long-term hydraulic conditions. Engineering Geology, **118**(1): 20–28.

Safehian, H., Rajabi, A.M., and Ghasemzadeh, H. 2018. Effect of diesel-contamination on geotechnical properties of illite soil. engineering geology, **241**: 55–63. Elsevier.

Saldanha, R.B., and Consoli, N.C. 2016. Accelerated Mix Design of Lime Stabilized Materials. Journal of Materials in Civil Engineering, **28**(3): 06015012. doi:10.1061/(ASCE)MT.1943-5533.0001437.

Saride, S., and Dutta, T.T. 2016. Effect of Fly-Ash Stabilization on Stiffness Modulus Degradation of Expansive Clays. Journal of Materials in Civil Engineering, **28**(12): 04016166. doi:10.1061/(ASCE)MT.1943-5533.0001678.

Saride, S., Puppala, A.J., and Chikyala, S.R. 2013. Swell-shrink and strength behaviors of lime and cement stabilized expansive organic clays. Applied Clay Science,. doi:10.1016/j.clay.2013.09.008.

Schroth, B.K., and Sposito, G. 1997. Surface charge properties of kaolinite. Clays and Clay minerals, **45**(1): 85–91. Springer.

Shafabakhsh, G.H., and Ani, O.J. 2015. Experimental investigation of effect of Nano TiO2/SiO2 modified bitumen on the rutting and fatigue performance of asphalt mixtures containing steel slag aggregates. Construction and Building Materials, **98**: 692–702. doi:10.1016/j.conbuildmat.2015.08.083.

Sherwood, P.T. 1993. Soil Stabilization with Cement and Lime: State-of-the-Art Review. *In* TRL STATE OF THE ART REVIEW.

Si, Z., and Herrera, C.H. 2007. Laboratory and Field Evaluation of Base Stabilization Using Cement Kiln Dust. Transportation Research Record: Journal of the Transportation Research Board, **1989**–**2**(1): 42–49. doi:10.3141/1989-47.

Sivapullaiah, P. V., and Moghal, A.A.B. 2011. Role of Gypsum in the Strength Development of Fly Ashes with Lime. Journal of Materials in Civil Engineering, **23**(2): 197–206. doi:10.1061/(ASCE)MT.1943-5533.0000158.

Sivapullaiah, P. V, Sridharan, A., and Ramesh, H.N. 2000. Strength behaviour of lime-treated soils in the presence of sulphate. Canadian Geotechnical Journal, **37**(6): 1358–1367. doi:10.1139/t00-052.

Skalny, J.P., Marchand, J., and Odler, I. 2001. Sulfate attack on concrete. CRC Press.

Sobolev, K., Flores, I., Torres-Martinez, L.M., Valdez, P.L., Zarazua, E., and Cuellar, E.L. 2009. Engineering of SiO2 Nanoparticles for Optimal Performance in Nano Cement-Based Materials. *In* Nanotechnology in Construction 3. Springer Berlin Heidelberg, Berlin, Heidelberg. pp. 139–148.

Soleimani Kutanaei, S., and Janalizadeh Choobbasti, A. 2017. Effects of Nanosilica Particles and Randomly Distributed Fibers on the Ultrasonic Pulse Velocity and Mechanical Properties of Cemented Sand. Journal of Materials in Civil Engineering, **29**(3): 04016230. doi:10.1061/(ASCE)MT.1943-5533.0001761.

Soosan, T., Sridharan, A., Jose, B., and Abraham, B. 2005. Utilization of Quarry Dust to Improve the Geotechnical Properties of Soils in Highway Construction. Geotechnical Testing Journal, **28**(4): 11768. doi:10.1520/GTJ11768.

Sreekrishnavilasam, A., Rahardja, S., Kmetz, R., and Santagata, M. 2007. Soil treatment using fresh and landfilled cement kiln dust. Construction and Building Materials, **21**(2): 318–327. doi:10.1016/j.conbuildmat.2005.08.015.

Sridharan, A., Soosan, T.G., Jose, B.T., and Abraham, B.M. 2006. Shear strength studies on soil-quarry dust mixtures. Geotechnical and Geological Engineering, **24**(5): 1163–1179. doi:10.1007/s10706-005-1216-9.

Stefanidou, M., and Papayianni, I. 2012. Influence of nano-SiO2 on the Portland cement pastes. Composites Part B: Engineering, **43**(6): 2706–2710. doi:10.1016/j.compositesb.2011.12.015.

Syed, I., and Scullion, T. 1998. In-Place Engineering Properties of Recycled and Stabilized Pavement Layers, Report 3903-S. Texas Transportation Institute, Texas A&M University, College Station, Texas.

Taha, M.R., and Taha, O.M.E. 2012. Influence of nano-material on the expansive and shrinkage soil behavior. Journal of Nanoparticle Research, **14**(10): 1190. doi:10.1007/s11051-012-1190-0.

Tajuelo Rodriguez, E., Garbev, K., Merz, D., Black, L., and Richardson, I.G. 2017. Thermal stability of C-S-H phases and applicability of Richardson and Groves' and Richardson C-(A)-S-H(I) models to synthetic C-S-H. Cement and Concrete

Research, **93**: 45–56. doi:10.1016/j.cemconres.2016.12.005.

Talluri, N., Puppala, A., Chittoori, B., Gaily, A., and Harris, P. 2013a. Stabilization of high-sulfate soils by extended mellowing. Transportation Research Record, (2363): 96–104. doi:10.3141/2363-11.

Talluri, N., Puppala, A.J., Chittoori, B.C.S., Gaily, A.H., and Harris, P. 2013b. Stabilization of High-Sulfate Soils by Extended Mellowing. Transportation Research Record: Journal of the Transportation Research Board, **2363**(1): 96–104. doi:10.3141/2363-11.

Talluri, N., Puppala, A.J., Congress, S.S.C., and Banerjee, A. 2020. Experimental Studies and Modeling of High-Sulfate Soil Stabilization. Journal of Geotechnical and Geoenvironmental Engineering, **146**(5): 04020019. doi:10.1061/(ASCE)GT.1943-5606.0002240.

Tasong, W.A., Wild, S., and Tilley, R.J.D. 1999. Mechanisms by which ground granulated blastfurnace slag prevents sulphate attack of lime-stabilised kaolinite. Cement and Concrete Research, **29**(7): 975–982. doi:10.1016/S0008-8846(99)00007-1.

Tatsuoka, F., Uchida, K., Imai, K., Ouchi, T., and Kohata, Y. 1997. Properties of cement-treated soils in Trans-Tokyo Bay Highway project. Proceedings of the Institution of Civil Engineers - Ground Improvement, **1**(1): 37–57. doi:10.1680/gi.1997.010105.

Texas Department of Transportation. 2005. Guidelines for Modification and Stabilization of Soils and Base for Use in Pavement Structures.

Thompson, M.R. 1968. Lime-treated soils for pavement construction. Journal of the Highway Division, Americal Society of Civil Engineers, **94**(2): 191–218.

Thompson, M.R. 1970. Suggested Method of Mixture Design Procedures for Lime Treated Soils. American Society of Testing and Materials Special Technical Publication, (479).

Toohey, N.M., Mooney, M.A., and Bearce, R.G. 2013. Stress-Strain-Strength Behavior of Lime-Stabilized Soils during Accelerated Curing. Journal of Materials in Civil Engineering, **25**(12): 1880–1886. doi:10.1061/(ASCE)MT.1943-5533.0000749.

Townsend, F.C., and Donaghe, R.T. 1976. Investigation of accelerated curing of soil-lime and lime-fly ash-aggregate mixtures. Soils and Pavements Laboratory (US).

Vakili, M.V., Chegenizadeh, A., Nikraz, H., and Keramatikerman, M. 2016. Investigation on shear strength of stabilised clay using cement, sodium silicate and slag. Applied Clay Science, **124**–**125**: 243–251. doi:10.1016/j.clay.2016.02.019.

Wang, Y.-H., and Siu, W.-K. 2006. Structure characteristics and mechanical properties of kaolinite soils. I. Surface charges and structural characterizations. Canadian Geotechnical Journal, **43**(6): 587–600. NRC Research Press Ottawa, Canada.

Wild, S., Kinuthia, J.M., Jones, G.I., and Higgins, D.D. 1999. Suppression of swelling associated with ettringite formation in lime stabilized sulphate bearing clay soils by partial substitution of lime with ground granulated blastfurnace slag (GGBS). Engineering Geology, **51**(4): 257–277. doi:10.1016/S0013-7952(98)00069-6.

De Windt, L., Deneele, D., and Maubec, N. 2014. Kinetics of lime/bentonite pozzolanic reactions at 20 and 50°C: Batch tests and modeling. Cement and Concrete Research, **59**: 34–42. doi:10.1016/j.cemconres.2014.01.024.

Wood, S.A., and Marek, C.R. 1993. Recovery and utilization of quarry by-products for use in highway construction, syposium on recovery and effective reuse of discarded materials and by-products for construction of highway facilities. Federal Highway Administration, Denver, Colorado,.

Yi, Y., Liska, M., and Al-Tabbaa, A. 2014. Properties and microstructure of GGBS–magnesia pastes. Advances in Cement Research, **26**(2): 114–122. doi:10.1680/adcr.13.00005.

Yuan, Y., and Chen, J. 2016. Nano-Welding of Multi-Walled Carbon Nanotubes on Silicon and Silica Surface by Laser Irradiation. Nanomaterials, **6**(3): 36. doi:10.3390/nano6030036.

Zhang, M., Zhao, M., Zhang, G., Nowak, P., Coen, A., and Tao, M. 2015. Calcium-free geopolymer as a stabilizer for sulfate-rich soils. Applied Clay Science, **108**: 199–207. doi:10.1016/j.clay.2015.02.029.

BIOGRAPHICAL INFORMATION

Nripojyoti Biswas grew up in Jalpaiguri, West Bengal, a picturesque town in the foothills of the Himalayas in India. Upon completion of his bachelor's studies in Civil Engineering from the Indian Institute of Engineering Science and Technology, Shibpur, India, in 2013, he worked for a year with Shapoorji Palonji Engineering Construction in Kolkata India. In 2015, he joined the Indian Institute of Technology, Kanpur, to pursue a master's degree in Civil (Geotechnical) Engineering. After graduation, he moved to the United States to start his doctoral studies at The University of Texas at Arlington in the spring of 2018. In the fall of 2019, he transferred from UT-Arlington to Texas A&M University, College Station, to complete his doctoral degree. He was awarded as an 'Outstanding Graduate Student' by the Department of Civil Engineering at UT Arlington. He has been a recipient of prestigious fellowships such as the Hooper Fellowship in Civil Engineering and the Terracon Endowed Fellowship in Civil engineering at Texas A&M University. He is an active member of the Geo-Institute Graduate Student Organization (ASCE) and a successful recipient of the Geo Institute-Student Travel Grant for participating in Geo-Congress 2020.